Changes in the ATP-binding cassette efflux transporters of the blood-brain barrier in glioma challenge

Georgian, Ana Ruxandra

Awarding institution:
King's College London

Changes in the ATP-binding cassette efflux transporters of the blood-brain barrier in glioma challenge

Ana Georgian

King's College London

Thesis submitted for the award of Doctor of Philosophy

November 2013

Abstract

The ATP-binding cassette (ABC) family of efflux transporters are expressed on the blood-facing (apical) surface of blood-brain barrier (BBB) endothelia and include P-glycoprotein (Pgp) and breast cancer resistance protein (BCRP). These neuro-protective transporters restrict the movement of compounds from the blood to the brain, including many chemotherapeutics; hence make treatment of brain tumours difficult. To further understand the role of efflux transporters in brain cancer, an *in vitro* model of primary porcine brain endothelial cells (PBECs) was used to explore changes in transporter expression at the BBB in response to glioma challenge. The *in vitro* results were then compared with changes in ABC transporter expression found within human brain tissue of glioma patients.

The activity and expression of Pgp and BCRP in PBECs were compared between PBECs in co-culture with glioma cells (glioma model) and PBECs in co-culture with normal astrocytes (normal model control), to identify any differences in ABC transporters. Further work was conducted to identify any signaling pathways involved in inducing ABC transporter changes during glioma challenge. For this purpose, PBECs were grown in media conditioned by either normal astrocytes or glioma cells, where the function of ABC transporters in response to modulators of Sonic and Wnt signaling was assessed. Finally, confocal microscopy was used to examine the expression of BCRP and Pgp in brain tissue of glioma patients.

The results have implication for the delivery of chemotherapeutics to the brain during tumour challenges.

Abbreviations

ABC	ATP-binding cassette
AJ	adhesion Junction
ALP	alkaline phosphatase
AsCM	astrocyte conditioned medium
AsM	astrocyte medium
BBB	blood brain barrier
BBECs	bovine brain endothelial cells
BCA	bicinchoninic acid
BCP	1 bromo-3-chloropropane
BCRP	breast cancer resistance protein
BECs	brain endothelial cells
BSA	bovine serum albumin
C6	Rat glial tumor cell line
C6CM	C6 conditioned medium
cAMP	cyclic adenosine monophosphate
Cav-1	caveolin-1
Caveolin-1-P	phosphorylated caveolin-1
CM	conditioned media
CNS	central nervous system
CO_2	carbon dioxide
COX-2	cyclooxygenase 2
CPYs	cytochromes

Ct	cycle of threshold
DAB	Digital Audio Broadcasting
dH_20	deionised water
Dkk-1	dickkopf 1
DMEM	Dulbecco's modified Eagle's medium
DMSO	dimethyl sulfoxide
ECs	endothelial cells
EDTA	ethylenediaminetetra acetic acid
ET_A	endothelin receptor a
ET_B	endothelin receptor b
FCS	fetal calf serum
FGF	fibroblast growth factor
Flk-1	VEGF receptor 2
gamma-GTP	gamma-glutamyl transpeptidase
GAPDH	glyceraldehyde 3-phosphate dehydrogenase
GBM	glioblastoma
GR	glucocorticoid receptor
HBSS	Hanks' Balanced Salt Solution
hCMEC/D3	human cerebral microvessel endothelial cells, D3 cell line
HEPES	hydroxyethyl piperazineethanesulfonic acid
HRP	horse radish peroxidase
IC_{50}	inhibition concentration at which 50% inhibition is achieved
IL-1β	interleukin -1β

IL-6	interleukin - 6
IR	insulin receptor
JAMs	junctional adhesion molecules
KCL	King's College London
KO	knock out
LDL	low density lipoprotein
MBECs	mouse brain endothelial cells
MEM	Essential Minimum Eagle's Medium
MPP^+	1-methyl-4-phenylpyridinium
MRP	multidrug resistance protein
MW	molecular weight
NaCl	sodium chloride
NEAAs	non-essential amino acids
NMDA	n-methyl-D-aspartate
NOS	nitric oxide signaling
NsM	neural stem cell media
NVU	neurovascular unit
O_2	oxygen
OAT	organic anion transporter
OCT	organic cation transporter
PBECs	porcine brain endothelial cells
PBECs-C6	PBECs grown on Transwells in co-culture with C6 glioma cells
PBECS-G7	PBECs grown on Transwells in co-culture with G7 glioma cells

PBECs-G7.4	PBECs grown on Transwells in co-culture with G7 glioma cells for 4 days
PBECs-hAs	PBECs grown on Transwells in co-culture with human astrocytes
PBECs-M	PBECs grown on Transwells in mono-culture
PBECs-P	PBECs grown in plates
PBECs-rAs	PBECs grown on Transwells in co-culture with rat astrocytes
PBS	phosphate buffered saline
PBST	phosphate buffered saline with Tween 20
PDGF	platelet-derived growth factor
Pgp	P-glycoprotein
PKA	protein kinase A
PKCβ1	protein kinase C β1
PPAR	peroxisome proliferator-activated receptors
PVDF	polyvinylidene difluoride
PXR	pregnane X receptor
RBE4	rat brain endothelial cell line
RBECs	rat brain endothelial cells
RFU	relative fluorescence units
RT-QPCR	reverse transcriptase quantitative polymerase chain reaction
SDS	sodium dodecyl sulfate
sfPBEC	serum-free PBEC medium
SHH	sonic hedgehog
SLCs	solute carrier family of transporters

Src kinase	Tyrosine-protein kinase CSK
$t_{1/2}$	half time
TCA	trichloroacetic acid
TEER	transendothelial electrical resistance
TEMED	tetramethylethylenediamine
Tf	transferrin
TfR	transferrin receptor
TJ	tight junction
TNF-α	tumour necrosis factor -α
TRI	total RNA isolation
Tyr14	tyrosine 14
UCL	University College London
Vd	volume of distribution
VEGF	vascular endothelial growth factor
ZO	zona occluden

Acknowledgements

I would like to acknowledge the advice and help of many others during the course of my PhD, most notably my supervisors from King's College London (KCL): Dr. Jane Preston, Prof Joan Abbott, and Dr. David Begley. I would also like to thank the other members of the BBB group at KCL especially Dr.Siti Yusof, Dr. Rachel C Brown, Dr. Diana Dolman and Dr. Svetlana Drndarski. In addition, thanks to Mem, Chris, Sarah, Gaya, Lisa, Peter, Charlie and Mourat. Also, a special mention for Francesca Davis who worked on the sonic signaling with me.

I would also like to thank my AstraZeneca supervisors Dr. Glynis Nicholls, Dr. Alex McCormick and Dr. Colin Howes. I would also like to acknowledge Dr. Phil Glaves and other members of the GSA team at AstraZeneca as well as Dr. Matt Arno (KCL) for help with PCR work and Patrick O'Brien (KCL) for help with the PCR calculations.

In addition I am thankful to Prof Sanjay Sisodiya and Dr. Joan Liu (Institute of Neurology, University College London (UCL)) for advice regarding immunohistochemistry as well as the Confocal Microscopy team at UCL and Dr. Paul Fraser (KCL). Also, a special mention to Dr. Marios Papadopoulous (St. George's Hospital) for some glioma samples.

Furthermore, I appreciate the cells and help obtained from Dr. Steven Pollard and other members of his group especially Sabine Gogolok (UCL).

Finally, thanks to my mum, my dad, Maria and Steven.

This project was sponsored by the BBSRC and AstraZeneca.

Table of Contents

List of Figures

List of Tables

1 General Introduction

1.1 The blood-brain barrier: historical background / physiological function

The existence of a physical barrier between the blood and brain parenchyma was first observed by Ehrlich, where peripherally injected water soluble dye did not stain the brain (Ehrlich, 1885). Together with Ehrlich's work and his own work using toxins Lewandowsky (1900), later went on to conclude that 'brain capillaries must hold back certain molecules' establishing the existence of a vascular blood-brain barrier (BBB). Since these early studies, much research over the last 130 year has demonstrated the importance and complexity of this BBB, to arrive at the understanding of today.

It is now known that the BBB is composed of endothelial cells of brain microvessels that form the interface between the blood and the brain parenchyma. The hallmark features of the brain endothelial cells, which differentiate them from non-brain endothelial cells, are their extremely "tight" tight-junctions (TJs), high expression of transporters (uptake and efflux) mediating and controlling transcellular transport, paucity of pinocytic vesicles but presence of specific receptor-mediated transcytosis, and low expression of adhesion molecules mediated leukocyte attachment and entry (Abbott, 2013).

The BBB endothelium has no fenestrations, but extremely "tight" TJs between neighbouring endothelial cells. This forms a physical barrier where TJs bring neighbouring endothelial cells into close contact, resulting in a very narrow intercellular gap (~5 Å) (Avdeef, 2011). Consequently, most molecules cannot fit through this gap and therefore cannot cross into the brain via this paracellular route (Abbott, 2013). Furthermore, TJ formation separates the apical and basolateral domains of the plasma membrane (the 'fence' foundation of the TJ), so that the apical (luminal) blood-facing surface and the basal (abluminal) brain-facing surfaces can have distinct functions (Abbott, 2013).

This polarity enables endothelial cells to correctly express uptake transporters, either on the apical and/or basal surfaces, to enable the uptake of necessary nutrients into the brain via passage through the endothelial cells themselves. Uptake of certain larger

molecules can occur via adsorptive-mediated or receptor-mediated endocytosis/transcytosis (AMT/RMT) (Abbott *et al.*, 2010)

The presence of enzymes (e.g. cytochrome P450s), within the membranes of the endothelial cells as well as extracellularly and intracellularly, forms a metabolic or enzymatic barrier to such transport systems (Kuhnline Sloan *et al.*, 2012). Efflux transporters on the apical surface of cells form an additional barrier to transport, which function in opposition to uptake transporters, pumping potentially neurotoxic compounds away from the brain and back into the blood (Begley, 2004). Thus, the BBB is not only a physical barrier but also transport barrier, that allows the transport of nutrients (such as glucose) into the brain, while restricting the entry of toxic and potentially damaging compounds to the brain (Abbott et al., 2010). All these processes work together to allow the BBB to maintain brain homeostasis and the correct microenvironment for neuronal function in the central nervous system (CNS).

The BBB does not exist in isolation, but is supported by other cells of the CNS to form a neurovascular unit (NVU), including astrocytes, pericytes, microglia and neurons (Abbott, 2013). These cells help in the development and maintenance of the BBB and are therefore crucial to its existence and dynamic nature.

Here, the different properties of the BBB will be discussed, together with ways in which the BBB is affected in cancer and the implications of the BBB efflux transporters for the treatment of primary brain tumours (gliomas).

1.2 The BBB: tight junctions and glycocalyx

The BBB acts as a physical barrier to most polar molecules as well as macromolecules such as proteins. The physical barrier is created by tight junctions (TJs) between neighbouring endothelial cells in the brain. Very “tight” TJs are a key feature of the BBB, whereas non-CNS endothelial cells have leakier cell:cell contacts (Coomber & Stewart, 1986). These TJs leave only a small gap, severely restricting the paracellular passage of ions and molecules from the blood to the brain (Avdeef, 2011).

Both adherens junctions (AJs) and TJs are found at the BBB. AJs are formed by protein complexes between transmembrane cadherin glycoproteins at the intercellular cleft that are linked to alpha, beta, and gamma catenin in the cytoplasm, which in turn are linked to the cytoskeleton of the cell (Steinberg & McNutt, 1999, Petty & Lo, 2002,

Brown & Davis, 2002, Paolinelli *et al.*, 2011) (Figure 1.1). Thus the AJs provide structural support to the endothelial cells and enable the formation of TJs.

The TJs are formed of a complex between occludin, claudins and junctional adhesion molecules (JAMs) (at the intercellular cleft) linked to the cytoplasm and cytoskeleton via zonula occludens (ZO) proteins and cingulin (Abbott et al., 2010, Liu *et al.*, 2012) (Figure 1.1). Several proteins are involved in TJ interaction and a comprehensive list is given in Table 1.1.

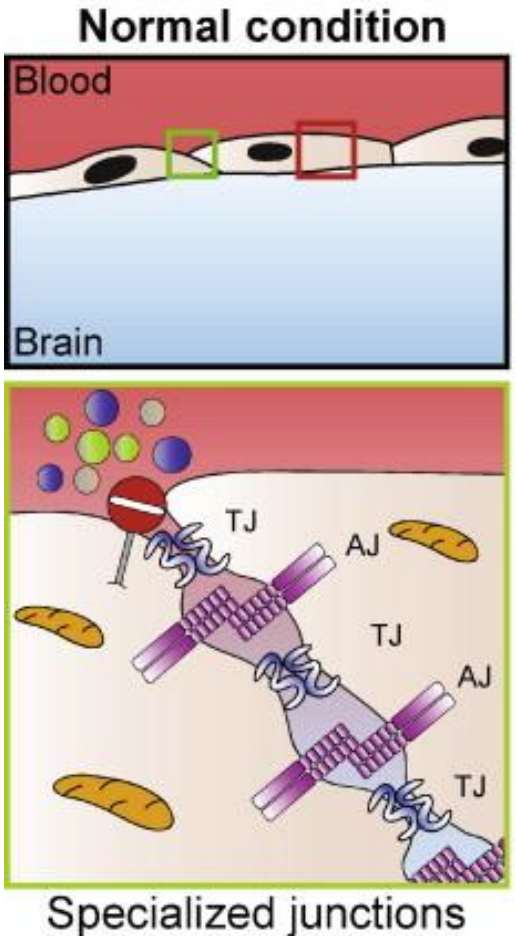

Figure 1.1 Brain capillaries under normal condition (Paolinelli et al.*, 2011)*

Cerebral endothelial cells form complex junctions sealing the paracellular route and blocking the passage of polar molecules.

TJs: Tight junctions such as claudins and occludin. AJs: Adherens junctions such as cadherins.

Table 1.1 Components of AJs and TJs on brain microvascular endothelial cells (Paolinelli et al., 2011).

2	AJs	TJs
Cell–cell adhesion membrane proteins	Cadherins (VE- and N-cadherin)	Claudins (1, 3, 5, 12) occludin JAMs, (A, B, C) ESAM, nectin
Cytoskeletal proteins	α-catenin, β-catenin, plakoglobin, p120, afadin or AF6, α-actinin, eplin	ZO proteins, cingulin ZONAB, afadin or AF6

The table reports the best characterised components of AJs and TJs only.

AJs, adherens junctions; TJs, tight junctions; ZO, zonula occludens; ZONAB, zonula occludens-1 associated nucleic-acid-binding protein; JAMs, junctional adhesion molecules; ESAM, endothelial cell-selective adhesion molecule.

Studies have shown that claudin 3, 5 and 12 are expressed at the BBB, while claudin 1 and 2 are not normally expressed in the parenchymal vessels of the CNS (Nitta *et al.*, 2003, Pfeiffer *et al.*, 2011) . A loss in the expression of these claudins has been shown to have consequences for BBB integrity. For example a loss of claudin 5 has been shown to result in barrier breakdown and paracellular leakiness (Nitta et al., 2003). Similarly, disruption of occludin, ZO-1 and ZO-2 proteins also leads to barrier breakdown and increased BBB permeability (Beauchesne *et al.*, 2009). This demonstrates the importance of TJs in establishing the low permeability of the BBB, where breakdown of TJs leads to leak of plasma constituents including serum proteins into the brain, resulting in disruption of CNS homoeostasis and consequently disruption in neuronal activity.

Another physical barrier present at the BBB, has recently been highlighted, namely the glycocalyx. This is a polysaccharide matrix that exists on the surface of the endothelial cells, which has been shown to have important functions at the BBB. It is composed of a negatively charged network of proteoglycan, glycoproteins, and glycolipids and it can act as a filter, by binding positively charged molecules. Thus, the glycocalyx restricts access of positively charged molecules to the endothelial cell surface and therefore restricts the transport of these molecules across the barrier (Li *et al.*, 2010, Yuan *et al.*, 2010).

2.1 Transport at the BBB

Due to the physical barrier of the BBB, most molecules can only enter the brain from the blood by crossing the endothelial cell layer.

There are several routes of entry for such molecules (Figure 1.2). Gases such as O_2 and CO_2 can freely diffuse across the barrier by passive diffusion, as can many small hydrophobic molecules (Liu *et al.*, 2004). Lipid-soluble molecules, can easily interdigitate between the phospholipids of the plasma membrane to reach the cell interior; entry into the brain has been shown to positively correlate with the degree of lipid solubility (Abbott et al., 2010).

The thinness of the BBB endothelial cell facilitates non-polar molecule diffusion, where flattening and elongation of the BBB endothelial cells decreases the distance over which a molecule must diffuse to reach from one side to the endothelium to the other side (Abbott et al., 2010). However, as a general rule the ability of molecules to diffuse decreases with increased surface charge and increased size of the molecule, with molecules of polar surface areas (PSA) above 80$Å^2$ and molecular weight (MW) greater that 450 Da showing restricted permeability (Abbott et al., 2010). Furthermore, positively charged molecules have the additional problem of binding to the glycocalyx before reaching the cell surface and therefore less readily cross the BBB (Abbott et al., 2010, Li et al., 2010).

For polar molecules, solute carriers (SLCs) can facilitate crossing of the BBB. Several members of the SLC family of transporters have been shown to be expressed at the BBB (Table 1.2), including GLUT1 for glucose transport, several amino acid and nucleoside/nucleotide transporters (e.g. LAT1), organic anion transporters (OATs) and organic cation transporters (OCTs) which allow negative and positive ionic compounds respectively into the brain (Kusuhara & Sugiyama, 2005, Abbott et al., 2010).

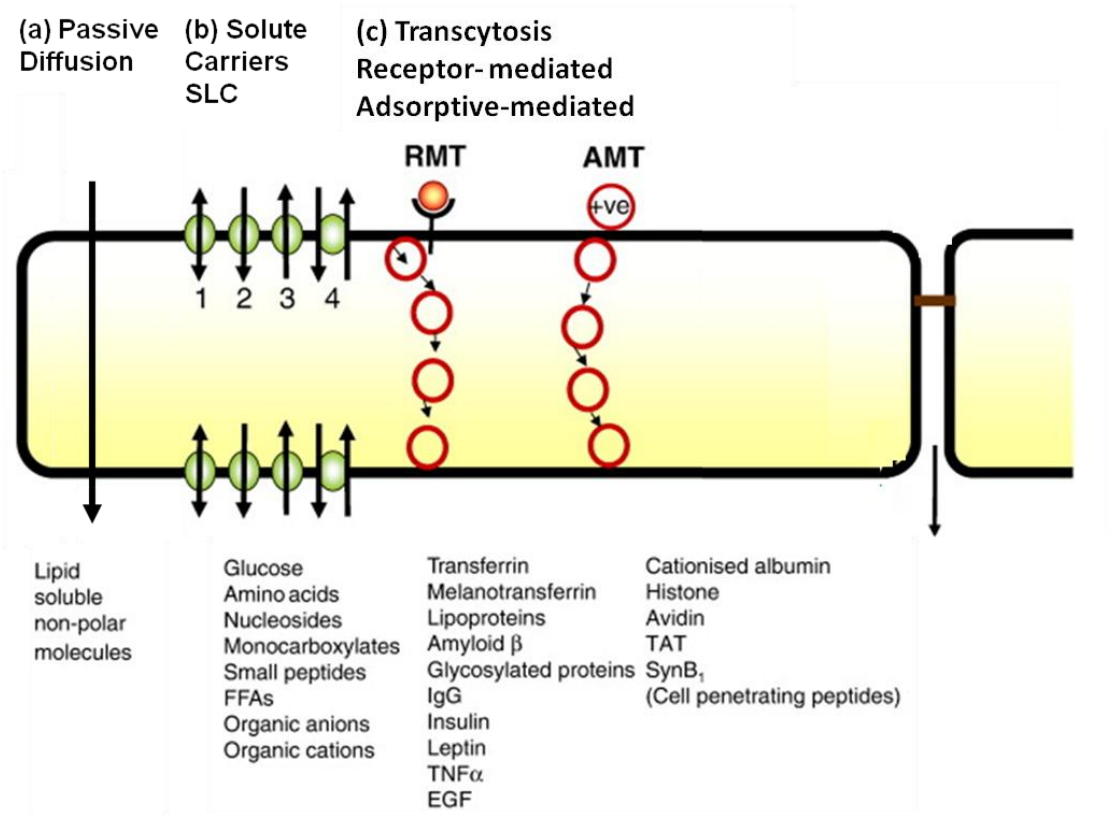

Figure 1.2 Transport mechanisms across the BBB. Modified from Abbott et al., (2010).

(a) Solutes may passively diffuse through the cell membrane and cross the endothelium. A higher lipid solubility and several other physico-chemical factors favour this process (see text). (b) Carrier-mediated influx via solute carriers (SLCs) may be passive or primarily or secondarily active and can transport many essential polar molecules such as glucose, amino acids and nucleosides into the CNS. The solute carriers may be bi-directional, the direction of net transport being determined by the substrate concentration gradient (1), unidirectional either into or out of the cell (2/3), or involve an exchange of one substrate for another or be driven by an ion gradient (4). In this last case the direction of transport is also reversible, depending on electrochemical gradients. (c) RMT (receptor mediated transcytosis) requires receptor binding of ligand and can transport a variety of macromolecules such as peptides and proteins across the cerebral endothelium (transcytosis). AMT (adsorptive mediated transcytosis) appears to be induced in a non-specific manner by positively charged macromolecules and can also transport across the endothelium. Both RMT and AMT appear to be vesicular-based systems which carry their macromolecule content across the endothelial cells.

Table 1.2 Solute carriers at the BBB. (Abbott et al. 2010)

Transporter (SLC)	Abbreviation and/or transporter subtype	EquivalentHuman Gene Name	BBB location	Orientation[a]	Example of endogenous substrates/mechanism
Glucose	GLUT1	SLC2A1	Luminal Abluminal	Blood to brain	Glucose (Facilitative, bi-directional)
Sodium-dependent glucose transporter	SGLT1	SLC5A1	Abluminal	Brain to endothelium	Glucose
Sodium myoinositol cotransporter	SMIT HMIT/GLUT13	SLC5A3 SLC2A13	Luminal	Blood to endothelium	Myoinositol (Sodium-dependent)
Cationic L-amino acid transporter	CAT1 (y^+) CAT3	SLC7A1 SLC7A3	Luminal	Blood to endothelium	Basic L-amino acids Lysine, arginine (Sodium-independent)
Large neutral amino acid transporter	LAT1 (system L)	SLC7A5	Luminal Abluminal	Blood to brain	Asparagine, glutamate, histidine, isoleucine, leucine, methionine, phenylalanine, threonine, tryptophan, tyrosine, valine (Facilitative, bi-directional)
Amino acid	y^+LAT2	SLC7A6	Luminal Abluminal	Blood to brain	Arginine, lysine, ornithine (Facilitative, bi-directional)
Amino acid	y^+LAT2 ? (Na^+-dependent LNAA, system y^+L)	SLC7A6?	Abluminal	Brain to endothelium	Alanine, glycine, histidine, isoleucine, leucine, methionine, phenylalanine, threonine, tryptophan, tyrosine, valine (Sodium-dependent)
Amino acid	SNAT2 (System A)	SLC38A2	Abluminal	Brain to endothelium	Small neutral amino acids Alanine, asparagine, proline, serine, glycine (Sodium-dependent)
Amino acid	SNAT 3 SNAT 5 (System N)	SLC38A3 SLC38A5	Abluminal	Brain to endothelium	Asparagine, glutamine, histidine, serine (Sodium-dependent)
Amino acid	System n	?	Luminal	Blood to endothelium	Asparagine, glutamine, histidine (Facilitative)
Amino acid	ASCT1 ASCT2 (System ASC)	SLC1A4 SLC1A5	Abluminal	Brain to endothelium	Alanine, cysteine, glycine, isoleucine, leucine, methionine, serine, threonine, valine (Sodium-dependent)
Amino acid	EAAT1 EAAT2 EAAT3	SLC1A3 SLC1A2 SLC1A1	Abluminal	Brain to endothelium	Anionic amino acids Glutamate, aspartate (Sodium-dependent)
Amino acid	x^-_G	SLC1A?	Luminal	Blood to endothelium	Glutamate (Facilitative)
Amino acid	GLYT	SLC6A9	Luminal?	Blood to endothelium	Glycine Na and Cl dependent
Amino acid	TAUT, β	SLC6A6	Luminal Abluminal	Brain to endothelium	Taurine, β-alanine (Sodium-dependent)
Nucleosides, nucleotides and nucleobases	ENT1 ENT2	SLC29A1 SLC29A2	Luminal	Blood to endothelium	Nucleosides, nucleotides, nucleobases (Facilitative, equilibrative)
Nucleosides, nucleotides and nucleobases	CNT1 CNT2 CNT3	SLC28A1 SLC28A2 SLC28A3	Abluminal	Endothelium to brain	Nucleosides, nucleotides, nucleobases (Sodium-dependent exchange)
Monocarboxylic acids	MCT1	SLC16A1	Luminal Abluminal	Blood to brain	Ketone bodies
Monocarboxylic acids	MCT2 ?	SLC16A7	Abluminal	Brain to endothelium	Lactate (Proton exchanger)
Thyroid hormone transporter	MCT8 (XPCT)	SLC16A2	Luminal Abluminal	Blood to brain	T3 thyroid hormone (Facilitative)
Organic anion transporters	OAT2 OAT3	SLC22A7 SLC22A8	Luminal	Blood to brain	Dicarboxylate exchange with α-ketoglutarate, bicarbonate, Cl^-
Organic anion transporting polypeptide	OATPB/OATP2B1 OATP1A4 OATP1C1	SLCO2B1 SLCO1A4 SLCO1C1	Luminal Abluminal	Blood to endothelium Endothelium to brain	Organic anion/bicarbonate exchangers
Organic cation transporters	OCT2 OCT3	SLC22A2 SLC22A3	Luminal	Blood to endothelium	Organic cation/proton exchange
Novel organic cation transporter	OCTN2	SLC22A5	Luminal Abluminal	Blood to endothelium Endothelium to brain	Organic cation/proton exchange
Amine transporter	PMAT	SLC29A4	Abluminal	Brain to endothelium	Organic cation/proton exchange, MPP^+, serotonin, dopamine
Choline transporter	CTL1	SLC44A1	Luminal Abluminal	Blood to endothelium Endothelium to brain	Choline Facilitative

Such transporters allow essential nutrients and amino acids to be transported into brain, where they are needed for the survival of the CNS cells. The polarity of transporters (either existing on the apical-luminal and/or basal-abluminal surface of the endothelia) is also key, since this determines the direction of flux into and out of the cell. For example GLUT1 needs to be expressed apically, in order to have access to the glucose in the circulation and also basally/abluminally to carry glucose into the brain. Basal/abluminal transporters are also necessary to allow the transport of intracellular molecules (those that have managed to pass across the luminal cell surface and enter the intracellular space) into the brain parenchyma.

Finally for larger molecules transcytosis of molecules is also possible. This is facilitated by pathways such as clathrin-mediated endocytosis and caveolae-mediated endocytosis (Abbott et al., 2010).

Clathrin-mediated endocytosis is a process where ligands bind to “clathrin-coated pits” on the plasma membranes. This is followed by small vesicle assembly (approximately 100 nm in diameter) and internalisation. Clathrin-coated pits can take up a variety of extracellular molecules, including low density lipoprotein (LDL), transferrin (Tf), growth factors and antibodies (McMahon & Boucrot, 2011, Xiao & Gan, 2013)

Caveolae are smaller flask-shape pits (approximately 50 nm in diameter) (Xiao & Gan, 2013). They express caveolin molecules (e.g. caveolin 1 and 2), which when phosphorylated, trigger vesicle internalisation (Fagerholm *et al.*, 2009).

In the BBB, molecule transport occurs via either adsorptive-mediated or receptor-mediated processes.

Adsorptive-mediated transport is a non-specific mode of transport, where positively charged ligands/molecules interact with the negative cell surface via electrostatic interaction. A vacuole is then formed around the molecule, which becomes internalised into the endothelial cell. This is a nonspecific process (i.e. not receptor-mediated) and is often via the clathrin-mediated mode (Xiao & Gan, 2013).

Receptor-mediated endocytosis is a specific process for cells to take up specific small and large molecular ligands, including hormones, growth factors, enzymes, and plasma proteins. In this process, the ligand binds to a receptor on the cell surface (usually found with clathrin-coated pits or caveolae). Due to a finite number of receptors on the cell surface, receptor-mediated endocytosis is normally a saturable process (Xiao & Gan, 2013). For example, transferrin receptor (TfR) and insulin receptor (IR), allow receptor mediated endocytosis of transferrin and insulin respectively (Haqqani *et al.*, 2013). A list of transcytotic mechanisms at the BBB is given in Table 1.3.

Table 1.3 Transcytosis mechanisms at the BBB (Abbott et al. 2010).

Transport system	Abbreviation (receptor)	Example ligands	Type	BBB direction
Transferrin	TfR	Fe-transferrin	RMT	Blood to brain
Melanotransferrin	MTfR	Melanotransferrin (p97)	RMT	Blood to brain
Lactoferrin	LfR	Lactoferrin	RMT	Blood to CSF
Apolipoprotein E receptor 2	ApoER2	Lipoproteins and molecules bound to ApoE	RMT	Blood to brain
LDL-receptor-related protein 1 and 2	LRP1 LRP2	Lipoproteins, Amyloid-β, lactoferrin, α 2-macroglobulin, melanotransferrin (p97), ApoE	RMT	Bi-directional
Receptor for advanced glycosylation end-products	RAGE	Glycosylated proteins, Amyloid-β, S-100, amphotericin	RMT	Blood to brain
Immunoglobulin G	Fcγ-R	IgG	RMT	Blood to brain
Insulin	–	Insulin	RMT	Blood to brain
Leptin	–	Leptin	RMT	Blood to brain
Tumour necrosis factor	–	TNFα	RMT	Blood to brain
Epidermal growth factor		EGF	RMT	Blood to brain
Heparin-binding epidermal growth factor-like growth factor (diphtheria toxin receptor)	HB-EGF (DTR)	Diphtheria toxin and CRM197 (protein)	RMT	Blood to brain
Leukaemia inhibitory factor	LIFRa (gp190)	LIF	RMT	Blood to brain/ spinal cord
Cationised proteins	+	Cationised albumin	AMT	Blood to brain
Cell penetrating peptides	+	SynB5/pAnt-(43–58)	AMT	Blood to brain

2.2 BBB metabolic barriers

Along with uptake processes and transporters, the BBB endothelial cells form a metabolic barrier. The thin nature of the endothelial cell to some extent aids rapid transport of molecules; however this does not completely prevent molecules from becoming degraded within the cell. Any molecule that enters the cells via any of the above processes is still vulnerable to metabolism and enzymatic degradation. For example even glucose is degraded in part as it crosses the BBB (McAllister *et al.*, 2001).

Enzymes can be found on the surface, the apical/luminal or basal/abluminal membranes or in the cytoplasm of endothelial cells. Enzymes such as gamma-GTP (Gamma-glutamyl transpeptidase) and ALP (Alkaline phosphatase) have been shown to be present in the apical/luminal membrane (Betz & Goldstein, 1978, Fukushima *et al.*, 1990), while cytochrome P450 (CYP) enzymes have been found intracellularly (Ghosh *et al.*, 2010).

The presence of such enzymes gives rise to a metabolic barrier in the BBB that can restrict and even prevent molecules crossing the BBB into the brain parenchyma.

2.3 BBB transport barrier: the ABC efflux transporters

In addition to metabolic processes, transport across the BBB is restricted by the presence of efflux transporters. These transporters tend to be localised on the apical/luminal surface of the endothelium and can pick up molecules from within the membrane lipid bilayer (Nervi *et al.*, 2010) and actively efflux them back into blood. Therefore, they too can retard molecules from crossing the BBB.

The most studied efflux transporters of the BBB are p-glycoprotein (Pgp), the multidrug resistance associated proteins (MRPs) and the breast cancer resistance protein (BCRP). They are all members of the ATP-binding cassette (ABC) transporter superfamily, characterised by their ability to use the energy from ATP-hydrolysis to transport their substrates against a concentration gradient (Begley, 2004, Abbott et al., 2010)

2.3.1 P-glycoprotein (Pgp)

Pgp was the first discovered ABC efflux transporter and has therefore been studied the most extensively. It is the ~180 kDa protein-product of the MDR1 gene in higher mammals such as pigs and humans (and mdr1a and mdr1b genes in rodents), composed of two functional units each formed of six transmembrane α-helices with one cytoplasmic domain responsible for ATP hydrolysis (i.e. a typical ABC-transporter conformation) (Bosch & Croop, 1998, Locher, 2009). In addition, two distinct substrate binding sites have been identified the R-site and the H-site (named after the drug specificities of Rhodamine 123 and Hoechst 33342) as well as a third M-site (modulation site) for modulators of Pgp (Ferreira *et al.*, 2013). Immunohistochemical studies and mRNA analysis have shown Pgp is expressed in the brain of humans, rats, mice and pigs (Warren *et al.*, 2009), where there is a consensus that it is predominantly expressed on the apical/luminal surface of BBB endothelia (Stewart *et al.*, 1996, Beaulieu *et al.*, 1997, Roberts *et al.*, 2008)

In vivo studies with single (mdr1a) and double (mdr1a/b) knockout (KO) mice have clearly shown that when Pgp is lacking there is an increase in BBB permeation of compounds such as quinidine and nelfinavir (Kusuhara *et al.*, 1997, Salama *et al.*, 2005). Similarly, Pgp inhibitor studies have found that certain molecules can more effectively cross the BBB in the absence of Pgp activity (Ibrahim *et al.*, 2000, Mittapalli

et al., 2013). Transfection experiments (with cloned full-length human and mouse Pgp cDNA) have demonstrated that the Pgp gene can confer, to otherwise sensitive cells, resistance against different cytotoxic agents, including alkaloids, anthracyclines (Gros *et al.*, 1986, Greenberger *et al.*, 1988). Taken together, all the above have demonstrated the role of Pgp in the BBB to be that of an efflux transporter, where the substrates it can transport include a variety of different pharmaceutics (Linnet & Ejsing, 2008, Matsson *et al.*, 2009).

In terms of Pgp modulation, this can involve changes in expression or changes in activity.

Changes in expression

Activation of the pregnane-X-receptor (PXR), constitutive androstane receptor (CAR) and glucocorticoid receptor (GR) pathways have been shown to lead to increased Pgp expression at the BBB (Narang *et al.*, 2008, Miller, 2010, Lemmen *et al.*, 2013). Similarly, glutamate via the NMDA/COX-2 pathway has been shown to increase Pgp expression (Yousif *et al.*, 2012). In addition, Lim *et al.* (2007) showed that activating the Wnt pathway increases Pgp mRNA, with the β-catenin pathway being implicated in this response.

The role of pro-inflammatory cytokines in Pgp regulation is still unclear, with different cytokines having different effects. IL-1β was shown to have no effect on Pgp mRNA, while IL-6 decreased Pgp mRNA levels and TNF-α increased Pgp mRNA expression in hCMEC/D3 endothelial cells (Poller *et al.*, 2010).

Changes in activity

Pgp activity has also been shown to be regulated via expression-independent pathways. For example, phosphorylation of Pgp by PKC (protein kinase C) has shown to increase (Chambers *et al.*, 1990) and decrease (Miller *et al.*, 1998) Pgp activity and it was suggested that different isomers of PKC could act to either increase or decrease Pgp activity (Sachs *et al.*, 1999).

Pgp decreases in activity were also shown to result in response to loss in luminal expression of Pgp, consistent with caveolae internalisation in a PCK-independent pathway (Hawkins *et al.*, 2010). Ubiquination of Pgp has also been shown to play a role in Pgp activity regulation, with increased ubiquination resulting in decreased activity (Zhang *et al.*, 2004).

2.3.2 Breast cancer resistance protein (BCRP)

BCRP is a 72 kDa protein, which unlike other efflux proteins (with two repeated halves), consists of a single nucleotide binding domain and a single membrane-spanning domain i.e. it is a half-transporter (Doyle *et al.*, 1998). BCRP has been suggested to be able to form heterodimers and homotetramers (Mao & Unadkat, 2005), although it is still debated whether such dimerisation is required for functional activity (Mitomo *et al.*, 2003, Mo & Zhang, 2009, Ni *et al.*, 2010). Cooray *et al*., showed the location of BCRP in human microvessels in 2002. BCRP has been shown to be luminally expressed in brain capillary endothelia of human (Zhang *et al.*, 2003), porcine (Eisenblatter *et al.*, 2003), rat (Hori *et al.*, 2004) and mouse (Lee *et al*., 2007, Lee *et al.*, 2005). However, its role at the BBB is still not fully characterised. Eisenblatter et al. (2003) suggested that the pig BCRP protein was able to actively transport the chemotherapeutic drug daunorubicin across a monolayer of primary cultured brain endothelial cells. Furthermore, Hori et al. (2004) showed that transfection of the BCRP gene into HEK293 cells resulted in decreased penetration of mitoxantrone into these cells. However, this study involved BCRP which was greatly over-expressed and so could not provide a true insight into the role of BCRP *in vivo*, since endogenous levels of BCRP are normally relatively lower (Lee et al., 2007). When BCRP was not hyper-expressed (i.e. was expressed at normal physiological levels), no mitoxantrone transport could be detected by Lee et al. (2007), suggesting that BCRP is not a major efflux protein at the BBB. However, Cisternino *et al.* (2004) using an *in situ* brain perfusion technique, showed that brain efflux of prazosin and mitoxantrone was inhibited by GF120918 (a Pgp and BCRP inhibitor) in both wild-type and mdr1a KO mice. Interestingly, in the mdr1a KO mice BCRP was also shown to be up-regulated greater than 3-fold, suggesting an adaptive response exists between efflux proteins (i.e. where BCRP expression is increased to perhaps compensate for the absence of Pgp) (Cisternino et al., 2004).

It should be mentioned that the relative expression levels of BCRP in rodent and human brain endothelia do not correlate well, with the protein expression of human BCRP measured to be 1.85 fold greater than that of mice (Uchida *et al.*, 2011). This suggests that there is a need to use alternative models to murine when addressing the relevance of BCRP *in vivo*.

Less is known about regulation of BCRP than Pgp. As for Pgp, BCRP expression has been shown to be increased in response to activation of PXR, CAR and GR receptors (Zhang et al., 2004, Narang et al., 2008, Lemmen et al., 2013), as well as to activation of the glutamate NMDA/COX-2 pathway and Wnt/β-catenin pathways (Lim et al., 2007, Yousif et al., 2012).

Differential regulation of BCRP versus Pgp has also been shown in response to cytokines, where TNF-α (which increased Pgp expression) was shown to decrease BCRP expression by Poller et al. (2010).

However, no pathways independent of Pgp regulation have been identified for BCRP nor have any expression-independent pathways and so further research on BCRP is still required.

2.3.3 Multidrug resistance associated proteins (MRPs)

Nine members of the MRP family have so far been discovered (MRP1-9); however, not all have been detected within brain capillary endothelia. Nies *et al.* (2004) found MRP1, MRP4 and MRP5 to be luminally localised on brain endothelial cells in human brain samples, but there was no positive staining for MRP 2, 3 or 6. However, this remains controversial since Potschka *et al.* (2003) and Soontornmalai *et al.* (2006) reported the presence of functional MRP2 at the BBB of rats and mice, respectively. In addition, more recent studies have additionally shown the expression of MRP8 and 9 mRNA in human brain microvessels or human brain endothelial cells (Dauchy *et al.*, 2008, Dauchy *et al.*, 2009). By contrast, one study in mice using liquid chromatography-tandem mass spectroscopy proteomics showed MRP4 to be the only MRP detected at the BBB (Kamiie *et al.*, 2008). The degree to which these differences can be attributed to differential expression between species is still unknown.

Functionally, MRP1, MRP2 and MRP3 have all been shown to have preferential substrates among conjugated lipophilic compounds (e.g. steroids conjugated with glutathione, glucuronate or sulphate), with MRP6 also being able to transport glutathione conjugates (Nies et al., 2004). MRP4 and MRP5 substrates include cyclic nucleotides such as cGMP (Jedlitschky *et al.*, 2000, Chen *et al.*, 2001). However, their function at the BBB remains just as elusive as their expression profiles. Although Sugiyama *et al.* (2003) showed that MRP1 may play a role in the efflux of estradiol glucuronide from the BBB, since mrp1 KO mice showed less efflux of this compound

than their wild-type counterparts, other mrp1 KO mice studies showed little alteration in the net substrate transport in KO mice compared with wild-type (Sun *et al.*, 2001, Cisternino *et al.*, 2003).

2.4 The neurovascular unit (NVU)

It is important to note that the BBB endothelial cells do not exist in isolation, but are part of a neurovascular unit (NVU) of supporting cells that aid the development and maintenance of the BBB. These include astrocytes, pericytes, microglia and neurons (Figure 1.3).

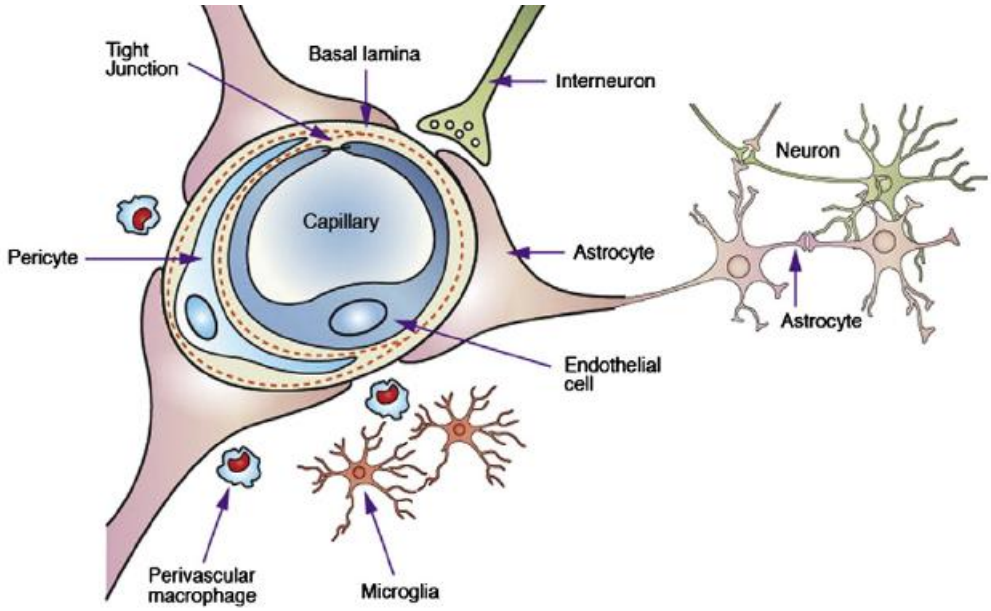

Figure 1.3 The BBB and the neurovascular unit. Chen and Liu (2012) based on Abbott et al. (2006).

Schematic representation of the blood–brain barrier (BBB) and other components of a neurovascular unit (NVU).

2.4.1 Astrocytes

The importance of astrocytes to the BBB has been hypothesised since 1967, where astrocytes were suggested to be involved in controlling the exit of materials from the brain capillaries (Davson & Oldendorf, 1967).

Astrocytes have since been shown important in glucose transport at the BBB, inducing the expression of GLUT1 on the luminal surface of endothelial cells (McAllister et al., 2001). Astrocytes were shown to induce more complex TJs (shown in electron microscope studies) (Dehouck *et al.*, 1990, Wolburg *et al.*, 2009), with high transendothelial electrical resistance (TEER) (measure of resistance to ion transport across the BBB) and low inulin (small paracellular molecule) permeability, as well as maintaining the transport of essential amino acids such as leucine (Dehouck et al., 1990, Kido *et al.*, 2002).

In vivo, chemical induction of astrocyte loss using a gliotoxin was shown to result in TJ breakdown and increased BBB leakiness which could be reversed by regrowth of astrocytes (Willis *et al.*, 2004), showing astrocytes to be important both *in vitro* and *in vivo*.

Astrocytes were shown to maintain Gamma-glutamyl transpeptidase (gamma-GTPase) enzyme activity in isolated microvessels places in culture, which is normally lost when microvessels are cultured alone (Kido et al., 2002). Furthermore, astrocytes were shown able to induce gamma-GTPase activity after it had been lost in culture (Dehouck et al., 1990). The presence of astrocytes has also been shown to increase the mRNA expression of efflux transporters such as Pgp in endothelial cells as well as increased levels of efflux activity (Kido et al., 2002, Berezowski *et al.*, 2004) and toxic depletion of astrocytes *in vivo* was also shown to result in decreased Pgp expression at the BBB (Willis *et al.*, 2007) .

Astrocytes have been shown to induce the expression of antioxidant proteins (manganese superoxide dismutase and heme oxygenase-1) in endothelial cells, thereby conferring protection against oxidative stress and free-radical induced damage (Schroeter *et al.*, 1999, Schroeter *et al.*, 2001, Son *et al.*, 2005).

Interestingly, astrocytes have been shown capable of inducing BBB markers (such as the transferrin receptor, Pgp, GLUT1 and gamma-GTPase activity as well as inducing close cell: cell interactions reminiscent of TJs (with decreased barrier permeability to inulin) in non-BBB endothelial cells such as human umbilical vein endothelial cells (Janzer & Raff, 1987, Tout *et al.*, 1993, Hayashi *et al.*, 1997)

Studies have shown that some of the same inductive properties could be achieved through the use of astrocyte-conditioned medium (such as decreased paracellular permeability and alkaline phosphatase activity, increased TEER and improved f-actin and e-cadherin distributions) (Rubin *et al.*, 1991, Sobue *et al.*, 1999) This

demonstrates that some astrocyte induction of the BBB phenotype involves the secretion of soluble factors by the astrocytes.

All this together shows that astrocytes play an important role in establishing and maintaining the normal BBB phenotype.

2.4.2 Pericytes

Recently studies have revealed the importance of pericytes in establishing and maintaining BBB phenotype.

Daneman *et al.* (2010) showed that the BBB is formed during embryogenesis in the absence of astrocytes (which only begin to be expressed postnatally), whereas pericytes are recruited to vessels over a week before astrocytes are generated. This indicates that pericytes may play a role in BBB development. Prenatal capillaries showed the presence of TJ protein, GLUT1 and Pgp. Interestingly, Pgp expression was present but only at low levels, with increases in expression occurring postnatally (which correlated with astrocyte expression, implicating astrocytes in the expression of efflux transporters).

By examining pericytes-deficient mice, BBB permeability was shown to inversely correlate with pericyte number (i.e. increased BBB permeability correlating with decreased pericyte number). Although the expression of TJ proteins did not appear affected in this study (occludin, Claudin 5 and ZO-1), structural abnormalities were clear in the endothelial junctions (e.g. the length of junctions were random, with altered parallel and perpendicular junctions), showing that pericytes are important in TJ formation. Transcytosis was also shown to increase with decreased pericyte numbers. The results indicated that pericytes do not induce BBB-specific gene expression but inhibit expression of molecules that increase vascular permeability, i.e. pericytes down regulate the expression of 'default' not brain endothelial characteristics, while astrocytes upregulate the specific BBB features.

In postnatal mice (2-8 months), Armulik *et al.* (2010) used mice with different deficiencies of pericytes (26-72% normal levels) and showed that increased blood vessel diameter and decreased vessel density correlated with decreased pericytes density. So pericytes were demonstrated to be important for angiogenesis in the brain. VE-cadherin, ZO-1 and Claudin-5 protein levels where not altered in pericytes-deficient

mice, but increased width of TJs was noted under the electron microscope (EM), as well as increased density of transcytotic vesicles (in agreement with the embryonic study above).

Microarray studies examined the expression of transporters, with GLUT1 unaffected but transferrin receptor showing decreased levels, with the decrease correlated with reduced pericyte density. This implicates pericytes in aspects of transporter expression and BBB uptake function (Armulik et al., 2010).

Similarly, Bell *et al.* (2010) used mice of increasing age (1,6-8,14-16 months) with different levels of pericyte deficiency to show that loss of pericytes at the capillaries, resulted in increased permeability of the BBB to macromolecules (e.g. serum proteins) indicative of deregulation of transcytotic pathways. This showed that BBB dysfunction of transcytosis can occur as a result of pericyte deficiency. Also, a decrease in ZO-1 and claudin 5 as well as decreased collagen IV and laminin correlated with increased age of the pericyte-deficient mice showing that a lack of pericytes also results in TJ and basal lamina dysfunction. This suggests that although initially a lack pericytes may not affect TJ protein expression, chronic lack of pericytes does eventually lead to TJ protein loss.

In summary, pericytes are important in BBB development and maintenance of the BBB. They are important in angiogenesis and in establishing capillary diameter (capillaries can act to constrict capillaries) (Winkler *et al.*, 2011) and therefore blood flow regulation of the brain. In addition they are important in the establishment of the basal lamina, secreting many molecules involved in the creation and remodelling of the basal lamina, and therefore are key players in the maintenance of the BBB and CNS microenvironment (Winkler et al., 2011).

2.4.3 Neurons

In addition to astrocytes and pericytes, neurons have also been shown to modulate the BBB. Duport *et al.* (1998) co-cultured endothelial cells with brain slices containing intact neural networks, which resulted in increased TJ expression and decreased BBB permeability. Similarly, Savettieri *et al.* (2000), showed that co-culture of endothelial cells with neurons increased the expression of occludin at the endothelium, indicating that neurons increased TJ protein expression.

2.4.4 Interactions between cells of the NVU

It is important to note that interactions between the cells of the NVU are also important in the modulation of the BBB. For example, the increase in BBB occludin in the presence of neurons has been shown to be enhanced/speeded up when astrocytes are also present (Schiera *et al.*, 2003).

Similarly, one study showed that addition of astrocytes to pericyte-endothelial cultures resulted in reorganisation of the 2D structure into a 3D structure, resulting in the formation of capillary-like structures and increased expression of the BBB marker GLUT1. This shows that both cell types are required for BBB formation (Ramsauer *et al.*, 2002).

In the same study, it was shown that astrocytes induce morphological changes in the pericytes, which then allows the pericytes to stabilise the capillary-like structures, conferring resistance against apoptosis (Ramsauer et al., 2002). Similarly, Armulik et al. (2010) showed that pericyte-deficient mice had altered astrocytes, with altered polarisation of astrocyte end-feet shown by changes in Aquaporin4 (marker of astrocyte polarisation) expression at the astrocyte end-feet in the deficient mice.

This demonstrates that the cells of the NVU work together and cross-communicate to form, maintain and modulate the BBB. Consequently, deregulation of the NVU cells, such as in brain cancer, can have a severe impact on the BBB.

2.5 Cancer and the CNS

Brain cancers make up 2-3% of total cancers, however survival rates are lower than for non-CNS with medium survival without treatment being only 1-2 months, while treatment through surgery and radiation only increases this to 6 months after surgery (Martinez *et al.*, 2013).

Although metastatic brain tumours do occur, this is uncommon, with only 10-20% of all systemic malignancies eventually metastasising to the brain (Gerstner & Fine, 2007). This is largely due to the barrier nature of the BBB, where metastasising cells in the

blood stream must attach and invade the BBB before they can reach the brain (Arshad *et al.*, 2010, Martinez et al., 2013).

Most CNS cancers arise from CNS cells themselves, giving rise to primary tumours. The most common primary tumours are gliomas (tumours originating from glial cell) accounting for over 30% of all brain tumours and 80% of malignant tumours (Agnihotri *et al.*, 2013). Gliomas can further be subcatagorised depending on their cell of origin (if known), e.g. gliomas arising from astrocytes are astrocytomas, and oligodendrogliomas arise from oligodendrocytes.

Cancer stem cells can also arise from neural stem cells and like their non-cancerous counterparts are capable of giving rise into a variety of different cell types resulting in mixed tumour cell populations (Wen & Kesari, 2008).

Irrespective of origin, the common feature of all tumours is aberrant growth and proliferation of the tumour cells. However, such growth requires a good supply of nutrients and O_2. Small tumours (<1-2mm) can survive by passive diffusion of nutrients/ O_2 from the existing BBB. However, as the tumour grows beyond 2mm it outgrows its supply of nutrients and O_2 (Jain *et al.*, 2012). This leads to the development of a hypoxic environment within the tumour and surrounding tissue. This triggers the expression of Hypoxia-inducible factor 1-α (HIF-1α) which in turn promotes angiogenic pathways, such as the VEGF (Vascular endothelial growth factor*)* pathway (Figure 1.4) (Jain et al., 2012). Non-VEGF pathways also exist that help promote angiogenesis (growth factors, FGF (Fibroblast growth factors*)*, PDGF (Platelet-derived growth factor)). Such angiogenic factors and pathways lead to the tumour developing its own blood vessels and thus gaining its own nutrient supply. However, these blood vessels are quite immature and leaky (Gerstner & Fine, 2007, Jain et al., 2012) and are often referred to as the blood-tumour barrier (BTB), to indicate differences from the normal BBB.

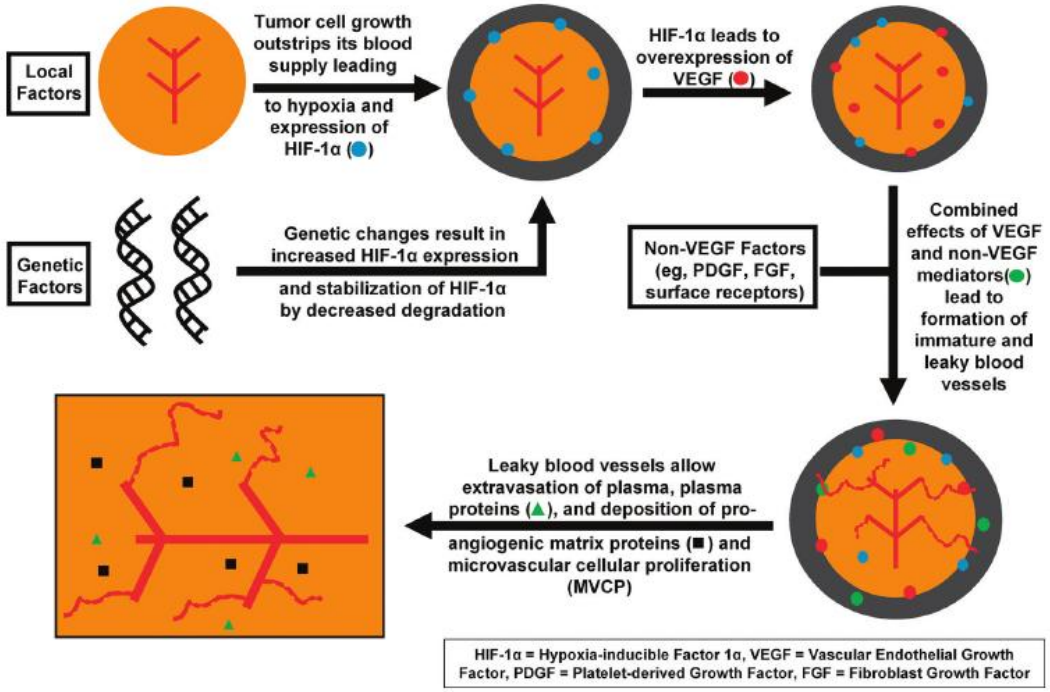

Figure 1.4 Tumour growth in angiogenesis in Glioma (Jain et al., 2012)

Tumour angiogenesis involves a multitude of controlled signaling cascades and structural changes

As the tumour continues to grow the tissue becomes hypervascularised to meet the nutrient /O_2 demands of the tumour's ever-increasing size. Thus one of the hallmarks of high grade tumours is the hypervascularisation, where the degree of vascularisation/endothelial proliferation helps categorise the tumours (Grier & Batchelor, 2006).

Together with the extent of endothelial proliferation, tumours are graded by four other histopathological characteristics associated with anaplasia, according to the WHO grading system. These are cellular density, nuclear atypia, mitosis and necrosis. Grades are given from I to IV, with IV being the most aggressive type of tumour. Grade I tumours are benign/non-malignant/non-cancerous tumours, that are slow-growing and resemble normal cells (Grier & Batchelor, 2006). Grade II tumours have some/moderate increase in cellular density with occasional nuclear atypia, with rare/absent mitotic activity and an absence of necrosis and endothelial proliferation. Grade III tumours have defined increases in cellular density with distinct nuclear atypia and marked mitotic activity, with an absence of necrosis and endothelial proliferation. Finally Grade IV tumours (e.g. glioblastomas) have all the features of Grade III tumours

together with high cellular density, necrosis and endothelial proliferation (Marquet *et al.*, 2007).

Survival times often correlate with tumour grades, with poor survival times for patients with high grade tumours (Agnihotri et al., 2013). This is because tumour growth can result in direct alterations to the brain and the brain microenvironment (e.g. through necrosis and hypoxia as detailed above), but also due to indirect effects. One crucial indirect effect is the alteration of the BBB by tumours, which leads to BBB dysfunction; a dysfunctional BBB can no longer maintain brain homeostasis leading to altered CNS microenvironment and changes in CNS activity (Deeken & Loscher, 2007).

2.6 Changes in the BBB in cancer challenge

2.6.1 The BBB and BTB in cancer

Several studies have examined the vasculature in and around tumours to assess the level of BTB and BBB breakdown.

In a study by Schlageter *et al.* (1999) several rat tumour models were used to identify differences between normal and tumour vessels. Tumour microvessels showed a tendency towards increased diameter and circumference with increases in intervessel distance from ~20 µm (normal) to > 50 µm (tumour). Tumour vessels also had increased capillary wall thickness and the presence of fenestrations, whereas normal vessels showed no fenestrations. There was also an increase in the number of interendothelial junctions and gaps.

Concerning transporters in tumour vessels, Guerin *et al.* (1992) using the rat 9L glioma model showed that GLUT1 coverage of vessels decreased from 100% (in normal) to 74% in tumour vessels (malignant glioblastoma). Hence decrease in GLUT1 positive density also occurs in tumour vessels, further distinguishing them from normal vessels.

Madden *et al.* (2004) harvested non-neoplastic and tumour-associated endothelial cells and conducted transcriptome analysis to identify differences in gene expression between the different endothelial cells. The results showed several genes to be induced (e.g. Endothelin receptor type B, HSPG2/Perlecan, RDC-1) or suppressed (1 NR4A1, Annexin A3 ANXA3, MT1A, HSP70, Syntaxin 7) in tumour vasculature when compared with non-neoplastic vessels (Table 1.4 and Table 1.5). This differential gene

expression between normal BBB and tumour BTB vessels, may be indicative of different BBB functional activity.

Table 1.4 Genes induced in tumour vasculature (Madden et al., 2004)

T/N	T/N prob.	SAGE tag	UG ID	UG description	Localization
17	95	GTCTCAGTGC	118893	Melanoma-associated gene MG50	Surface/secreted
14	90	CTTATGCTGC	82002	Endothelin receptor type B	Surface
13	99	CCACCCTCAC	211573	HSPG2 Perlecan	Extracellular
13	94	GTGCTACTTC	119129	Collagen, type IV, alpha 1	Extracellular
12	98	GAGTGAGACC	345643	Thy-1 cell surface antigen	Surface
10	94	ATGGCAACAG	149609	ITGA5 integrin alpha 5 (Fn receptor) receptor	Surface
9	91	TCACACAGTG	23016	G protein-coupled receptor RDC-1	Surface
8	100	GACCGCAGG	119129	Collagen, type IV, alpha 1	Extracellular
8	97	GGGAGGGGTG	2399	Matrix metalloproteinase 14 (membrane-inserted)	Extracellular
7	99	CCCTACCCTG	75736	Apolipoprotein D	Extracellular
8	97	TTCTCCCAAA	75617	Collagen, type IV, alpha 2	Extracellular
8	98	GGATGCGCAG	302741	Homo sapiens mRNA full length insert cDNA clone EU	
5	98	GTGCTAAGCG	159263	Collagen, type VI, alpha 2 Exon 1	Extracellular
4	93	CCCAGGACAC	110443	Homo sapiens cDNA: FLJ22215 fis, clone HRC01580	

Table 1.5 Genes suppressed in tumour vasculature (Madden et al., 2004)

Brain N/T	Brain N/T prob.	SAGE tag	UG ID	UG description	Localization
9	72	TAGTTGGAAA	1119	Nuclear receptor subfamily 4, group A, member 1 NR4A1	Nuclear membrane
9	72	AAGGGCGCGG	1378	Annexin A3 ANXA3	Membrane
9	72	AGCTGTGCCA	348254	Metallothionein 1A (functional) MT1A	Extracellular
7	60	ACAAAATCAA	110613	Nuclear pore complex interacting protein SMG-1	Membrane
6	68	GCCTGCAGTC	31439	Serine protease inhibitor, Kunitz type, 2 SPINT2	Extracellular
6	52	ACCAGGTCCA	5167 334549	Solute carrier family 5 (sodium-dependent vitamin)	Membrane
6	52	GGCTAATTAT	34114	ATPase, Na+/K+ transporting, alpha 2 (+)	Membrane
6	75	TTTAAATAGC	7934	KLF4 Kruppel-like factor 4 (gut)	Intracellular
5	81	CAGTTCATTA	326035	Early growth response 1 EGR1	Intracellular
5	61	CTGCCGTGAC	75462	BTG family, member 2 BTG2	Extracellular
5	65	TTTTAACTTA	160483	Erythrocyte membrane protein band 7.2 (stomatin)	Membrane
4	77	TAGAAACCGG	8997	Heat shock 70-kd protein 1A HSP70	Intracellular
4	77	CTTCTTGCC	272572 347939	Hemoglobin, alpha 2	Intracellular
4	53	TAGAAAAAAT	8906	Syntaxin 7	Surface

In a study by Shibata (1989), electron microscope imaging was used to compare glial, non-glial and metastatic brain vasculature from human brain tumours.

In glial tumours, capillaries had thickened walls and irregular cell junctions (that were short or elongate), with surface infolding of endothelial cells as well as increased numbers of pinocytic vesicles. There was also irregularity in basal lamina and the presence of a large extravascular space. However, although such changes were pronounced in malignant gliomas (high grade tumours), only slight changes were noted in benign astrocytomas (low grade tumours), which had normal capillary width, TJs, basal lamina, perivascular space and only moderate surface infolding and increase in pinocytic vesicles (Shibata, 1989).

Similarly, Larsson *et al.* (1990), used gadolinium-DTPA (a molecule normally BBB impermeable) to assess BBB permeability and showed that in low grade tumours the

BBB is largely intact. Grade II astrocytomas showed no or little gadolinium-DTPA permeability, with more permeability in Grade III astrocytoma, and Grade IV glioblastomas showing the highest permeability. This showed that BBB dysfunction correlates with tumour grade.

Interestingly these observations are in agreement with Schlageter et al. (1999), who showed that the increase in vessel size was greater in larger tumours than in smaller tumours.

Furthermore, Shibata 1989 showed that vessel alterations were more pronounced in the tumour centre than in the periphery of the tumour and even less so in the surrounding brain which appeared normal in most cases (Shibata, 1989). This demonstrated that blood vessels within a tumour (i.e. the BTB) are not only heterogeneous, but that they are more normal with increased distance from the tumour core. Consequently, the BBB surrounding tissue furthest from the tumour core is left intact is most cases. However, the fact that the surrounding brain was affected in some cases (Schlageter et al., 1999), does show that the tumour can influence the surrounding parenchyma although any effects should diminish with increased distance from the tumour.

The grade and proximity to tumour core are not the only factors that can affect the blood vessels. The origin of the tumour and its microenvironment have been shown to be important in the development of the tumour blood vessels (Hobbs *et al.*, 1998, Regina *et al.*, 2001).

Although there are many features in common among glial, non-glial and metastatic tumours, there are also clear differences.

In the Shibata (1989) study, non-glial tumour vessels showed increased surface infolding, increased vesicles and many fenestrations, with discontinuous TJs and irregular basal lamina. In metastatic tumours, endothelial cells were shown to be proliferating and had marked infolding with increased number of pinocytic vesicles and a high degree of fenestrations. However, tumours of glial origin showed no endothelial fenestration, irrespective of grade. This links tumour origin to tumour vasculature, with the vasculature of non-glial tumours more like the vasculature found in the tissue of origin (Regina et al., 2001).

The tissue/cell of origin is not the only determinant in the development of tumour vasculature. Hobbs et al. (1998), showed that the microenvironment of the tumours is

important to vascularisation. In this study, mice were implanted with the same tumour type but in different locations; the results showed that cranial tumours grew twice as fast as subcutaneous tumours. Furthermore the cranial tumour vasculature had smaller transvascular gaps between endothelial cells. This suggests that the cranial microenvironment favours tumour growth and also alters the phenotype to become more like of that of the CNS vasculature.

Factors such as tumour grade, origin and microenvironment result in the high heterogeneity of tumour vasculature and therefore make targeting brain tumours difficult, since it is unclear whether the BTB and the surrounding BBB are intact.

Chemotherapy is becoming increasingly important in glioma treatment since traditional brain tumour treatments (involving radiotherapy and/or surgery), do not guarantee complete removal of cancerous cells, often resulting in reoccurrence (Wen & Kesari, 2008). However, if the BTB and BBB are intact, this becomes a problem for chemotherapeutic treatment of brain tumours since many chemotherapeutics cannot cross the BBB under normal circumstances, largely due to the presence of ABC efflux transporter (see Section 1.5.). Although in later stages of cancer the BTB and surrounding BBB are more permeable to drugs, there are other problems by this stage such as oedema and high levels of necrosis (Dinda *et al.*, 1993). Furthermore, cancer stem cells may also exist within tumours, which have been shown to confer resistance of malignant tumours to chemotherapy, making treatment of such tumours even more difficult (Wen & Kesari, 2008, Agarwal *et al.*, 2011).

It should also be mentioned that in CNS-cancer (including late stage cancer) not all cancer cells are always in the form of tumours, as some of the cancer cells may have migrated away from the site of origin (Agarwal et al., 2011). Therefore, even if every cancer cell of the original tumour is surgically removed or irradiated, the undetected and untreated invasive cancer cells are left behind which can grow into a new tumour (Agarwal et al., 2011).

These invasive cells fall into the ‘small tumour’ category (<2mm) and so do not require their own nutrients/O_2 supply and therefore do not have their own BTB (Agarwal et al., 2011, Jain et al., 2012). This means they are situated within an area with intact BBB that is not readily permeable to chemotherapeutics (see Figure 1.5) (Agarwal et al., 2011).

It is clear that considerable research is needed to enhance the effectiveness of CNS chemotherapeutics.

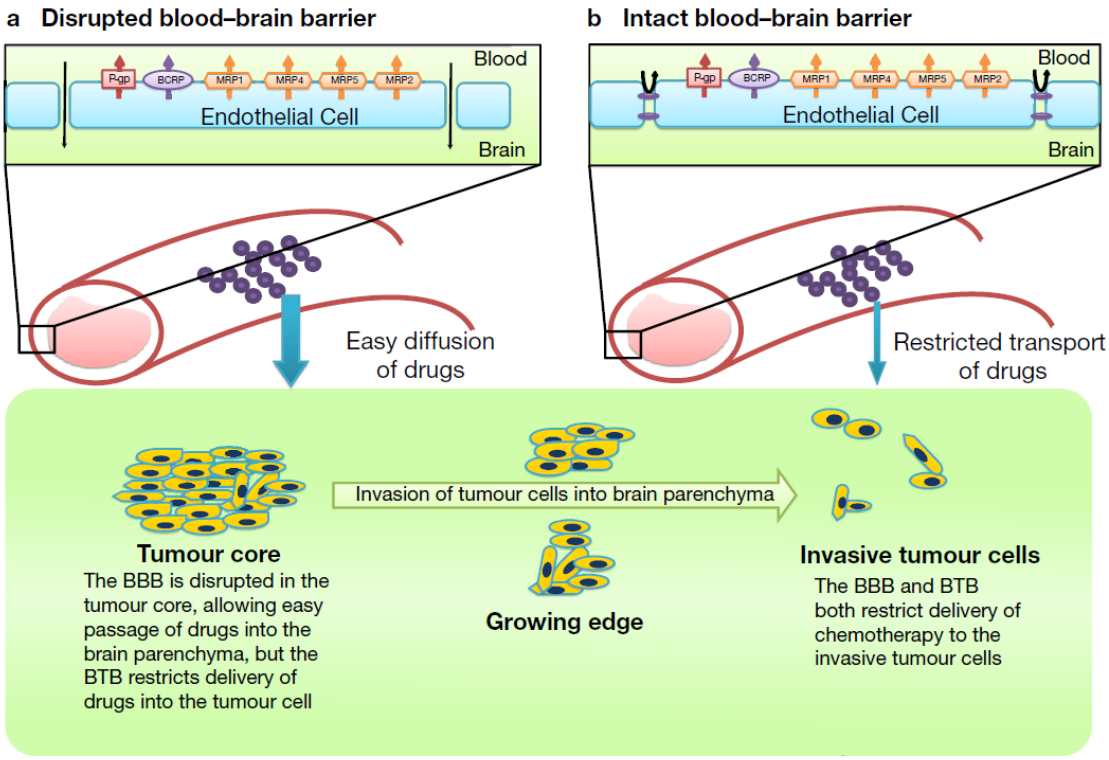

Figure 1.5 Multiple mechanisms and barriers that limit drug delivery to glioma (Agarwal et al., 2011)

The blood–brain barrier (BBB) and the blood–tumour-cell barrier (BTB) form barriers that a systemically administered drug must cross to reach the tumour. The centre of the figure shows the invasion of glioma cells from the tumour core into the normal brain parenchyma. Above this, parts a and b show how the integrity of the BBB affects drug delivery in these different locations (a) The BBB is often disrupted at the site of the tumour, with the lack of TJs allowing for easy diffusion of drugs and small molecules into the tumour. However, this is also the part of the tumour that gets removed after surgery. (b) The BBB is intact in areas centimeters away from the tumour core. Drug delivery across this barrier is restricted by the presence of TJs between endothelial cells and more importantly by drug efflux transporters that pump drugs back into the blood. The amount of drug that is able to cross this barrier and reach the brain is usually a fraction of what reaches the tumour core. Nests of tumour cells in such locations protected by the intact BBB eventually give rise to the recurrent tumour after surgery.

2.6.2 Efflux transporters at the BBB in CNS cancer

As mentioned previously, one of the major reasons that chemotherapeutics cannot cross the BBB is the presence of BBB ABC efflux transporters, where many

chemotherapeutics have been shown to be substrates for one and usually more than one efflux transporter (Matsson et al., 2009).

In spite of this, relatively little research has been focused on understanding the efflux transporters of the BBB during cancer challenge. Although some studies have examined alterations in the ABCs during cancer challenge, there are many discrepancies between studies.

As with the morphological changes in the BBB (detailed previously) the expression of the efflux transporters in the vasculature has also been shown to be dependent on the tumour origin (Deeken & Loscher, 2007).

Metastatic tumours in the brain

In one histological study examining 137 metastatic tumour samples (breast, lung and prostate carcinomas) none of the tumour capillaries of these samples were found to be positive for Pgp expression. Conversely, 86% of the glioma tumour vessels showed positive Pgp staining, while normal brain vessels showed 100% Pgp positive staining (Toth *et al.*, 1996). However, other studies showed different results. Regina et al. (2001) showed that in lung carcinoma brain metastases, the capillaries did possess Pgp, but that this was only 40% of the level of normal brain vessels. Similarly, melanoma metastases tumour vasculature possessed diminished Pgp level, with only 5% that of normal brain vessels.

Regina et al. (2001), suggested that the Pgp levels were linked to the tissue of origin, with Pgp levels of the original tissue influencing levels of Pgp expressed in the newly formed blood vessels. This may explain why glial tumours maintain BBB phenotypes (i.e. the same level of Pgp as normal brain vasculature) in some cases (Toth et al., 1996).

Non-glial tumours in the brain

Non-metastatic, primary non-glial tumours (e.g. meningiomas originating from the meninges) have also been compared with glial tumours, showing similar results to the metastatic tumours.

In an immunohistological study on microvessels of 22 primary CNS lymphoma and 30 glioma samples, decreases in both Pgp and BCRP were detected in 63% and 93% of the lymphoma areas tested, respectively, with BCRP undetectable in 50% of subjects. Conversely, most gliomas were found to express Pgp and BCRP at similar levels as

normal brain vessels although decreases in Pgp and BCRP were noted in higher grade tumours, especially in proliferating endothelia and around necrotic foci (Sakata *et al.*, 2011). Interestingly, the decrease in the transporter expression of lymphoma vessels was more prominent in areas of dense and perivascular tumour cell infiltration compared to sparse areas of infiltration. This suggests that alterations to efflux transporter expression are more pronounced nearer the tumour core, similar to other morphological changes that occur during cancer challenge at the BBB (see section 1.8.1).

For MRPs, no MRP1-positive vessels were detected in either lymphoma or glioma vessels (Sakata et al., 2011). This agrees with a study by Cooray *et al.* (2002) examining the vasculature in normal tissue, tumours of glial origin and tumour meningiomas, finding no MRP1, 3 or 5 detected in any of the tumour types tested. However, Cooray et al. (2002) did find BCRP to be present luminally in all cases. However, the levels of expression were not quantified here so cannot be compared to those of Sakata et al. (2011).

When intracranial ependymal tumours and spinal tumours were examined by Ginguene *et al.* (2010), Pgp and BCRP were both shown to be present luminally on tumour vessels. In both tumour types, the tumour microvessels showed heterogeneous Pgp labelling (weak and strong), while BCRP showed consistently strong labelling (Ginguene et al., 2010). This is in keeping with the results of Regina et al. (2001) in metastatic tumours, which together suggest that Pgp levels in the vasculature of tumours from metastatic and non-glial origins tend to have weaker/more heterogeneous Pgp expression than normal brain or glial tumours. By contrast BCRP expression appears to remain strong irrespective of tumour type (Ginguene et al., 2010).

Although metastatic and non-glial brain tumours appears to have lower levels of Pgp, Allen *et al.* (2000) showed that even low levels of Pgp and MRPs can still significantly deter drug passage. Hence, although levels of Pgp in some tumours may be low, they may still pose a problem for chemotherapy delivery.

Chemotherapeutic challenges would also exist (perhaps to an even greater extent) for glial tumours with fully expressed ABC transporters in their vessels. However, some studies suggest that even glial tumours are susceptible to changes in ABC transporters (e.g. loss in Pgp).

Glial tumours

Concerning Pgp expression in the microvessels of gliomas, Toth et al. (1996) found that Pgp expression was lower in glioma than in normal vasculature (86% in tumour compared with 100% Pgp in normal brain). Interestingly, there was no difference in the relative staining intensity of Pgp in endothelial cells of normal brain versus tumour periphery, however the most central regions of tumours were unreactive for Pgp. Conversely, Toth et al. (1996) did show that the areas surrounding the brain tumours maintained an intact BBB in terms of Pgp expression. This shows that like other morphological features of the BTB/BBB (see section 1.8.1), the degree of Pgp expression varies with distance from the tumour core (inversely correlated).

Furthermore, Toth et al. (1996), showed that in Grade I and II tumours Pgp staining was just as strong as normal brain, while Grade IV glioblastoma vessels showed more heterogeneous staining, with both weak and strong Pgp staining observed and with 4 of the 18 samples tested being completely negative.

Sawada *et al.* (1999) also showed a trend towards decreased Pgp expression in tumour microvasculature with tumour grade, finding weaker Pgp staining in new tumour blood vessels compared to normal cerebral blood vessels (although Pgp was shown to retain luminally expression). An inverse correlation between Pgp expression and the proliferation of endothelial cells was noted, with proliferating cells shown to be functionally immature (Sawada et al., 1999). This suggests that in proliferating cells Pgp expression is reduced.

By contrast, some studies have shown increased levels of Pgp with tumour grade. Nabors *et al.* (1991), showed Pgp-positive tumour vessels only in high grade tumours and not in low grade tumours. Tews *et al.* (2000), showed Pgp in tumour glioblastoma vessels with strong Pgp expression in both non-neoplastic and tumour tissue (i.e. no diminution in Pgp expression in high grade tumours).

Concerning expression of the other ABC transporters, Zhang et al. (2003) compared non-malignant tumours to glioblastoma to determine the relative mRNA expression levels of BCRP, MRP1 and Pgp (using laser capture microscopy to isolate tumours vessels for QPCR). The vessels were shown to have similar levels of BCRP and PGP mRNA, but the highest levels of mRNA were found to be for MRP1 (8 fold greater than the other two transporters). The results also showed significantly higher BCRP mRNA in glioblastoma vessels compared to non-malignant vessels, while MRP1 decreased in glioblastoma.

Calatozzolo *et al.* (2005), showed that in endothelial cells of gliomas MRP1, 3 and 5 and Pgp were expressed both at the mRNA and protein levels, with the highest mRNA levels found to be for MRP1.

By contrast, Tews et al. (2000) found no MRP1 in tumour glioblastoma vessels and no MRP1 was detected by the Sakata et al. (2011) study in glioma vessels.

The differences reported may be due to lack of correlation between mRNA and protein expression, where mRNA translation into protein may be prevented, resulting in little low or no protein expression.

Bronger *et al.* (2005) used PCR and immunostaining methods in combination to show the presence of MRP4 and MRP5 expression at both mRNA and protein level in glioma vasculature. However, no MRP2 and MRP3 could be detected in tumour vasculature at either the protein or mRNA level. Interestingly, although MRP6 mRNA could be detected, no detectable MRP 6 protein was observed. This shows that discrepancies between mRNA and protein levels of the MRP proteins can occur.

Bronger et al. (2005) showed MRP4 and MRP5 proteins to be luminally expressed with the proteins showing positive staining in 87% and 86% of the tumour capillaries tested, respectively. Staining was weak/low, but consistent expression was observed across Grade II to Grade IV glioma. So unlike some Pgp studies, MRP4 and MRP5 expression in tumour endothelial does not appear to correlate with tumour grade. However this is only one study and is therefore not conclusive.

Interestingly, the capillaries that failed to stain in the Bronger et al. (2005) study were shown to be proliferating, linking the proliferative state of the blood vessels to poor expression of MRPs. This agrees with the earlier observations concerning Pgp, indicating that proliferation in endothelial cells of tumour microvessels results in decreased expression of multiple efflux transporters.

The appearance of MRPs is interesting, since there is still controversy as to whether these are expressed in normal tissue. Regina *et al.* (1998), suggested that in normal brain, astrocytes act to suppress MRP1. However, MRP1 expression has been shown present in normal brain endothelial microvessels as has MRP4 (See section on MRPs).

Concerning BCRP, Bronger et al. (2005) showed that BCRP is expressed at both the mRNA and the protein levels (luminally) in tumour vessels.

Sakata et al. (2011) found BCRP to behave like Pgp, where in low grade gliomas all samples showed strong BCRP and Pgp staining of capillaries (stronger than normal brain), while in high grade gliomas (28 samples) only 77% showed strong BCRP and Pgp staining, with the rest showing weaker staining relative to normal brain. This suggests that both Pgp and BCRP may first increase in low grade tumours (showing stronger expression than normal brain vessels), but then decrease in higher grade tumours (showing weaker expression than normal brain vessels).

In summary, the data concerning efflux transporter expression is inconclusive with differences in protein expression being shown by different studies. Furthermore there is a lack of correlation between mRNA levels and protein expression, not only between different studies, but within the same study, that also complicates the matter. In addition, there are no studies comparing protein expression with the transporter function and so no indication as to whether increases/decreases in protein levels actually lead to altered ABC transporter activity.

Some clear patterns concerning tumour vasculature are beginning to emerge (e.g. link between ABC transporter expression and the proliferative state of capillaries), but more research is needed. Furthermore, the surrounding tumour tissue (with an established/mature BBB) is rarely investigated, so there is no real knowledge of how the established BBB efflux transporters are affected by tumours. Clearly more work needs to be done to investigate this.

2.7 Aims and Objectives

The aim of the project was to better understand how the BBB reacts to the presence of glioma cells. It was aimed to identify any differences in ABC transporter activity/expression in normal BBB and glioma BBB as well as identifying possible factors responsible for any differences.

Towards this aim the following objectives were defined:

a) To identify and characterise an appropriate model for the ‘normal’ BBB that could be used as a reference control for a glioma BBB model consisting of endothelial cells co-cultured with glioma cells.

b) To compare the ABC transporter activity/expression in endothelial cells co-cultured with glioma cells with the normal reference control, to determine any changes in ABC transporters induced by the glioma cells.
c) To assess possible glioma factors involved in altering ABC transporter activity/expression within endothelial cells.
d) To determine any changes in ABC transporter expression in human brains in response glioma challenge using confocal microscopy on human tissue from control and glioma brains.
e) To correlate *in vitro* results concerning ABC transporter changes with the expression changes in human brains to identify any common effects on ABC transporters in the BBB as a results of glioma challenge.

3 Materials and Methods

All chemicals were purchased from Sigma unless otherwise stated.

3.1 Coating plastics for cell culture

For cell culture involving porcine brain endothelial cells (PBECs), plastics required pre-coating with fibrous proteins. Plastics were coated with rat tail collagen (0.33 $mg.ml^{-1}$, isolated in accordance with Strom and Michalopoulos (1982)). For T-75 flasks, 4ml of collagen was used and the collagen was left on the flasks for 2 hours at room temperature. The collagen was then removed and the flasks were washed twice with equal volumes (i.e. 4 ml) of Hanks' Balanced Salt Solution (HBSS). Then 4 ml of 7.5 $\mu g.ml^{-1}$ fibronectin was added to the flask and the flask was incubated for 2 hours at room temperature. The flasks were then washed with HBSS (as above), before the addition of porcine brain capillaries (see section 2.4).

Transwell inserts (polycarbonate, 0.45 µm pore, Corning) were similarly coated using 500µl of collagen for each 12-Well Transwell and 1.5 ml for each 6-Well Transwell (for 2 hours), followed by 500µl of fibronectin for each 12-Well Transwell and 1.5 ml for each 6-Well Transwell (for 2 hours).

For 96 and 24 well plates, these were coated with collagen only using 200µl and 500µl of collagen per well, respectively, with the collagen left on the plates for 2 hours at room temperature.

For rat astrocyte cell culture, plastics were coated with 10 $\mu g.ml^{-1}$ poly-L-Lysine for 1 hour at 37˚C, 5% CO_2 in air, using the same volumes as for the collagen. The coating was then removed and the plastics allowed to dry before the addition of cells.

For human astrocyte cell culture, plastics were coated with 15 $\mu g.ml^{-1}$ poly-L-Lysine , using the same volumes as for the collagen. Coating occurred for 24 hours at 37˚C, 5% CO_2 in air, followed by washing twice with dH_20 before the addition of cells.

3.2 Isolation of porcine brain microvessels

To obtain PBECs, the culture begins with 3 porcine brains (from Cheale Meats Ltd abattoir, immediately dispatched after euthanisation), and generates 6 cryovials (3 vials of PBEC 60s and 3 vials of PBEC 150s) (see terminology below). One vial yields 10 - 15 12-well Transwell inserts ($1x10^5$ cells per Transwell).

PBECs isolation was in accordance with Patabendige *et al.* (2013). The brains were removed from the skulls, cut into hemispheres and placed on ice in Iscove's Dulbecco's Modified Eagle's medium (DMEM) medium with 100 $\mu g \cdot ml^{-1}$ penicillin and 100 $U \cdot ml^{-1}$ streptomycin. From each hemisphere only the cortex was used for PBEC isolation, with the rest of the brain matter discarded (i.e. the cerebellum, diencephalon and brain stem were removed). The meninges and white matter were removed from the cortices using surgical instruments, to give clean cortices. The clean cortices from all 3 brains were pooled together and then passed through a 50 ml syringe into a solution of Eagle's Minimum Essential Medium (MEM), with 25 mM hydroxyethyl piperazine-ethanesulfonic acid (HEPES) containing 10% fetal calf serum (FCS), 100 $\mu g \cdot ml^{-1}$ penicillin and 100 $U \cdot ml^{-1}$ streptomycin. The cortical matter was then homogenised 30 times (15 times with a loose pestle followed by 15 times with a tight pestle) (Dounce 40 ml Homogeniser). The homogenate was divided into 3 sections (1 section per porcine brain used) and was filtered through nylon meshes. Each section was filtered through its own set of 2 meshes.

Firstly, a 150 µm mesh was used, with the microvessel fragments, large capillaries of sizes greater than 150 µm becoming trapped on the mesh, while capillary fragments smaller than 150 µm pass through the mesh and into the filtrate. Secondly, the filtrate was re-filtered through a 60 µm mesh, where the enriched capillary fragments greater than 60 µm (but smaller 150 µm since they had already been filtered through the 150 µm mesh) were retained on the 60 µm mesh. The capillaries on the 150 µm mesh were then used to generate PBEC '150s', while the capillaries on the 60 µm were used to generate PBEC '60s' and were therefore kept separate from this point onwards.

In total, 3 meshes of 60 µm and 3 meshes of 150 µm were generated, one of each kind from each section filtered. The meshes containing the capillaries were then incubated with a digest mix (composed of M199 medium containing 10% FCS, 100 $\mu g \cdot ml^{-1}$ penicillin, 100 $U \cdot ml^{-1}$ streptomycin, 210 $U \cdot ml^{-1}$ collagenase type III (VWR International), 90 $U \cdot ml^{-1}$ Trypsin (VWR International), 115 $U \cdot ml^{-1}$ DNase I (VWR International) for 1

hour at 37˚C, 5% CO_2 in air. All 3 meshes of 150s were digested together separate from the 60s meshes and *vice versa*.

The digest mixes containing the digested capillaries of either 150s or 60s, were then centrifuged at 105 x g for 5 minutes at 4˚C. The pellets containing the capillaries were then washed twice, by firstly resuspending the capillary pellet in MEM medium and then by centrifugation at 105 x g for 5 minutes at 4˚C. The washed pellets were then each resuspended in 3 ml freezing medium (10% dimethyl sulfoxide (DMSO) in FCS), and aliquoted into cryovials as 1 ml aliquot of PBECs. The 3 PBEC 150s and 3 PBECs 60s cryovials were then placed at -80˚C in a Mr. Frosty container for 24 hours and then moved to liquid nitrogen for long-term storage.

3.3 Primary rat astrocyte isolation

To obtain primary rat astrocytes, the culture begins with 6-10 rat pups (postnatal 0-2 days, Sprague-Dawley) and produces 6-12 cryovials (~800,000 cells/vial, passage 1 (p1))

Rat cortical astrocytes were prepared according to Rist *et al.* (1997).

Animals were killed by neck dislocation and decapitated. The skin of the head was incised longitudinally using a scalpel and the bone was then cut and removed. The brain was eased out of the skull and placed in Dissection Buffer (HBSS without Ca^{+}, Mg^{+}, with 10 mM HEPES, 100 $U{\cdot}ml^{-1}$ penicillin and 100 $\mu g{\cdot}ml^{-1}$ streptomycin). The cortex was isolated and the remaining brain matter was removed. The meninges were removed and the brains placed back into Dissection Buffer (~12.5 ml) and cut into pieces using a scalpel. This cortical matter was then mixed with 1.25 $mg{\cdot}ml^{-1}$ trypsin in a 50:50 ratio, and was digested for 30 minutes at 37°C. After digestion, 10 ml of Rat Astrocyte Medium A was added (DMEM containing 4.5 $g{\cdot}L^{-1}$ glucose and 2 mM L-alanyl glutamate (Glutamax), 10% fetal calf serum, 100 $U{\cdot}ml^{-1}$ penicillin, 100 $\mu g{\cdot}ml^{-1}$ streptomycin). The suspension was centrifuged at 360 x g and the pellet was suspended in 5 ml of medium and triturated with a fine–bore polished pipette. The suspension was centrifuged as before and the supernatant was filtered using a 73.5 μm mesh tissue sieve and the filtrate was plated into flasks (pre-coated with poly-L-lysine).

Cells were isolated by Siti Yusof (BBB group Kings College London, 2008/9).

Medium was changed one day after the preparation and then every three days until cells were confluent (~7 days). On day 14–16 after plating, the medium was changed to Rat Astrocyte Medium A containing 10 μM cytosine arabinoside (to eliminate dividing cells). At this stage, the astrocytes were confluent, and the contaminating cells, which are not contact-inhibited, are susceptible to cytosine arabinoside. The flasks were shaken at 37°C for 24 hours to dislodge contaminating cell types and the medium was changed to remove the dislodged cells. This procedure was repeated for five days in total. The cells were then allowed to reach confluence. The cells were then trypsinised by washing the cells twice with HBSS without Ca^{2+} or Mg^{2+}, before incubation with X1 Trypsin/EDTA for 1-3 minutes at 37°C, 5% CO_2 . The trypsin was then quenched with medium and the cells were centrifuged at 360 X g for 5 minutes and the spent medium/ trypsin was discarded. The cells were resuspended in Freezing Medium and aliquoted into 1 ml aliquots (of ~800,000 cells). The cells were placed at -80˚C in a Mr. Frosty container for 24 hours and then moved to liquid nitrogen for long-term storage.

3.4 Cell Culture

Cells were kept at 37˚C, 5% CO_2 in air unless stated otherwise.

3.4.1 Culture of primary porcine brain endothelial cells (PBECs)

Porcine brain microvessels were defrosted and grown in collagen and fibronectin coated T-75 flasks, in PBEC Medium (DMEM containing 1 $g.L^{-1}$, 100 $\mu g \cdot ml^{-1}$ penicillin, 100$U \cdot ml^{-1}$ streptomycin, 125 $\mu g \cdot ml^{-1}$ heparin, 2 mM L-glutamine and 10% Bovine Plasma Derived Serum (BPDS) (First Link UK)) and 4 $\mu g \cdot ml^{-1}$ of puromycin. Puromycin is a toxin that is also a substrate of P-glycoprotein (Pgp) and so selectively eliminates any cells that do not express Pgp at sufficiently high levels to exclude the puromycin (such as pericytes, which are the major contaminant of the preparation), without affecting the endothelial cells which do express Pgp at sufficiently high levels.

The microvessels were kept at 37°C, 5% CO_2 and endothelial cells were seen to grow out of the microvessels. These porcine brain endothelial cells (PBECs) were passaged when ~ 50% confluent (usually within 3 days). If the cells did not reach 50% confluence

within 3 days, the cells were fed on Day 3 with fresh PBEC Medium (without puromycin, since contaminants would have already been eliminated by this stage), and allowed to grow further at 37°C, 5% CO_2 until 50% confluence was reached (in another 2-3 days).

The cells were then washed twice with HBSS without Ca^{2+} or Mg^{2+}, before being incubated with X1 Trypsin/EDTA for 8-15 minutes at 37°C, 5% CO_2 which allowed the cells to become detached from the flask. The trypsin was quenched with PBEC medium and the cells were centrifuged at 360 X g for 5 minutes, and the spent medium/trypsin was discarded. The cells were resuspended and seeded into the plates/Transwells at a density of 100,000 cells/cm^2.

PBECs were passaged to either 96-Well or 24-Well plates pre-coated with collagen or onto 12-Well or 6-Well polycarbonate Transwells (0.45 µm pore, Corning) that had been pre-coated with collagen and fibronectin.

PBECs in plates

For PBECs in plates (PBECs-P), PBEC-60s were left at 37°C, 5% CO_2 for 2-3 days to reach confluence. The cells were either immediately assayed after confluence was reached or fed with fresh medium and left at 37°C, 5% CO_2 for another 1-3 days until the cells were used.

PBECs in mono-culture or in co-culture with human astrocytes or G7 glioma cells

For mono-cultured PBECs (PBECs-M), PBECs in co-culture with human astrocytes (PBECs-hAS) and PBECs in co-culture with G7 glioma cells (PBECs-G7), PBECs-60s were passaged into PBEC Medium and placed in Transwell inserts pre-coated with collagen/fibronectin. The Transwell inserts were then placed above an empty well containing PBEC Medium and grown to confluence, which occurred in 3 days.

For PBECs-M, on the fourth day after passaging the medium was changed to PBEC Serum Free Medium (DMEM containing 1 $g{\cdot}L^{-1}$ glucose, 100 $\mu g{\cdot}ml^{-1}$ penicillin, 100 $U{\cdot}ml^{-1}$ streptomycin, 125 $\mu g{\cdot}ml^{-1}$ heparin, 2 mM L-glutamine, 550 nM hydrocortisone) containing 250 µM CPT-cAMP and 17.5 µM RO-20-1724 (CalbioChem) both apically and basally, and 24 hours later the cells were assayed (see assay sections).

For PBECs-hAS and PBECs-G7, on day 4 after passaging the medium on the apical chamber was changed to PBEC Serum Free Medium containing 250 µM cAMP and 17.5 µM RO-20-1724 and the Transwell insert was placed above a well containing either human or G7 Cells at ~50% confluence in Neural Stem Cell Medium composed of DMEM/F-12 Medium (1:1 mix) with 365 $mg \cdot L^{-1}$ L-glutamine and additionally containing 29 mM Glucose, X1 non-essential amino acids (NEAAs) (PAA, GE healthcare), X1 Penicillin/Streptomycin (PAA, GE healthcare, 10 mM HEPES, 0.012% BSA, 0.1% β-mercaptoethanol, X0.5 B27 supplement (PAA, GE healthcare) and X0.5 N2 supplement (PAA, GE healthcare), 1 $\mu g \cdot ml^{-1}$ laminin, 10 $ng \cdot ml^{-1}$ Mouse EGF and 10 $ng \cdot ml^{-1}$ basic human FGF. The TEER was monitored once a day for 48 hours and after 48 hours the PBECs were ready to be assayed.

Alternatively, for PBECs-G7, PBECs-60s were passaged to a Transwell insert (in PBECs medium) which was immediately placed above ~50% confluent G7 cells (in Neural Stem Cell Medium). After 4 hours the PBECs were moved to a new well of ~50% confluent G7 cells (in Neural Stem Cell Medium), then moved again every 12 hours for a total of 4 days. On the fourth day after passaging, the medium on the PBECs was changed to PBEC Serum Free Medium with 250 µM CPT-cAMP and 17.5 µM RO-20-1724, and the cells were left in co-culture with G7s (in Neural Stem Cell Medium) for a further 24 hours before use.

PBECs in co-culture with normal rat astrocytes or C6 glioma cells

For PBECs in co-culture with primary rat astrocytes (PBECs-rAS) or C6 glioma cells (PBECs-C6), PBEC-60s were passaged into PBEC Medium and placed in Transwells and immediately placed above confluent normal rat astrocytes or C6 glioma cells in Rat Astrocyte Medium B (DMEM containing 4.5 $g \cdot L^{-1}$ glucose, 10% fetal calf serum, 100 $U \cdot ml^{-1}$ penicillin, 100 $\mu g \cdot ml^{-1}$ streptomycin). The cells were grown in co-culture for 3 days, and then on the fourth day after passaging, the medium was changed to PBEC Serum Free Medium, both apically and basally, for 24 hours. The PBECs were then ready for use.

PBECs in conditioned medium

For PBECs grown in conditioned medium, the PBECs-150s were passaged into 50% Conditioned Medium (consisting on a 1:1 mix of PBEC Medium and Conditioned

Medium) and seeded into plates coated with collagen. The medium was changed in 2 days to fresh 50% Conditioned Medium with or without a drug treatment. The cells were then left for 2 days before being assayed. For further details regarding conditioned medium (i.e. type and composition) see section 2.4.6.

3.4.2 Primary rat astrocyte cell culture

Primary rat astrocytes were grown in Rat Astrocyte Medium B (DMEM containing 4.5 $g \cdot L^{-1}$ glucose, 10% fetal calf serum, 100 $U \cdot ml^{-1}$ penicillin and 100 $\mu g \cdot ml^{-1}$ streptomycin) with medium changed every 3 days.

For PBEC co-culture experiments, primary rat astrocytes were defrosted 4 days before co-culturing with PBECs. The astrocytes (p1) were defrosted in Astrocyte Medium B and seeded into 12-Well or 6-Well plates (pre-coated with poly-L-lysine) at a seeding density of 1.75 x 10^4 cells/cm^2. The medium was changed 3 hours after defrosting (to remove DMSO from within the freezing medium of the cells) and again 3 days after confluence, (1 day before the start of co-culture).

Twenty-four hours later, PBECs were placed in co-culture with the confluent astrocytes, by placing a Transwell insert containing the PBECs above the well in which the astrocytes were grown.

On the fourth day of co-culture, the medium on both the PBECs and astrocytes was changed to PBEC Serum Free Medium (DMEM containing 1 $g \cdot L^{-1}$ glucose, 100 $\mu g \cdot ml^{-1}$ penicillin, 100 $U \cdot ml^{-1}$ streptomycin, 125 $\mu g \cdot ml^{-1}$ heparin, 2 mM L-glutamine, 550 nM hydrocortisone) containing 250 µM CPT-cAMP and 17.5 µM RO-20-1724 (CalbioChem). The PBECs were ready for use 24 hours later and the astrocytes were discarded.

3.4.3 Human astrocyte cell culture

Human astrocytes were purchased from Science Cell Research Laboratories at (p1) and grown in Human Astrocyte Medium (Science Cell Research Laboratories) until passage 3.

For PBEC co-culture, human astrocytes (p3) were defrosted into Human Astrocyte Medium and seeded directly into plates (coated with poly-l-lysine) at a density of 3.2 x 10^4/cm^2. The next day the medium was changed to Neural Stem Cell Medium, 24 hours later (2 days before the start of the co-culture).

Two days later confluent PBECs were placed above the human astrocytes, when human astrocytes were ~50% confluent. The co-culture was maintained for 48 hours and then the PBECs were removed for further experiments and the astrocytes were discarded.

3.4.4 C6 glioma cell culture

C6 were received as a gift from the late Irving Fritz (Babraham Institute, Cambridge). For PBEC co-culture experiments, C6 glioma cells (p129-133) were defrosted 3 days before co-culturing with PBECs. The C6s were defrosted into Rat Astrocyte Medium B and seeded into plates at a density of 2.20 x 10^4 cells/cm^2. The medium was changed 1 hour after defrosting and then again 2 days later when the C6s were confluent (1 day before co-culturing with PBECs began).

The PBECs were then placed above the C6s 24 hours later to begin the co-culturing process.

Two days after the start of co-culture the media on the PBECs and C6 was changed to fresh media in all cases except for some RNA studies, see Results sections.

On the fourth day of co-culture the medium on both the PBECs and C6s was changed to PBEC Serum Free Medium, containing CPT-cAMP and Ro-20-1724. The PBECs were ready for use 24 hours later and the C6s were discarded.

3.4.5 Primary G7 glioma cell culture

Human primary cell lines used in this study were obtained from Steven Pollard (UCL) in accordance to UK regulations and following approval from the local and ethical review board (Lothian Regulatory Ethics Committee; Ref LREC/2002/6/15). Tissue was donated using written informed consent from patients or next of kin for tumour biopsies and foetal tissue, respectively.

G7 cells (p26-29) were obtained from the Cancer Institute (UCL). G7s are glioma cells isolated from a glioblastoma multiform patients and have tested positive for stem cell markers. G7 cells were obtained directly on plates at ~30% confluence in Neural Stem Cell Medium. The medium was changed 24 hours later to fresh Neural Stem Cell Medium (2 days before the start of the PBEC co-culture).

Two days later confluent PBECs (in PBEC Serum-Free Medium with 250 µM CPT-cAMP and 17.5 µM RO-20-1724) were placed above the G7 glioblastoma cells, which were at ~50% confluence. The co-culture was maintained for 48 hours and then the PBECs were removed for further experiments and the G7 were discarded.

Alternatively, non-confluent PBECs (in PBEC Medium) were placed above ~50% confluent G7s for 4 hours. The PBECs were then moved to new G7s (~50% confluence) and then moved again every 12 hours for a total of 3 days. On the fourth day the medium on the PBECs was changed to PBEC Serum Free Medium with 250 µM CPT-cAMP and 17.5 µM RO-20-1724 and the PBECs were placed above new G7s for a final 24 hours.

3.4.6 Collection of conditioned medium

For collection/production of primary rat astrocyte-conditioned medium, cells were defrosted into Rat Astrocyte Medium B and placed in a T-75 flask (pre-coated with poly-L-lysine) at a density of 800,000 cells per flask. The medium was changed 3 hours later and then every 3 days until cells were confluent (~7-9 days).

When the astrocytes became confluent, 10 ml of fresh medium was placed on the cells and left for 48 hours. Two different media were used, Rat Astrocyte Medium B or Serum Free PBEC medium.

The medium was collected 48 hours later and stored at -80˚C as Rat Astrocyte Conditioned Medium. Fresh medium was then placed on the cells and the collection process was repeated.

For collection/production of C6 glioma conditioned medium, cells were defrosted into Rat Astrocyte Medium B and placed in a T-75 flask at a density of 1,000,000 cells per

flask. The medium was changed 1 hour later and then every 2 days until cells were confluent (~4-5 days).

When the C6s were confluent, the cells were treated the same as the astrocytes (detailed above) to produce C6-conditioned medium.

Conditioned Neural Stem Cell Media from normal glial cells (Cb660s) and glioma cells (G7s, G15s and G26s), were obtained from the Institute of Cancer Research (UCL) (with all cells positive for stem cell markers). The media consisted of Neural Stem Cell Medium that had been placed on cells (at 40-60% confluence) for 48 hours before being collected.

3.5 Treatment of PBECs with reagents

PBECs in 50% conditioned medium were treated with one or more of the following drugs for 48 hours.

To target the Wnt Pathway, human Dickkopf-related protein 1 (Dkk-1) a Wnt receptor inhibitor was used at a final concentration of 0.1 $mg \cdot ml^{-1}$ (Aviscera Bioscience). To promote the pathway, BIO (a GSK-3β inhibitor) was used at a final concentration of 1 µM.

To target the Sonic Hedgehog Pathway, SHH (recombinant human) was used at a final concentration of 1 $\mu g \cdot ml^{-1}$ (Source Bioscience), while cyclopamine (SMO receptor inhibitor) was used at 30 µM to inhibit the pathway.

A summary of the drugs used is given in Table 2.1.

Table 3.1. Drug treatments

Drug	Conc.	Target	Action	Ref
BIO	1 µM	GSK3β	Agonist	Lim *et al.* (2008)
Dickkopf	0.1 $mg \cdot ml^{-1}$	Frizzled Receptor	Antagonist	Lim et al. (2008)
SHH	1 $\mu g \cdot ml^{-1}$	Sonic Receptor	Agonist	Chen *et al.* (2012) (used 0.1 $mg \cdot ml^{-1}$)
Cyclopamine	30 µM	SMO receptor	Antagonist	Yauch *et al.* (2008)

The drug treatment was given on the day the medium on the PBECs was changed and all drug treatments were administered with either DMSO, dH_20 or PBS vehicle (where the final concentration of vehicle was ≤1%) in the final medium.

3.6 Monitoring trans-endothelial electrical resistance (TEER)

The resistance (Ω) of the PBECs that had been grown on Transwells was measured using an STX100 probe and EVOM volt-ohmmeter, where a jig was used to dock the chopsticks during the measurement in order to ensure that the chopstick was inserted at the same point and distance from filter for all Transwells. The resistance of a blank Transwell filter (without any cells) was also measured, and this was subtracted from the resistance of the PBECs on the Transwells. TEER was then expressed as $\Omega \cdot cm^2$.

3.7 Viability assay

To determine the viability of cells, an MTT viability assay was used.

MTT (3-(4,5-Dimethylthiazol-2-yl)-2,5-diphenyltetrazolium bromide) is a yellow organic heterocyclic compound that can be reduced enzymatically to an insoluble purple salt. The assay is based on the reduction of MTT to an insoluble purple tetrazolium salt by dehydrogenases (mainly mitochondrial succinate dehydrogenase) in live cells, where a colour change (yellow to purple) is measured in terms of absorbance.

All cells were washed with PBS prior to the addition of (100 µl) 1 $mg \cdot ml^{-1}$ MTT in DMEM without phenol red (Invitrogen 1188028), and incubated at 37˚C in 5% CO_2 for 4 hours. The medium was then removed and the crystals that had formed were dissolved in 100 µl isopropanol for 10 minutes. The plate was then shaken and read at 560 nm using Labsystems Multiscan Ascent plate reader and viability was measured as the levels of absorbance.

3.8 Activity assays

Activity assays were used to determine the uptake and efflux activity of PBECs as detailed below.

3.8.1 Uptake assay

An uptake assay was used to assess the uptake of ^{3}H-1-methyl-4-phenylpyridinium (^{3}H-MPP^{+}) by PBECs**.** MPP^{+} is a common substrate for Pgp, BCRP and the MRPs (Unpublished work by the BBB group 2008).

Unless stated otherwise steps were conducted at 37˚ C.

Confluent PBECs in 96-well plates were incubated with 200 µl ^{3}H-MPP^{+} Buffer consisting of 27.55 KBq·ml^{-1} of ^{3}H-MPP^{+} (Perkin Elmer) in Assay Buffer (25 mM HEPES, 0.1% BSA in HBSS, pH 7.35) and ^{14}C-sucrose 5.55 KBq·ml^{-1} (Movarek Biosciences) for either 30 minutes, 1 hour or 4 hours. ^{14}C-sucrose was used as an extracellular space marker, since it is not taken up by the PBECs. After the incubation time, the ^{3}H-MPP^{+} buffer was removed and the cells were washed with PBS (4°C).
To determine the amount of ^{3}H-MPP^{+} taken up, the cells were then lysed for 1 hour in Assay Lysis Buffer (1% Triton X-100 in dH_20). From the lysate 100 µl was mixed with 3.5 ml of Scintillation Fluid (Ultima Gold, Perkin Elmer) and counted for ^{3}H and ^{14}C signals using 1219 RackBeta Liquid Scintillation counter (LKB Wallac), while another 100 µl of the lysate was removed for BCA Analysis (see Section 2.9.1).
Alternatively, to determined the viability of the cells after exposure, after washing cells underwent an MTT Assay (see section 2.7)

3.8.2 ^{3}H-MPP^{+} efflux assay – 24 well plate

The efflux of ^{3}H-MPP^{+} from the PBECs was then assessed using a ^{3}H-MPP^{+} Efflux Assay in a 24-Well plate format. Since MPP^{+} is a common substrate for Pgp, BCRP and MRPs, it was used as a tool to assay the activity of these efflux transporters. The assay involves an initial loading stage (where ^{3}H-MPP^{+} is taken up by the PBECs) and a secondary efflux stage (where efflux of ^{3}H-MPP^{+} from inside the PBECs and into an extracellular buffer is directly measured). In the presence of an ABC transporter inhibitor the efflux of ^{3}H-MPP^{+} should be lower than in the absence of the inhibitor (if the ABC transporter is present and acting to efflux the ^{3}H-MPP^{+}). Therefore, the inhibitable level of ^{3}H-MPP^{+} efflux is a measure of ABC transporter activity.

Unless stated otherwise steps were conducted at 37˚ C.

Confluent PBECs in 24 well plates were preloaded with ^{3}H-MPP^{+} by incubating the cells for 60 minutes with Assay Buffer A (25 mM HEPES in HBSS, pH 7.35, 0.1% BSA) containing ^{3}H-MPP^{+} (27.75 KBq·ml^{-1}) and ^{14}C-sucrose (5.55 KBq·ml^{-1}). ^{14}C-sucrose was used as an extracellular space marker in this assay, since it does not enter the cells.

After the hour, the buffer was removed and the cells were washed with PBS (4°C). Non-radioactive Assay Buffer A with vehicle control (DMSO or methanol) or with ABC transporter inhibitors was then added to the loaded cells.

The ABC transporter inhibitors used were haloperidol and verapamil (Pgp inhibitor/ substrate) (Matsson *et al.*, 2009), Ko143 and prazosin (BCRP inhibitor/substrate) (Matsson et al., 2009) and MK571 (inhibitor to all MRP transporters) (Weksler *et al.*, 2005, Poller *et al.*, 2008, Matsson et al., 2009, Cioni *et al.*, 2012).

The cells were incubated in the buffer for between 30 seconds and 35 minutes. The buffer was then removed and kept as the Extracellular Efflux Sample. The cells were then lysed with 1% Triton-X-100 for 45 minutes and the lysate was collected as the Intracellular Retention Sample.

The Extracellular Efflux Sample and Intracellular Retention Sample were then mixed with 3.5 ml Ultima Gold Scintillation Fluid (Perkin Elmer) and counted for the amount of ^{3}H and ^{14}C within each sample using a 1219 RackBeta Liquid Scintillation counter (LKB Wallac).

3.8.3 ^{3}H-MPP^{+} efflux assay – 12- well Transwells

The ^{3}H-MPP^{+} Efflux Assay was also conducted in a Transwell format, to assess polarised efflux activity of the ABC Transporters. The assay in this format varies from the 24-well format, so details are given separately.

Unless stated otherwise steps were conducted at 37˚ C.

Confluent PBECs on Transwells were first loaded with ^{3}H-MPP^{+} by incubating the cells for 60 minutes with Assay Buffer A containing ^{3}H-MPP^{+} (27.75 KBq·ml^{-1}) only, with the buffer added to both the apical (0.5 ml in the Transwell) and basal (1 ml surrounding

the Transwell) chambers. After the incubation both chambers were washed with PBS (4˚C) and the cells were then incubated with Assay Buffer A containing 0.185 KBq·ml^{-1} ^{14}C-sucrose in the apical chamber (0.5 ml) and Assay Buffer A without any radioactivity in the basal chamber (1 ml), for 30 seconds to 35 minutes. In this assay ^{14}C-sucrose was used as a paracellular transport marker to assess the integrity of the PBEC monolayer. Since ^{14}C-sucrose cannot cross the cells directly, any ^{14}C-sucrose transport from the apical chamber to the basal chamber must occur via the paracellular route.

After the incubation time, the Apical buffer was removed and kept as the Apical Efflux Sample and the Basal Buffer was removed and kept as the Basal Efflux Sample. The cells were then lysed in 1% Triton-X-100 (0.5 ml apically and 1 ml basally) for 45 minutes and the lysate (apical and basal lysates pooled) was collected as the Intracellular Retention Sample

All samples were mixed with 3.5 ml of Scintillation Fluid and counted for amount of ^{3}H and ^{14}C within each samples using a 1219 RackBeta Liquid Scintillation counter (LKB Wallac).

3.8.4 Hoechst 33342 uptake assay

The Hoechst 33342 Assay was used to determine the efflux activity of PBECs grown in 96-well plates.

Hoechst is a nucleotide-binding dye that upon binding to DNA becomes fluorescent. It enters cells by diffusion across the cell surface membrane (Zhang *et al.*, 1999). However, Hoechst is a substrate for the ABC efflux transporters, Pgp (Shapiro *et al.*, 1997, Tang *et al.*, 2004) and BCRP (von Wedel-Parlow *et al.*, 2009). Therefore, the uptake of Hoechst is retarded by the presence of ABC transporters with the level of retardation in uptake being proportional to the efflux activity of the transporters. Inhibition of an efflux transporter should result in less dye being actively effluxed (than in the absence of inhibitor) and therefore more of the dye can reach and bind to DNA within the cells.

Unless stated otherwise steps were conducted at 37˚ C

PBECs grown in 96 well plates were incubated for 1 hour with a Preincubation Buffer consisting of 25 mM HEPES, in HBSS, pH 7.35, 0.1% BSA with vehicle control

(DMSO) or with inhibitor (0.2 µM Ko143 or 60 µM Haloperidol). The Preincubation Buffer was removed and the cells were incubated with Hoechst Assay Buffer (25 mM HEPES, in HBSS, pH 7.35, 0.1% BSA with 10 µM Hoechst 33342).

The Hoechst Assay buffer was left on the cells for 1 hour, the cells were then washed with PBS (4˚C) and the cells were analysed with a Bio-Tek Synergy HT plate reader at 360 nm excitation and 460 nm emission wavelengths to give Relative Fluorescence Units (RFUs) per well.

The method was adapted from von Wedel-Parlow *et al*, 2009, where all conditions apart from the inhibitors used were maintained as published previously.

The cells were then lysed for 45 minutes with 1% Triton-X-100 and the protein content of the lysate was measured in µg with a BCA assay (see section 2.9.1).

Results were then expressed as RFUs/µg protein in a well.

3.9 Expression studies

3.9.1 BCA Assay

The Pierce protein assay was used to quantify proteins. The assay is based on the reduction of Cu^{2+} to Cu^{1+} by protein (in an alkaline environment), where Cu^{1+} reacts with bicinchoninic acid (BCA) in a colourimetric reaction that can be measured in terms of absorbance. The BCA assay was conducted according to the Pierce Kit instructions to measure total cellular protein levels. Protein samples (e.g. 100 µl of cell lysate) were incubated at 37°C for 30 minutes with equal volumes of Pierce Reagent Mix (a mixture of Reagents A and B in a 50:1 ratio, respectively), before absorbance readings were measured at 540 nm in Labsystems Multiscan Ascent plate reader.

BSA protein standards of known concentrations were measured alongside protein samples, to construct a calibration curve of absorbance against protein concentration, from which the absorbance measured with a sample of unknown protein concentration, could be used to determine the protein concentration within the sample.

3.9.2 mRNA expression

RNA was isolated at different stages of the PBEC culturing process for analysis. The cell culture process involves the growing endothelial cells out from capillaries isolated from pig brain (See Section 2.4). Therefore the RNA from capillaries was initially isolated at cell culture day 0 (Day 0 Samples). The capillaries were grown for 3 days in puromycin, with RNA isolated after these 3 days (Day 3 Samples). Puromycin was then removed from the medium and 3 days later the cells were passaged to the Transwells with RNA isolated on the Day of Passaging.

The PBECs were passaged and grown in 6 well Transwells either alone (i.e. in mono-culture) or in co-culture with normal rat astrocytes. Once on the Transwell, the PBECs were grown to confluence which occurred in 3 days, and RNA was isolated from the confluent PBECs (3 Days Co-culture Samples). In addition, the confluent PBECs were incubated for 24 hours in PBEC serum-free medium containing 250 µM CPT-cAMP and 17.5 µM RO-20-1724 and RNA was isolated after these 24 hours (4 Days in Co-culture Sample).

RNA isolation was conducted using TRI (Total RNA Isolation) Reagent® (Sigma). The PBECs were lysed for 5 minutes in 450 µl – 1000 µl of TRI. BCP (1-bromo-3-chloropropane) was then added; 100 µl per 1 ml of TRI solution, and the solution was mixed and then incubated at room temperature for 15 minutes. The mixture was then centrifuged at 12000 x g for 15 minutes (4˚C). The aqueous phase of the mixture (containing the RNA) was then removed to a fresh tube for further processing. The interphase and organic phases were then processed separately for Protein Isolation (see section 2.9.3)

Isopropanol was added to the aqueous phase, 500 µl for 1 ml TRI solution initially used, and vortexed for 10 second. The mixture was incubated at room temperature for 10 minutes and then centrifuged at 12000 x g for 8-15 minutes (4˚C) until a white precipitate of RNA was formed. The RNA pellet was washed with 75% ethanol (1 ml per 1 ml of TRI solution) and centrifuged at 7500 x g for 5 minutes (4˚C). The ethanol was discarded and the pellet was air-dried for 3-5 minutes. The pellet was resuspended in dH_20 and the RNA was stored at -80˚C.

The RNA isolated was purified using the miniElute Clean Up kit (Qiagen) with the RNase-free DNase Set. RNA samples (45 µg or less) were each combined with 10 µl RDR buffer, 2.5 µl DNase I stock and made up to 100 µl with dH_2O. The mixture was

incubated at room temperature for 10 minutes, then mixed with 350 µl of RLT buffer and 250 µl ethanol. The mixture was placed on a miniElute column and centrifuged for 15 seconds using Heraeus Biofuge Pico centrifuge (max speed). 500 µl RPE buffer was then added to the column and the column was re-centrifuged for 15 second. Then 500 µl 80% ethanol was added to the column and the column was centrifuged for 2 minutes. The column was then left to dry (for 5 minutes) and 14µl -100µl of dH_20 was used to elute the RNA from within the column.

The RNA was quality checked using the Aligen RNA 6000 Pico Kit. To a Pico Microchip, 1 µl of RNA was added per well (for a total of 9 wells/ 9 samples per chip) containing the RNA ladder. The chip was then analysed with the Bioanalyzer 2100 and Software Version 2.6 and RNA purity measurements given a number of 1-10 (10 being the purest). RNA sample of ≥ 7 were considered of good quality for PCR work.

A 2 step RT-QPCR reaction was conducted on purified and high quality RNA. Step 1, the RNA was converted to cDNA, Step 2, QCPR analysis was conducted on the cDNA.

To convert the RNA into cDNA the TaqMan® Reverse Transcription Reagents were used (Life Technologies).

Each RNA sample underwent the DNase Reaction, where per 10 µl reaction, 100 ng RNA was combined with 1 µl X10 Reaction buffer, 2.2 µl 25 mM $MgCl_2$, 2 µl deoxyNTPs, 0.5 µl Random Hexamers, 0.2 µl RNase Inhibitor 0.25 µl MultiScript DNase enzyme and volumes were made up to 10 µl using dH_20. For each sample, a negative reaction was also run, where no MultiScript was used.

The reaction mix was then thermo cycled using a robocycler (25˚C for 10 minutes, 48˚C for 30 minutes, 95˚C for 5 minutes then held at 4˚C).

The cDNA was then used in the second step for the PCR reaction. For the PCR reactions, a Pooled Standard Sample was created as a positive control, by pooling ~20% of the cDNA from each sample. The cDNA samples were then diluted in a 1 in 4 ratio with dH_20 for the next step.

For the PCR reaction, 4 µl (~10ng) of the diluted cDNA was combined with 1 µl TaqMan Probes per 20 µl reaction and 10 µl TaqMan® Fast Universal PCR Master Mix (2✕), No AmpErase® UNG to give a final concentration of X1 (5 µl water was used to make up the solution to the final volume). The following probes were used Ss03373435_m1 (MDR1) (for Pgp), Ss03393456_u1 (ABCG2) (for BCRP), Ss03376563_uH (ACTB) (for β-actin), Ss03373286_u1 (GAPDH) (for GAPDH), with all

probes obtained from Life Technologies (details of probes can be found in the Appendix, Section 9.4, however exact probe sequences were not disclosed by the company).

Reactions were run on MicroAmp Fast 96-Well Plates, 0.1 ml, in duplicates or triplicates per plate, for all samples except the negative control (where no MultiScript had been added) which was a single well per sample on the plate. Alternatively, reactions were scaled down to 10 µl and run on 394 well plates (MicroAmp) by Matt Arno (Genomics Center, KCL) with all reactions in quadruplicate.

A standard curve and blank controls (of water) were also run in duplicates per plate. The standard curve was made from the serial dilution of the Pooled Standard Sample (mentioned above).

All reactions were then run on the 7900HT Fast Real-Time PCR System and software using default setting of 20 seconds at 95˚C, then 40 cycles of 1 second 95˚C and 20 seconds 60˚C. The cycle of threshold (Ct) values were then analysed (see calculations section 2.10.5).

3.9.3 Isolation of protein from PBECs and western blotting (see Appendix for results)

Organic/interphase samples obtained from section 2.9.2 were processed to isolate the total cellular protein. Per 1 ml of TRI solution used in the initial isolation, 300 µl of 100% ethanol was added and the samples were mixed by inversion and incubated at room temperature for 3 minutes. The samples were then centrifuged at 2000 x g for 5 minutes (4˚C) and the supernatant (containing the protein) was then further processed.

Acetone was added to the supernatant to precipitate the protein (X3 volumes of acetone were added to X1 the volume of the supernatant) and the samples were incubated at room temperature for 10 minutes. The samples were centrifuged and the supernatant discarded. The protein pellet was washed with 1 ml of Protein Wash 1 (300 mM guanidine hydrochloride in 95% ethanol, with 2.5% glycerol). The samples were centrifuged after incubation with the protein wash for 10 minutes at room temperature. Centrifugation was at 8000 X g for 5 minute (4˚C). The protein was washed twice more with Protein wash 1 then once with Protein Wash 2 (100% ethanol containing 2.5% glycerol). The pellets were resuspended in 1% Triton-X-100, 6 M urea

containing EDTA-free protease inhibitor cocktail (Rouche) and protein samples were stored at -80˚C.

Isolated Protein then underwent SDS-PAGE. For SDS-PAGE, polyacrilamide gels were made to 0.75 mm thickness. The resolving portion of the gel was made using 8% Acrylamide/Bis (BioRad), 375 mM Tris-HCl pH 8.8, 0.1% SDS, 0.1% APS, 0.06% TEMED (GE Healthcare). The stacking portion of the gel was made with 4% Acrylamide/Bis (BioRad), 375 mM Tris-HCl pH 6.8, 0.1% SDS, 0.05% APS, 0.1% TEMED).

The protein samples (7.5 µg – 100 µg) were prepared, by mixing protein with X5 Sample Dye (62.5 mM Tris-HCl pH6.8, 10% Glycerol, 2% SDS, 5% β-mercaptoethanol, 0.025% bromophenol Blue) so that the final concentration of the dye was X1. The samples were then heated at 95˚C for 10 minutes, centrifuged (pulse spun for 10 seconds) and allowed to cool at room temperature for 1 minutes. The cooled samples were loaded onto the gel with 5 µl SeeBluePlus2 (Invitrogen) ladder and/or 5 µl MagicMark (Invitrogen) ladder and ran at 120 Volts for 1 hour in Tris-Glycine Running Buffer (240 mM Tris, 190 mM Glycine, 0.1% SDS, pH 8.3)

The gel was transferred onto a PVDF membrane (Millipore, 0.45 µm pore) using the Novex Semi Dry Western Blotting System (Invitrogen). A sandwich was made composed of one 2.5 mm Filter Paper (Invitrogen) soaked in Transfer Buffer (25 mM Tris, 190 mM glycine, 10% methanol, pH 8.5 or 10 mM $NaHCO_3$, 3 mM $NaCO_3$, 20% methanol pH 9.9) , followed by the PVDF membrane (that had been soaked in 100% methanol for 5 minutes), then the SDS-gel, then a final 2.5mm filter paper soaked in Transfer Buffer (25 mM Tris, 190 mM glycine, 10% methanol, pH 8.5 or 10 mM $NaHCO_3$, 3 mM $NaCO_3$, 0.1% SDS, pH 9.9). The sandwich was then transferred for 30-75 minutes at 20 Volts.

The PVDF membrane was then placed in Blocking Buffer (20mM Tris-HCl, 137mM NaCl, 0.1% Tween 20 (Fisher Scientific) and 5% milk powder (Marvel), pH 7.6) for 1 hour at 4˚C. The membrane was then incubated with primary antibodies in Antibody Diluent Buffer (0.5% BSA in PBS, pH 7.4) overnight at 4˚C.

The antibodies used include BXP-21 (mouse IgG2A, 1:200 dilution) (Calbiochem), C219 (mouse IgG2A, 0.25 $\mu g \cdot ml^{-1}$ dilution) (Calbiochem) and C11 (goat IgG, 1:1000 dilution) (Santa Cruz).

The membrane was then washed in PBST (PBS+0.1% Tween 20) 3 times (15 minutes each wash) and the washed membrane was incubated with secondary antibodies in Antibody Diluent Buffer overnight at 4˚C.

The secondary antibodies used include Goat, anti-mouse IgG2A HRP (1:1000 dilution) (GeneTex) and Donkey, Anti-goat IgG HRP (1:1000 dilution) (Alpha Diagnostics).

The membrane was washed 3 times with PBST as before and then washed with a final 30 minute wash in PBS.

The membrane was then incubated in a 50:50 solution of West Dura Pico Kit (Pierce) for 1 minute and visualised using Syngene Imager and software.

3.9.4 Confocal microscopy

Wax embedded slides of normal brain tissue, Grade I and Grade II astrocytomas obtained from US Biomax or Biochain or were either a gift from Dr. Marios Papadopoulous (St. George's Hospital).

Slides were dewaxed and prepared for staining as follows: Slides were placed in 100% xylene for 5 minutes and repeated with fresh xylene. This was followed by 3 minutes in 100% ethanol that was repeated with fresh ethanol. The slides were then placed for 3 minutes in 70% ethanol and then under running water for 2 minutes. The slides were then incubated in 3% H_2O_2 for 15 minutes and then placed in running water for 10 minutes. The slides were then incubated with 1% Antigen Unmasking Solution (Vector Laboratories) in dH_20 and microwaved (full power for 15 minutes). The slides were left to cool for 20 minutes at room temperature and then underwent staining.

The primary antibodies used included BXP-21 (anti-BCRP, mouse IgG2A), JSB-1 (anti-Pgp, mouse IgG1) (GeneTex GTX23366), anti-von Willebrand factor (VWF) (Rabbit IgG1) (Millipore AB7356) and anti-CD34 (Rabbit IgG1) (GeneTex GTX61737). Antibody dilutions were made using Antibody Diluent (Dako) (1:200 BXP-21, 1:40, 1:200 JSB-1, 1:100 anti VWF or 1:100 anti-CD34) and dilutions were added to slides. Slides were then placed at 4˚C overnight, then washed 3 times (5 minutes a wash) with X1 PBST (made from X10 stock from Dako)

Alexa Fluor secondary antibodies were used (Invitrogen) and diluted in Antibody Diluent. Red-Alexa Fluor-546 (against mouse IgG2A – BCRP, 1:80 dilution), Green –

Alexa Fluor-488 (against mouse IgG1-Pgp 1:100 dilution) and Far Red-Cy5 (against Rabbit IgG1- VWF or CD34, 1:50 dilution). The secondary antibodies were added to the slides and left to incubate for 3 hours at room temperature in the dark. The slides where then washed 3 times in 1X PBST (5 minutes each wash) and then rinsed with dH_20. VECTASHIELD DAPI mounting medium (Vector Laboratories) was then added and coverslips were placed onto the slides.

Images were taken with either the Leica SP8vis microscope (UCL Confocal Imaging Unit) taking 290 µm² images in z-stacks (0.5 micron step size) using an 40X objective (oil immersion) or Nikon Diaphot DTM Microscope (Paul Fraser, KCL) single images using 40X objective (water immersion).

With the Leica SP8vis, sequential imaging was conducted first assessing DAPI and BCRP, then assessing Pgp and VWF or CD34, so as to avoid bleed through.

Images were then analysed as detailed in Section 2.10.6.

3.10 Calculations

3.10.1 Uptake of ^{3}H-MPP^{+} into PBECs in plates

The uptake of ^{3}H-MPP^{+} into PBECs grown in 96-well plates was calculated as the Volume of Distribution (Vd). This is the volume that the ^{3}H-MPP^{+} would occupy (within the cells) if it reached the same concentration in the cell as in the medium.

All samples were corrected for background radioactivity (in blank samples) before calculations, with blank/background radioactivity measured as the DPMs in the non-radioactive assay buffer (for efflux samples) or 1 % Triton-X 100 lysis buffer (for intracellular retention samples).

Equation 1 was used to determine the Vd of ^{3}H-MPP^{+} within cells, correcting for the Vd of the extracellular marker ^{14}C sucrose. Here ^{14}C-Sucrose was used as a marker for extracellular space, since it does not enter the cells and therefore any ^{14}C-Sucrose detected would only be present in the extracellular space at the end of the experiment. The corrected Vd was then divided by the protein content of a well (i.e. the total protein in a well measured using a BCA assay).

Equation 1: Volume of distribution (Vd)

$$Vd\ (\mu l.mg^{-1}) = \left[\frac{^{3}H\ I}{^{3}H\ To} - \frac{^{14}C\ I}{^{14}C\ To}\right] / Tot\ prot$$

NB. All samples were taken from the same well.

Vd = Volume of distribution measured in **µl.mg^{-1}**

^{3}H I = The total **dpms** of ^{3}H-MPP^{+} detected intracellularly (within the lysate of a well) at the end of the experiment

^{14}C I = The total **dpms** of ^{14}C-Sucrose detected in the same lysate sample as ^{3}H I

^{3}H To = The initial concentration **(dpms.µl^{-1})** of ^{3}H-MPP^{+} at the beginning of the experiment

^{14}C To = The initial concentration **(dpms.µl^{-1})** of ^{14}C-Sucrose at the beginning of the experiment

Tot Prot = Total protein in **mg** (in the well from which ^{3}H I was measured)

3.10.2 Calculations for ^{3}H-MPP^{+} efflux assay in 24 Well plate format

To calculate the Total ^{3}H-MPP^{+} Loaded into PBECs during a ^{3}H-MPP^{+} Efflux Assay using either 24-Well plate format or Transwell format, firstly samples were corrected for ^{14}C-sucrose.

For the 24-Well format, ^{14}C-Sucrose was used as an extracellular space marker; the extracellular efflux samples and intracellular retention samples (lysates) were corrected for ^{14}C-sucrose using Equation 2.

Equation 2 : Correction for extracellular space

$$Corrected\ \ ^{3}H\ S = \ ^{3}H\ S - \ ^{14}C\ S \times \frac{^{3}H\ To}{^{14}C\ To}$$

^{3}H S = The total **dpms** of ^{3}H-MPP^{+} detected within the sample

^{14}C S = The total **dpms** of ^{14}C-Sucrose detected within the sample

^{3}H To = The total **dpms** of ^{3}H-MPP^{+} added at the beginning of the experiment (in the Loading Buffer)

^{14}C To = The total **dpms** of ^{14}C-Sucrose added at the beginning of the experiment (in the Loading Buffer)

The Total ^{3}H-MPP^{+} Loaded for 24-Well Efflux assay was then calculated as the sum of the corrected ^{3}H-MPP^{+} in the Extracellular efflux Sample and the corrected ^{3}H-MPP^{+} in the Intracellular sample (lysate) per well (Equation 3).

Equation 3 : Total ^{3}H-MPP^{+} Loaded

$$Total\ {}^{3}H\ Loaded = Corrected\ \ {}^{3}H\ E + \text{Corrected}\ \ {}^{3}H\ I$$

NB. All samples were collected from the same well, and represent measurements from a single well.

Total ^{3}H Loaded = Total ^{3}H-MPP^{+} loaded into PBECs per well.

Corrected ^{3}H E = The ^{3}H-MPP^{+} in the Extracellular Efflux Sample after correction for ^{14}C-sucrose (with **Eq 2.)**

Corrected ^{3}H I = The ^{3}H-MPP^{+} detected Intracellularly (within the lysate) after correction for ^{14}C-sucrose (with **Eq.2**).

The Total ^{3}H-MPP^{+} Loaded was then used to calculate the percentage of ^{3}H-MPP^{+} effluxed, as shown in Equation 4.

Equation 4: Percentage Efflux

$$^{3}H\ Effluxed\ (\%) = \left[\frac{Corrected\ \ {}^{3}H\ E}{Total\ {}^{3}H\ Loaded}\right] \times 100$$

Total ^{3}H Loaded = Total ^{3}H-MPP^{+} loaded into PBECs per well (calculated using **Eq 3)**.

Corrected ^{3}H E = The ^{3}H-MPP^{+} in the Extracellular Efflux Sample after correction for ^{14}C-sucrose (using **Eq.2**)

WORKED EXAMPLE (From haloperidol dose-response curve)

NB. All samples have been corrected for blank

Extracellular Efflux sample = 2118 ^{3}H dpms, 3 ^{14}C dpms

Intracellular lysate sample = 2046 ^{3}H dpms, 0 ^{14}C dpms

Initial amount of ^{3}H added (^{3}H To) = 1465200 dpms

Initial amount of ^{14}C added (^{14}C To) = 144400 dpms

Step 1. Correction for ^{14}C-Sucrose

$$Corrected\ {}^{3}H\ S = {}^{3}H\ S - {}^{14}C\ S \times \frac{{}^{3}H\ To}{{}^{14}C\ To}$$

a) Extracellular Efflux Buffer

$$\begin{aligned} Corrected\ {}^{3}H\ S &= 2118\ dpms - 3dpms \times \frac{1465200\ dpms}{144400\ dpms} \\ &= 2118\ dpms - 30\ dpms \\ &= 2088\ dpms \end{aligned}$$

b) Intracellular (Lysate) Sample

$$\begin{aligned} Corrected\ {}^{3}H\ S &= 2046\ dpms - 0\ dpms \times \frac{1465200\ dpms}{144400\ dpms} \\ &= 2046\ dpms - 0\ dpms \\ &= 2046\ dpms \end{aligned}$$

Step 2. Calculation of the Total ^{3}H-MPP^{+} Loaded

$$Total\ {}^{3}H\ Loaded = Corrected\ {}^{3}H\ E + \text{Corrected}\ {}^{3}H\ I$$

$$\begin{aligned} &= 2088 + 2046\ dpms \\ &= 4134\ dpms \end{aligned}$$

Step 3. Calculation of % Efflux

$$Eq.3\ \%\ {}^{3}H\ Effluxed = \left[\frac{Corrected\ {}^{3}H\ E}{Total\ {}^{3}H\ Loaded}\right] \times 100$$

$$\begin{aligned} \%\ {}^{3}H\ Effluxed &= \frac{2088\ dpms}{4134\ dpms} \times 100 \\ &= 50.5\% \end{aligned}$$

3.10.3 Calculation for PBECs on Transwells

In the Transwell experiments ^{14}C-sucrose was used as a paracellular permeation marker. Since it does not enter endothelial cells, the only way for ^{14}C-sucrose to cross from the Apical Chamber to the Basal Chamber of the Transwells is via the paracellular route. Therefore its flux can be used as a measure of the paracellular flux/ leakiness of a monolayer. The apparent permeability (Papp) of ^{14}C-sucrose (i.e. the leakiness of the monolayer) was calculated in some cases using Equation 5 (Avdeef, 2011).

Equation 5 : Apparent Permeability (Papp)

Papp (cm.s^{-1}) = dQ/(dT x A X Co)

dQ = transported amount (dpms in Basal Chamber)

dT = time (seconds)

A = surface area of filter (in cm)

Co= initial concentration (dpms.µl^{-1})

For calculations concerning the efflux of ^{3}H-MPP^{+}, the Intracellular Retention Samples obtained from the ^{3}H-MPP^{+} Assay in the Transwell format were corrected for ^{14}C-Sucrose using Equations 6 and 7. Firstly the percentage of ^{14}C-sucrose in the Intracellular Retention Samples was calculated using Equation 6. Secondly, this was then used to correct the ^{3}H-MPP^{+} Intracellular Retention Sample against ^{14}C-sucrose using Equation 7.

The total ^{3}H-MPP^{+} Loaded was then calculated as the sum of the ^{3}H-MPP^{+} measured in the Apical plus Basal Efflux Samples, together with the ^{14}C-Sucrose corrected Intracellular Retention Sample (as shown in Equation 8).

For the efflux percentage calculations, the Apical and Basal Samples were expressed as a percentage of the Total ^{3}H-MPP^{+} Loaded in the PBECs (Equation 4).

To convert the Total ^{3}H-MPP^{+} Loaded into mol, Total ^{3}H-MPP^{+} Loaded was expressed as a percentage of the ^{3}H-MPP^{+} dpm in the Loading Buffer where 1.5 ml of ^{3}H-MPP^{+} Loading Buffer was added per Transwell at a concentration of 9 nM ^{3}H-MPP^{+} i.e. a total of 13.5 pmol was added per Transwell.

Equation 6: ^{14}C-Sucrose in Intracellular Retention Sample

$$\%\ ^{14}C\ Intra = \frac{^{14}C\ I}{^{14}C\ I + {}^{14}C\ A\ + {}^{14}C\ B} \times 100$$

NB. All samples were collected from the same Transwell

^{14}C I = The total ^{14}C **dpms** in the Intracellular Rentention Sample (i.e. in the Lysate Sample)

^{14}C B = The total ^{14}C **dpms** in the Basal Chamber (i.e. in the Basal Efflux Sample)

^{14}C A = The total ^{14}C **dpms** in the Apical Chamber (i.e. in the Apical Efflux Sample)

Equation 7: Correction for ^{14}C-sucrose in Intracellular Retention Sample

$$Corr\ \ ^{3}H\ Intra\ (dpms) = \ \ ^{3}H\ I - \left(\ \ ^{3}H\ I \times \frac{\%\ \ ^{14}C\ I}{100} \right)$$

NB. All samples were collected from the same Transwell

Corr ^{3}H Intra= The total ^{3}H-MPP^{+} **dpms** in the Intracellular Retention Sample (i.e. lysate) after correction for ^{14}C-Sucrose

^{3}H I= The total ^{3}H **dpms** in the Intracellular Retention Sample (i.e. in the lysae sample)

% ^{14}C = the percentage of ^{14}C-sucrose within the lysate sample (measured using **Eq.6**)

Equation 8: Total ^{3}H-MPP^{+} Loaded per Transwell

$$Total\ \ ^{3}H\ MPP+\ Loaded\ (dpms) = \ \ ^{3}H\ A + \ \ ^{3}H\ B + \ Corr\ ^{3}H\ I$$

NB. All sample were collected from the same Transwell

^{3}H B = The total ^{3}H-MPP^{+} **dpms** in the Basal Efflux Sample

^{3}H A= The total ^{3}H **dpms** in the Apical Chamber (i.e. in the Apical Efflux Sample)

Corr ^{3}H I = The total ^{3}H-MPP^{+} **dpms** in the Intracellular Retention Sample after correction for ^{14}C-Sucrose (calculated using **Eq 7**).

WORKED EXAMPLE (Mono-culture, 35 minute efflux, no inhibitor)

Basal Efflux Sample = **5444 ^{3}H dpms, 2191 ^{14}C dpms**

Apical Efflux Sample = **2516 ^{3}H dpms, 4022 ^{14}C dpms**

Intracellular Sample (Lysate) = **3352 ^{3}H dpms, 92 ^{14}C dpms**

Initial ^{14}C = **6644 dpms** (total dpms)

Initial ^{3}H = **5,355,000 dpms** (total dpms) = **13.5 pmol**

Step 1. ^{14}C-Sucrose correction of Intracellular Sample

$$\%\ ^{14}C\ Intra = \frac{^{14}C\ I}{^{14}C\ I + {}^{14}C\ A + {}^{14}C\ B} \times 100$$

$$\%\ ^{14}C\ Intra = \frac{92}{92 + 4022 + 2191} \times 100$$

$$= 1.45\ \%$$

$$Corr\ \ ^{3}H\ Intra\ (dpms) = {}^{3}H\ I - \left({}^{3}H\ I \times \frac{\%\ \ ^{14}C\ I}{100} \right)$$

$$Corr\ \ ^{3}H\ Intra\ (dpms) = 3352 - \left(3352 \times \frac{1.45}{100} \right)$$

$$= 3303\ dpms$$

Step 2. Calculation of Total ^{3}H-MPP$^+$ Loaded and % Efflux

$$Total\ \ ^3H\ MPP+\ Loaded\ (dpms) = \ \ ^3H\ A + \ \ ^3H\ B + \ Corr\ ^3H\ I$$

$$= 2516 + 5444 + 3303$$
$$= 11263\ dpms$$

- **% Efflux calculations**

$$\%\ Effluxed\ Apically = 100 \times \frac{^3H\ Apical}{Total\ \ ^3H\ Loaded}$$

$$\%\ Effluxed\ Apically = 100 \times \frac{2516\ dpms}{11263\ dpms}$$

$$= 22.3\ \%$$

$$\%\ Effluxed\ Basally = 100 \times \frac{^3H\ Basal}{Total\ \ ^3H\ Loaded}$$

$$\%\ Effluxed\ Basally = 100 \times \frac{5444\ dpms}{11263\ dpms}$$

II. **fmol loaded calculations**

$$\%\ ^3H\ in\ Loading\ Buffer = 100 \times \frac{Total\ ^3H\ Loaded}{^3H\ To}$$

$$\%\ ^3H\ in\ Loading\ Buffer = 100 \times \frac{Total\ ^3H\ Loaded}{^3H\ To}$$

$$\%\ \ ^3H\ in\ Loading\ Buffer = 100 \times \frac{11263\ dpms}{5355000\ dpms}$$

$$= 0.210\ \%$$

Where 0.210% of 13.5 pmol (total mol in loading buffer) is 0.0284 pmol

3.10.4 Calculation of inhibitable Hoechst 33342 uptake

To calculate the inhibitable Hoechst 33342 Uptake, was a 2 Step Process.

Step 1: Calculating the Inhibitable Uptake (Inh U)

$$\mathbf{InhU = Inh - no\ Inh}$$

Inh = Uptake in the presence of inhibitor (RFU/µg protein)

No Inh = Uptake in the absence of inhibitor (RFU/µg protein)

Step 2: Normalising against Baseline Uptake (i.e. uptake in untreated and uninhibited control)

$$\text{Normalised Inhibition} = \frac{\text{Inh U} + \text{Baseline}}{\text{Baseline}}$$

Baseline= Uptake in the absence of any drug treatment and in the absence of any inhibitor (RFU/µg protein)

3.10.5 Calculations for mRNA levels

To calculate the fold change of the Gene of interest was a 3 step process.

Step 1: First the ΔCt for a gene of interest (GOI) was calculated as follows from the cycle of threshold (Ct) values of the PCR reaction:

$$\Delta Ct_{GOI} = Ct_{GOI} - Ct_{Ref\ G}$$

$CT_{Ref\ G}$ = The CT of the reference gene (in the Same Sample)

Step 2: The ΔΔCt of the GOI was then calculated using the ΔCt as follows:

$$\Delta\Delta Ct_{GOI} = \Delta Ct_{GOI} - \Delta Ct_{Ref\ S}$$

$\Delta CT_{Ref\ S}$ = The ΔCt of reference sample (i.e. mono-culture sample)

Step 3: The fold change of the GOI was then was calculated as follows:

$$\text{n-fold change} = 2^{-\Delta\Delta Ct}$$

3.10.6 Calculation from confocal imaging

In an image, CD34-positive pixels were initially isolated (Image Hopper Software), where only CD34-positive vessels less than 7 µm width were analysed (size determined using ImageJ Software). The intensity of Pgp or BCRP signal in the CD34-positive pixels was then measured across all images in a z-stack. The data were then pooled and expressed as a histogram using Image Hopper Software. The area under the curve (AUC) was calculated and divided by the number of pixels analysed to give Pgp or BCRP expression.

3.11 Statistics

All statistics was conducted using Graph Pad Prism 5 Software.

For comparisons of 2 data sets, t-tests were conducted (e.g. between no inhibitor (vehicle control) and inhibitor data sets).

For comparisons of 3 or more data sets, 1-way ANOVA analysis was conducted. If the ANOVA analysis showed $p<0.05$ significance the data sets were then compared using post-hoc tests. For comparisons of 3 data sets a Newman-Keuls Multiple Comparison Test was then used. However, the Newman-Keuls Multiple Comparison Test is not appropriate for comparisons of more than 3 data sets (Graph Pad Prism Guidelines),

therefore for comparison of 4 or more data sets the Tukey's Multiple Comparison Test was used.

4 *In vitro* BBB Models

4.1 Results

In this chapter, cell culture systems were modified to allow study of efflux transporter activity in normal BBB endothelial cells and assessed to determine their suitability for later use during co-culture with glioma cells. Primary porcine brain endothelial cells (PBECs) were used as an *in vitro* cell model of the blood-brain barrier (BBB). These cells have been shown to have high transendothelial electrical resistance (TEER) (Cohen-Kashi Malina *et al.*, 2009, Patabendige *et al.*, 2013a, Patabendige *et al.*, 2013b) and a similar expression pattern of efflux transporters to the human BBB, thus making them a good BBB model (Warren *et al.*, 2009). To study the ABC transport activity within PBECs, ^{3}H-MPP^{+} was used. MPP^{+} was previously shown to be a substrate for Pgp, with MPP+ flux across Caco-2 cells increasing in the apical to basal direction and decreasing in the basal to apical direction in the presence of the Pgp inhibitor Cyclosporin A (Bleasby *et al.*, 2000). In a different study, MPP+ uptake into MDCK cells was increased by the Pgp/BCRP inhibitor PMEO-DAPy (Mandikova *et al.*, 2013). Matsson *et al.*, (2009) also showed that MPP+ can inhibit MRP2 substrate transport (ATP-dependent transport of estradiol-17β-glucuronide), indicating that MPP+ is either an inhibitor or competitive substrate of MRP2. This together with unpublished data by the BBB group at KCL (Patabendige, 2008) indicates that MPP+ is a common substrate of the main ABC transporters (i.e. Pgp, BCRP and MRPs). Using MPP+ as a substrate, a ^{3}H-MPP^{+} efflux assay was developed that directly measures efflux from endothelial cells and polarised efflux from both the apical and basal surfaces can be assessed separately.

4.1.1 Viability of PBECs after ^{3}H-MPP^{+} incubation

To determine whether ^{3}H-MPP^{+} is toxic to PBECs, their viability was measured (using an MTT assay) after the cells had been exposed to ^{3}H-MPP^{+} for up to 4 hours. No differences were seen in PBEC viability between those exposed to ^{3}H-MPP^{+} and those not exposed (control conditions) (Figure 3.1).

Figure 3.1 Viability of PBECs after exposure to ^{3}H-MPP^{+}

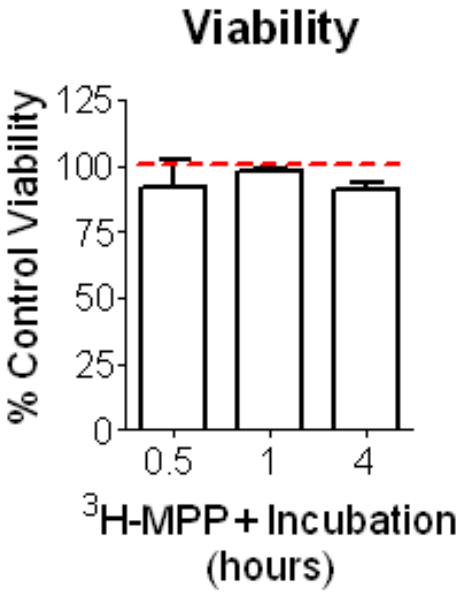

The viability of the PBECs was measured using an MTT assay after the cells had been incubated with 9 nM (27.75 KBq.ml^{-1}) ^{3}H-MPP^{+} and ^{14}C-sucrose (5.55 KBq.ml^{-1}) or incubated with ^{14}C-sucrose (5.55 KBq.ml^{-1}KBq.ml^{-1}) alone (control) for up to 4 hours.

The results are expressed as % control, with control results represented by the dotted line.

Values are mean ± SEM of n=11-16 wells from 3 different plates using 3 different batches of PBECs.

No significant differences were found between any condition and its control in unpaired 2-tailed t-tests.

4.1.2 Uptake of ^{3}H-MPP^{+} into PBECs

^{3}H-MPP^{+} uptake was measured for up to 4 hours and the results showed an increase in the volume of distribution (Vd) of ^{3}H-MPP^{+} between 30 minutes and 1 hour, but no further increase between 1 hour and 4 hours (Figure 3.2). This indicates that uptake of ^{3}H-MPP^{+} reaches steady-state/saturation within 1 hour and for further work, 1 hour incubation was used.

Figure 3.2 ^{3}H-MPP^{+} uptake by PBECs

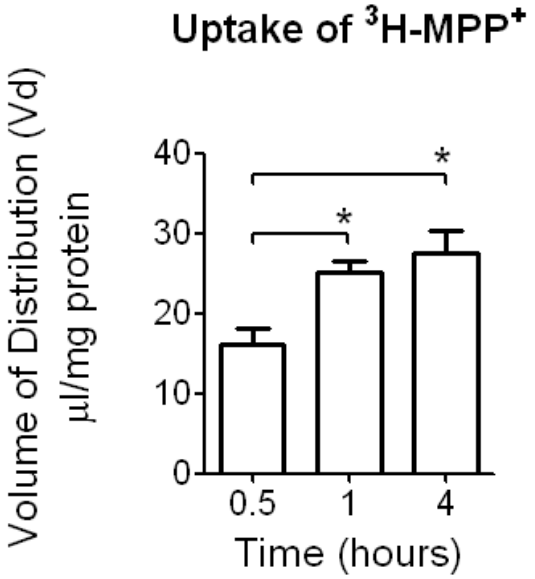

PBECs were incubated with 9 nM (27.75 KBq.ml^{-1}) ^{3}H-MPP^{+} and ^{14}C-sucrose (5.55 KBq.ml^{-1}) for 30 minutes, 1 hour or 4 hours, with ^{14}C-sucrose as a marker for extracellular space. The cells were then washed and lysed. Half the lysate was analysed for ^{3}H-MPP^{+} and ^{14}C-sucrose and the other half of used for protein content measurement using a BCA assay.

Results are expressed as volume of distribution (Vd) in µl.mg^{-1} of protein after correction for ^{14}C-sucrose.

Values are mean ± SEM of n=10-13 wells from 3 different plates using 3 different batches of PBECs.

*p<0.05 significant difference between indicated conditions using 1-way ANOVA and Newman-Keuls Multiple Comparison post test.

4.1.3 Rate of ^{3}H-MPP^{+} efflux by PBECs in plates

PBECs in 24 well plates were loaded with ^{3}H-MPP^{+} and then efflux from the loaded cells was measured between 30 seconds and 35 minutes.

^{3}H-MPP^{+} efflux is shown plotted against time in Figure 3.3, where efflux was shown to increase with time. There appeared to be more than 1 component to the rate of ^{3}H-MPP^{+} efflux, with the line plotted deviating from linear by 35 minutes of efflux. The efflux half times $t_{1/2s}$ were calculated as 37 minutes (all data points) The initial rate could not have been release of non-specific binding since a thorough wash process was conducted prior to the efflux stage of the experiment and in addition, efflux was corrected for ^{14}C-sucrose (extracellular space marker). In addition, non-specific binding analysis was conducted previously, which showed that no significant level of non-specific binding of ^{3}H-MPP^{+} occurred to the PBECs cell surface (see Appendix 9.1.2).

A

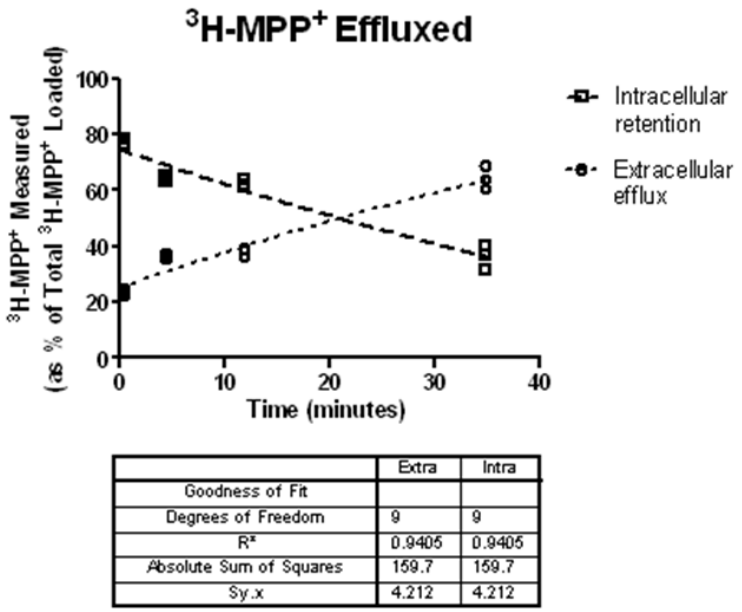

	Extra	Intra
Goodness of Fit		
Degrees of Freedom	9	9
R²	0.9405	0.9405
Absolute Sum of Squares	159.7	159.7
Sy.x	4.212	4.212

B

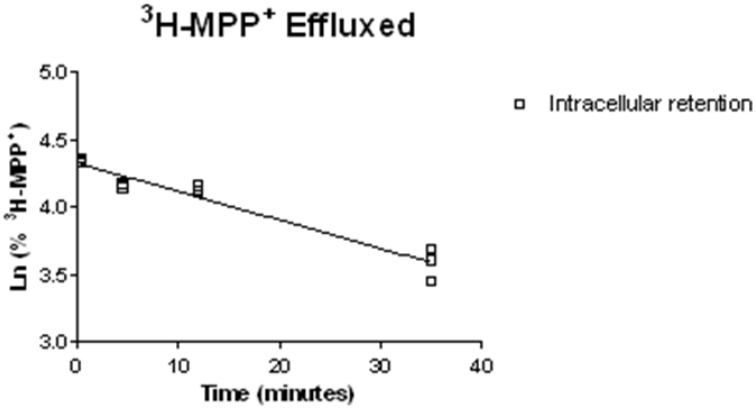

Slope (K constant) = -0.0211 ± 0.0002
R^2=0.9409
P = <0.0001

Figure 3.3 Rate of ^{3}H-MPP$^+$ efflux from PBECs in plates

PBECs were grown in 24 well plates (PBECs-P) until confluent and then underwent ^{3}H-MPP$^+$ efflux assays.

The PBECs were loaded with ^{3}H-MPP$^+$. The loaded cells were then incubated with efflux buffer for the times shown. The buffer was then collected, the cells were lysed, and the buffer and lysate were analysed by liquid scintillation counting. All data were corrected for ^{14}C-sucrose.

The ^{3}H-MPP$^+$ effluxed or retained intracellularly was then expressed as a percentage of the ^{3}H-MPP$^+$ initially loaded into the cells (A). Results of non-linear regression analysis are shown in table.

To calculate the efflux rate constant (K) the intracellular retention data were plotted on an Ln scale (B); the rate of efflux (over the 35 minutes) is shown by the solid line.

All data points collected are shown on the graph, where there are n=3 measurements for each time point.

4.1.4 ^{3}H-MPP^{+} efflux from PBECs on Transwells

To assess whether ^{3}H-MPP^{+} efflux from PBECs is polarised, the ^{3}H-MPP^{+} efflux assay was conducted on PBECs grown on Transwells.

^{3}H-MPP^{+} efflux from PBECs in mono-culture (PBECs-M) or in co-culture with rat astrocytes (PBECs-rAS) was assessed over time. Efflux into both the apical and basal chambers of the Transwells were measured between 30 seconds and 35 minutes, together with the intracellular retention of ^{3}H-MPP^{+}.

The results (Figure 3.4) show decreased intracellular ^{3}H-MPP^{+} with time that begins to plateau within the first 12 minutes for the PBECs-M and PBECs-rAS (Figure 3.4 AIII and BIII). However, when the efflux to the apical and basal chambers were analysed separately, the results showed that for both the PBECs-M and PBECs-rAS, the apical efflux continued to increase after 12 minutes, whereas basal-directed efflux reached a plateau at 12 minutes (Figure 3.4 AI-AII and BI-BII). The apical linear correlation suggests an active process, while the plateau at the basal surface suggests an equilibrative process.

The results showed faster efflux in the PBECs-rAS than PBECs-M, and the half time for total efflux were calculated as 55 minutes and 32 minutes for PBECs-M and PBECs-rAS respectively (Figure 3.4 AIV and BIV). This was not due to greater ^{3}H-MPP^{+} uptake, since the data was corrected for potential differences in uptake by being expressed as a percentage of the total ^{3}H-MPP^{+} loaded per well. Therefore, increases in overall efflux rate may indicate increased efflux transporter activity in the PBECs-rAS.

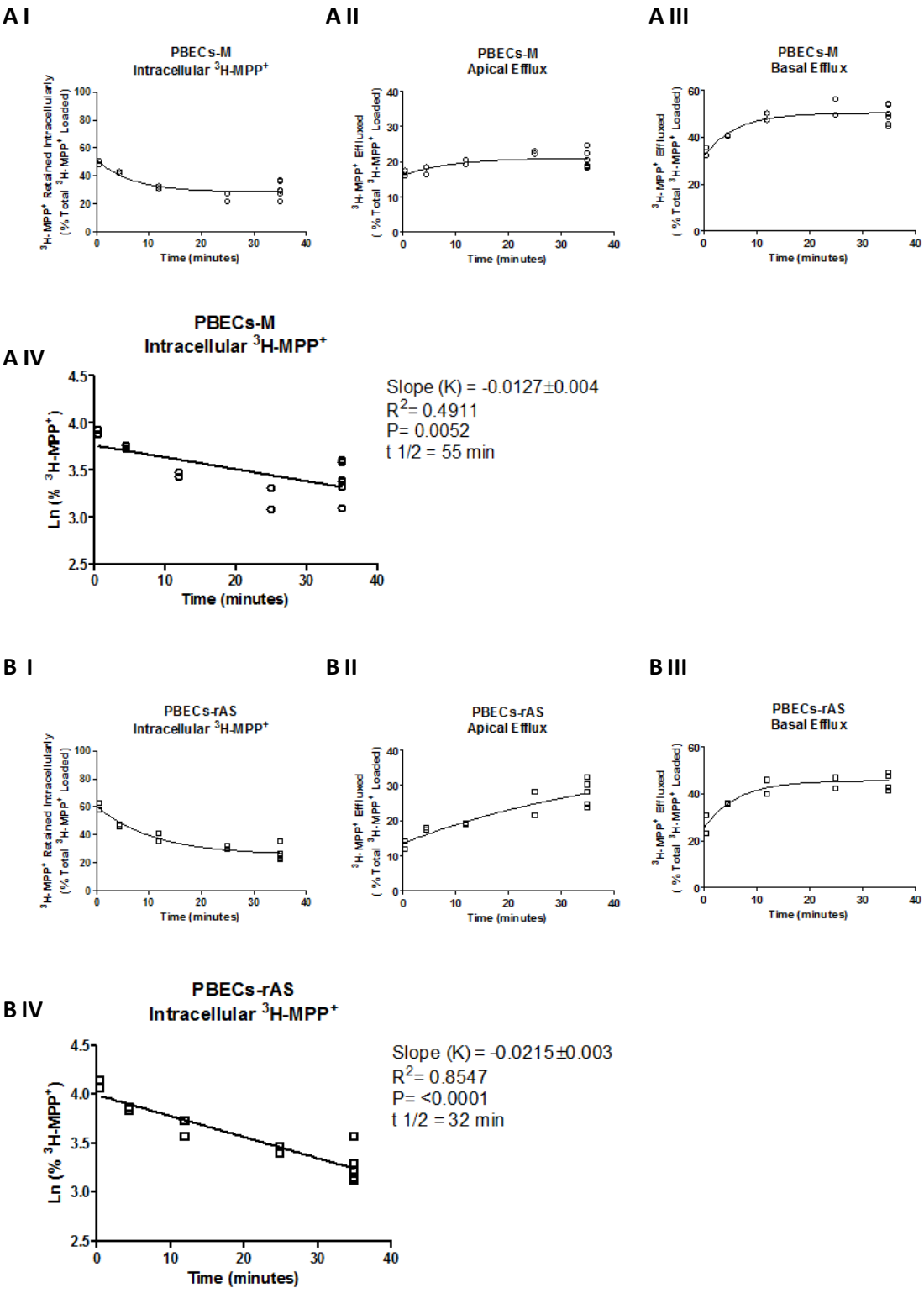

Figure 3.4 Polarised efflux of ^{3}H-MPP$^+$ over time

PBECs were grown on Transwell filters in either in mono-culture (PBECs-M, A) or in co-culture with rat astrocytes (PBECs-rAS, B) for a total of 4 days, before undergoing ^{3}H-MPP$^+$ efflux assays.

The PBECs were loaded with ^{3}H-MPP^{+}. The loaded cells were then incubated with efflux buffer in both the apical and basal chambers of the Transwells for the times shown. The buffers were then collected and analysed separately by liquid scintillation counting for ^{3}H-MPP^{+}. The cell lysate was also analysed by liquid scintillation counting for ^{3}H-MPP^{+}with correction for ^{14}C-sucrose (Intracellular retention).

The ^{3}H-MPP^{+} effluxed apically or basally, or retained intracellularly was then expressed as a percentage of the ^{3}H-MPP^{+} initially loaded into the cells.

I) Intracellular retention, II) Apical efflux, III) basal-directed efflux, IV) Ln Intracellular retention (for rate constant (K) and t ½ analysis) with the rate of ^{3}H-MPP^{+} efflux (over 35 minutes) (shown by the solid line in IV).

The graphs show all the data point collected from a total of 4 experiments together.

To estimate the rates of efflux at the apical and basal surfaces, the efflux constant obtained from the percentage efflux in 35 minutes was divided by the estimated intracellular retention at 17.5 minutes (halfway through the 35 minutes) (extrapolared from the lines drawn in Figure 3.4 IV). The resulting rate constants are given in Table 3.1, which show that there is no differences in the basal rates of ^{3}H-MPP^{+} efflux between PBECs-M and PBECs-rAS, but a greater apical efflux rate of PBECs-rAS together with a greater overall rate (measured from the intracellular retention data). This suggests that the greater rate of efflux in PBECs-rAS is as a result of greater apical efflux with no difference in basal efflux.

This implies that the basal astrocytes are having an effect on the apical surface, but not on the basal surface.

Table 3.1 Rates of efflux

	Efflux rate constant K (min^{-1})		
	Loss of total intracellular pool	**Apical**	**Basal**
PBECs-M	0.013 ± 0.004	0.003± 0.001	0.010 ± 0.003
PBECs-rAS	0.022 ± 0.003 *	0.011 ± 0.001 ***	0.011 ± 0.003

*p <0.05, *** p<0.001 difference in 1-tailed unpaired t-test between PBECs-M and PBECs-rAS

To study the contribution of different efflux transporters to ^{3}H-MPP^{+} efflux, efflux was assessed at a single time, using PBECs-M, PBECs-rAS and PBECs-hAS (PBECs grown in co-culture with human astrocytes).

Before the start of the assay, the integrity of the PBECs' tight junctions (TJs) was assessed using transendothelial electrical resistance (TEER) measurements (Figure 3.5), which showed a barrier was in place under all conditions with average TEER of ~ 200Ω.cm^{2} or greater.

Figure 3.5 TEER measurements of PBECs

PBECs were grown on Transwells either alone in mono-culture (PBECs-M) or in non-contact co-culture with primary rat astrocytes (PBECs-rAS) or human astrocytes (PBECs-hAS).

The chart shows the TEER measurements for the different cultures. For PBECs-M and PBECs-rAS, the cells were kept in serum-free medium for 1 day with TEER measured after this day. For the PBECs-hAS, the cells were kept in serum-free medium for 2 days prior to the assay and TEER measured on the 2nd day.

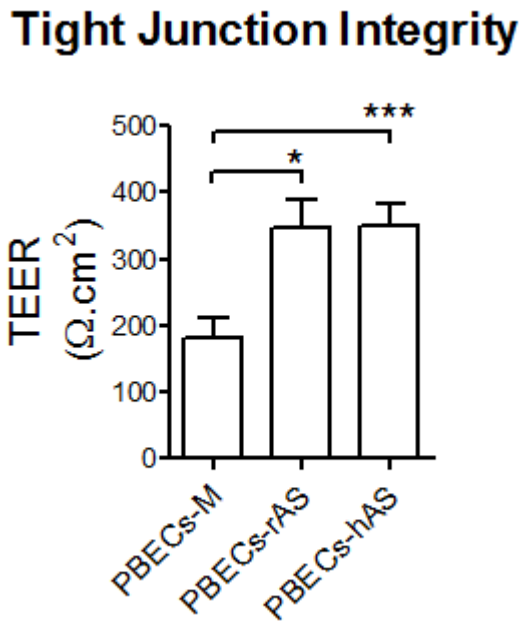

* p<0.05, *** p<0.001 differences between indicated conditions using 1-way ANOVA, Values are mean ± SEM of n=10-34 wells from 3-5 different plates.

For the assay, the efflux time of 35 minutes was used since previous results indicated this to be the approximate apical $t_{1/2}$ of ^{3}H-MPP^{+} efflux for PBECs-M (apical $t_{1/2,}$ total rate) (Table 3.1).

Significant differences in ^{3}H-MPP^{+} efflux were seen between the different PBEC conditions, with the greatest overall efflux shown by PBECs-rAS followed by the PBECs-M and finally by the PBECs-hAS (Figure 3.6C). There was a significant difference in apical efflux, with PBECs-rAS showing greater efflux than the other 2

models (Figure 3.6A). At the basal face PBECs-hAS showed lower basal-directed efflux than the other 2 models (Figure 3.6B).

This indicates that basal astrocytes may exert effects on PBEC efflux capacity at both the apical and basal surfaces.

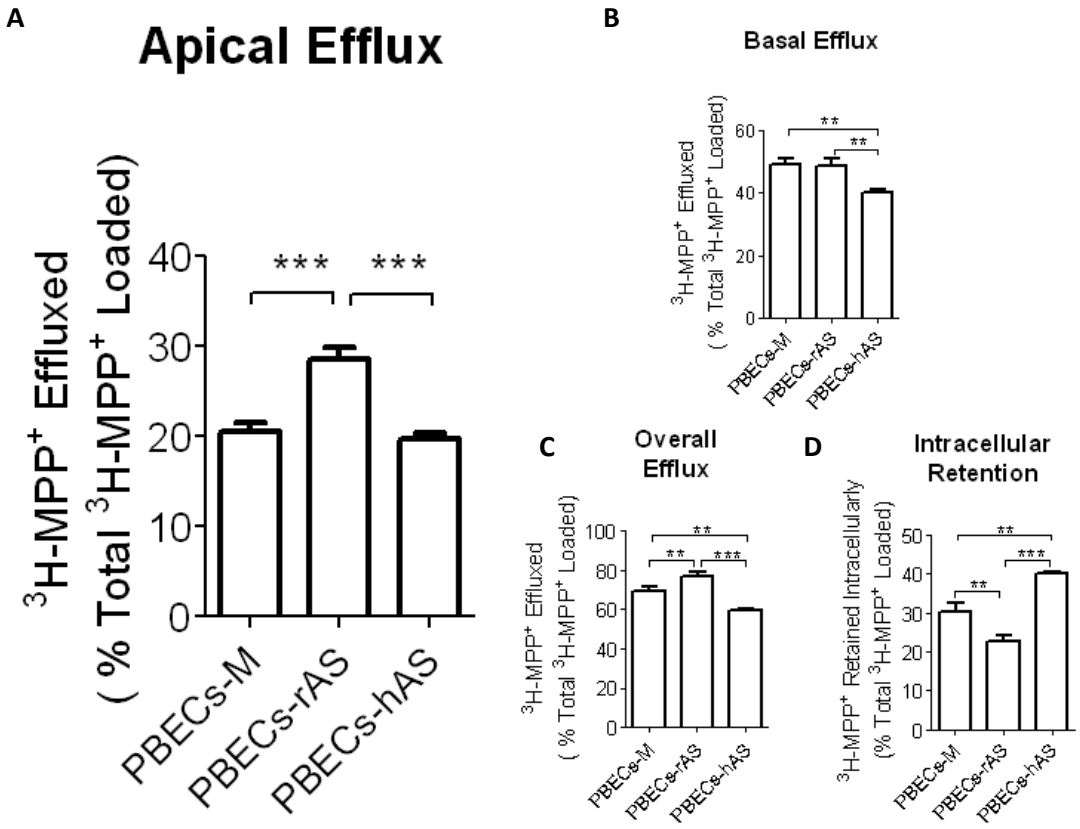

Figure 3.6 Efflux of ^{3}H-MPP$^+$ by PBECs on Transwells

PBECs were grown on Transwells in mono-culture (PBECs-M) or co-culture with either rat astrocytes (PBECs-rAS) for a total of 4 days or in co-culture with human astrocytes (PBECs-hAS) for 2 days, before undergoing ^{3}H-MPP$^+$ efflux assays.

The PBECs were loaded with ^{3}H-MPP$^+$. The loaded cells were then incubated with efflux buffer in both the apical and basal chambers of the Transwells for 35 minutes. The buffers were then collected separately and the cells were lysed. The buffers and lysate (intracellular sample) were analysed by liquid scintillation counting for ^{3}H-MPP$^+$ with correction for ^{14}C-sucrose for the lysate sample.

The ^{3}H-MPP$^+$ effluxed apically or basally were then expressed as a percentage of the ^{3}H-MPP$^+$ initially loaded into the cells, as was the ^{3}H-MPP$^+$ remaining intracellularly (from lysate analysis).

A) Apical efflux, B) basal-directed efflux, C) overall efflux (the sum of the apical and basal efflux), D) intracellular retention.

Values are mean ± SEM of n=4-6 wells from 3-6 experiments using 3-4 different batches of PBECs.

*p<0.05 **p<0.01, ***p<0.001 difference in 1 way ANOVA analysis and Newman-Keuls Multiple Comparison post test

Differences in ^{3}H-MPP^{+} loading between the different PBEC systems were assessed (Figure 3.7) with significant differences measured: The PBECs-rAS showed greater loading than the PBECs-hAS.

Figure 3.7 PBECs on Transwells: ^{3}H-MPP^{+} loading

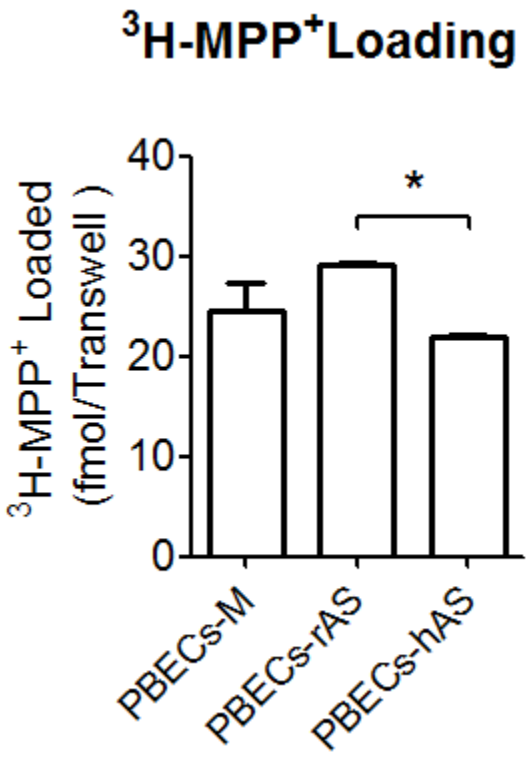

PBECs were grown on Transwells in mono-culture (PBECs-M) or co-culture with either rat astrocytes (PBECs-rAS) for a total of 4 days or in co-culture with human astrocytes (PBECs-hAS) for 2 days.

The PBECs then underwent ^{3}H-MPP^{+} efflux assays, where the ^{3}H-MPP^{+} loaded into the cells was analysed by liquid scintillation counting for ^{3}H-MPP^{+} with correction for ^{14}C-sucrose and expressed as fmol/Transwell.

Values are the mean ± SEM of n=10-34 wells from 3-4 different plates.

* p<0.05 in a 1-way ANOVA analysis with Newman-Keuls Multiple Comparison post test.

Differences in TJ integrity were also shown, where both of the co-culture systems had greater TEERs, indicative of "tighter" TJs, than the PBECs-M (Figure 3.5). This demonstrates that in addition to differences in uptake and efflux characteristics (above), the different PBEC models also differ at the tight-junction level.

4.1.5 Effect of ABC transporter inhibitors on ^{3}H-MPP^{+} efflux

To determine whether ^{3}H-MPP^{+} efflux was due to the activity of ABC transporters, ABC transporter inhibitors were added during the efflux phase of the assay.

Haloperidol (specific non-competitive inhibitor) and verapamil (non-specific competitive substrate) were used to assess Pgp activity, while Ko143 (specific non-competitive inhibitor) and prazosin (non-specific competitive substrate) were used to assess BCRP activity (Weksler *et al.*, 2005, Poller *et al.*, 2008, Matsson *et al.*, 2009, Cioni *et al.*, 2012).

The efflux results (Figure 3.8) showed decreased efflux with increasing concentrations of inhibition. IC_{50} values were calculated as follows: haloperidol 52.48 ± 0.23 µM; verapamil 23.99 ± 0.04 µM, Ko143 0.21 ± 0.26 µM; and prazosin 37.77 ± 0.16 µM (Figure 3.8) (Raw inhibition data is shown in the Appendix Section 9.2). This demonstrated that efflux was at least in part due to the action of both Pgp and BCRP.

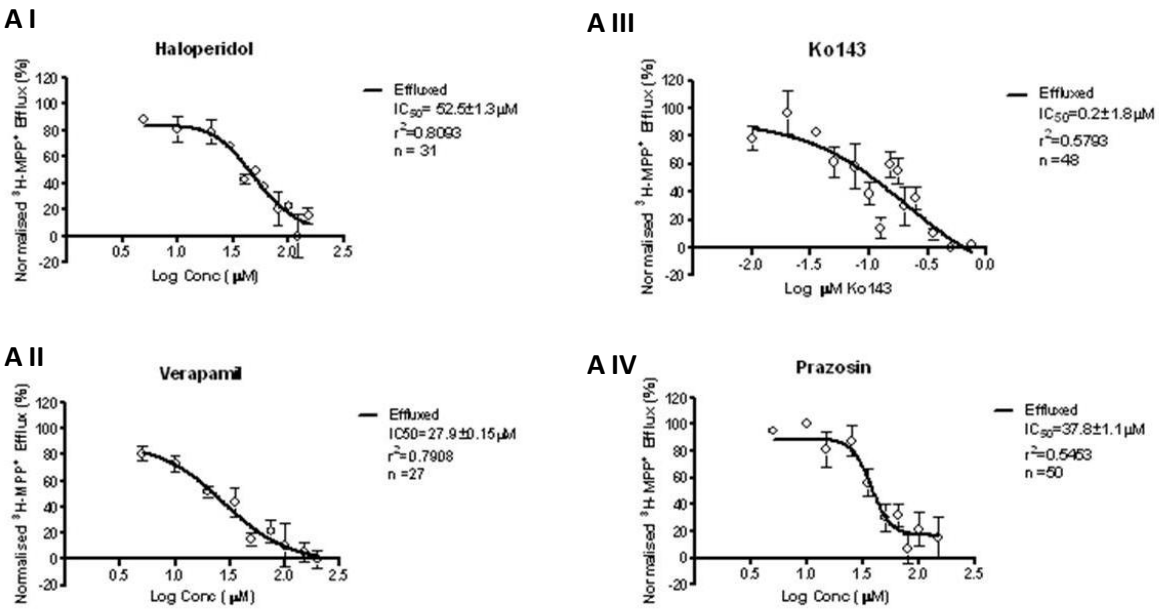

Figure 3.8 Dose Response Inhibition of ^{3}H-MPP^{+} efflux by ABC Inhibitors

The PBECs grown on plates (PBECs-P) were loaded with ^{3}H-MPP^{+}. The loaded cells were then incubated with efflux buffer with or without ABC inhibitors (0 – 300 µM) for 35 minutes. The inhibitors used were the Pgp inhibitors haloperidol (A I) and verapamil (A II), and the BCRP inhibitors Ko143 (A III) and prazosin (A IV).

The buffer was then collected and analysed by liquid scintillation counting for ^{3}H-MPP^{+} with correction for ^{14}C-sucrose.

The ^{3}H-MPP^{+} effluxed was then expressed as a percentage of the ^{3}H-MPP^{+} initially loaded into the cells.

The data were normalised to the minimum and maximum efflux per inhibitor across all the concentrations tested, with the minimum efflux becoming 0% and the maximum efflux becoming 100%.

The values are shown as mean ± SEM of 3-5 wells where possible, or as single point when less than 3 wells were tested at the same concentration. Values are pooled from 3-5 plates.

The dose-response data were also analysed by Lineweaver-Burk plots. The Lineweaver-Burk plots for all the inhibitors gave good linear correlation ($r^2 > 0.7$ for Ko143 ($p<0.0001$), $r^2 > 0.8$ for prazosin ($p=0.0003$), and $r^2 > 0.9$ for haloperidol ($p<0.0001$) and verapamil ($p<0.0001$) (Figure 3.9A), suggesting that, over the concentration ranges tested, the inhibitors were acting on a single binding site (i.e. a single transporter) or that inhibitors may be acting on multiple sites with the same affinity.

Eadie-Hofstee plots were constructed in addition to Lineweaver-Burk plots. The Eadie-Hofstee plots showed linear relationships for all inhibitors at the higher inhibitor concentrations tested, however at the lowest concentrations, where efflux inhibition was not seen (see 3.8), the plot deviated from linear. The inhibitors used here have been previously assessed by Matsson *et al*., (2009) in a study examining the effects of ABC transporter inhibitors known to act on multiple transporters. Matsson *et al*., (2009) showed that prazosin had IC50s of 36 µM for BCRP and 240 µM for Pgp, with a low concentration of Prazosin having no significant effect on Pgp or MRP2 activity (Prazosin did not inhibit MRP2 at any concentration). Similarly, Haloperidol (Pgp IC50 = 39 µM) did not result in inhibition of BCRP or MRP2 activity until concentrations reached greater than 100µM. Ko143 (BCRP IC50 = 0.2 µM), did not affect Pgp or MRP2 activity even at concentrations greater than 1 µM, when BRCP inhibition was

maximal (Matsson *et al*., 2009). This demonstrates that at certain concentrations inhibitors may be transporter specific.

In the current study, the Km values measured using the Lineweaver-Burk plots were similar to the IC_{50} values of the dose-response curves for haloperidol and Ko143 (58.9 µM for Haloperidol and 0.12 µM for Ko143), but the competitive substrates verapamil and prazosin showed Km of approximately twice the IC_{50} values calculated (63.6 µM for prazosin and 66.4 µM for verapamil), which may be a reflection of substrate specificity. Based on these results and similar results within the literature it was concluded that the best concentrations to use were as follows: 60 µM haloperidol, 50 µM verapamil (Fricker *et al.*, 2002), 0.2 µM Ko143 and 35 µM prazosin (Matsson *et al*., 2009).

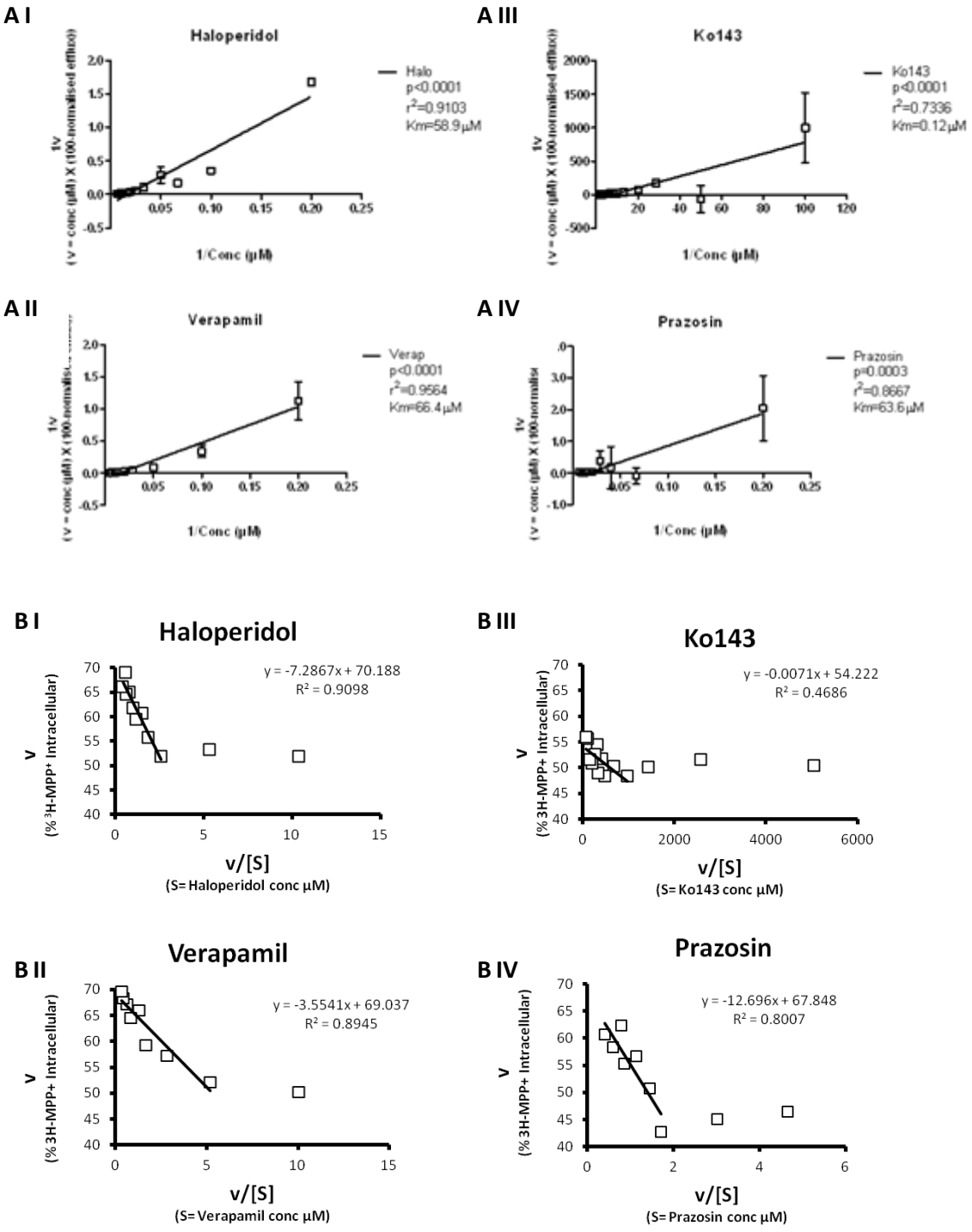

Figure 3.9 Kinetic analysis of dose-response data of ABC Inhibitors

The Lineweaver-Burk Plot analysis of the dose response effects of the ABC inhibitors on ^{3}H-MPP^{+} efflux are shown in A I - IV.

Eadie-Hofstee Plot analysis of the dose response effects of the ABC inhibitors on ^{3}H-MPP^{+} efflux are shown in B I - IV.

To investigate the polarisation of transporters, ^{3}H-MPP^{+} efflux was separately assessed apically and basally with ABC transporter inhibitors, using PBECs grown on Transwells (PBECs-M, PBECs-rAS and PBECs-hAS).

In addition to haloperidol and verapamil (to assess Pgp activity), Ko143 and prazosin (to assess BCRP activity), the MK571 inhibitor, a non-specific inhibitor for the MRP family of efflux transporters, was used at a concentration of 10 µM to assess MRP activity (Weksler et al., 2005, Poller et al., 2008, Matsson et al., 2009, Cioni et al., 2012)**.** Due to the scarce availability of human astrocytes, only Ko143 was tested on the PBECs-hAS.

For the PBECs-M and PBECs-rAS, the results showed inhibitable efflux (i.e. decreased efflux in the presence of inhibitors) by one or both Pgp inhibitors (haloperidol and verapamil) and the BCRP inhibitor prazosin on the apical surface but not on the basal surface, (Figure 3.10). Similarly, for the PBECs-hAS, the Ko143 inhibitor only inhibited efflux on the apical surface and not on the basal surface, suggesting that BCRP-dependent efflux was only present apically. In addition, the inhibitions in apical efflux agreed with increases in the percentage of ^{3}H-MPP^{+} retained intracellularly for the PBECs in co-culture (Figure 3.10 CII and CIII), with significant intracellular retention increases, in the presence of inhibitors, seen for the PBECs-rAS (by haloperidol, verapamil, Ko143 and prazosin) and the PBECs-hAS (by Ko143).

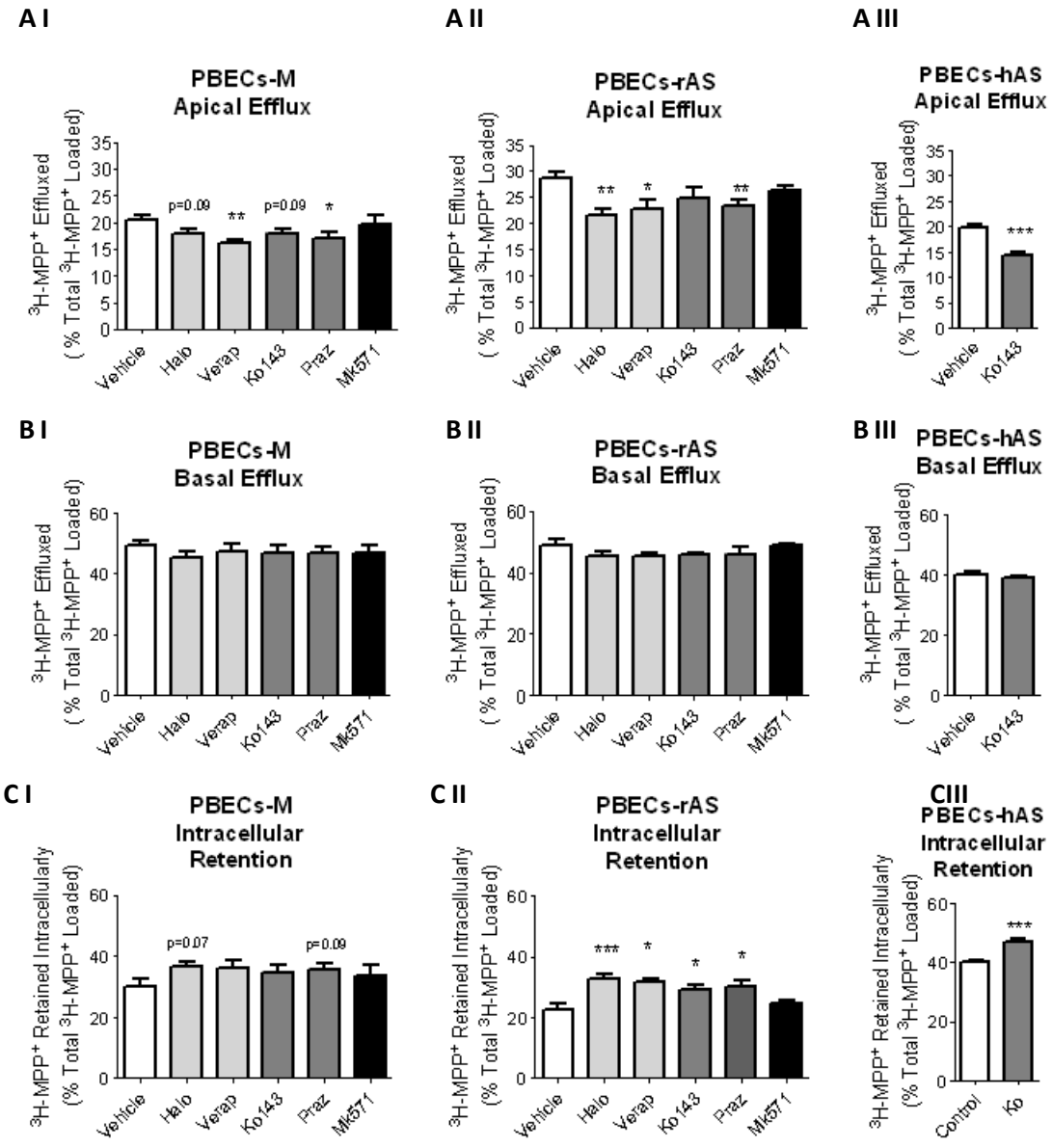

Figure 3.10 Polarised ABC Transporter Activity in PBECs

PBECs were grown on Transwells in mono-culture (PBEC-M, I) or in non-contact co-culture with primary rat astrocytes (PBECs-rAS, II) or human astrocytes (PBECs-hAS, III) before undergoing ^{3}H-MPP^{+} efflux assays.

The PBECs were loaded with ^{3}H-MPP^{+}. The loaded cells were then incubated with efflux buffer containing ABC inhibitors in both the apical and basal chambers of the Transwells for 35 minutes. The inhibitors used were the Pgp inhibitors haloperidol (60 µM) and verapamil (50 µM), the BCRP inhibitors Ko143 (0.2 µM) and prazosin (35 µM) and the non-specific MRP family inhibitor MK571 (10 µM).

The buffers were then collected and the cells were lysed. The buffers and the lysate were analysed by liquid scintillation counting for ^{3}H-MPP^{+} with correction for ^{14}C-sucrose for lysate samples.

The ^{3}H-MPP^{+} effluxed apically or basally were then expressed as a percentage of the ^{3}H-MPP^{+} initially loaded into the cells, as was the ^{3}H-MPP^{+} remaining intracellularly (from lysate analysis).

A) Apical efflux, B) basal-directed efflux, C) intracellular retention.

Values are mean ± SEM of n=3-6 wells from 3-6 experiments using 3-4 different batches of PBECs.

* P<0.05, ** P<0.01, *** P<0.001 significantly different from vehicle control using an unpaired t-test.

Since inhibitors were able to show complementary effects on apical efflux and intracellular retention, the results indicate that the polarised co-cultured PBECs are appropriate tools for measuring ABC transporter activity. However, there was no effect of MK571 inhibitor (10 µM) (Figure 3.10), indicating that no detectable MRP activity was present using this model and method.

To compare the levels of Pgp and BCRP activity between the different systems, the percentage inhibition was assessed for the inhibitors (Table 3.2), with greater inhibition being indicative of greater transporter activity.

Table 3.2 ABC transporter dependent ^{3}H-MPP^{+} efflux

	Inhibitable Pgp-dependent Efflux (% Control)		**Inhibitable BCRP-dependent Efflux (% Control)**		**Inhibitable MRP-dependent Efflux (% Control)**
APICAL	**Haloperidol**	**Verapamil**	**Ko143**	**Prazosin**	**MK571**
PBECs-M	NSD	21.1±2.5	NSD	17.6±3.3	NSD
PBECs-rAS	24.6±2.3*****	20.6±3.3	NSD	17.8±2.0	NSD
PBECs-hAS			**26.7±6.8**		

Inhibitable efflux was calculated as the inhibition of ^{3}H-MPP^{+} efflux in the vehicle control, expressed as a percentage of efflux in vehicle efflux.

*p<0.05 difference in a 1-tailed unpaired t-test between PBECs-M and PBECs-rAS.

NSD = no significant difference.

The results (Table 2) showed greater apical haloperidol-inhibitable efflux in PBECs-rAS than in PBECs-M. Significant apical Ko143-dependent efflux was shown in PBECs-hAS but not the other two conditions. This suggests differences in Pgp and BCRP activity exist between the different PBEC culture formats used.

4.1.6 mRNA expression of the ABC transporters

To analyse the mRNA expression of Pgp and BCRP transporter in PBECs, β-actin and GAPDH were first assessed to determine whether they could be used as reference genes (i.e. if they were good indicators for general gene expression). β-actin is an important component of the cell cytoskeleton and is essential for cell survival. Similarly, GAPDH is a component of glycolysis, an essential process in cell function. Since both genes are essential to cell survival they are constitutively expressed and have been used as reference genes in previous studies on endothelial cells (Yin *et al.*, 2010, Dwyer *et al.*, 2012), with GAPDH regularly used as a reference gene in PBEC studies (Warren et al., 2009, Lemmen *et al.*, 2013)

RNA was isolated at different stages of the PBEC culturing process and was analysed by RT-PCR. The PCR Ct values for both β-actin and GAPDH showed variation across the samples (Figure 3.11). There were significant increases in Ct values after passaging, with greater increases the longer the cells were in culture. A higher Ct indicates lower levels of RNA since more PCR cycles of amplification are required to reach the cycle of threshold (Ct). Therefore the results suggest that both β-actin and GAPDH mRNA levels decrease after passaging, with greater decreases in later stages of the cell culture process. However, there was a good correlation between the β-actin and GAPDH Cts (R^2=0.9917, $p<0.0001$) (Figure 3.12), suggesting that both these "house-keeping" gene were altered in approximately the same proportions, indicating common changes in gene expression. Hence, these genes appear to be good measures of generalised gene expression and were used as reference genes in further work. However, it should be noted that despite the good correlation, GAPDH Ct values were consistently lower than those of β-actin, indicating higher expression of GAPDH than β-actin.

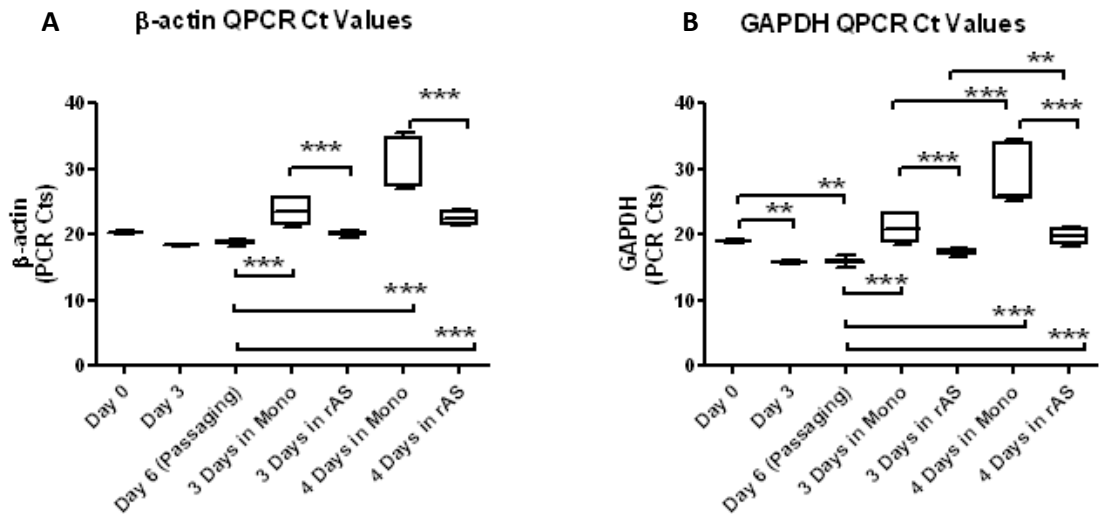

Figure 3.11 β-actin and GAPDH Ct (cycle of threshold) values from RT-QPCR experiments

The results show the Ct values for β-actin (A) and GAPDH (B) RNA from RT-QPCR experiments conducted on RNA collected from PBECs at different stages of the cell culture process.

Day 0 represents the primary isolated porcine capillaries. The PBECs were grown out from the capillaries for up to 6 days (the first 3 days in puromycin containing medium). RNA was isolated after the 3 days of puromycin treatment (Day 3) and on day 6 when the cells were passaged to Transwells (Day 6).

Once on Transwells, the PBECs were either grown alone (i.e. in mono-culture, Mono) or in co-culture with primary rat astrocytes (rAS). The PBECs, in either mono-culture or in co-culture with the rAS, were grown on the Transwells for 3 days in serum-containing medium after which RNA was isolated (3 Days in Mono or 3 Days in rAS). Alternatively, the PBECs, in either mono-culture or in co-culture with the rAS, were grown on the Transwells for 3 days in serum-containing medium, followed by 24 hours in serum-free medium containing 550 nM hydrocortisone, 250 µM CPT-cAMP and 17.5 µM Ro-20-1724, before RNA isolation (4 Days in Mono or 4 Days in rAS).

The Ct values obtained per condition are expressed as box and whisker plots, showing the range of Ct obtained per sample type. Values were obtained from 3 samples per condition, where PCR was conducted on triplicates per plate and n=3 plates were run.

** $p<0.01$, *** $p<0.001$ significance in unpaired 2 tailed t-test.

Figure 3.12 Correlation of β-actin and GAPDH

The graph shows the correlation of Ct values of β-actin and GAPDH RNA from RT-QPCT experiments conducted on RNA collected from PBECs at different stages of the cell culture process.

Each point shows the average Ct of a single sample; PCR experiments were conducted in triplicates of a sample per plate and 3 plates were run.

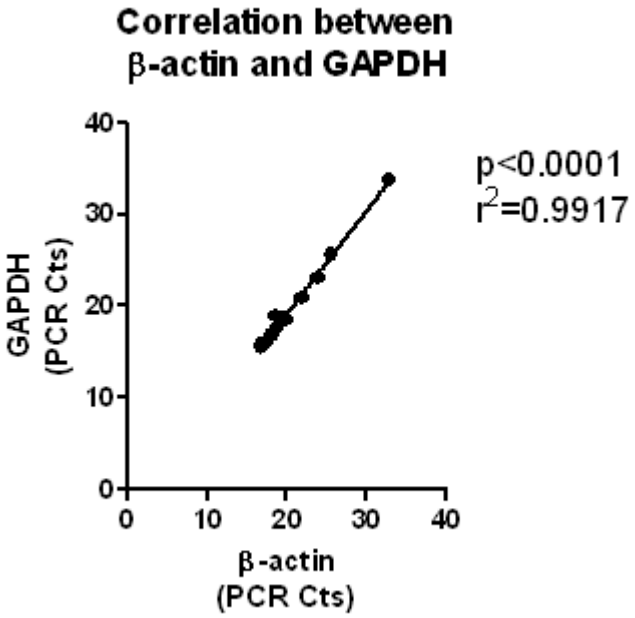

To assess the expression of Pgp and BCRP, the RNA samples collected previously underwent RT-QPCR with either Pgp or BCRP primers, with resulting Ct values normalised against the reference genes (β-actin and GAPDH) (Pgp and BCRP Ct values obtained from the different samples are shown in the Appendix Section 9.4) .

The results indicate that the Pgp and BCRP mRNA levels in the capillaries (Day 0) were significantly greater than after the cells had been in culture (Figure 3.13). This is consistent with other work showing transporter expression decreases in primary cell culture (Torok et al., 2003).

The mRNA levels of Pgp and BCRP in the cells after 3 days in puromycin (Day 3) and on the Day of Passaging were not significantly different, indicating that the removal of puromycin from the medium did not change the expression of efflux transporters (Figure 3.13). However, changes in mRNA levels were seen after the PBECs were passaged to Transwells. Firstly, Pgp mRNA levels were significantly increased by 2.7 or 3.3 fold (depending on the reference gene used) after 3 days on the Transwells, when PBECs had reached confluence (Figure 3.13).

For mRNA levels after 4 days on Transwells, the results were inconclusive, with normalisation against β-actin showing no change in Pgp mRNA levels from the Day of

Passaging, but normalisation against GAPDH showing increased mRNA levels (3.5 fold compared to the Day of Passaging, similar increases to those shown after 3 days on the Transwells) (Figure 3.13).

No changes in BCRP mRNA were shown after 3 days on Transwells, however significant increases in BCRP levels were noted after 4 days on Transwells (3.5 fold or 5.3 fold, depending on the reference gene used) (Figure 3.13).

This implied that mRNA changes for Pgp occurred within 3 days, while BCRP changes in mRNA required the fourth day of growth, at which time the fold change in BCRP mRNA was greater than that of Pgp. This may be indicative of different transcriptional times required by the two different ABC genes or differential effects of using serum-free medium for 24 hours.

No significant differences between PBECs in mono-culture and in co-culture with rat astrocytes were detected suggesting equal levels of Pgp and BCRP mRNA transcription within these systems (Figure 3.14 and Figure 3.15). Therefore, any differences in activity (shown previously) are likely to be due to post-transcriptional events of the gene-expression process.

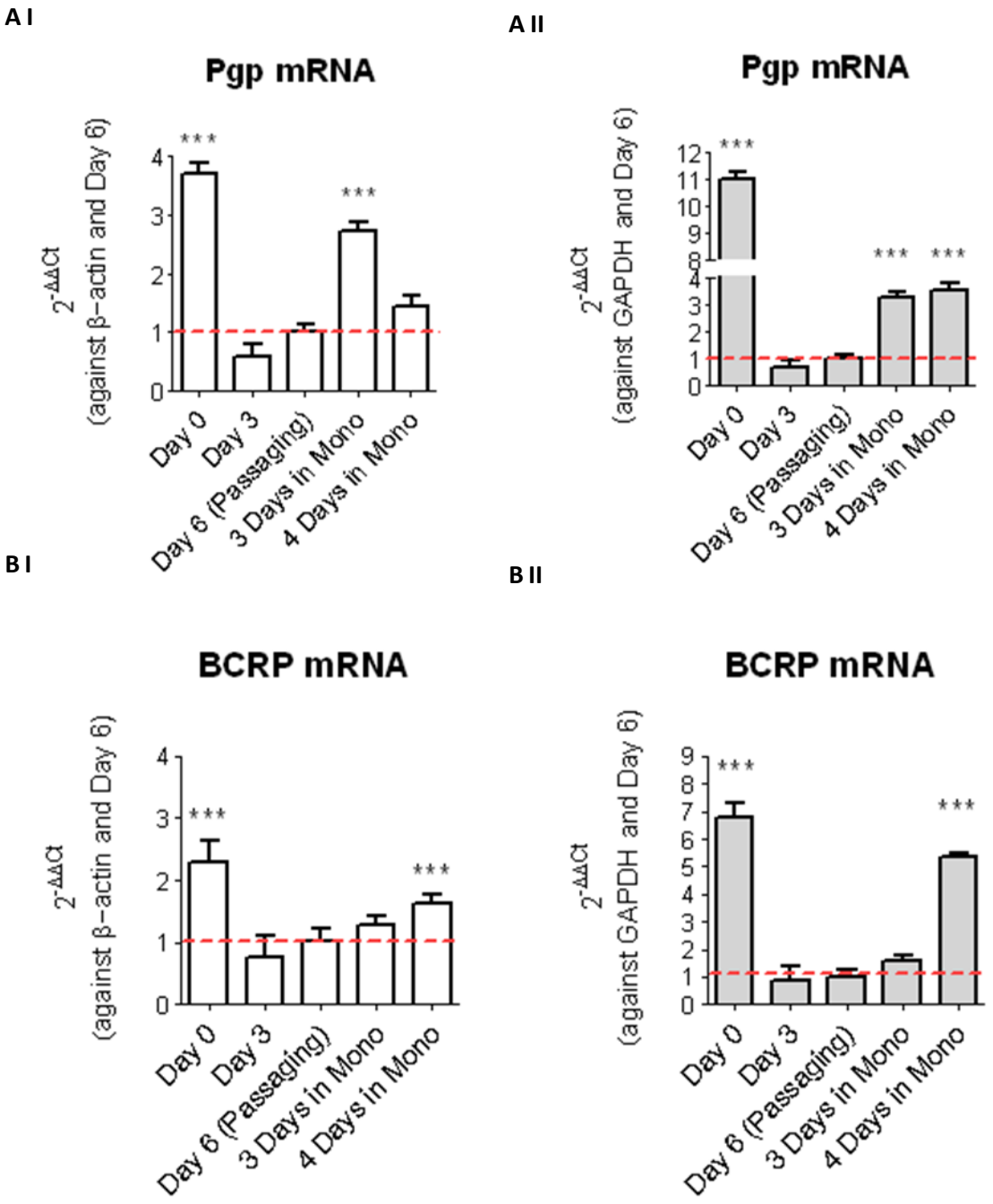

Figure 3.13 mRNA levels of Pgp and BCRP throughout the cell culture process

Total RNA was isolated from PBECs grown on Transwell filters in mono culture. The RNA underwent RT Q-PCR using Pgp (A) or BCRP (B) primers.

Ct values obtained per gene per sample were normalised against either β-actin (light bars, I) or GAPDH (dark bars, II) Ct values obtained for the sample (to give the ΔCt) then further normalised against the average ΔCt at Day 6 to give the ΔΔCt, which was then used to calculate the fold change $2^{-\Delta\Delta Ct}$ shown above.

Day 0 represents the primary isolated porcine capillaries. The PBECs were grown out from the capillaries for up to 6 days (the first 3 days in puromycin-containing medium). RNA was isolated

after the 3 days of puromycin treatment (Day 3) and on day 6 when the cells were passaged to Transwells (Day 6).

Once on Transwells, the PBECs were grown alone (i.e. in mono-culture) for 3 days in serum-containing medium after which RNA was isolated (3 Days in Mono). Alternatively, the PBECs, were grown on the Transwells for 3 days in serum-containing medium, followed by 24 hours in serum-free medium containing 550 nM hydrocortisone, 250 µM CPT-cAMP and 17.5 µM Ro-20-1724, before RNA isolation (4 Days in Mono)

Values are mean ± SEM of n=3 samples per condition, where PCR was conducted on triplicates per plate and n=3 plates were run.

** $p<0.01$, ***$p<0.001$ difference in unpaired 2 tailed t-test to Day 6

Figure 3.14 Pgp and BCRP mRNA levels of PBECs after 3 days on Transwells

Total RNA was isolated from PBECs grown on Transwell filters either in mono culture (Mono) or co-culture with normal rat astrocytes (AS) for a total of 3 days in serum-containing medium. The RNA underwent RT Q-PCR using Pgp (A) or BCRP (B) primers.

Ct values obtained per gene per sample were normalised against either β-actin (light bars, I) or GAPDH (dark bars, II) Ct values obtained for the sample (to give the ΔCt) then further normalised against the average ΔCt of the mono-cultured cells to give the ΔΔCt, which was then used to calculate the fold change $2^{-\Delta\Delta Ct}$ shown right.

Values are mean ± SEM of n=3 samples per condition, where PCR was conducted in triplicates per plate and n=3 plates were run.

No significant differences in unpaired 2 tailed t-test

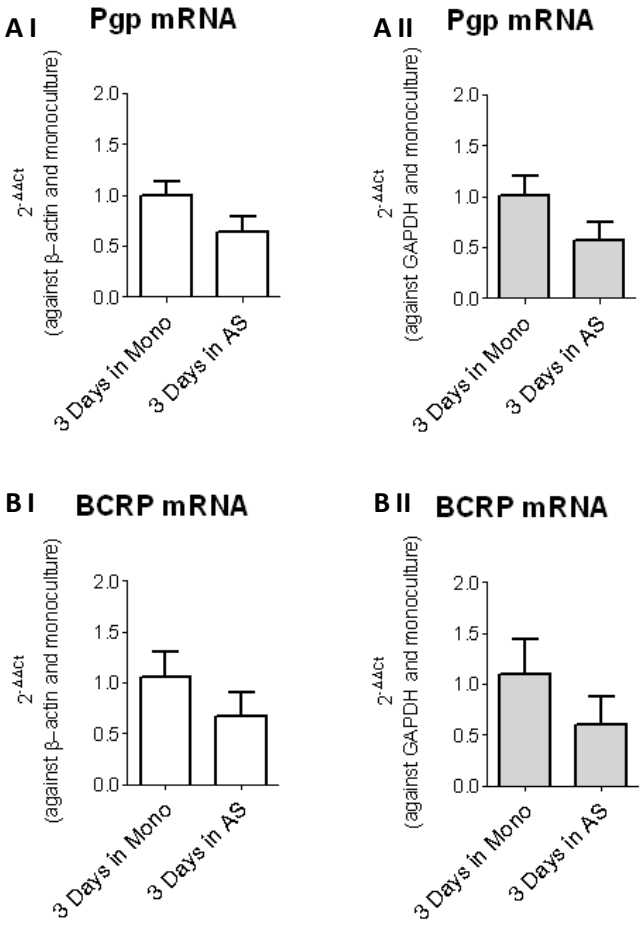

Figure 3.15 Pgp and BCRP mRNA levels of PBECs after 4 days on Transwells

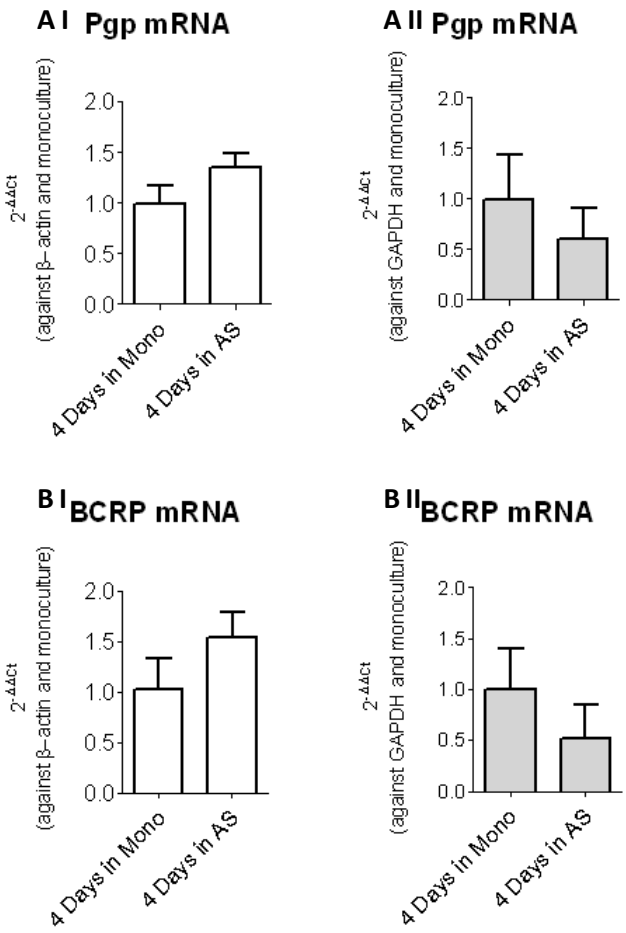

Total RNA was isolated from PBECs grown on Transwell filters either in mono culture (Mono) or co-culture with normal rat astrocytes (AS) for a total of 4 days (3 days in serum-containing medium and a further day in serum-free medium with 550 nM hydrocortisone, 250 µM CPT-cAMP and 17.5 µM Ro-20-1724).

The RNA underwent RT Q-PCR using Pgp (A) or BCRP (B) primers.

Ct values obtained per gene per sample were normalised against either β-actin (light bars, I) or GAPDH (dark bars, II) Ct values obtained for the sample (to give the ΔCt) then further normalised against the average ΔCt of the mono-cultured cells to give the ΔΔCt, which was then used to calculate the fold change $2^{-\Delta\Delta Ct}$ shown right.

Values are mean ± SEM of n=3 samples per condition, where PCR was conducted in triplicates per plate and n=3 plates were run.

No significant differences in unpaired 2 tailed t-test

4.2 Discussion

Initial studies were conducted to find a suitable BBB model that would enable comparisons between BBB efflux transporter activities in different culture conditions, for later use with a glioma cell co-culture.

Focus was initially placed on the "normal" conditions as detailed in this chapter.

The primary porcine brain endothelial cells (PBECs) used have been shown to maintain the characteristics of the BBB *in vivo*, with "tight" TJ formation (measured by high transendothelial electrical resistance and low paracellular substrate transport (Cohen-Kashi Malina *et al.*, 2009, Patabendige *et al.*, 2013a, Patabendige *et al.*, 2013b). In addition, PBECs have been shown to have a similar expression pattern of ABC transporters to the human BBB (Warren et al., 2009), which is of particular importance when addressing the aim of studying the ABC efflux transporters (in normal and glioma conditions). Together this indicated that PBECs would be a good model for the study.

To optimise the PBEC model to better suit the aim of the overall study, different culture conditions were considered: PBECs grown on Transwells and in non-contact co-culture with astrocytes. Transwells allow separate apical and basal surface analysis that is more representative of the *in vivo* BBB, and several studies have shown that co-culture of endothelial cells with rat astrocytes helps to induce and maintain features of the *in vivo* BBB. Furthermore, human astrocytes were used to assess the suitability of a humanised model.

In addition, the ^{3}H-MPP efflux assay was developed to assess the activity of ABC efflux transporters within the different PBEC conditions.

4.2.1 Differences in ^{3}H-MPP^{+} Loading

Significant differences in the amount of ^{3}H-MPP^{+} loaded between PBECs-rAs and PBECs-hAS were shown in the study, indicating different influences of these astrocytes on the uptake of ^{3}H-MPP^{+} by these models (Figure 3.7).

Uptake of ^{3}H-MPP^{+} has been previously studied in brain endothelium. Early studies by Martel *et al.* (2001), showed uptake of ^{3}H-MPP^{+} into RBE4s (immortalised rat

endothelial cell line) to be Na^+- independent, energy dependent and pH dependent. The study further showed uptake of ^{3}H-MPP$^+$ was not affected by OAT inhibitors but was inhibited by OCT inhibitors, inhibiting either OCT1 or OCT2, both of which had been shown to be expressed in RBE4 cells. Liou *et al.* (2007) showed inhibition of OCT1 decreased ^{3}H-MPP$^+$ uptake into primary rat brain endothelial cells (RBECs), although the study of OCT2 and OCT3 effects were not possible since the RBECs were not shown to express these transporters. Together the studies implicate the OCT family of transporters in the transport of ^{3}H-MPP$^+$ at the BBB.

Lin *et al.* (2010), showed that OCT1 and OCT2 are expressed mainly apically in human and rat microvessels. This apical expression agreed with the earlier Martel et al. (2001) study that found that only ^{3}H-MPP$^+$ transport in the apical to basal direction was subject to inhibition by OCT inhibitors. Together this shows that uptake of ^{3}H-MPP$^+$ occurs via OCT transporters on the apical surface of the BBB.

In addition, unpublished work by the BBB group at King's College London (2008) has shown the activity of OCT transporters in PBECs, where MPP$^+$ uptake in PBECs was inhibited by OCT1/2 inhibitors.

Taken together, this suggests the differences in loading between PBECs-rAS and PBECs-hAS noted here (Figure 3.7) indicate different levels in the activity/expression of these uptake transporters within the different systems.

It should be noted that any differences in loading will not affect efflux, as results were expressed as a percentage of the total ^{3}H-MPP$^+$ loaded. In addition, during the course of the experiment the concentration of extracellular ^{3}H-MPP$^+$ is much lower than the intracellular concentration, so the concentration gradient favors efflux, even if loading is lower in the PBECs-hAS.

Also, experiments have shown that the OCT uptake transporters do not significantly contribute to efflux, with inhibition of OCTs by amantadine (OCT1/2 inhibitor) during the course of a ^{3}H-MPP$^+$efflux assay yielding no difference in ^{3}H-MPP$^+$ efflux compared with control (See Appendix Section 9.3). Therefore, OCT uptake transporters do not play a significant role in efflux of ^{3}H-MPP$^+$ in this model.

4.2.2 Differences in ^{3}H-MPP^{+} efflux

Differences between the different PBEC culture systems were shown when examining the efflux of ^{3}H-MPP^{+}.

Firstly, differences in the initial rates of ^{3}H-MPP^{+} efflux from PBECs-P and PBECs-M were seen, with slower efflux when cells were on Transwells (i.e. PBECs-M). The different rates of efflux could be due to differences in exposed surfaces, where the polarisation effect (i.e. creation of both apical and basal surfaces) caused by the use of Transwells decreased the rate of overall efflux. However, it should be noted that the efflux rate of the PBECs-rAS was similar to the efflux rate shown by the PBECs-P. This indicates that the PBECs-P are also a good model for the study of apical efflux.

Differences in the media used could also have contributed to the differences in efflux between PBECs-P and PBECs-M, with the latter having the medium changed to serum-free medium with hydrocortisone, CPT-cAMP and Ro-20-1724 supplements for the last 24 hours of culture. The use of hydrocortisone, CPT-cAMP and Ro-20-1724 correlated with increases in the mRNA expression levels of BCRP here (Figure 3.13) and are also implicated in Pgp and MRP mRNA changes by Perriere *et al.* (2007). Therefore, medium differences may have affected the efflux, contributing to the slight differences seen, i.e. PBECs-M had slower initial $t_{1/2}$ than the PBECs-P.

Differences in the use of hydrocortisone, CPT-cAMP and Ro-20-1724 could not explain differences in efflux noted between the PBECs-M and the PBECs-rAS, since both cultures were exposed to hydrocortisone, CPT-cAMP and Ro-20-1724. In spite this, differences were noted. Higher TEER, indicative of tighter TJs in the PBECs-rAS were seen (Figure 3.5). This is in agreement with a number of studies showing that co-culturing endothelial cells with astrocytes improves tight junction formation, increasing TEER and decreasing paracellular permeability (Gaillard *et al.*, 2001, Tan *et al.*, 2001, Helms *et al.*, 2010, Patabendige et al., 2013a).

Comparing co-cultured and mono-cultured PBECs, the PBECs-rAS were shown to have higher rates of ^{3}H-MPP^{+} efflux than PBECs-M (Figure 3.4). Furthermore, efflux from the apical surface was greater in PBEC-rAS in single-time point experiments (Figure 3.6), with no differences in basal efflux. Together this indicates that the factors regulating efflux may be greater in the co-culture system.

The transporters at least partially responsible for the efflux of ^{3}H-MPP^{+} were shown here to be Pgp and BCRP (Figure 3.10). Results showed more conclusive Pgp and BCRP activity in the astrocyte co-culture compared to monoculture, with ABC transporter inhibition of efflux correlating with increased intracellular retention of ^{3}H-MPP^{+} (Figure 3.10 and Table 3.2). Although MPP^{+} is positively charged, it has a $logD_{7.4}$ of 0.5, similar to other known ABC transporter substrates (e.g. Taurocholate $logD_{7.4}$ of 0.1, Quercetin $logD_{7.4}$ of 1.0, Bromosulfalein $logD_{7.4}$ of 0.4 and doxorubicin $logD_{7.4}$ of 0.2 (Matsson *et al*., 2009). Furthermore, Bleasby *et al.,* (2000), suggested the possibility that MPP+ was sufficiently lipophilic to passively diffuse across cell membranes. Further, Tsinman *et al*, 2011 showed that bases can traverse porcine plasma membranes effectively, with results correlating well with rodent in situ brain perfusions, demonstrating that basic compounds (such as MPP+) can cross lipid membranes despite their positive charge. Together this suggests that MPP+ is sufficiently lipophilic to interact with the ABC-efflux transporter active sites located within the hydrophobic transmembrane regions of the ABC transporters (Nervi *et al,* 2010).

Several studies have shown that co-culturing endothelial cells with rat astrocytes leads to up-regulation of Pgp mRNA, protein and activity. Gaillard *et al.* (2000), compared primary bovine brain endothelial cells (BBECs) in mono-culture with 50% astrocyte-conditioned medium, with BBECs in contact co-culture with rat astrocytes, showing that in co-culture Pgp protein expression increased together with increased Pgp activity (vinblastine exclusion assay and daunorubicin transport). Similarly, Dohgu *et al.* (2004) using a mouse BBB model, compared mono-cultured endothelial cells and astrocyte contact co-cultured endothelial cells and showed increased Pgp activity in the astrocyte co-culture system from Rhodamine123 (Rho123) accumulation assay. Xue *et al.* (2013) also showed increased Pgp protein expression when endothelial cells were in contact co-culture with astrocytes when compared to endothelial cells in mono-culture.

Many earlier findings on the effects of astrocytes have come from contact co-culture (above), however the results here are using a non-contact co-culture system, since it allows for straight forward comparisons of mono-cultured cells with co-cultured cells. It is not possible to rigorously compare transport through two layers of cells (contact-co-culture) with transport through one layer of cells (mono-culture or non-contact co-culture), since the underlying cell layer of astrocytes could itself alter the flux of substrates, especially since astrocytes have been shown to express low levels of Pgp and BCRP (Ballerini *et al.*, 2002, Hirrlinger *et al.*, 2005). In addition, since the overall aim of the project involves the assessment and therefore use of glioma cells, and since

gliomas have been reported to express extremely high levels ABC efflux transporters (Sharom, 2008, Decleves *et al.*, 2008), the use of glioma in a contact-co-culture would likely alter the transport flux of a substrate. For such reasons focus was placed on non-contact co-culture models in the current study.

The results obtained in the current study differ from the studies reported above in some respects. In the current study, the non-contact co-culture model did not show any significant differences in mRNA levels between the PBECs-M and the PBECs-rAS. However, the activity results were more conclusive in both the co-culture models than in the mono-culture model. PBECs-M showed no significant changes in intracellular retention of ^{3}H-MPP^{+} upon addition of inhibitors, despite significant inhibition of apical efflux, while PBECs-rAS did (Figure 3.10). This, together with the observed increased efflux rates (Figure 3.4) and greater apical efflux but no difference in basal efflux (Figure 3.6) suggests greater activity of ABC transporters in the co-cultured model, despite no increase in mRNA levels being detected (Figure 3.13 and Figure 3.14). Therefore the results indicate that Pgp and BCRP activity can be increased by non-contact co-culture with astrocytes independently of increases in mRNA levels of the ABC transporters. Whether this is via post-transcriptional effects or other factors, e.g. greater tight-junction integrity in the PBECs-rAS leading to more polarised transporter expression is unclear. However, since this is a non-contact model, it does suggests that any effects are a result of diffusible factors, secreted by the astrocytes or by the PBECs themselves as a response to the presence of astrocytes.

Increases in Pgp activity have also been shown in other non-contact co-culture models Cohen-Kashi Malina et al. (2009) compared PBECs in mono-culture, contact co-culture and non-contact co-culture, and although significant increases in Pgp activity could only be seen when comparing the contact co-culture with mono-culture, the non-contact co-cultured PBECs showed Pgp activity level similar to that of the contact co-culture model.

Both protein and mRNA levels were assessed in Lim *et al.* (2007), where RBECs in mono-culture and in non-contact co-culture with astrocytes were compared. The results showed increased mdr1a mRNA and Pgp protein levels as well as a higher ratio of Pgp activity (although activity was not significant), showing that similar effects on Pgp transporter mRNA levels can be achieved using contact and non-contact co-culture. However, it should be noted that in this study, co-culture with astrocytes occurred over 9 days, compared to the current study where co-culture with the rat astrocytes was for 4 days. This suggests that in the short term (up to 4 days) ABC transporter activity is

regulated post-transcriptionally via diffusible factors, however in the long term (9 days) the diffusible factors may induce mRNA changes as well.

In the study by Perriere et al. (2007), where ABC transporter mRNAs from RBECs in mono-culture were compared with mRNAs from RBECs in optimised non-contact astrocyte co-culture, the co-culture conditions showed increased mdr1a mRNA (not significant), increased BCRP mRNA and decreased mdr1b, showing that BCRP mRNA levels can also be elevated in non-contact co-culture. However, in the Perriere et al. (2007) study a simple mono-culture model was compared to a highly optimised co-culture model, where medium differences may have played a role. In the optimised model, hydrocortisone, CPT-cAMP and Ro-20-1724 were used together with the addition of astrocytes, which was compared to a mono-culture without hydrocortisone, CPT-cAMP and Ro-20-1724. In the current study, the use of hydrocortisone, CPT-cAMP and Ro-20-1724 correlated with the mRNA increases in BCRP (Figure 3.13, Day 4). Therefore, increases in mRNA levels shown by Perriere et al. (2007), may be due to the addition of hydrocortisone, CPT-cAMP and Ro-20-1724 and not solely due to the presence of astrocytes.

Considering MRP activity, in-house evidence suggested that ^{3}H-MPP^{+} is effluxed via MRPs (BBB Group King's College London, 2008, Unpublished). However, no inhibitable MRP activity was detected in the current study. This may indicate that the assay used is not sensitive enough to detect MRP activity changes.

A similar study using daunorubicin (also a common substrate of Pgp, BCRP and MRPs), was unable to show MRP activity in 3 hours, but could after 24 hours, suggesting that MRP efflux is slow, and may require longer times to see its effects (Perriere et al., 2007). However, as some studies have shown suppression of endothelial MRP expression by astrocyte co-culture (Regina *et al.*, 1998), the undetectable contribution of MRP activity in the PBECs in astrocyte co-culture systems could have reflected such suppression in the PBEC system (Figure 3.10). Early work by Seetharaman *et al.* (1998) indicated that MRP1 is weakly detected in human brain microvessels and only appears in culture, suggesting that its expression is suppressed *in vivo*.

It is also clear that astrocytes from different species have different effects on the PBECs, with PBECs-hAS showing higher BCRP activity (Ko143-dependent efflux, Table 3.2) than PBECs-rAS. However, higher overall efflux was achieved by the PBECs-rAS (Figure 3.6) suggesting that other factors/transporters involved in efflux may be more active in the PBECs-rAS. It should be noted that the culture conditions

between the two systems were different. The PBECs-rAS were co-cultured for a total of four days, with the final day in serum-free PBEC medium with hydrocortisone, CPT-cAMP and Ro-20-1724. By contrast, the PBECs-hAS were only in co-culture for two days, both days in serum-free PBEC medium with hydrocortisone, CPT-cAMP and Ro-20-1724. The prolonged exposure of PBECs-rAS to the rat astrocytes could have led to the greater expression of more than one efflux transporter (indicated by the greater overall efflux). Moreover, the longer time spent in hydrocortisone, CPT-cAMP and Ro-20-1724 medium by the PBECS-hAS may have led to higher levels of BCRP specifically.

Perriere et al. (2007) did show more significant elevation in BCRP mRNA than in Pgp mRNA as a result of hydrocortisone, CPT-cAMP and Ro-20-1724. Increases in Pgp mRNA were inconclusive since a rodent model was used, where two genes control expression of Pgp (mdr1a and mdr1b) and the only significant increases in mRNA were for the mdr1b gene (Perriere et al., 2007). Interestingly, the pig and human MDR1 genes (the sole genes responsible for Pgp expression in the porcine and human BBB) share more homology with the mrd1a gene (Smith *et al.*, 1998). Furthermore, the regulation of human MDR1 has been shown to be similar to the mdr1a (and not 1b) gene via p53 (Thottassery *et al.*, 1997). Therefore, is it not clear how hydrocortisone, CPT-cAMP and Ro-20-1724 would affect pig MDR1 expression, with the results obtained in this study also being inconclusive (showing either a decrease or no change in Pgp mRNA (Figure 3.13, Day 4).

Finally, there is the question of the species-specificity of any astrocytic effects. Human astrocytes have been used in BBB co-culture models previously, but this was in co-culture with human BBB models (Cucullo *et al.*, 2007, Hatherell *et al.*, 2011), and no comparison was made between the influence of rat and human astrocytes. It is clear that further work needs to be done to clarify the extent to which astrocyte-endothelial influences on ABC transporters in species-specific.

4.2.3 PBECs as a tools for further study

It should be mentioned that the polarity of Pgp and BCRP activity observed in all the cultures was apical (Figure 3.10), which is in agreement with the literature, where there is a consensus that these transporters are found on the luminal/apical blood-facing surface (Beaulieu *et al.*, 1997, Eisenblatter *et al.*, 2003, Begley, 2004, Roberts *et al.*,

2008). In this respect, all the models used in the current study are good tools for the assessment of ABC transporter activity *in vitro*, although the co-culture models did show more consistent results.

One of the aims of this phase of the current study was to establish the baseline/reference conditions before moving to examine co-culture of PBECs with glioma cells. Co-culture of PBECs with normal astrocytes did alter Pgp and BCRP activity. Hence, to distinguish glioma effects from normal astrocytic effects, glioma co-culture cannot be compared with mono-culture, but must instead be compared with an astrocyte co-culture system. Therefore the choice of an appropriate “normal” BBB condition depends on the type of glioma model used, and the control species will have to match as closely as possible the glioma model.

Furthermore, since the results suggested that different species of astrocytes may have differential effect on PBECs, comparisons of glioma co-culture should be species-specific, i.e. rat glioma compared with rat astrocytes and human glioma compared with a human astrocyte system. Therefore the choice of appropriate ‘normal’ BBB condition depends on the type of glioma model used and the control species will have to match as closely as possible the glioma model.

5 The Effect of Glioma Co-culture on PBEC Efflux Transporter Activity

5.1 Results

In the previous chapter it was found that PBEC activity was differently affected by rat and human astrocyte co-culture. The aim in this part of the project was to assess the effect of glioma co-culture on PBEC efflux, primarily using rat C6 glioma cells (PBECs-C6s) compared with rat astrocyte co-culture (PBECs-rAS). A limited stock of clonal human malignant glioma G7 cells (isolated from a glioblastoma multiform patient, from Dr Steven Pollard, UCL) were available and their effect on PBEC efflux (PBECs-G7s) was compared with human astrocyte co-culture (PBECs-hAS).

Ideally, the time of co-culture with the C6s or G7s should be the same but unfortunately this was not possible since the G7s become senescent in the presence of serum, which is essential for PBEC growth. Conversely, serum-free conditions were detrimental to PBEC after 2 days. Therefore, PBECs were co-cultured with human cells for 2 days in serum-free conditions (compared with 4 days for the C6 co-culture in a combination of serum and serum-free conditions). In addition, attempts were made to replicate the longer C6-coculture, by moving the PBECs (in serum) to fresh G7s (in serum-free medium) every 12 hours for a total of 3 days and then changing the medium to serum-free for a further 24 hours (for a total of 4 days in culture) (PBECs-G7.4).

5.1.1 ^{3}H-MPP^{+} efflux by PBECs in glioma co-culture

As described in Chapter 3, the rate of ^{3}H-MPP^{+} efflux was measured to assess the effects of glioma co-culture on PBECs. Due to limited availability of G7 cells, the rate was only assessed for the PBECs-C6s (Figure 4.1).

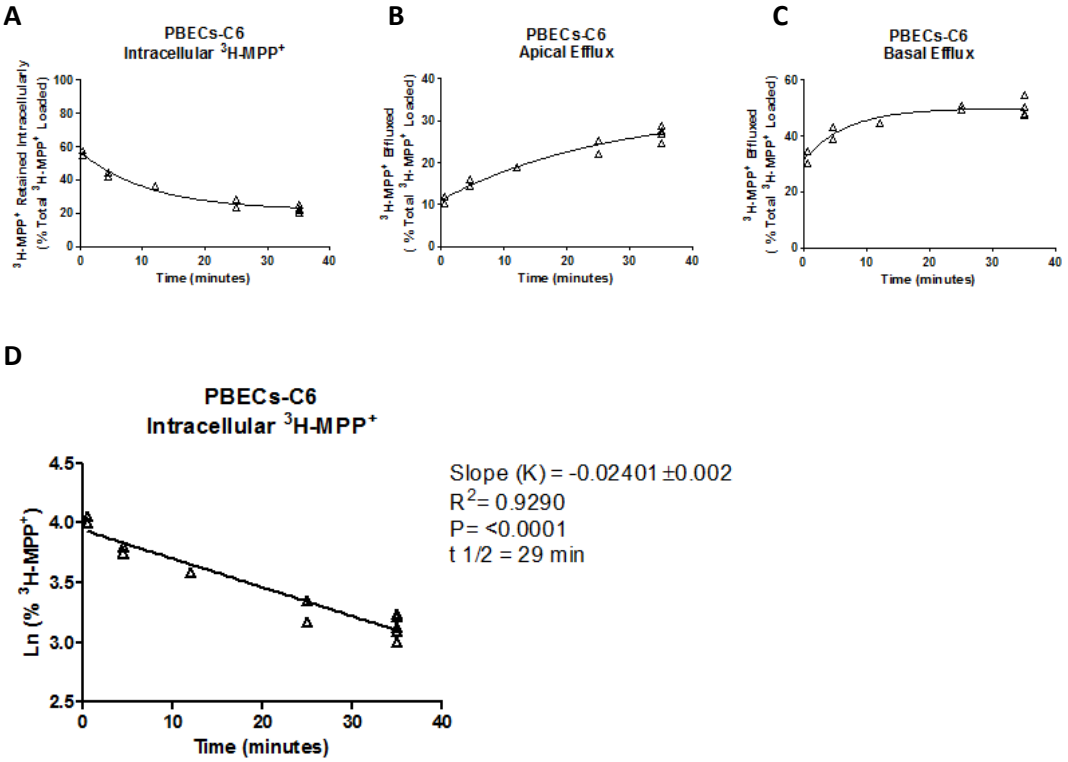

Figure 5.1 Rates of ^{3}H-MPP$^+$ efflux by PBECs in co-culture with C6 glioma cells.

PBECs were grown in co-culture with rat glioma C6s (PBECs-C6s) for a total of 4 days, before undergoing ^{3}H-MPP$^+$ efflux assays.

The PBECs-C6s were loaded with ^{3}H-MPP$^+$. The loaded cells were then incubated with efflux buffer in both the apical and basal chambers of the Transwells for the times shown. The buffers were then collected and analysed separately by liquid scintillation counting for ^{3}H-MPP$^+$ with correction for ^{14}C-sucrose.

The ^{3}H-MPP$^+$ effluxed apically or basally was then expressed as a percentage of the ^{3}H-MPP$^+$ initially loaded into the cells.

A) Intracellular retention B) Apical efflux, C) basal-directed efflux, and D) Ln plot of the Intracellular retention.

The graphs show all the data points collected from a total of 4 experiments together with the rate of ^{3}H-MPP$^+$ efflux (over 35 minutes) shown in D by the overlaid line.

The intracellular retention of ^{3}H-MPP^{+} by PBECs-C6s decreased with time, indicating efflux of ^{3}H-MPP^{+}. As with the PBECs-rAS, intracellular retention began to plateau by 35 minutes, while the profiles of the separated apical and basal efflux graphs were similar to those for PBECs-rAS suggesting plateauing of basal efflux which may be due to an equilibrative process (Figure 4.1)

The PBECs-C6 demonstrated similar rates of ^{3}H-MPP^{+} efflux as the PBECs-rAS with similar $t_{1/2s}$ of 29 minutes and 32 minutes, respectively.

As in Chapter 3 with the PBECs-rAS, the rates of apical and basal efflux from PBECs-C6s were also estimated (Table 4.1). The results showed no significant difference between rates from PBECs-rAS and PBECS-C6s either apically or basally. However, both showed increased apical efflux compared to PBECs-M.

Table 5.1 Rates of efflux by PBECs-C6s

	Efflux rate constant K (min^{-1})		
	Loss of total intracellular pool	**Apical**	**Basal**
PBECs-M	0.013 ± 0.004	0.003± 0.001	0.010 ± 0.003
PBECs-rAS	0.022 ± 0.003 *	0.011 ± 0.001 ***	0.011 ± 0.003
PBECs-C6	0.024 ± 0.002 *	0.013 ± 0.001 ***	0.012 ± 0.002

*p <0.05, *** p<0.001 difference in 1-tailed unpaired t-test between PBECs-M and indicated pair.

No significant differences between PBECs-rAS and PBECs-C6s were observed.

To further asses any differences in ^{3}H-MPP^{+} efflux between PBECs-C6s and the PBECs-rAS, ^{3}H-MPP^{+} efflux by the PBECs at a single time point (35 minutes) was assessed. In addition, PBECs-G7s were compared with PBECs-hAS.

For the rat co-cultures, no significant differences were noted in the apical and basal-directed efflux of ^{3}H-MPP^{+}, with the PBECs-C6 showing similar overall efflux and intracellular retention of ^{3}H-MPP^{+} to PBECs-rAS (Figure 4.2). This agreed with the previous observations concerning the rate of ^{3}H-MPP^{+} efflux, which showed the PBECs-C6s had a similar efflux rate (Figure 3.4 and Figure 4.1).

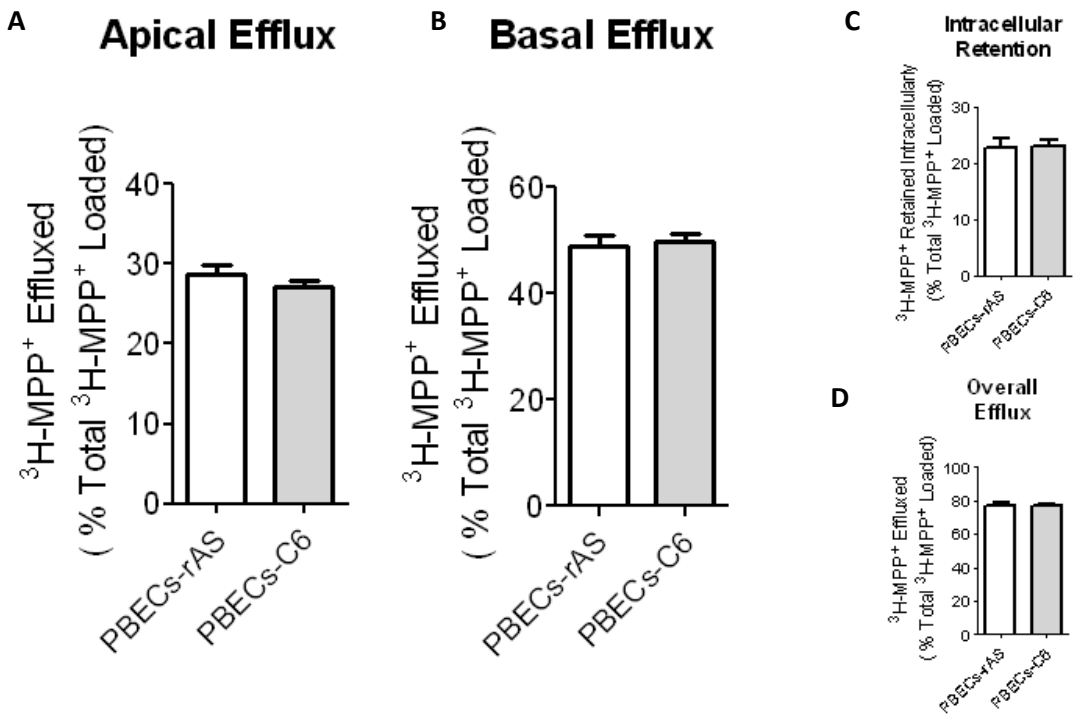

Figure 5.2 ^{3}H-MPP$^+$ efflux from PBECs in C6 glioma co-culture

PBECs were grown in co-culture with either rat astrocytes (PBECs-rAS) or rat glioma C6s (PBECs-C6s) for a total of 4 days, before undergoing ^{3}H-MPP$^+$ efflux assays.

The PBECs-C6s were loaded with ^{3}H-MPP$^+$. The loaded cells were then incubated with efflux buffer in both the apical and basal chambers of the Transwells for 35 minutes. The buffers were then collected and the cells were lysed. The buffers and lysate were analysed separately by liquid scintillation counting for ^{3}H-MPP$^+$ with correction for ^{14}C-sucrose.

The ^{3}H-MPP$^+$ effluxed apically or basally were then expressed as a percentage of the ^{3}H-MPP$^+$ initially loaded into the cells, as was the ^{3}H-MPP$^+$ remaining intracellularly (from lysate analysis).

A) Apical efflux, B) basal-directed efflux, C) intracellular retention, D) overall efflux (the sum of the apical and basal efflux).

Values are mean ± SEM of n=4-6 wells from 3 independent plates.

No significant differences in unpaired 2 tailed t-test.

For the human co-culture, the PBECs-G7 after 2 days of co-culture showed significantly higher overall ^{3}H-MPP^{+} efflux than their human astrocyte counterpart (also in 2 days of co-culture) (Figure 4.3). This was due to a significant increase in apical, but not basal-directed efflux under the G7 condition. However, in longer co-cultures with the G7s i.e. PBECs-G7.4 (where co-culture was maintained for 4 days), basal-directed efflux was lower than in the PBECs-G7 co-cultured for 2 days. However, no human astrocyte control was conducted for the longer 4 days co-culture, therefore it is not possible to distinguish whether the lower basal-directed efflux is due to a genuine decrease with time spent in co-culture with the G7s or results from changes during the cell culture process itself which may have influenced baseline levels of basal-directed efflux.

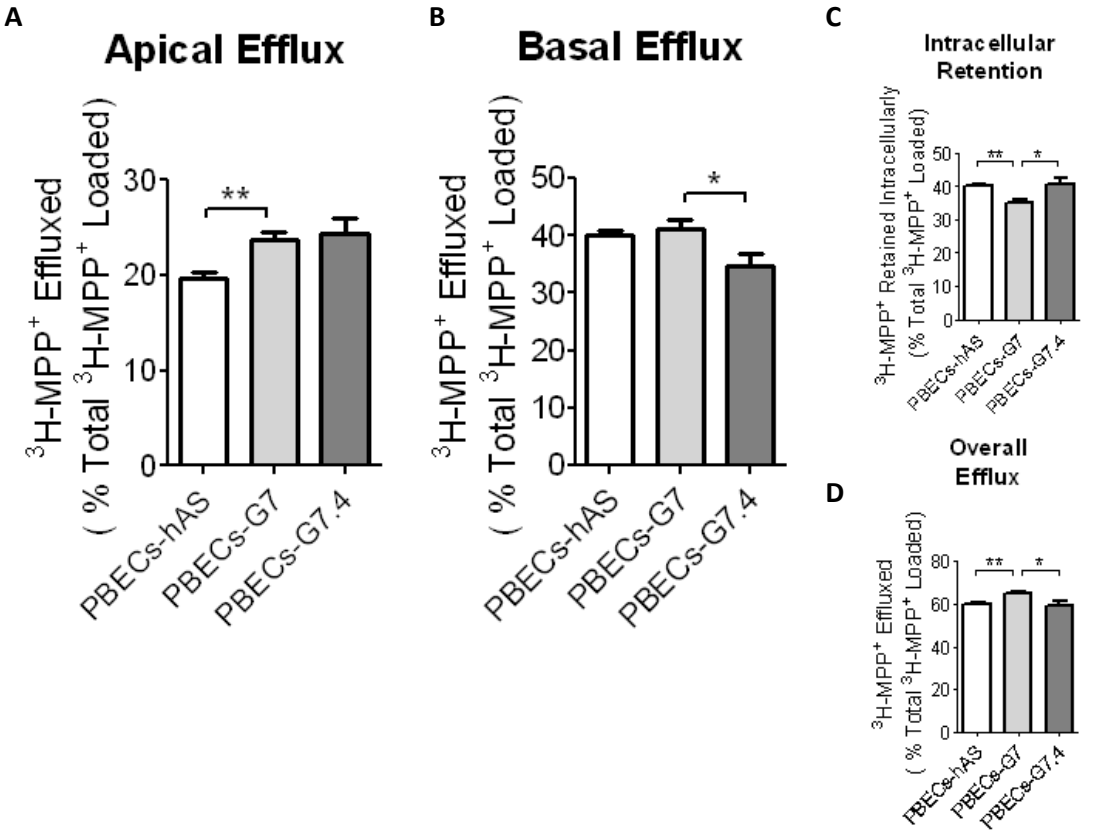

Figure 5.3 ^{3}H-MPP^{+} efflux from PBECs in G7 glioma co-culture

PBECs were grown in co-culture with either human astrocytes (PBECs-hAS) or human glioma G7s (PBECs-G7s) for a total of 2 days under serum-free condition, before undergoing ^{3}H-MPP^{+} efflux assays. Alternatively, PBECs were grown in co-culture with G7s for a total of 4 days in a combination of serum and serum-free conditions (PBECs-G7.4) and then assayed.

The PBECs were loaded with ^{3}H-MPP^{+}. The loaded cells were then incubated with efflux buffer in both the apical and basal chambers of the Transwells for 35 minutes. The buffers were then collected and the cells were lysed. The buffers and lysate were analysed separately by liquid scintillation counting for ^{3}H-MPP^{+} with correction for ^{14}C-sucrose.

The ^{3}H-MPP^{+} effluxed apically or basally were then expressed as a percentage of the ^{3}H-MPP^{+} initially loaded into the cells, as was the ^{3}H-MPP^{+} remaining intracellularly (from lysate analysis).

A) Apical efflux, B) basal-directed efflux, C) intracellular retention, D) overall efflux (the sum of the apical and basal efflux).

Values are mean ± SEM of n=4-7 wells from 3 independent plates.

*p<0.05, difference in an unpaired 2 tailed t-test.

All 3 glioma co-cultures, PBECs-C6, PBECs-G7 and PBECs-G7.4, showed similar levels of overall apical ^{3}H-MPP^{+} efflux 27.2±0.7%, 23.7±0.9% and 24.4±1.6% respectively, irrespective of the species of the co-culture cells used. By contrast, previous results (Chapter 3, Figure 3.6) showed significant differences in apical efflux in PBECs in different astrocyte co-cultures (rat or human), with PBECs-rAS showing greater levels of ^{3}H-MPP^{+} apically effluxed than PBECs-hAS (28.6±1.3% and 19.8±0.6% respectively). This could indicate greater similarities between the influence of the different glioma cells, compared with their normal astrocyte counterparts.

The integrity of the PBEC TJs was also assessed in the different glioma conditions. TEER measurements were taken before the start of the experiment and ^{14}C-sucrose permeability was measured during the course of the 35 minute efflux assay (Figure 4.4).

Interestingly, the TEER and ^{14}C-sucrose permeability of the PBECs in co-culture with the rat cells were different between the rat astrocyte and glioma co-cultures. The PBECs-C6s had higher TEERs and lower paracellular permeability of ^{14}C-Sucorse, indicating “tighter” TJs than their normal astrocyte counterparts. However, the TEER measurements and ^{14}C-sucrose permeability were not different between the PBECs-G7s and PBEC-hAS in the 2 day co-culture, indicating the TJ integrity of these PBECs were similar. There was no difference between the PBECs-G7 after 4 days compared with 2 days of co-culture, demonstrating that the different co-culture lengths or methods did not influence TJ integrity.

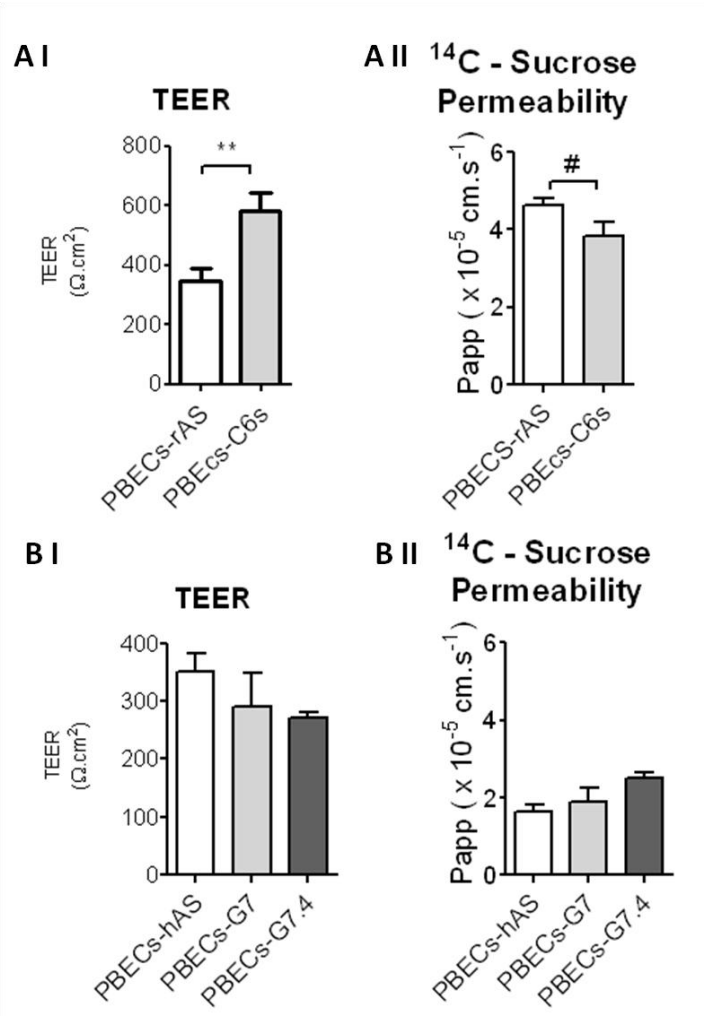

Figure 5.4 Tight junction integrity of PBECS in co-culture with glioma cells.

The tight junction integrity of PBECs co-cultured with normal astrocytes or glioma cells was measured in two ways.

Firstly, the transendothelial electrical resistance (TEER) of the PBEC monolayer was measured before the start of a Transwell ^{3}H-MPP^{+} efflux experiment (I). Secondly, the permeability of the paracellular marker ^{14}C-sucrose (apical to basal direction) was measured over 35 minutes during the efflux stage of the ^{3}H-MPP^{+} efflux experiment (II).

A) PBECs grown in co-culture with either normal rat astrocytes (PBECs-rAS) or rat C6 glioma cells (PBECs-C6s) for a total of 4 days.

B) PBECs grown in co-culture with either human astrocytes (PBECs-hAS), human glioma G7s (PBECs-G7s) for a total of 2 days (serum-free) or for a total of 4 days in a combination of serum and serum-free conditions (PBECs-G7.4).

Mean ± SEM, n=6-35 wells

** $p<0.01$, unpaired 2-tailed t-test, # $p<0.05$ unpaired 1 tailed t-test

No significant differences were found in unpaired t-tests between PBECs-hAS and PBECs-G7, or PBECs-G7 and PBECs-G7.4.

The amount of ^{3}H-MPP^{+} loaded into the different PBECs was also assessed. Figure 4.5 shows that co-culture of PBECs with C6s for 4 days or G7s for 2 days did not change ^{3}H-MPP^{+} loading when compared with their respective astrocyte co-culture controls, when compared with each other, or compared with the PBECs in G7 co-culture for 4 days. This indicates that glioma cells have no additional effect(s) on uptake other than the "normal" astrocytic effect(s), at least for ^{3}H-MPP^{+} uptake, indicative of transporters such as OCT1 and OCT2.

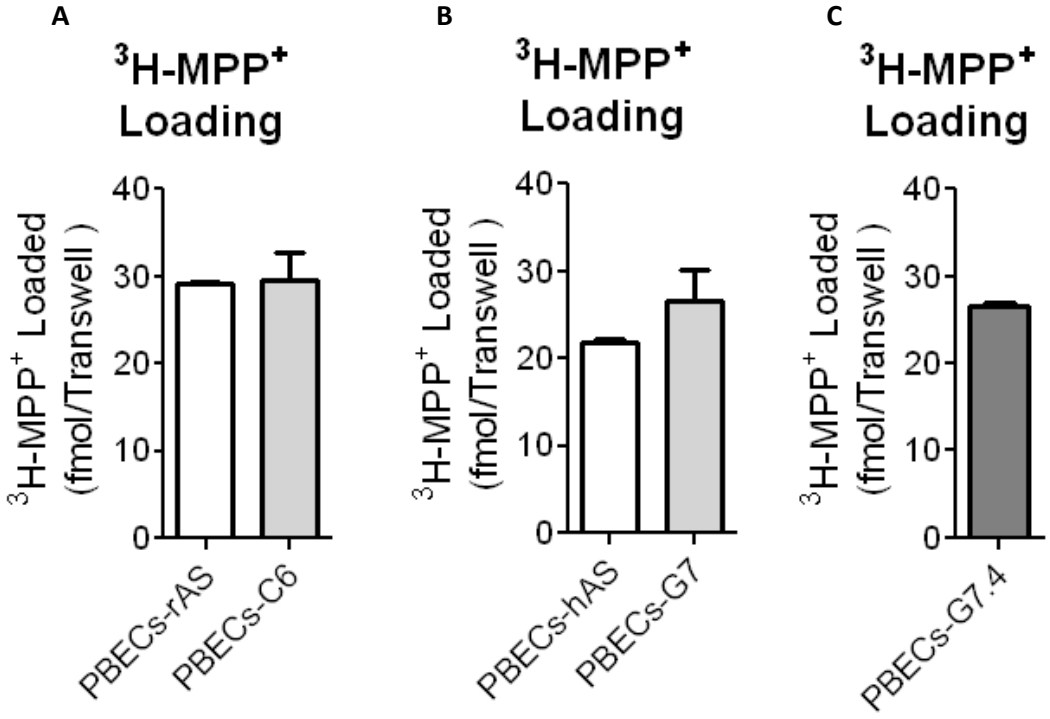

Figure 5.5 ^{3}H-MPP^{+} loaded into PBECs grown in glioma co-culture

The ^{3}H-MPP^{+} loaded into PBECs during ^{3}H-MPP^{+} efflux was analysed by liquid scintillation counting for ^{3}H-MPP^{+} with correction for ^{14}C-sucrose and expressed as fmol/Transwell.

A) PBECs grown in co-culture with either normal rat astrocytes (PBECs-rAS) or rat C6 glioma cells (PBECs-C6s) for a total of 4 days.

B) PBECs grown in co-culture with either human astrocytes (PBECs-hAS) or human glioma G7s (PBECs-G7s) for a total of 2 days under serum-free condition.

C) PBECs grown in co-culture with human glioma G7s for a total of 4 days in a combination of serum and serum-free conditions (PBECs-G7.4).

Values are mean ± SEM of n=4-7 wells from 3 different plates.

No significant differences were found in unpaired t-tests between PBECs-rAS and PBECs-C6, or PBECs-hAS and PBECs-G7, or PBECs-G7 and PBECs-G7.4, or PBECs-G7.4 and PBECs-C6s.

Together the results showed differences between the PBECs in co-culture with rat cells and the PBECs in co-culture with the human model. This could be due to differences between species, but also due to differences between the different co-culture methods or the times spent in co-culture.

The PBECs were in co-culture with the rat cells for 4 days, while only 2 days were spent in co-culture with the human cells. Mimicking the 4 day co-culture process of the PBECs in rat co-culture using G7s (PBECs-G7.4) did result in different efflux activity than the PBECs in the 2 day co-culture, showing that the culture method or time-spent in co-culture does influence efflux activity.

Therefore the human 2 day co-cultured may indicate earlier changes in efflux characteristics while the 4 day co-culture with rat cell or the human G7s may indicate later changes in efflux characteristics. Alternatively, the differences noted could arise if human-porcine cell interactions induce faster changes than rat-porcine cell interactions.

5.1.2 ABC transporter activity in PBECs grown in glioma co-culture

To determine whether the differences in ^{3}H-MPP^{+} efflux noted above were due to differences in the activity of ABC transporter, a ^{3}H-MPP^{+} efflux assay was conducted on the different PBECs in the presence of ABC transporter inhibitors.

As previously, haloperidol (60 µM) and verapamil (50 µM) were used to assess Pgp activity, Ko143 (0.2 µM) and prazosin (35 µM) were used to assess BCRP activity and MK571 (10 µM) to asses MRP activity. Due to the scarce availability of human astrocytes and G7 cells, only the effect of Ko143 was tested on the PBECs with human cells after 2 days of co-culture and only haloperidol and Ko143 were tested for the PBECs in G7 co-culture for 4 days with results shown in Figure 4.6.

The previous chapter (Chapter 3, Figure 3.6) shows the inhibition of PBECs-rAS by both Pgp inhibitors and one BCRP inhibitor (prazosin) only on the apical surface, with no significant inhibition by the MRP inhibitor MK571. Here, the PBECs-C6s also showed Pgp and BCRP mediated efflux at the apical surface, however there were some differences compared with the PBECs-rAS.

Firstly, the PBECs-C6s showed Pgp-dependent ^{3}H-MPP^{+} efflux on the basal surface, with haloperidol significantly decreasing efflux (Figure 4.6). By contrast, the PBECs-rAS did not show any inhibitable Pgp activity on the basal surface. In addition, apical Pgp-dependent efflux was significantly decreased during C6 co-culture, compared with PBECs-rAS (Figure 4.7 with Pgp inhibitors, haloperidol and verapamil).

Secondly, both Ko143 and prazosin BCRP inhibitors showed significant effects on the apical ^{3}H-MPP^{+} efflux from PBECs-C6s, while only prazosin showed significant effects in the PBECs-rAS (Figure 4.6). In addition, the BCRP-dependent component was shown to increase apically for both BCRP inhibitors in the C6 co-culture (Figure 4.7, with BCRP inhibitors, Ko143 and prazosin).

Finally, the MRP inhibitor Mk571 significantly inhibited efflux at the apical surface of the PBECs-C6 in conjunction with increased intracellular retention (Figure 4.6), indicating the presence of MRP activity at the apical surface of PBECs-C6, which the PBECs-rAS did not show.

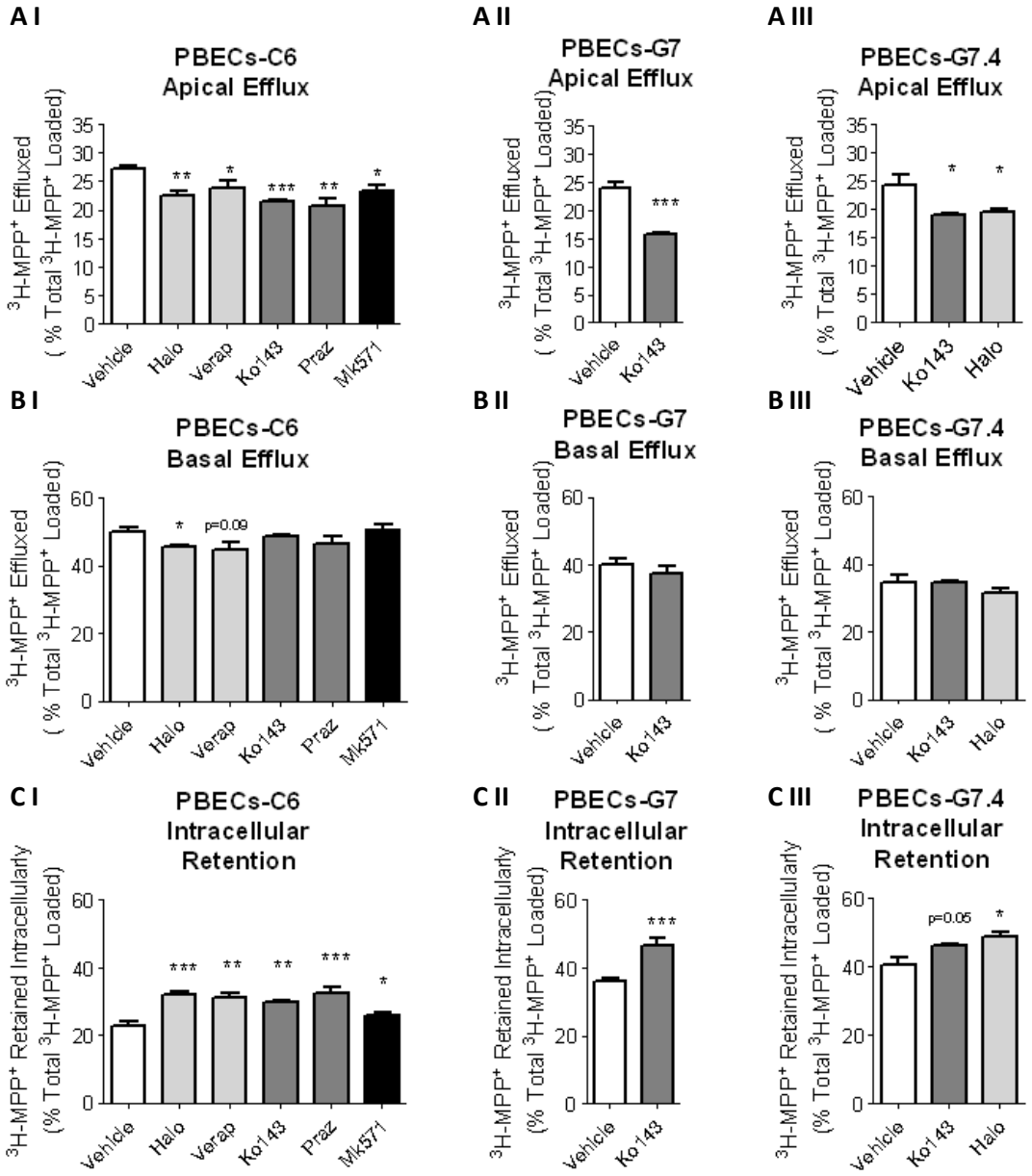

Figure 5.6 Efflux of ^{3}H-MPP$^+$ from PBECs in glioma co-culture

PBECs were grown on Transwells in co-culture with either or C6 glioma cells (PBECs-C6s) for a total of 4 days or G7 glioma cells for either 2 days (PBECs-G7) or 4 days (PBECs-G7.4).

The PBECs were loaded with ^{3}H-MPP$^+$. The loaded cells were then incubated with efflux buffer, without (vehicle) or with an inhibitor, in both the apical and basal chambers of the Transwells for 35 minutes. The inhibitors used were the Pgp inhibitors haloperidol (60 µM) and verapamil (50 µM), the BCRP inhibitors Ko143 (0.2 µM) and prazosin (35 µM) and the non-specific MRP family inhibitor MK571 (10 µM).

The buffers were then collected and analysed separately by liquid scintillation counting for ^{3}H-MPP$^+$, along with the cell lysate.

The ^{3}H-MPP^{+} effluxed apically or basally were then expressed as a percentage of the ^{3}H-MPP^{+} initially loaded into the cells.

A) Apical efflux, B) basal-directed efflux and C) intracellular retention.

Values are mean ± SEM of n=3-6 wells from n=3 plates

* p<0.05, ** p<0.01, ***p<0.001, p=0.05, p=0.09 difference in unpaired 2 tailed t-test between efflux in the presence or absence of the inhibitor.

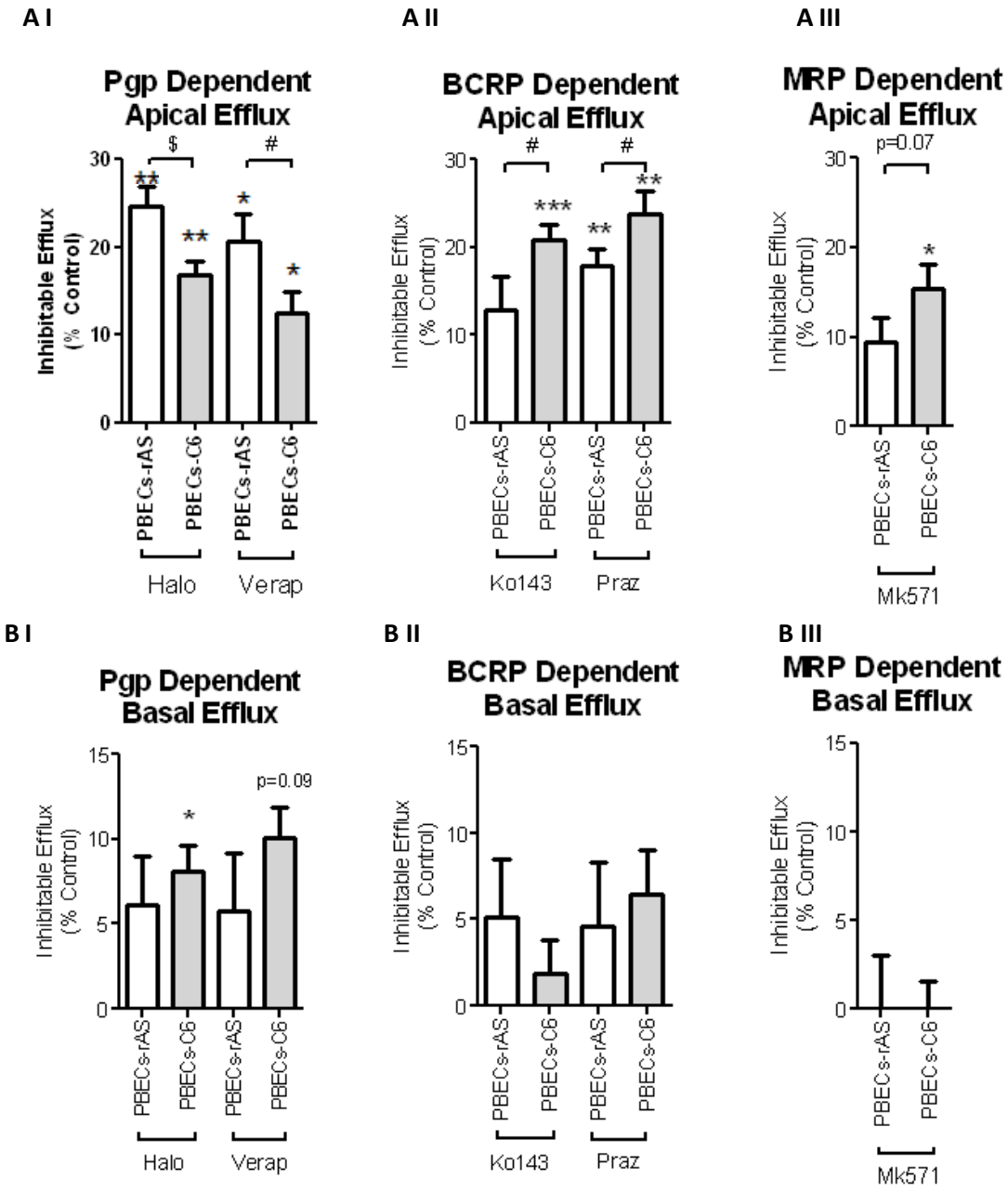

Figure 5.7 ABC Transporter activity in PBECs grown in co-culture with rat glioma cells

PBECs were grown on Transwells in co-culture with either rat astrocytes (PBECs-rAS) or C6 glioma cells (PBECs-C6s) for a total of 4 days.

The PBECs-C6s were loaded with ^{3}H-MPP^{+}. The loaded cells were then incubated with efflux buffer, without (vehicle) or with an inhibitor, in both the apical and basal chambers of the Transwells for 35 minutes. The inhibitors used were the Pgp inhibitors haloperidol (60 µM) and

verapamil (50 µM), the BCRP inhibitors Ko143 (0.2 µM) and prazosin (35 µM) and the non-specific MRP family inhibitor MK571 (10 µM).

The buffers were then collected and analysed separately by liquid scintillation counting for ^{3}H-MPP^{+} with correction for ^{14}C-sucrose.

The ^{3}H-MPP^{+} effluxed apically or basally were then expressed as a percentage of the ^{3}H-MPP^{+} initially loaded into the cells.

The inhibitable efflux was calculated for each inhibitor, as the efflux in the absence of inhibitor minus the efflux in the presence of inhibitor and expressed as a percentage of the efflux in the absence of inhibitor (% Control).

A) Apical inhibition and B) inhibition at the basal surface, with I) showing Pgp inhibition, II) showing BCRP inhibition and III) showing MRP inhibition.

Values are mean ± SEM of n=3-6 wells from n=3 plates

* $p<0.05$, ** $p<0.01$ difference in unpaired 2 tailed t-test between efflux in the presence of the inhibitor and efflux in the absence of that inhibitor.

$ $p<0.05$, difference in unpaired 2-tailed t-test between the indicted pairs

# $p<0.05$ difference in unpaired 1-tailed t-test between the indicted pairs.

In the PBECs co-cultured with human cells, only the Ko143 BCRP inhibitor was tested which inhibited apical (but not basal-directed) efflux (Figure 4.6). However, the Ko143-inhibitable component on the apical surface changed from 26.7±2.3 % in PBECs-hAS to 32.8±1.5% in PBECs-G7 in the 2 days co-culture (Figure 4.8), indicating increased BCRP activity on the apical surface in agreement with the increased overall apical efflux shown in Figure 4.3.

Interestingly, the PBECs-G7.4 (4 days of co-culture) showed similar levels of apical haloperidol-inhibitable efflux (19.5 ± 5.4%) as the PBECs-C6s (16.8 ± 1.7%) and similar levels of apical Ko143-inhibitable efflux (21.1 ± 3.4% and 20.9 ± 1.7 % respectively). This shows similar BCRP and Pgp transporter activities with the two systems yielding comparable results when co-cultured for 4 days.

This also indicates that differences between the rat co-cultures and the 2 day co-cultures with human cells are likely due to differences in the culturing process, either in the time of culture or the method. However, despite the differences between the rat 4 day co-culture and human 2 days co-cultures, both showed increases in apical BCRP-

dependent efflux in glioma co-culture when compared with their respective controls (i.e. astrocyte co-cultures), indicating that BCRP activity in PBECs is increased by co-culture with glioma.

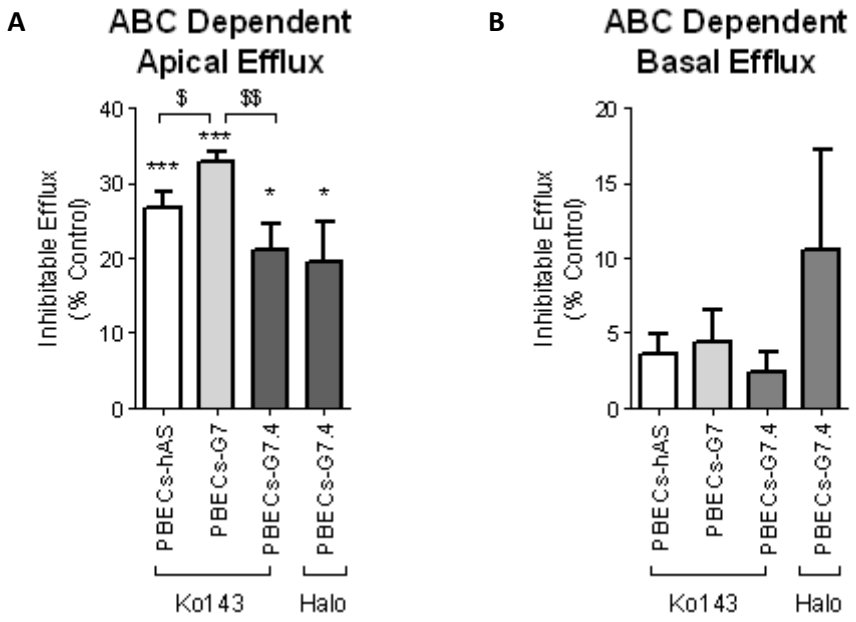

Figure 5.8 ABC transporter activity in PBECs grown in co-culture human glioma cells.

PBECs were grown in co-culture with human astrocytes (PBECs-hAS) or G7 glioma cells (PBECs-G7) for 2 days, under serum-free conditions or in co-culture with G7s for a total of 4 days in a combination of serum and serum-free conditions (PBECs-G7.4) and then assayed.

The PBECs-C6s were loaded with ^{3}H-MPP^{+}. The loaded cells were then incubated with efflux buffer, without (vehicle) or with an inhibitor, in both the apical and basal chambers of the Transwells for 35 minutes. The inhibitors used were the Pgp inhibitors haloperidol (60 µM) and verapamil (50 µM), the BCRP inhibitors Ko143 (0.2 µM) and prazosin (35 µM) and the non-specific MRP family inhibitor MK571 (10 µM).

The buffers were then collected and analysed separately by liquid scintillation counting for ^{3}H-MPP^{+} with correction for ^{14}C-sucrose.

The ^{3}H-MPP^{+} effluxed apically or basally were then expressed as a percentage of the ^{3}H-MPP^{+} initially loaded into the cells.

The inhibitable efflux was calculated for each inhibitor, as the efflux in the absence of inhibitor minus the efflux in the presence of inhibitor and expressed as a percentage of the efflux in the absence of inhibitor (% Control).

A) Apical inhibition and B) inhibition at the basal surface.

Mean ± SEM of n=3-6 wells from n=3 plates

* p<0.05, **p<0.01, difference in unpaired 2 tailed t-test between efflux in the presence of the indicated inhibitor and efflux in the absence of that inhibitor.

$ p<0.05 difference in unpaired 2-tailed t-test between indicated pairs.

5.1.3 Pgp and BCRP expression in PBECs during glioma co-culture

To determine whether the differences in Pgp and BCRP activity noted above relate to their mRNA expression, comparisons were made between PBECs co-cultured with normal astrocytes and PBECs co-cultured with glioma cells.

For the PBECs in rat co-cultures, mRNA expression was measured after the cells had been in co-culture for 3 days (when the PBECs reached confluence) or 4 days (after 24 hour treatment with PBEC serum-free medium containing hydrocortisone, CPT-cAMP and Ro-20-1724). Two different C6 conditions were tested, one where the medium was changed on day two of co-culture and the other where the medium was not changed (the second is denoted by C6* in Figure 4.9 and Figure 4.10). Since C6 cells use up nutrients quickly and apoptose when nutrients are depleted, more cell death was expected when medium was not changed; apoptotic factors could influence the Pgp and BCRP mRNA expression in PBECs. However, the results in Figure 4.9 and 4.10 showed that frequency of medium change did not affect expression.

For the PBECs in human co-cultures RNA was measured after only 2 days of co-culture, due to the difficulties in co-culturing the cells for longer, as described previously.

There was little change in Pgp or BCRP mRNA after 3 days in co-culture with C6s (Figure 4.9). However, after 4 days in co-culture there was ~3 fold greater BCRP mRNA expression under the C6 co-culture condition compared with rat astrocyte co-culture. Pgp expression did not change (Figure 4.10).

Figure 5.9 BCRP and Pgp mRNA in PBECs after 3 days in co-culture with rat glioma cells

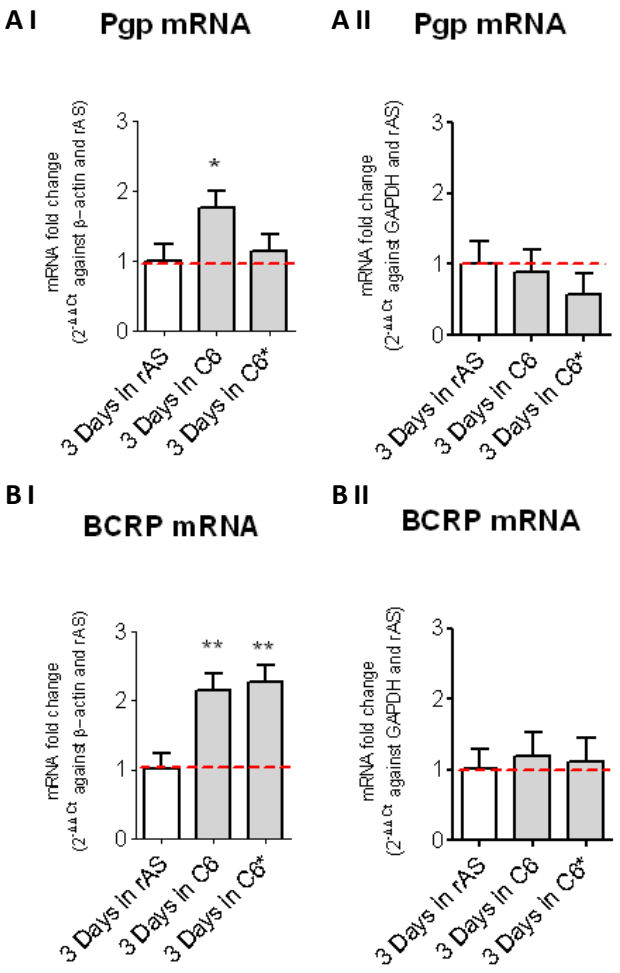

Total RNA was isolated from PBECs grown on Transwell filters in co-culture with normal rat astrocytes (rAS) or C6 glioma cells (C6 or C6*) for 3 days in serum-containing media. The C6* denotes a condition where medium was not changed on day 2 of co-culture.

The RNA underwent RT-QPCR using Pgp (A) or BCRP (B) primers.

Ct values obtained per gene per sample were normalised against either β-actin (I) or GAPDH (II). Ct values obtained for the sample (to give the ΔCt) then further normalised against the average ΔCt of the rat astrocyte-cultured cells to give the ΔΔCt, which was then used to calculate the fold change $2^{-\Delta\Delta Ct}$ shown right.

Mean ± SEM of n=3 samples per condition; PCR conducted in triplicate per plate on n=3 plates.

* p<0.05, **p<0.01 difference from rAS control in unpaired 2 tailed t-test.

The mRNA results after 4 days in co-culture agreed with the activity data for BCRP, with greater BCRP mRNA in the PBECs-C6s corresponding with greater BCRP activity results. However, mRNA levels for Pgp did not show any differences between PBECs-rAS and PBECs-C6s, despite greater Pgp-dependent activity measured in the PBECs-C6s than the PBECs-rAS.

This suggests that BCRP activity is regulated at the transcriptional level in this co-culture systems but that Pgp activity is not. It is possible that Pgp activity may be regulated post-transcriptionally.

Figure 5.10 BCRP and Pgp mRNA in PBECs after 4 days in co-culture with rat glioma cells

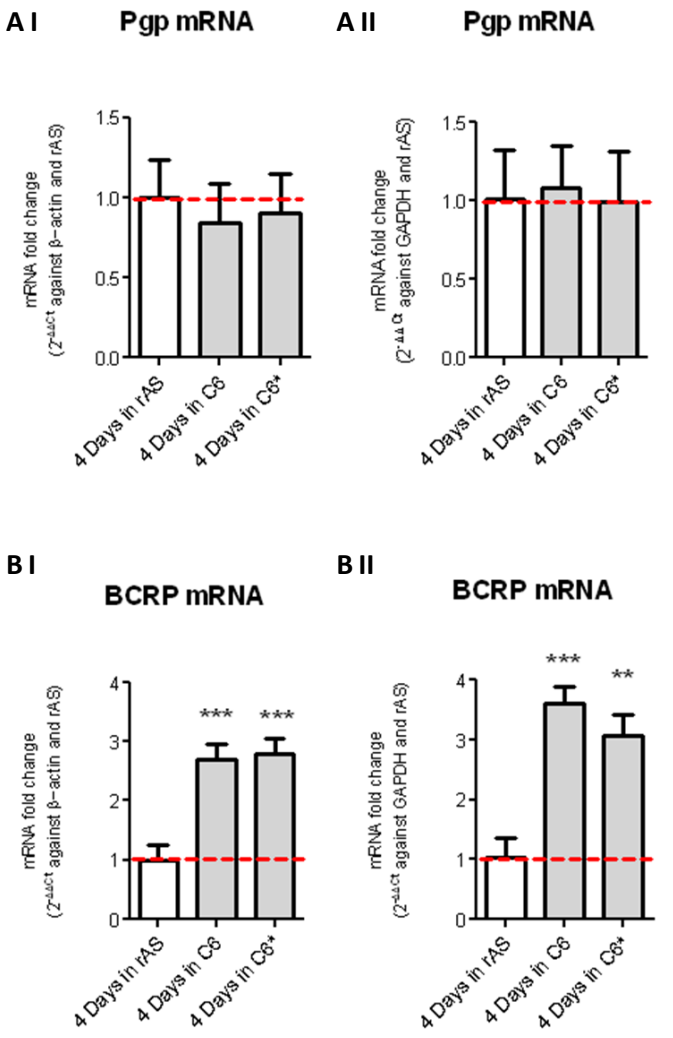

Total RNA was isolated from PBECs grown on Transwell filters either in co-culture with normal rat astrocytes (rAS) or C6 glioma cells (C6 or C6*) for 3 day in serum-containing media and for a further 24 hours is serum-free medium, for a total of 4 days in co-culture. The C6* denotes a condition where media was not changed on day 2 of co-culture.

The RNA underwent RT-QPCR using Pgp (A) or BCRP (B) primers.

Ct values obtained per gene per sample were normalised against either β-actin (I) or GAPDH (II). Ct values obtained for the sample (to give the ΔCt) then further normalised against the average ΔCt of the rat astrocyte-cultured cells to give the ΔΔCt, which was then used to calculate the fold change $2^{-\Delta\Delta Ct}$ shown right.

Mean ± SEM of n=3 samples per condition; PCR conducted in triplicates per plate on n=3 plates.

**p<0.01, ***p<0.001 difference from rAS control in unpaired 2 tailed t-test from

In the human co-cultures (Figure 4.11), no differences in Pgp or BCRP mRNA were seen when comparing the PBECs in human astrocyte co-culture with the PBECs in G7 glioma co-culture. However, BCRP activity was shown to be significantly greater in PBECs-G7s, demonstrating greater levels of Ko143-inhibitable activity than PBECs-hAS (Figure 4.8). This suggests that the greater BCRP activity noted was not directly

influenced by BCRP mRNA expression, indicating an mRNA-independent cause for the differences in BCRP activity, for example, possible post-transcriptional regulation.

The differences in the rat and human BCRP expressions could be due to differences in the times the PBECs spent in co-culture. The rat model was co-cultured for 4 days and mRNA changes in BCRP were only consistently seen on the fourth day.

Figure 5.11 Pgp and BCRP mRNA expression in PBECs co-cultured with human glioma cells for 2 days

Total RNA was isolated from PBECs grown on Transwell filters either in co-culture with normal human astrocytes (PBEC-hAS) or human G7 glioma cells (PBECs-G7) for 2 days in serum-free medium.

The RNA underwent RT Q-PCR using Pgp (A) or BCRP (B) primers.

Ct values obtained per gene per sample were normalised against either β-actin (I) or GAPDH (II). Ct values obtained for the sample (to give the ΔCt) then further normalised against the average ΔCt of the rat astrocyte-cultured cells to give the ΔΔCt, which was then used to calculate the fold change $2^{-\Delta\Delta Ct}$ shown right.

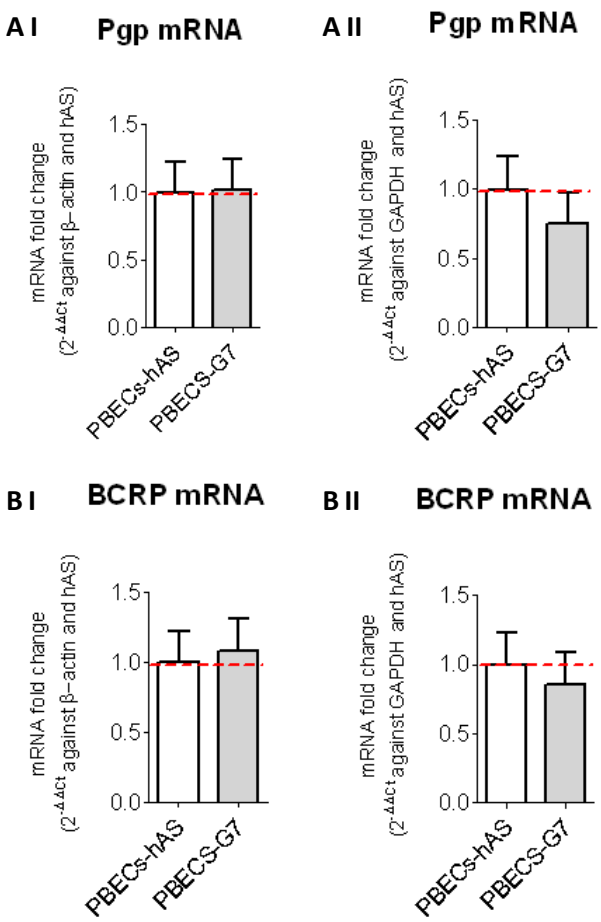

Mean ± SEM of n=3 samples per condition; PCR was conducted in quadruplicate per plate.

No significant differences were found using unpaired 2-tailed t-tests between PBECs-hAS and PBECs-G7.

5.2 Discussion

This chapter focused on identifying the contribution of the major efflux transporters to apical efflux and how this is affected by normal astrocytes and glioma in co-culture.

^{3}H-MPP^{+} loading, the first step in the efflux assay used, showed that PBECs co-cultured with glioma cells did not differ from co-culture with normal astrocytes. As described previous (Chapter 3), MPP^{+} uptake most likely occurs via OCT transporter (Martel *et al.*, 2001). The lack of difference in loading, indicates that glioma cells have no glioma-specific effects on OCTs, beyond normal astrocytic effects. This could be a useful target for glioma therapy since intact OCT transporters could be a useful entry point for chemotherapeutic drugs to the brain.

PBECs co-cultured with rat C6 cells showed lower apical Pgp activity than in PBECs-rAS as well as some significant Pgp activity on the basal surface, which the PBECs-rAS did not (Figure 4.7). No differences were seen between Pgp mRNA expression between the PBECs-C6s and PBECs-rAS (Figure 4.9 and Figure 4.10), which suggests that differences in Pgp activity between the PBECs-C6 and PBECs-rAS were not due to differences in mRNA levels. However, it is possible that Pgp activity was regulated post-transcriptionally (i.e. independent of mRNA levels). Further, since some Pgp-dependant basal activity was detected, it may indicate that differences between the PBECs-C6s and the PBECs-rAS may involve differences in the regulation of Pgp apical:basal polarity and transporter localisation.

BCRP showed greater apical activity in PBECs co-cultured with C6 than in PBECs co-cultured with normal astrocytes (Figure 4.7). This correlated with increased mRNA expression of BCRP, indicating that increases in BCRP activity could be due to transcriptional changes.

Comparisons between endothelial cells in astrocyte and C6 co-cultures have been conducted previously. Dohgu *et al.* (2004) showed that after 3 days in contact co-culture mouse brain endothelial (MBEC4) cells in culture with C6 showed greater (paracellular) permeability to sodium fluorescein and decreased Pgp activity (measured via Rho 123 accumulation) compared with mono-cultured cells, whilst MBEC4 co-cultured with astrocytes showed decreased permeability to sodium fluorescein and increased Pgp activity. This decrease in Pgp activity with C6 co-culture agrees with the current finding. By contrast, in the current study, the lower Pgp activity apically is

accompanied by increased barrier tightness (increased TEER and reduced ^{14}C-Sucrose Papp, Figure 4.4).

Boveri *et al.* (2005) using bovine brain endothelial cells showed decreased Pgp protein expression and activity when co-cultured with C6s compared with normal astrocytes. Furthermore, the bovine brain endothelial cells did not differentiate as well as in the presence of C6 cells, with a less well developed pattern of TJ proteins (12 days in non-contact co-culture).

Taken together these studies suggest a link between the differentiation state of the BBB and Pgp expression, with a less differentiated BBB showing lower levels of Pgp.

Interestingly, Boveri et al. (2005) showed increased secretion of vascular endothelial growth factor (VEGF) by the C6 cells (with 40-fold higher levels detected in conditioned medium from C6s than from normal astrocytes), which was suggested to lead to the lack of differentiation in their study. However, in the current shorter-term study, absence of BBB TJ breakdown suggests that the VEGF has not yet had such effects here. However, VEGF has been shown to decrease Pgp apical localisation/activity (see below). Therefore, in the current study VEGF secretion by the C6s could have led to Pgp activity decreases that were independent of BBB TJ breakdown.

VEGF is a growth factor associated with angiogenesis and the growth and development of the BBB under normal condition (Ferrara *et al.*, 2003). However, its over-expression by glioma cells has been implicated in tumour development and growth (Merrill & Oldfield, 2005), with the majority of gliomas showing increased expression of VEGF (Merrill & Oldfield, 2005).

A direct link between BCRP activity or expression and VEGF has not been reported, but a link between Pgp activity and VEGF has been shown at the BBB. Hawkins *et al.* (2010b), showed both *in vitro* and *in vivo* (rat models) that VEGF decreases Pgp activity. Using rat capillaries and a fluorescent specific Pgp substrate ([N-ε(4-nitrobenzofurazan-7-yl)-D-Lys(8)]-cyclosporin A), it was shown that the loss in Pgp activity after exposure to VEGF resulted from a loss of luminal expression of Pgp. Overall protein expression was not altered, indicating that Pgp was not proteolytically degraded in response to VEGF. VEGF effects on Pgp were shown to be dependent on the activation of the VEGF receptor (flk-1) and scr kinase, the latter being involved in the caveolae phosphorylation pathway.

Jodoin *et al.* (2003) showed that around 70% of the Pgp in bovine brain capillary endothelial cells co-cultured with astrocyte, was found in isolated caveolae fractions. Similarly, 80% of the Pgp expressed in human capillaries was found co-localised with caveolin-1 and caveolin-2 within isolated caveolae fractions. In the caveolae fractions of the bovine brain endothelial cells Pgp was shown to interact with caveolin-1 and caveolin-2 and to be active within the caveolae, with disruption of caveolae decreasing Pgp activity (Jodoin et al., 2003).

Barakat *et al.* (2007), showed that Pgp/caveolin-1 co-localised via direct interaction of the two proteins, where Pgp activity was suppressed by phosphorylated caveolin-1. Knock-down of caveolin-1 via siRNA resulted in increased Pgp activity in RBE4 cells (with Pgp substrate accumulation assay, showing decreased accumulation when caveolin-1 was silenced). The study further showed that src kinase and/or phosphorylation of tyrosine14 on caveolin-1 did not affect expression of Pgp, however did decrease Pgp activity. It was concluded that phosphorylation of tryosine14 on caveolin-1 increased its interactions with Pgp, resulting in down-regulation of Pgp activity, without altering expression.

Caveolae have been shown to be largely expressed on the surface of plasma membranes with slow rates of endocytosis (Fagerholm *et al.*, 2009). This maintenance at the plasma membrane has been suggested to be linked by caveolin-1 within the caveolae, which interacts with f-actin to maintain the caveolae at the plasma membrane. However, Fagerholm et al. (2009) showed in adipocytes that phosphorylation of tyrosine14 on caveolin-1 can result in rapid internalisation of caveolae and endocytosis, with the phosphorylated caveolin-1 being internalised within an endosome.

Hawkins et al. (2010b) showed that VEGF treatment resulted in the phosphorylation of caveolin-1 (via src kinases), therefore VEGF acts via activation of flk-1 and src to mediate phosphorylation of caveolin-1 resulting in internalisation of Pgp via caveolae vesicle endocytosis. In addition, Hawkins *et al.* (2010a) showed that VEGF could protect Pgp from protease kinase cleavage at the apical surface, by a mechanism consistent with internalisation via caveolae endocytosis.

Together these studies indicates that Pgp activity can be regulated by VEGF without affecting Pgp expression, acting via src kinase phosphorylation of caveolin-1, leading to interaction of Pgp and phosphorylated calveolin-1, with the Pgp/phosphorylated caveolin-1 complex then internalised via caveolae endocytosis.

Early studies showed increases in the number of vesicles within brain microvasculature during tumour challenge (Dinda *et al.*, 1993, Bertossi *et al.*, 1997). Bertossi et al. (1997) showed no statistical difference in the number of vesicles between normal and peritumoural microvessels, however did show that in peritumoural vessels there were three times as many vesicles attached to the luminal surface. Regina *et al.* (2004) showed down-regulation of caveolin-1 and increases in phosphorylated caveolin-1 in glioma vasculature. In accordance with the above studies; increases in phosphorylation could then lead to increased internalisation of vesicles as well as decreases in Pgp activity. Similarly Zhao *et al.* (2011) showed that VEGF leads to increased caveolae endocytosis at the BBB.

Taken together, these studies suggest that in the current study, Pgp differences under the influence of glioma co-culture (more particularly the lower apical Pgp activity of the PBECs in C6 co-culture) could have been (in part) due to altered Pgp/caveolae internalisation brought about by increased VEGF expression of glioma cells.

Dinda et al. (1993), showed that in peritumoural microvasculature there were increased numbers of pinocytic vesicles and large vacuoles (mainly below the luminal surface), but also an increase in these at the abluminal/basal surface, where the number of abluminal vesicles increased with tumour grade/oedema. This indicates glioma can alter caveolae organisation at the plasma membrane of the BBB (shifting from luminal/apical to abluminal/basal surfaces). Furthermore, if Pgp is contained within the caveolin it could result in a reshuffling of Pgp from the luminal to the abluminal surface. This reshuffling contributes to the decreases apical Pgp activity but increased Pgp activity at the basal surface in this study.

Together this suggests that one of the effects of glioma on the BBB is increased internalisation of caveolae/Pgp by endothelial cells, probably through VEGF/src/Cav-1-P pathway, with potential reorganisation of Pgp/vesicles to the abluminal/basal surface.

Pgp expression has been claimed at the basal surface under normal conditions (Bendayan *et al.*, 2006). Here we showed that C6 cells induced Pgp activity at the basal surface, while rat astrocyte did not, demonstrating that any Pgp activity at the basal surface was increased due to the presence of C6 cells and did not occur under normal conditions. Hence, the Bendayan et al. (2006) needs to be treated with caution.

The physiological implication of these finding is that under glioma challenge the BBB could have decreased Pgp activity at the apical surface and increased Pgp activity at

the basal surface, which could decrease the ability of the BBB to remove potentially dangerous chemicals but increase chemotherapeutic entry.

Loss of Pgp in the BBB has been shown previously to result in BCRP upregulation (Cisternino *et al.*, 2004), suggesting that endothelial cells can increase BCRP to compensate for a loss in Pgp. Here it was shown that BCRP activity was greater on the apical surface in the PBECs-C6 (as well as some evidence of greater MRP activity) where apical Pgp activity decreased (Figure 4.6 and Figure 4.7). Furthermore, in this study, there was no difference in overall efflux at the apical surface (Figure 4.2), demonstrating that increases in BCRP activity (and possibly MRP activity) did enough to compensate for the loss of apical Pgp activity.

Concerning the changes in the PBEC BCRP expression under the normal and glioma co-culture, there was greater BCRP activity in rat glioma co-culture that correlated with the increased BCRP mRNA expression, suggesting BCRP activity may be regulated transcriptionally during glioma co-culture, with greater BCRP mRNA expression leading to greater protein expression and greater levels of BCRP activity. Furthermore, since BCRP mRNA was greater but Pgp mRNA was not, it suggests that BCRP is regulated by a different pathway to Pgp. Therefore joint pathways of regulation, such as glucocorticoid receptors (GRs), pregnane X receptor (PXR), glutamate/n-methyl-D-aspartate (NMDA)/ cyclooxygenase 2 (COX-2) which have been shown to up-regulate both transporters together can be excluded (Lemmen *et al.*, 2013, Narang *et al.*, 2008, Yousif *et al.*, 2012).

Lemmen et al. (2013) used PBECs to show that activation of PXR leads to increased BCRP and Pgp mRNA within 6 hours and increased protein/activity by 12 hours. Similarly, Narang et al. (2008), showed PXR expression correlated with increased BCRP and Pgp expression in response to dexamethasone (which occur quickly within 6 hours) and inhibiting GRs prevented the increases, indicating that activation of both GR and PXR increased Pgp and BCRP mRNA/protein levels (using rat BBB model).

Yousif et al. (2012) showed that morphine increased Pgp and BCRP mRNA and protein within 24 hours and that these effects were blocked by inhibiting NMDA receptors or COX-2, while activation of prostaglandin E2 receptors increased Pgp and BCRP mRNA. This implicated the glutamate NMDA/COX2 pathway in up-regulating Pgp and BCRP in response to morphine (using rat and human BBB models).

Pathways which have opposing effects on Pgp and BCRP transporters have been identified. Liu *et al.* (2008) showed than insulin treatment of rat endothelia for 72 hours

increases Pgp mRNA and protein, while in another study Liu *et al.* (2011) showed that the same insulin treatment results in decreased BCRP mRNA and protein. Chernausek *et al.* (1993) did show that C6s secrete twice the amount of insulin-like growth factor-1 (which acts on the same receptors as insulin) than normal glial cells. However, this cannot be the cause of the differences seen in the present study since this would lead to increased Pgp and decreased BCRP in accordance with the findings from Liu et al. (2008) and Liu et al. (2011).

Poller *et al.* (2010) also showed opposite regulation of Pgp and BCRP (in human hCMEC/D3 BBB model). The study showed that pro-inflammatory cytokines affected transporter expression. Interleukin-1β (IL-1β) decreased BCRP mRNA but had no effect on Pgp mRNA, while interleukin 6 (IL-6) decreased both Pgp and BCRP mRNA and tumour necrosis factor-α (TNF-α) decreased BCRP and increased Pgp mRNA expression (72 hour treatments). Similarly, von Wedel-Parlow *et al.* (2009), showed TNF-α and IL-1β decreased BCRP mRNA expression of PBECs with no effect on Pgp mRNA (after just 6 hours of treatment). By 24 hours decreased protein levels of BCRP were noted with both treatments, while Pgp protein levels where only shown to decrease by 24 hours for IL-1β and 48 hours for TNF-α. Interestingly endothelin-1 treatment (a upstream trigger of TNF-α) caused an increase in BCRP and a decrease in Pgp protein after 48 hours, implicating the endothelin-1 and TNF-α pathways, which according to Rigor *et al.* (2010) work via activation of endothelin B (ET_B) receptor, nitric oxide signaling (NOS) and protein kinase C β1 (PKCβ1) to reduce Pgp.

Conversely, von Wedel-Parlow et al. (2009) showed that treatment with an anti-inflammatory glucocorticoid (hydrocortisone) (for 48 hours) increased BCRP mRNA (3 fold) and slightly decreased Pgp mRNA, more in agreement with the current study.

This shows opposite regulation effects of inflammation on BCRP and Pgp. However in the current study in contrast to the above study with anti-inflammatory agents, although there was up-regulation of BCRP mRNA no effect on Pgp mRNA was noted. Therefore a truly independent pathway for BCRP mRNA is required to explain the results obtained here. However, very few individual pathways for BCRP mRNA regulation (independent of Pgp regulation) have been identified.

One study by Hoque *et al.* (2012), showed that in hCMEC/D3 BBB cells, PPARα activation led to increased BCRP mRNA, protein and activity (in a time-dependent and ligand-concentration dependent manner) via PPARα binding to the BCRP promoter. Studies involving PPARα activation have shown either no effect or decreases in Pgp activity (Ehrhardt *et al.*, 2004). Interestingly, Weiss *et al.* (2009), showed that treatment

with PPARα/γ ligands resulted in increased BCRP mRNA with no effect on Pgp mRNA. These studies are consistent with the findings of the current study, which may implicate the PPAR nuclear receptors in the effect seen here in C6 co-culture.

Since the current study showed that BCRP mRNA expression increased on day 3 of co-culture prior to addition of CPT-cAMP and Ro-20-1724 (Figure 4.9), this indicates that the pathways responsible for BCRP mRNA increases can be independent of elevating cAMP. However, conclusive mRNA increases in BCRP (when using both reference genes) correlated with the addition of CPT-cAMP and Ro-20-1724 (Figure 4.9), indicating that CPT-cAMP and Ro-20-1724 can enhance the C6 effects seen on day 3 of co-culture. Therefore, this indicates that BCRP mRNA is up-regulated by a pathway that can be influenced by, but is not dependent on, CPT-cAMP and Ro-20-1724. Interestingly, cAMP can work via PKA to increase the phosphorylation of PPAR proteins, resulting in their activation/DNA binding capabilities, however phosphorylation/activation can also occur via other means (Diradourian *et al.*, 2005). Therefore, this too implicates the PPAR pathway in the regulation of BCRP mRNA under C6 conditions. However, the way in which C6s could trigger PPAR responses in PBECs is unclear, with no studies conducted on the matter. Therefore, this is only a possibility, and other yet undiscovered pathways could be involved in BCRP regulation during glioma challenge.

In the human co-cultures no notable changes in BCRP mRNA expression were seen in the glioma co-cultures (Figure 4.11), which was different to the greater BCRP mRNA expression shown in the rat glioma co-cultures by the PBECs-C6s, when compared to the PBECs-rAS. This difference could be due to the length of the co-culture or differences in the methods of co-culture.

In the rat co-cultures, the rat cells were in co-culture for 4 days, while the human cells were in co-culture for only 2 days; the latter may not be enough time to induce mRNA changes. Similarly, Boveri et al. (2005), who used cells for 12 day co-culture with bovine endothelia, could not replicate the results of Raub *et al.* (1992) who only conducted the co-culture for 2 days. However, even though there was no change in mRNA expression in the current study, increased BCRP activity was seen (Figure 4.8), suggesting that, like Pgp, BCRP can also be regulated post-transcriptionally. Although no post-transcriptional regulation of BCRP has yet been reported, regulation via dimerisation of BCRP (where a dimer is needed for BCRP activity) had been suggested as a means of regulating BCRP activity post-transcriptionally (Mo & Zhang, 2009, Ni *et al.*, 2010), suggesting an expression-independent regulation of BCRP is possible.

Furthermore, the co-cultures with the rat cells began while the PBECs were proliferating, but in the 2 day human co-cultures the PBECs were co-cultured after confluence had been reached. An early study could not induce BBB enzymes through astrocyte co-culture when using a non-proliferation confluent monolayer of brain endothelial cells, but could when co-culturing the endothelial cells with the astrocytes during proliferation (Meyer *et al.*, 1990). .

This has implications for glioma development *in vivo*, indicating that new BBB formation is more vulnerable to the influence of glioma than an established BBB. Therefore in glioma, where VEGF has been shown to be commonly increased and be involved in promoting angiogenesis (Jain *et al.*, 2012), the new BBB or blood-tumour barrier could be compromised. In addition this may have implications for repair of the BBB during glioma, where the new BBB formed after apoptosis, necrosis or hypoxia, may be compromised. This agrees with previous studies showing that the BBB in early tumour challenge is tight, while later stages of glioma show increased BBB permeability (Larsson *et al.*, 1990) and also that the newly-formed vasculature of glioma is leaky (Jain et al., 2012).

Understanding such differences in the BBB during tumour challenge may help in the development of pharmaceuticals that can more effectively treat glioma. Since in the current study, both the proliferating PBECs (4 day rat co-culture) and the confluent PBECs (2 day human co-cultures) showed glioma to increase BCRP activity, increases in BCRP activity may be a common feature of both the established and newly formed BBB, and its increased activity should be considered in pharmaceutical treatment of gliomas.

6 Investigation of Signaling Mechanisms

6.1 Results

Previous results (Chapter 4) indicated that PBEC BCRP is transcriptionally regulated in the presence of glioma cells, with mRNA expression in PBECs co-cultured with C6s increasing 3-4 fold when compared with PBECs in co-culture with normal rat astrocytes. However, no Pgp modulation in mRNA expression was observed. This suggested independent pathways exist for BCRP and Pgp regulation.

Since the Wnt and Hedgehog signaling pathways are known to modulate BCRP and Pgp expression (Sims-Mourtada *et al.*, 2007, Lim *et al.*, 2008) and since the glioma secretome contains modulators of these systems (Zhou *et al.*, 2010, Braun *et al.*, 2012), the effect of signaling agonist and antagonist were tested.

PBECs were grown in either astrocyte-conditioned medium, C6-conditioned medium or human glioma-conditioned medium, to try and identify any pathways responsible for the effects noted previously.

To assess differences in Pgp and BCRP activity between the PBECs in normal and glioma-conditioned media a modified Hoechst assay was used based on the cell accumulation of Hoechst 33342 dye which is both a Pgp and BCRP substrate (Shapiro *et al.*, 1997, Tang *et al.*, 2004, von Wedel-Parlow *et al.*, 2009). This allowed rapid screening in a 96-well format, which the ^{3}H-MPP^{+} assay did not. Hoechst 33342 is a nucleotide-binding dye that can freely diffuse through the plasma membrane and reach the nucleus and bind to DNA. Once bound to the DNA, Hoechst 33342 becomes fluorescent at a wavelength of ~460 nm (Zhang *et al.*, 1999). Inhibition of efflux transporters reduces efflux of the dye, enhancing dye accumulation; thus transporter activity can be assessed indirectly.

6.1.1 PBECs grown in different media

Since each co-culture cell type required different growth media, the effects of non-conditioned media on PBECs efflux activity were compared.

PBECs were grown in either 50% serum-free PBEC medium (sfPBEC), 50% Astrocyte Medium (AsM/sfPBEC) or 50% Neural Stem Cell medium (NsM). The growth was conducted as follows over a period of 4 days (Table 5.1):

Table 6.1 PBEC media composition

Medium Label	**Days After Passaging**			
	Day 1	**Day 2**	**Day 3**	**Day 4**
sfPBEC [a]	100% PBEC Medium	100% PBEC Medium	50% PBEC Medium 50% serum-free PBEC Medium	50% PBEC Medium 50% serum-free PBEC Medium
AsM/ sfPBEC [b]	50% PBEC Medium 50% Astrocyte Medium B	50% PBEC Medium 50% Astrocyte Medium B	50% PBEC Medium 50% serum-free PBEC Medium	50% PBEC Medium 50% serum-free PBEC Medium
NsM [c]	50% PBEC Medium 50% Neural Stem Cell Medium	50% PBEC Medium 50% Neural Stem Cell Medium	50%PBEC Medium 50% Neural Stem Cell Medium	50% PBEC Medium 50% Neural Stem Cell Medium

[a] sfPBEC replicates the condition of Mono-cultured PBECs (PBECs-M),

[b] AsM/sfPBEC replicates the condition of the rat astrocyte and C6 co-cultures (PBECs-rAS and PBECs-C6)

[c] NsM replicates the condition of the human astrocyte and G7 2 day co-cultures (PBECs-hAS and PBECs-G7).

After four days the PBECs were then assayed using the Hoechst Uptake assay in the absence or presence of Ko143 (BCRP inhibitor) or haloperidol (Pgp inhibitor) (Figure 5.1).

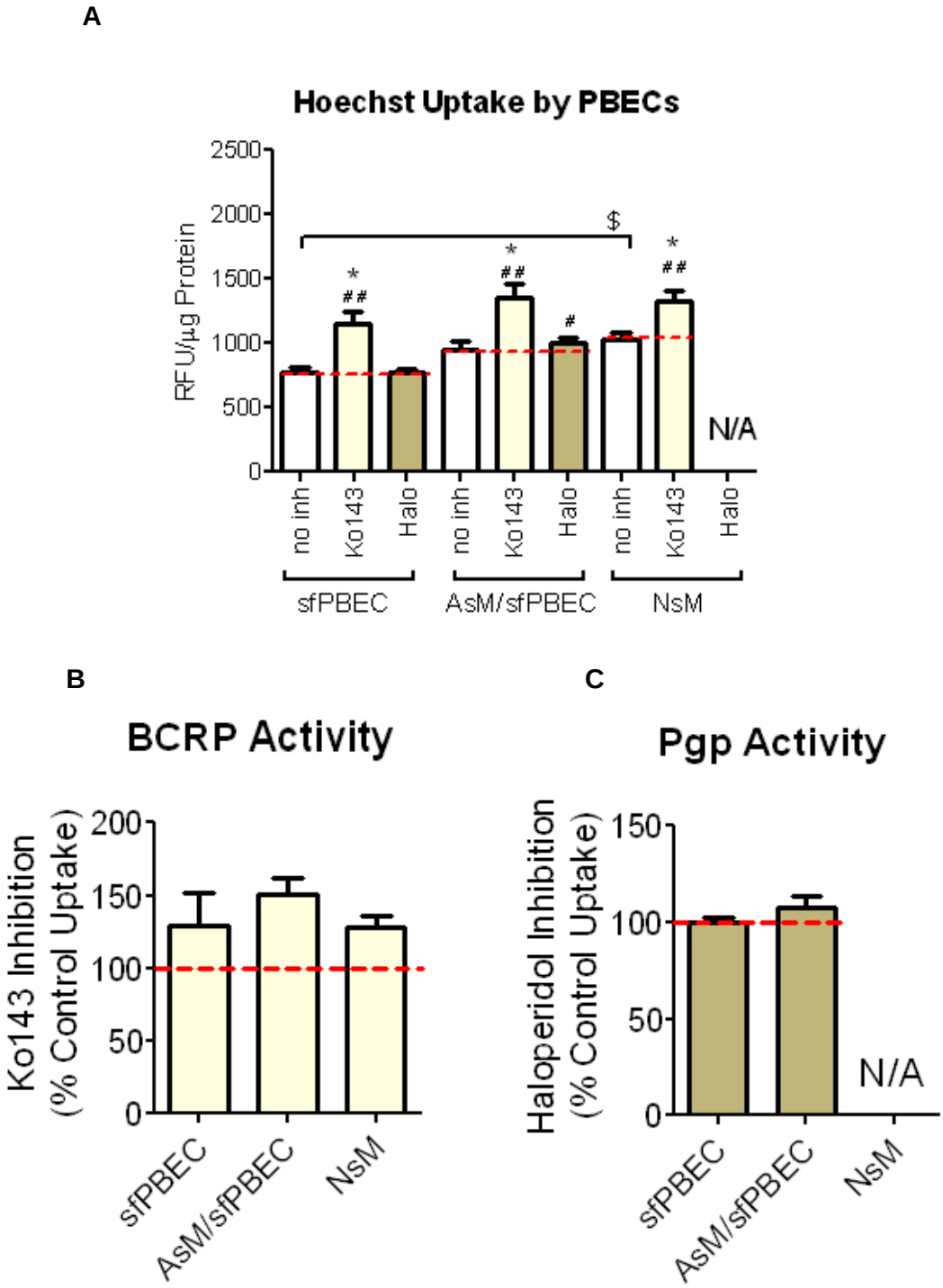

Figure 6.1 BCRP and Pgp activity of PBECs grown in standard media

PBEC efflux activity was assayed using the Hoechst Uptake assay. Hoechst 33342 (10 µM) was incubated with the PBECs for 1 hour in the absence or presence of ABC transporter inhibitors Ko143 (0.2 µM) or haloperidol (60 µM) and Hoechst accumulation expressed as Relative Fluorescence Units (RFU) per µg protein.

A) The Hoechst uptake per µg protein by PBECs grown in different media compositions; sfPBEC = 100% serum-free PBEC medium; AsM/sfPBEC= 50% Astrocyte Medium and 50% serum-free PBEC medium; NsM = Neural Stem Cell Medium.

The RFU/ µg protein data under the inhibitor conditions for a given medium type was then normalised against the control (no inhibitor, indicated by the dotted red lines) data for that same medium type to give the relative inhibition of BCRP (B) and Pgp (C) by the Ko143 and Haloperidol inhibitors respectively.

The results are expressed as % control RFU/µg protein (with control uptake indicated by the red dotted line). Values are mean ± SEM of n=3 wells from 2-3 plates.

* $p<0.05$ difference in unpaired 2-tailed t-test, between the indicated inhibitor and its own no inhibitor control.

# $p<0.05$, ##$p<0.01$, ## $p<0.001$ difference in a paired 2-tailed t-test, between the indicated inhibitor and its own no inhibitor control on the same plate.

For BCRP activity, analysis by 1 way ANOVA showed no significant differences, $p=0.4794$, $F=0.8182$, $R^2=0.1895$, $df=9$

For Pgp activity, analysis by unpaired 2-tailed t-test showed no significant differences, $p=0.3495$, $t=1.058$ $R^2=0.2188$, $df=4$

N/A = not assessed

The results (Figure 5.1 B and C) showed similar levels of Ko143 and of haloperidol inhibition between all the conditions, indicating similar levels of BCRP and Pgp activity respectively.

PBECs were then grown for four days in conditioned medium from normal rat astrocytes (AsCM), rat C6 cells (C6CM), normal human neural stem cells (Cb660CM) or human malignant glioma cells with neural stem cell markers G15 (G15CM), G7 (G7CM) or G26 (G26CM) (Table 5.2). However, due to low availability of the human cell-conditioned media only the BCRP activity was assessed.

Conditioned medium (C6CM or AsCM) had no effect on Pgp activity compared with the non-conditioned medium equivalent (AsM/sfPBEC) (Figure 5.2A). However, growing PBECs in AsCM suppressed BCRP activity when compared with non-conditioned medium. BCRP activity was greater in C6CM than in than in AsCM (Figure 5.2A) but not significantly different from non-conditioned medium.

Similarly, G7- and G26-conditioned medium also showed increased BCRP activity when compared with Cb660CM (Figure 5.2C).

This indicates that the glial cells supplement the medium with one or more factors that can influence PBEC ABC transporter activity.

Table 6.2 Conditioned media composition

Medium Label	Days After Pass aging			
	Day 1 (Media Change)	Day 2	Day 3 (Media Change)	Day 4
AsCM	50% PBEC Medium 50% Astrocyte Medium B conditioned by rat Astrocytes	50% PBEC Medium 50% Astrocyte Medium B conditioned by rat Astrocytes	50% PBEC Medium 50% serum-free PBEC Medium conditioned by rat Astrocytes	50% PBEC Medium 50% serum-free PBEC Medium conditioned by rat Astrocytes
C6CM	50% PBEC Medium 50% Astrocyte Medium B conditioned by C6s	50% PBEC Medium 50% Astrocyte Medium B conditioned by C6s	50% PBEC Medium 50% serum-free PBEC conditioned by C6s	50% PBEC Medium 50% serum-free PBEC Medium conditioned by C6s
Cb660CM	50% PBEC Medium 50% Neural Stem Cell Medium conditioned by Cb660s	50% PBEC Medium 50% Neural Stem Cell Medium conditioned by Cb660s	50% PBEC Medium 50% Neural Stem Cell Medium conditioned by Cb660s	50% PBEC Medium 50% Neural Stem Cell Medium conditioned by Cb660s
G15CM	50% PBEC Medium 50% Neural Stem Cell Medium conditioned by G15s	50% PBEC Medium 50% Neural Stem Cell Medium conditioned by G15s	50% PBEC Medium 50% Neural Stem Cell Medium conditioned by G15s	50% PBEC Medium 50% Neural Stem Cell Medium conditioned by G15s
G7CM	50% PBEC Medium 50% Neural Stem Cell Medium conditioned by G7s	50% PBEC Medium 50% Neural Stem Cell Medium conditioned by G7s	50% PBEC Medium 50% Neural Stem Cell Medium conditioned by G7s	50% PBEC Medium 50% Neural Stem Cell Medium conditioned by G7s
G26CM	50% PBEC Medium 50% Neural Stem Cell Medium conditioned by G26s	50% PBEC Medium 50% Neural Stem Cell Medium conditioned by G26s	50% PBEC Medium 50% Neural Stem Cell Medium conditioned by G26s	50% PBEC Medium 50% Neural Stem Cell Medium conditioned by G26s

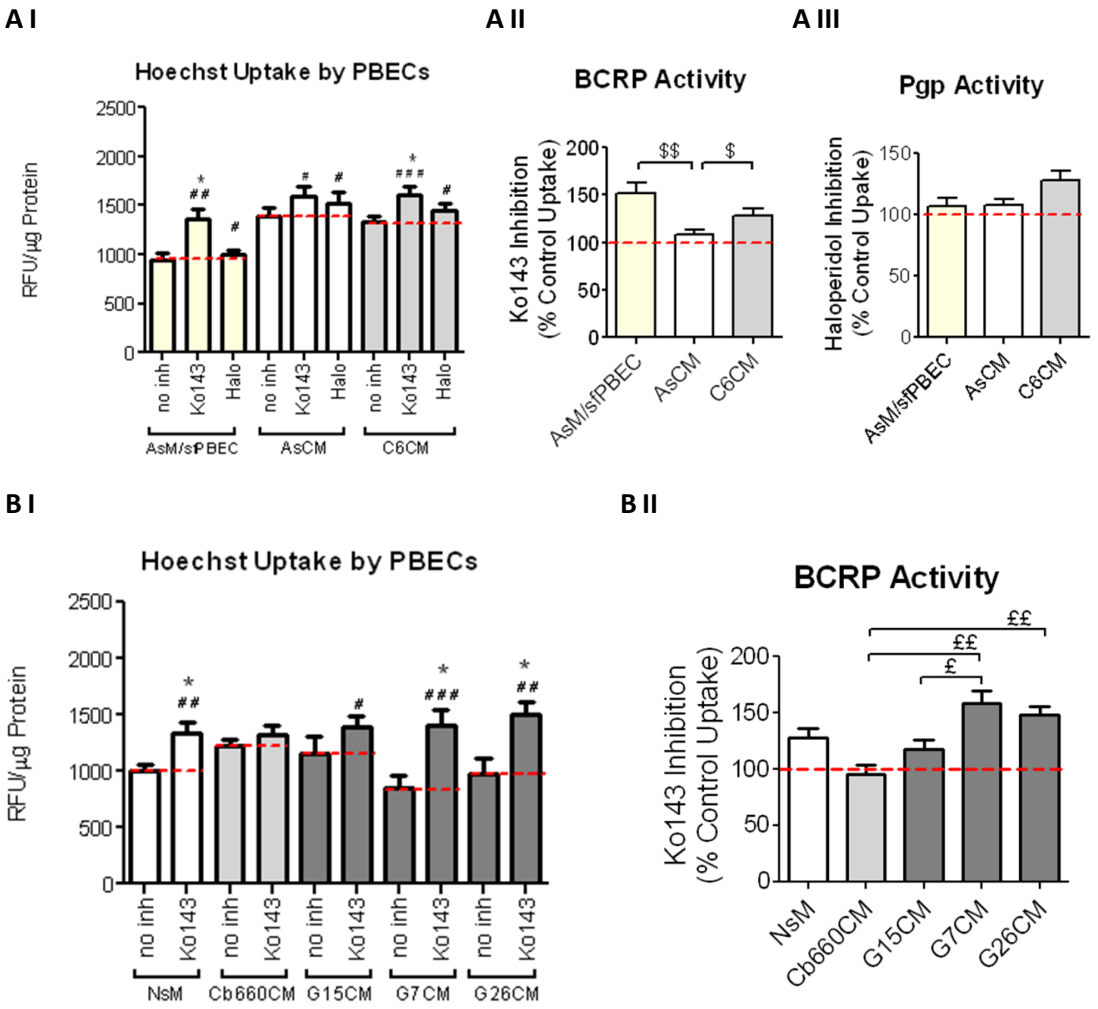

Figure 6.2 BCRP and Pgp activity of PBECs grown in conditioned media

PBECs were grown in media conditioned by rat or human cells and efflux transporter activity was assessed using the Hoechst Uptake assay. Hoechst 33342 (10 µM) was incubated with the PBECs for 1 hour in the absence or presence of ABC transporter inhibitors Ko143 (0.2 µM) (A) or haloperidol (60 µM) (B) and Hoechst accumulation expressed as Relative Fluorescence Units (RFU) per µg protein.

I) The Hoechst uptake per µg protein by PBECs grown in different media compositions; AsM/sfPBEC= 50% Astrocyte Medium and 50% serum-free PBEC medium; AsCM = rat astrocyte conditioned medium, C6CM = G6 glioma conditioned medium; NsM = Neural Stem Cell Medium, Cb660CM = conditioned medium from normal human neural stem cells, G15, G7 and G26 CM = conditioned medium from different human glioma cell lines.

The RFU/ µg protein data under the inhibitor conditions for a given medium type was then normalised against the control (no inhibitor, indicated by the red dotted lines) data for that same medium type to give the relative inhibition of BCRP (II) and Pgp (II) by the Ko143 and Haloperidol inhibitors respectively.

The results are expressed as % control RFU/µg protein (with control uptake indicated by the red dotted line). Values are mean ± SEM of n=3 wells from 2-3 plates.

* p<0.05 difference in unpaired 2-tailed t-test, between the indicated inhibitor and its own no inhibitor control.

# p<0.05, ##p<0.01, ### p<0.001 difference in a paired 2-tailed t-test, between the indicated inhibitor and its own no inhibitor control on the same plate.

$ p<0.05, $$ p<0.01 statistically significant differences in 1-way ANOVA using Newman-Keuls Multiple Comparison post test

£ p<0.05, ££ p<0.01 statistically significant differences in 1-way ANOVA using Tukey's Multiple Comparison post test

For Pgp activity, 1 way ANOVA analysis showed no significant differences, p=0.2447, F=1.490, R^2=0.1065 df=27

6.1.2 PBEC efflux transporter: Hedgehog and Wnt signaling

To investigate whether the Hedgehog and Wnt signaling pathways could affect PBEC ABC transporter activity, PBECs were grown in AsCM or C6CM with agonists and antagonists of these systems for 48 hours (Table 5.3, Figure 5.3). PBECs grown in AsCM were used as the normal condition since AsCM influenced PBEC transporter activity and hence was deemed a more physiologically normal control than non-conditioned medium.

Table 6.3 Drug treatments

Pathway	Treatment	Treatment Type	Target	Concentration	Ref
Hedgehog	SHH Cyclopamine	Agonist Antagonist	Patch Receptor Smo membrane receptor	1µg/ml 30 µM	Chen et al 2012 Yauch et al 2008
Wnt	BIO Dkk-1	Agonist Antagonist	GSK-3β Frizzled Receptor	1 µM 0.1mg/ml	Lim JC 2008 Lim JC 2008

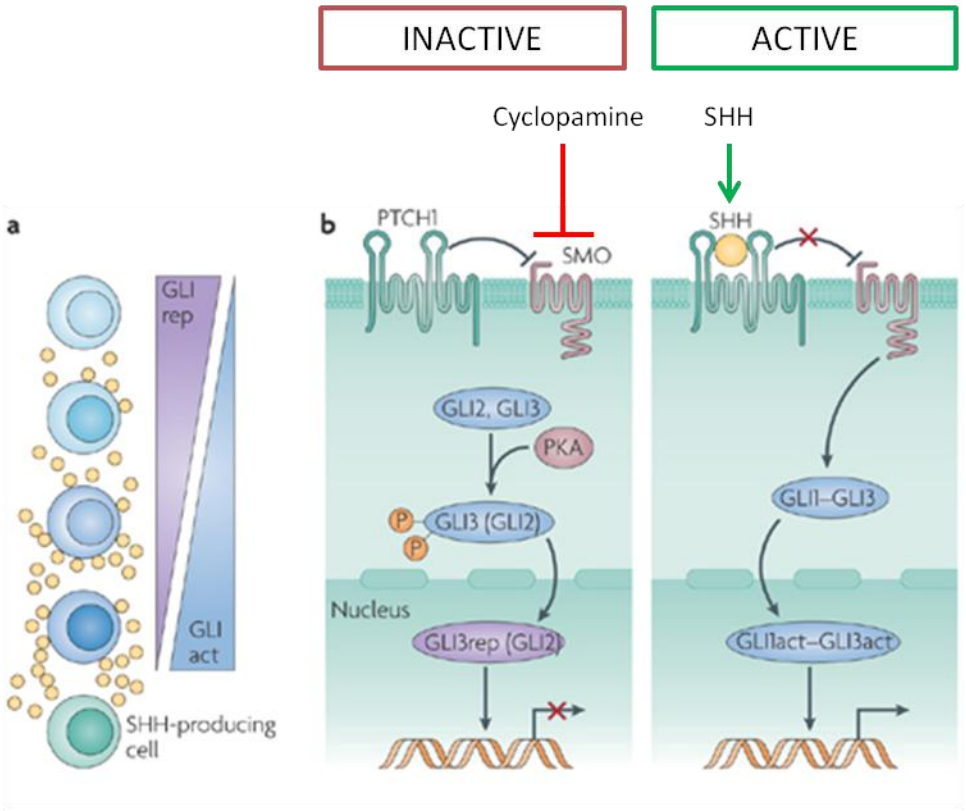

Figure 6.3 Sonic Signaling (Modified from Comptom et al., 2007)

a) Sonic hedgehog (SHH) secreted by a localised source (shown in green) creates a gradient of concentration that provides positional information to the cells in the gradient, dependent on the concentration and duration of the signal, and specifies distinct cell fates accordingly (represented by different shades of blue). The amount of SHH signal received by a cell affects the ratio of glioma-associated oncogene (GLI) activator form–GLI repressor form (GLIact–GLIrep) protein content, with increased amount of GLIact in cells closer to the SHH secreting source and increased GLIrep in cells receiving low or no SHH. The ratio of GLIact:GLIrep proteins is instrumental in the interpretation of the SHH gradient.

b) In the absence of SHH protein, patched (PTCH1) inhibits smoothened (SMO) activity allowing the protein kinase A (PKA)-mediated phosphorylation and truncation of GLI2 and GLI3. GLI2rep and GLI3rep are transported to the nucleus where they negatively regulate gene transcription. In the presence of SHH, interaction of SHH with PTCH1 relieves the inhibition of SMO. Activated SMO protects the GLI proteins from PKA-mediated modification and activates them. GLI1act–GLI3act are translocated to the nucleus where they activate target gene transcription.

Cyclopamine inhibits SMO activity inducing an inactive state, while SHH treatment alleviates SMO inhibition activating the pathway.

The results (Figure 5.4) show that for PBECs in AsCM, the sonic pathway agonist, SHH, increased BCRP activity, but inhibition of the sonic downstream receptor Smo alone had no effect. Conversely, for PBECs in C6CM, treatment with SHH decreased both BCRP and Pgp activity, while treatment with the sonic receptor antagonist (cyclopamine) increased BCRP activity, indicating that the response to sonic signaling is altered by C6CM.

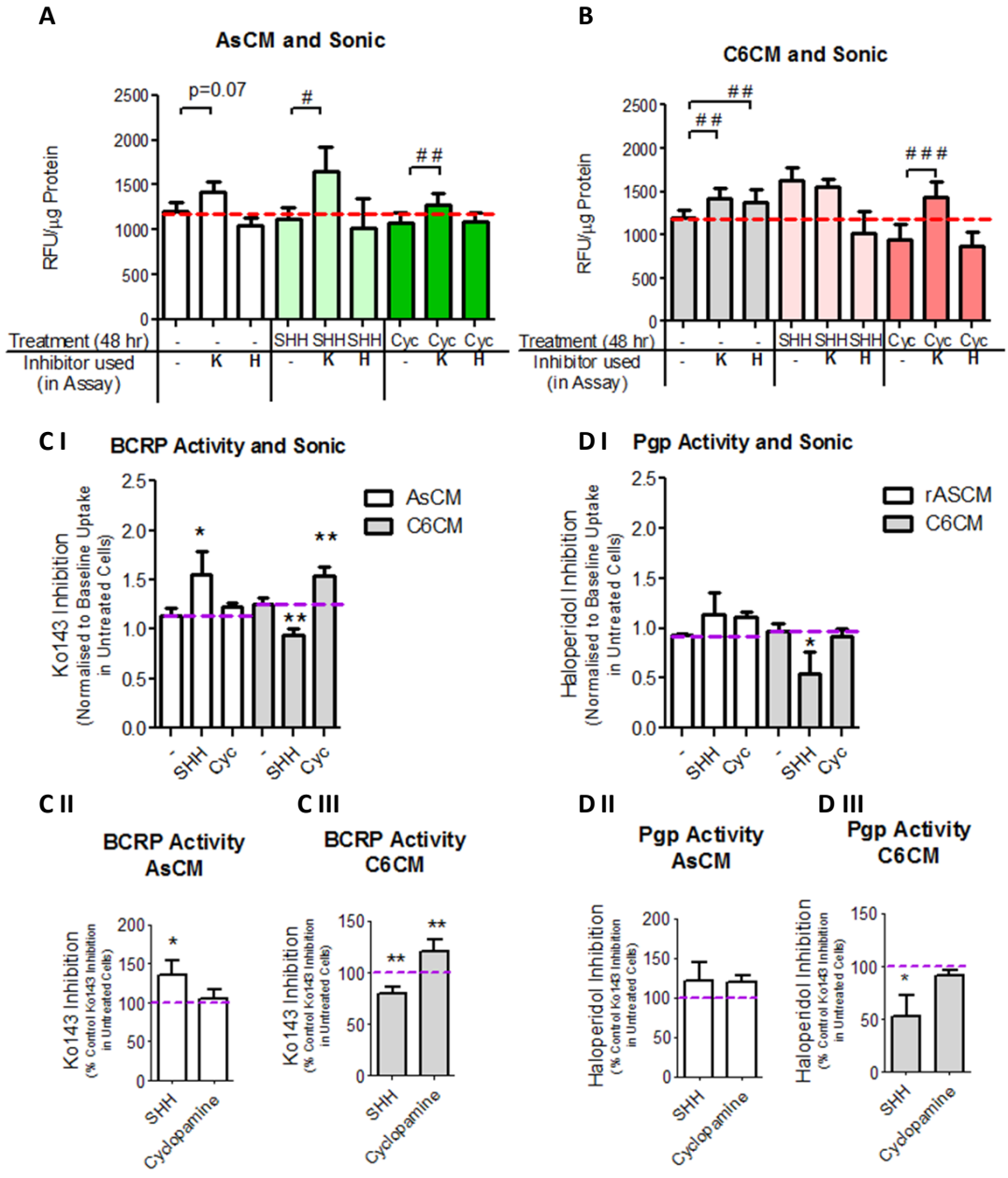

Figure 6.4 Sonic Hedgehog and ABC transporter activity

PBECs grown in either rat astrocyte-condition medium (AsCM, light bars) or C6-conditioned medium (C6CM, dark bars) and treated for 48 hours with either recombinant sonic hedgehog

(SHH, 1µg/ml), cyclopamine (Cyc, 30 µM) or vehicle control (-), were assayed using a Hoechst Uptake assay.

Hoechst 33342 (10 µM) was incubated with the PBECs for 1 hour in the absence or presence of ABC transporter inhibitors Ko143 (0.2 µM, BCRP inhibitor, K) or haloperidol (60 µM, Pgp inhibitor, H) and Hoechst accumulation is expressed as Relative Fluorescence Units (RFU) per µg protein.

The inhibition effect of the transporters was calculated as the increase in RFU/µg protein in the presence of inhibitor when compared to the RFU/µg protein in the absence of that inhibitor on the same plate. The inhibition effect was then normalised to baseline Hoechst uptake on the same plate (i.e. the uptake in the absence of any treatment or inhibitors) (indicated by the red dotted lines in A and B), with normalised inhibition data given in C I and D I for Ko143 and Haloperidol respectively.

Ko143 inhibition was used to determine BCRP activity (C) and Haloperidol was used to determine Pgp activity (D).

The normalised inhibition data in the SHH or cyclopamine treated PBECs were then expressed as a percentage of the normalised Ko143 and haloperidol inhibitions measured in untreated PBECs (as shown in CII-CIII and DII- DIII).

Mean ± SEM of n=4-10 wells from 3-5 plates.

#p<0.05, ##p<0.01, ###p<0.001 statistically significant differences in a 2-tailed paired t-test between the indicated inhibitor condition and its respective no inhibitor control from the same plate.

*p<0.05, **p<0.01 statistically significant differences in a paired t-test between the indicated condition and its respective untreated control from the same plate.

To investigate the Wnt pathway, PBECs were treated with BIO to upregulate signaling, and Dkk-1 to inhibit signaling (see Table 5.3, Figure 5.5).

The data (Figure 5.6) show that for PBECs in AsCM, activation of the Wnt pathway increased both BCRP and Pgp activity, while inhibition of Wnt signaling using Dkk-1 alone decreased BCRP activity, demonstrating endogenous Wnt activity in PBEC in AsCM. By contrast, for PBECs in C6CM neither intervention had any significant effect. This indicated that there are one or more factors in the C6CM that inhibit Wnt activity.

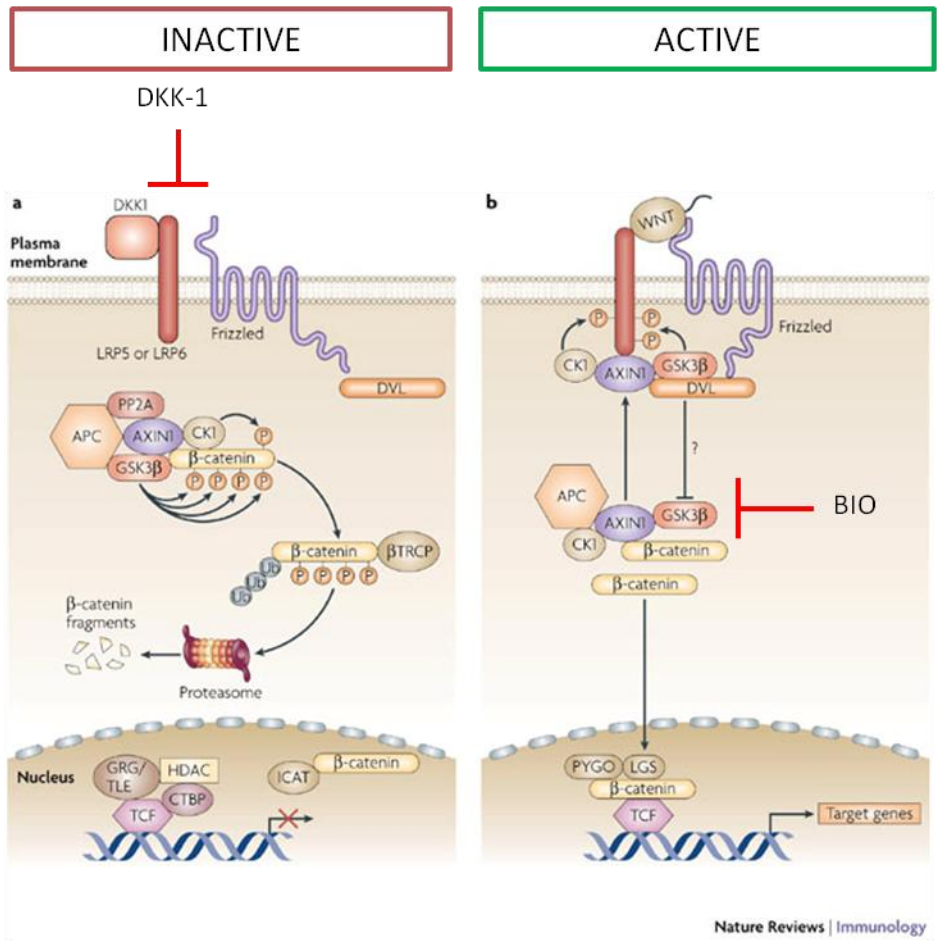

Figure 6.5Wnt Signaling (Modified from Staal et al., 2008)

a) In the absence of WNT signalling, β-catenin levels in the cytoplasm and nucleus are low as a result of continuous phosphorylation by the serine/threonine kinases CK1 (casein kinase 1) and GSK3β (glycogen synthase kinase 3β), leading to binding of -transducin-repeat-containing protein (TRCP) and to ubiquitylation and degradation by the proteasome. The destruction complex is composed of CK1 and GSK3β, as well as the anchor proteins AXIN1 (axis inhibition protein 1) and APC (adenomatous polyposis coli). In the nucleus, TCF (T-cell factor) molecules

are bound by co-repressors such as GRG/TLE (Groucho/transducin-like enhancer) proteins that shut off expression of WNT target genes. Other components of the repressor complex include CTbP (C-terminal binding protein) and HDACs (histone deacetylases). β-catenin in the nucleus is inhibited from binding TCF by ICAT (cell autonomous inhibitor of β-catenin and TCF) . The Frizzled receptor complex — composed of Frizzled and LRP5 (LDL-receptor-related protein 5) or LRP6 — can also be actively inhibited by receptor-bound soluble inhibitors such as DKK1 (Dickkopf homologue 1).

b) Upon binding of a lipid-modified WNT protein to the receptor complex, a signaling cascade is initiated. LRP is phosphorylated by CK1 and GSK3β, and AXIN1 is recruited to the plasma membrane. The kinases in the β-catenin destruction complex are inactivated and β-catenin translocates to the nucleus to form an active transcription factor complex with TCF, leading to transcription of a large set of target genes. In the nucleus, β-catenin binds to TCF and LEF factors and recruits co-factors such as legless (LGS; also known as BCL9) and Pygopus (PYGO), CBP/p300, Brahma and MED12 to initiate transcription DVL, mammalian homologue of Drosophila Dishevelled; PP2A, protein phosphatase 2A.

Dkk-1 treatment acts to inactivate the Wnt pathway, while BIO inhibits GSK3β acting to promote the active Wnt state.

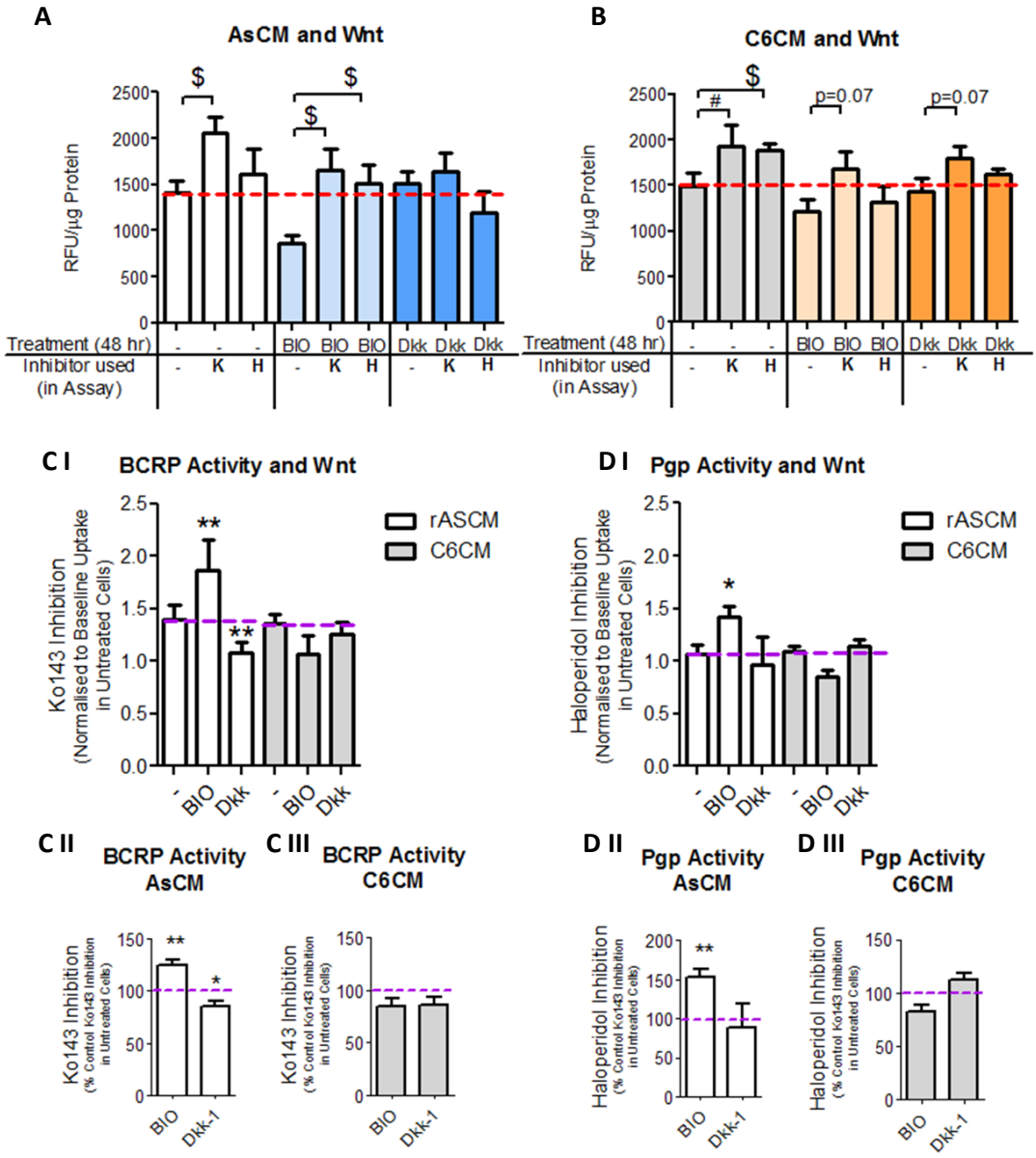

Figure 6.6 Wnt and ABC transporter activity

PBECs grown in either rat astrocyte-condition medium (AsCM, light bars) or C6-conditioned medium (C6CM, dark bars) and treated for 48 hours with either BIO (1 µM), recombinant Dkk-1 (0.1mg/ml) or vehicle control (-), were assayed using a Hoechst Uptake assay.

Hoechst 33342 (10 µM) was incubated with the PBECs for 1 hour in the absence or presence of ABC transporter inhibitors Ko143 (0.2 µM, BCRP inhibitor, K) or haloperidol (60 µM, Pgp inhibitor, H) and Hoechst accumulation is expressed as Relative Fluorescence Units (RFU) per µg protein.

The inhibition effect of the transporters was calculated as the increase in RFU/µg protein in the presence of inhibitor when compared to the RFU/µg protein in the absence of that inhibitor on the same plate. The inhibition effect was then normalised to baseline Hoechst uptake on the

same plate (i.e. the uptake in the absence of any treatment or inhibitors) (indicated by the red dotted line in A and B), with normalised inhibition data given in CI and D I for Ko143 and Haloperidol respectively.

Ko143 inhibition was used to determine BCRP activity (C) and Haloperidol was used to determine Pgp activity (D).

The normalised inhibition data in the SHH or cyclopamine treated PBECs were then expressed as a percentage of the normalised Ko143 and haloperidol inhibitions measured in untreated PBECs (as shown in CII-CIII and DII- DIII).

Mean ± SEM of n=4 from 2 plates.

$ $p<0.05$, statistically significant differences in a 2-tailed unpaired t-test between the indicated inhibitor condition and its respective no inhibitor control.

#$p<0.05$, ##$p<0.01$, ###$p<0.001$ statistically significant differences in a 2-tailed paired t-test between the indicated inhibitor condition and its respective no inhibitor control from the same plate.

*$p<0.05$, **$p<0.01$ statistically significant differences in a paired t-test between the indicated condition and its respective untreated control from the same plate.

6.2 Discussion

The current study aimed to investigate Wnt and Hedgehog signaling in PBECs grown in AsCM and glioma CM.

The results showed that in PBECs in AsCM, activation of the canonical Wnt/β-catenin pathway (by inhibiting GSK-3β with BIO) led to increased BCRP and Pgp activity in PBECs. Conversely, inhibition of Wnt (by inhibitor of the Wnt Frizzled receptor, Dkk-1) decreased BCRP activity (Figure 5.4). This showed not only that Wnt can increase BCRP and Pgp activity in PBECs, but that for PBECs in AsCM medium, the Wnt pathway is constitutively active, since the inhibitor did have an effect.

The constitutive activity of Wnt in the PBECs is not necessarily derived from the AsCM. Similar results of Wnt activation and inhibition in both primary rat and human endothelial cells in non-conditioned medium, have been shown by Lim et al. (2008). In that study, Wnt activation using BIO led to increased mdr1a (rat endothelial cells) and MDR1 (human endothelial cells) mRNA and Pgp protein expression. ABCG2 mRNA

and BCRP protein expression also increased. The increases correlated with increased β-catenin translocation to the nucleus, implicating β-catenin/TCF/LEF in the transcriptional regulation of the ABCs. Conversely, the addition of Wnt inhibitors to the endothelial cells, caused decreased Pgp and BCRP mRNA and protein expression.

This together demonstrates that Wnt in constitutively active within brain endothelial cells and that this is partly responsible for the basal expression levels/activity of BCRP and Pgp.

Harati *et al.* (2013) also investigated the link between the Wnt/β-catenin pathway and Pgp/BCRP expression. Harati et al. (2013) examined capillaries isolated from rats at different stages of development and showed that Pgp and BCRP mRNA expression increased with rat maturation. Pgp protein expression also increased with rat maturation, however, BCRP protein expression did not, with BCRP protein expression stabilising early in the development process. Furthermore, neither Pgp nor BCRP activity changed throughout development, showing that despite changes in the protein and/or mRNA expression of Pgp and BCRP, activity was constant.

Interestingly, β-catenin expression (both mRNA and protein expression) was shown to decrease with rat brain development. There was an inversely correlation between with the mRNA expression of Pgp and BCRP and β-catenin expression, showing that despite decreases in Wnt signaling, BCRP and Pgp mRNA expression continued to increase (Harati et al., 2013). This indicates that factors other than Wnt are also involved in the regulation of BCRP and Pgp expression. However, as with the Lim et al. (2008) study, Harati et al. (2013) did show that, activation of Wnt (with BIO) increased β-catenin mRNA and protein expression. Wnt activation *in vivo* also resulted in higher nuclear levels of β-catenin that correlated with increased BCRP and Pgp mRNA/protein and activity. In addition, Harati et al. (2013) further showed the endothelin-1 (ET-1) mRNA and protein were increased in response to BIO *in vivo* and that the BIO effect on BCRP could be countered by simultaneous administration of an ET_A receptor (receptor for ET-1) inhibitor. This demonstrates that Wnt effects on the ABC transporters could be ET-1 dependent.

In the current study, the involvement of the Hedgehog pathway was also investigated. Although the role of the Hedgehog pathway has been investigated in the BBB previously, no effects of Hedgehog on the BBB ABC transporters has been reported.

Alvarez *et al.* (2011) did show that the Sonic hedgehog pathway can be activated in endothelial cells, with activation promoting BBB integrity. In this study, Alvarez et al.

(2011) showed that the SHH protein precursor is made and secreted by astrocytes; human foetal astrocytes (but not human brain endothelial cells) demonstrated the expression of the SHH precursor and cleaved SHH protein was detected in astrocyte-conditioned medium. Similarly SHH was found in human and mouse astrocytes *in vivo*, but not in endothelial cells or pericytes (Alvarez et al., 2011). Furthermore, brain endothelial cells were shown to express the Hedgehog receptor and respond to SHH signals.

Treatment of brain endothelial cells *in vitro* with either astrocyte-conditioned media (ACM) or recombinant SHH was shown to have similar effects, which included increased Hop, Gli1 and SOX-18 transcription. Furthermore, SHH and ACM treatment of endothelial cells increased occludin and claudin-5 mRNA and protein expression in the endothelial cells, increased TEER and decreased ^{14}C-Sucrose permeability across the endothelial cells. Conversely, inhibiting the hedgehog pathway with cyclopamine (Smo inhibitor) reduced the effects of ACM on human brain endothelial cells. These findings demonstrate that astrocytes can secrete SHH that can in turn affect endothelial cells.

In the current study, cyclopamine had no effect on the PBECs in AsCM (either on BCRP or Pgp activity), suggesting that for the PBECs in AsCM no Hedgehog activity was present to be inhibited. This therefore indicates that the rat astrocytes did not secrete SHH into the medium or did not secrete sufficient SHH, to elicit an effect that could be significantly inhibited by cyclopamine.

Interestingly, the use of AsCM combined with SHH treatment of PBECs increased the activity of BCRP, when compared with the use of AsCM alone. However no effect on Pgp activity was noted. This indicates that the pathway (although not constitutively active) can be activated, with effects leading to increased BCRP activity.

Similar effects of SHH on BCRP have been reported in non-BBB cells. In cancer cell lines, Sims-Mourtada et al. (2007) showed SHH increased chemotherapeutic resistance of cells by increasing efflux of the chemotherapeutics from the cells, which was attributed to the increased expression of ABC efflux transporters in response to SHH. SHH treatment resulted in increased Gli-1 (sonic transcription factor), BCRP and Pgp protein expression and activity. Furthermore, siRNA against Gli-1 and inhibition by cyclopamine decreased BCRP and Pgp protein expression and activity, implicating SHH, Gli-1 and Smo (cyclopamine target) in the regulation of both efflux transporters.

Singh *et al.* (2011) showed the presence of a Gli-1 binding site in the BCRP promoter region. SHH treatment of lymphoma cells resulted in a concentration-dependent increase in the expression of BCRP mRNA and protein, while Smo inhibition by cyclopamine led to decreased Gli-1 and BCRP mRNA and protein expression. siRNA against Gli-1 also decreased BCRP mRNA and protein expression, showing BCRP is downstream of Gli-1 and that regulation of BCRP involves SHH, Smo and Gli-1.

The current results concerning BCRP are consistent with these earlier studies, which together demonstrate that active sonic hedgehog pathway increases BCRP mRNA and protein expression, leading to increased activity of BCRP. However, the current study diverges from these previous studies concerning Pgp activity, where PBECs treated with SHH in AsCM did not show increased Pgp activity, while the older studies showed that as for BCRP, sonic activation leads to increased Pgp mRNA and protein, and increased activity.

In ovarian cancer cells normally resistant to paclitaxel (a Pgp substrate), resistance was decreased by knocking down or inhibiting Smo (using siRNA or cyclopamine). Decreased drug resistance to the Pgp substrates again implicated the Hedgehog pathway in Pgp regulation (Steg *et al.*, 2012)

Chen *et al.* (2012) showed that in MCF-7 cancer cells the addition of SHH increased Pgp expression in MCF-7 sensitive cells, making them resistant to Pgp substrates. Conversely, siRNA against mdr1a had no effect on SHH or Smo expression, showing Pgp to be downstream of SHH/Smo and not upstream.

The differences between the current studies and earlier studies concerning Pgp and sonic signaling could be due to differences between BBB and non-BBB cells in Pgp regulation or to other factors influencing Pgp activity in the BBB but not in the other cell types.

Teng *et al.* (2012) showed a link between SHH and VEGF in the BBB, with SHH shown to increase VEGF expression (both mRNA and protein) in mouse brain endothelial cells. Furthermore, Hawkins *et al.* (2010) showed that VEGF could decrease Pgp activity without changes in overall Pgp expression, by causing Pgp internalisation. Therefore, in the current study SHH treatment could have resulted in the activation of VEGF pathway leading to Pgp internalisation, where any increases in Pgp expression (in response to SHH) could be masked by loss of Pgp activity in response to VEGF.

Concerning the effects of SHH on the PBECs in C6CM in the current study combined, C6CM and SHH treatment of PBECs resulted in decrease in both BCRP and Pgp activity (when compared with the effect of C6CM alone). This indicates that as a result of glioma-secreted factors the sonic pathway in these BBB endothelial cells is altered. Similarly, Wnt pathway regulation of BCRP and Pgp was altered in PBECs in C6CM, as neither BIO (increased BCRP and Pgp activity in AsCM) nor Dkk-1 (decreased BCRP activity in AsCM) had any effect on the activity of BCRP or Pgp in the PBECs under C6CM conditions.

Interestingly, sonic hedgehog and the Wnt/β-catenin pathways do interact. Meng *et al.* (2001) showed that SUFU, a negative regulator of Hedgehog that controls the nuclear-cytoplasmic distribution of Gli transcription factors by binding Glis and preventing them from reaching their nuclear targets, also complexes with β-catenin, preventing it from acting in the nucleus as a transcription factor (with TCF/LEF protein) (Meng et al., 2001).

In *Xenopus* development, SUFU was shown to integrate Wnt and Hedgehog signals (Min *et al.*, 2011). SUFU was shown to suppress both pathways by binding to β-catenin and Gli-1 respectively. Interestingly, Gli1 was shown to inhibit Wnt under β-catenin over-expression (preventing TCF-transcription), while β-catenin was shown to stimulate Hedgehog pathway when Gli-1 was over-expressed (increased Gli-1 transcription); these effects where both SUFU dependent.

In addition, GSK-3β, the same protein involved in phosphorylation and subsequent ubiquination of β-catenin (in Wnt inactive state), is involved in the sonic signaling pathway (Kise *et al.*, 2009, Chen *et al.*, 2011). Chen et al. (2011) showed that SUFU is also phosphorylated by GSK-3β at Ser 342, which stabilises the SUFU against SHH signaling-induced degradation via ubiquination. In addition, Kise et al. (2009) showed that SUFU (known to suppress Gli-dependent transcription) mediated the processing of Gli3 Repressor (acts as a repressor of Gli-1 and Gli-2 transcription) by GSK-3β. SUFU mediates processing of Gli3 by acting as a bridge between GSK-3β and the unprocessed form of Gli3, facilitating the phosphorylation processing of Gli3 by GSK-3β by bringing the two proteins into close contact. It was shown that SUFU is essential for Gli3 phosphorylation via GSK-3β to occur, as GSK-3β could not interact with Gli3 in the absence of SUFU. Activation of the sonic pathway by SHH was shown to stimulate the dissociation of SUFU/GSK-3β complex from Gli-3, preventing Gli3 repressor processing.

Together this shows that the Sonic and Wnt pathways are linked by at least three proteins SUFU, GSK3B and β-catenin. Therefore, incorrect regulation of one pathway may influence the other pathways. Furthermore, the active Hedgehog pathway has been shown able to negatively regulate Wnt, while active Wnt pathway has been shown to act as a positive regulator of the Hedgehog pathway (Min et al., 2011)

Since the two pathways are interlinked and do influence each other, it is not possible to completely differentiate between the two in the current study. Therefore it is not possible to determine whether the alterations in the pathway responses that were seen in the PBECs in C6CM exist within one or both pathways, nor whether alteration in one pathway may be influenced by the other pathway.

Research into gliomas has given some insight into Wnt signaling under glioma conditions. Zhou et al. (2010) investigated the expression of Dkk-1 in normal and glioma cell lines as well as in normal and glioma tissue samples. The culture medium of all 12 glioblastoma cell lines tested positive for expression of Dkk-1 while normal and medulloblastoma cell line media were negative. Similarly, in human tissues, in normal tissues 9/11 samples tested negative for Dkk-1 while the remaining two only showed weak expression. Conversely, in glioma tissues 28/47 showed strong staining for Dkk-1, 15 tissues showed weak staining and only 4 tissues were negative. In addition, Dkk-1 expression was shown to positively correlate with tumour grade, with more Dkk-1 expressed in higher grade tumours. Zhou et al. (2010) concluded that Dkk-1 was a good marker of gliomas.

In the current study, conditioned medium was also obtained from a glioblastoma cell line, the C6 cells, where Dkk-1 secretion is possible although not confirmed.

The presence of Dkk-1 in the medium could explain why BIO could not elicit an increase in the BCRP and Pgp activity of PBECs in C6CM. Similarly, if Dkk-1 were already present in the medium, the Wnt-dependent expression of BCRP and Pgp would already have been suppressed and so the addition of more Dkk-1 would have no effect. Due to the common pathways shared by the Sonic and Wnt pathways, Dkk-1 may also influence the sonic pathway, however how that might happen is still unknown. Interaction between the two pathways needs to be further explored in PBECs both in AsCM and C6CM.

Other research into gliomas has shown high expression of SHH in glioma cells as well as high expression of members of the signaling pathway (Patch-1, Smo and Gli1) (Braun et al., 2012). If, like their astrocyte counterparts, the glioma cells can secrete

the SHH protein, then gliomas would be able to influence nearby endothelial cells via activation of the Hedgehog pathway, promoting the expression of the ABC transporters. However, in the current study SHH treatment of PBECs in C6CM resulted in PBECs with decreased BCRP and Pgp activity, while cyclopamine increased BCRP activity (opposite effects to those seen under AsCM condition and in previous studies), implying some alterations of the Hedgehog pathway caused by the C6CM.

As detailed above, the presence of Dkk-1 in the C6CM is a candidate, which could have caused a change in Wnt, which may have in turn interfered with the hedgehog pathway. However, other factors may also be acting on the PBECs in C6CM, for example Boveri *et al.* (2005) showed C6s to secrete 40 times more VEGF than astrocytes, and VEGF has been shown to decrease Pgp activity without affecting expression, via caveolae internalisation of Pgp (Hawkins et al., 2010b). Therefore, activity levels of Pgp in the PBECs could have been influences by high levels of VEGF in the C6CM.

Other yet undetermined glioma factors may also have influenced any of the other signaling pathways involved in ABC transporter regulation. Therefore due to the complexity of signaling cascades (e.g. the involvement of Wnt in Hedgehog signaling, as well as the effect of ET-1 signaling on Wnt and the possible influence of the VEGF pathway on Pgp), definitive conclusions concerning the influence of the Hedgehog pathway on the ABC transporters, in endothelial cells in glioma-conditioned media cannot be reached. However, alterations of normal Wnt and Sonic Hedgehog pathways are apparent.

Further work is needed on brain endothelial cells concerning the composition of C6CM as well as work dissecting the influences of sonic on Wnt and vice versa.

7 ABCs in Human Brain

7.1 Results

In order to assess changes in ABC efflux transporter in human brain, an immunohistochemical study was conducted on brain tissue samples from control, Grade I and Grade II astrocytoma patients (Table 6.1).

Table 7.1 Tissue descriptions

No	Sex	Age	Organ	Pathology diagnosis	Grade[a]	Stage	TNM[b]	Sample Type
1	F	28	Cerebrum	Normal cerebral tissue	–	–	–	Control
2	F	20	Cerebrum	Normal cerebral tissue	–	–	–	Control
3	M	26	Cerebrum	Normal cerebral tissue	–	–	–	Control
4	F	24	Cerebrum	Normal cerebral tissue	–	–	–	Control
5	F	24		Normal cerebral tissue				Control
6	M	32		Normal cerebral tissue				Control
7	M	54	Brain	Normal brain				Control
8	M	50's	Brain	Normal brain				Control
9	M	30	Cerebrum	Astrocytoma	1	IIA	T1M0	Grade I
10	M	33	Cerebrum	Astrocytoma	1	I	T1M0	Grade I
11	F	37	Cerebrum	Astrocytoma	1	I	T1M0	Grade I
12	M	39	Cerebrum	Astrocytoma	1	I	T1M0	Grade I
13	F	15	Left Frontal Lobe	Astrocytoma	1			Grade I
14	F	29	Right Frontal Lobe	Astrocytoma	1			Grade I
15	M	62	Cerebrum	Astrocytoma	2	II	T1M0	Grade II
16	M	31	Cerebrum	Astrocytoma	2	IIB	T2M0	Grade II
17	F	47	Cerebrum	Astrocytoma	2	II	T2M0	Grade II
18	F	48	Cerebrum	Astrocytoma	2	II	T1M0	Grade II
19	M	25	Left Frontal Lobe	Astrocytoma	2			Grade II

Tissues 1-4,9-12 and15-18, were all contained on a single slide as a tissue array, with all other samples obtained as 1 tissue per slide.

a Grade 1 or well-differentiated: Cells appear normal and are not growing rapidly.
a Grade 2 or moderately-differentiated: Cells appear slightly different from normal.

b TNM grading:

T - Primary tumour

Tx - Primary tumour cannot be assessed
T0 - No evidence of primary tumour
Tis - Carcinoma *in situ*; intraepithelial or invasion of lamina propria
T1 - Tumour invades submucosa
T2 - Tumor invades muscularis propria

N - Regional lymph nodes

Nx - Regional lymph nodes cannot be assessed
N0 - No regional lymph node metastasis
N1 - Metastasis in 1 to 3 regional lymph nodes

M - Distant metastasis

Mx - Distant metastasis cannot be assessed
M0 - No distant metastasis
M1 - Distant metastasis

BCRP and Pgp staining intensity was determined using antibodies BXP-21 and JSB-1 respectively, which have been used to identify BCRP and Pgp in human brain capillaries/tissue (Sawada *et al.*, 1999, Lee *et al.*, 2007).

For each tissue, once a capillary was identified and the image captured, the image pixels staining for endothelial marker CD34 were specifically analysed further for BCRP and Pgp staining. This procedure therefore excluded as far as possible any background or other non-specific staining from the analysis. Tissue No.3 was eliminated from analysis since no capillaries were identified within the tissue.

7.1.1 Identifying capillaries

Two different endothelial markers were tested, von Willebrand Factor (VWF) and glycoprotein CD34, both of which are established endothelial cell markers (Muller *et al.*, 2002) used on human brain samples previously (Zhang *et al.*, 2011, Wang *et al.*, 2013).

Antibodies against both markers positively stained blood vessels in the tissues tested. However, more background (non-specific staining) was observed with the anti-VWF antibody (Figure 6.1), hence, the anti-CD34 antibody was used for the next stage of analysis.

Three criteria were used to select capillary images for analysis:

a) CD34 positive staining

b) The CD34 marker was used in conjunction with DAPI staining of nuclei within the same z-stack to confirm the presence of live cells.

c) Diameter of vessels used was measured using ImageJ software from the z-stacks and only vessels < 7µm were selected for analysis since capillary diameters in human brain have been reported as 4-7 µm (Patel *et al.,* 2008).

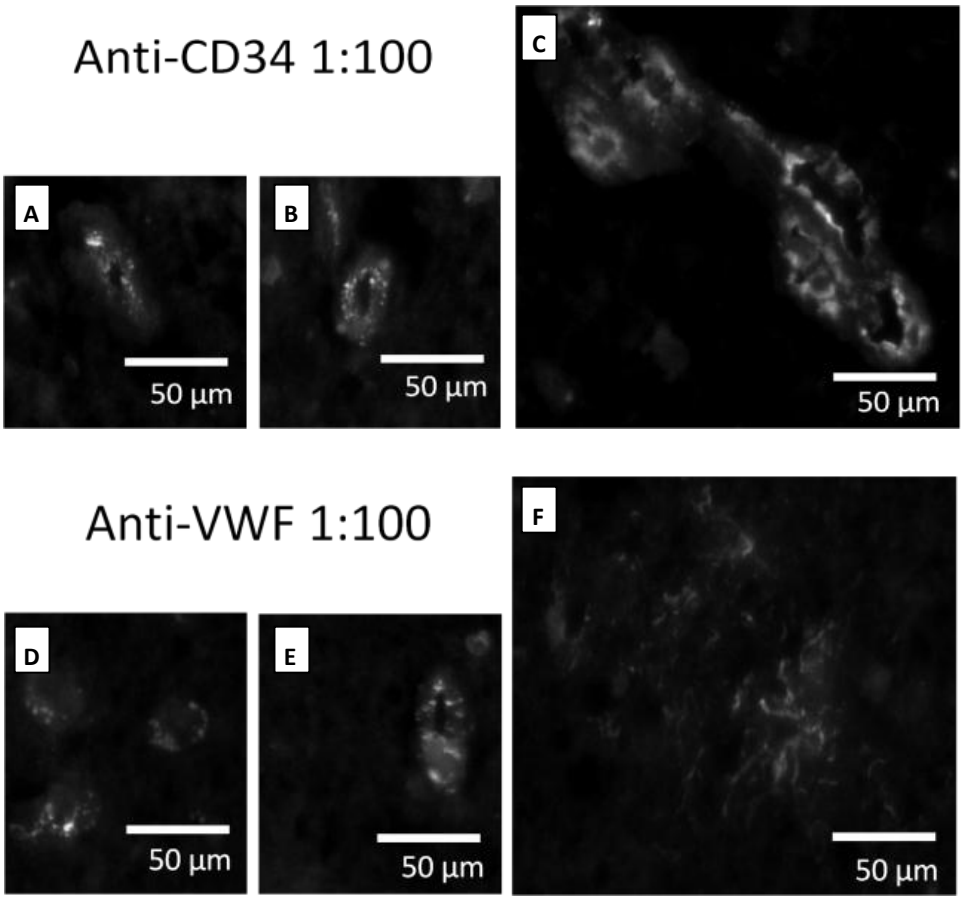

Figure 7.1 CD34 and VWF staining in astrocytoma Grade I tissue (No. 14)

The images show CD34 stained tissue (A, B, C) and VWF stained images (D, E, F), from the same patient (No.14).

Images were captured with a Nikon Fluorescence microscope.

7.1.2 BCRP and Pgp Quantification

Tissues sections, 5 µm thick (control, Grades I and II astrocytoma) were stained with anti-BCRP antibody (BXP-21, 1:200), anti-Pgp antibody (JSB-1, 1:40), anti-CD34 antibody (1:100) and DAPI to detect nuclei. The tissues were then counterstained with secondary antibodies coupled to AlexaFluor 488 (Pgp), 562 (BCRP) and Cy5 (CD34) respectively.

Examples of the staining are shown in Figure 6.2.

The results showed BCRP and Pgp to co-localise with the CD34 endothelial cell marker, showing the ABC transporters to be expressed on brain microvessels. In addition areas of co-localisation of Pgp and BCRP were also noted (indicated by the arrows in Figure 6.2).

The BCRP and Pgp staining intensity was semi-quantified based on intensity for each pixel also showing staining for the endothelial marker CD34.

The data from all images in one z-stack of a capillary were combined to obtain data that reflected expression over the whole thickness of the slide. Intensity was represented by a number from 0 (no staining) to 1 (maximum intensity). Since all samples underwent simultaneous staining and imaging with the same parameters, the maximum staining intensity found throughout all the samples tested became 1. The intensity was plotted as a histogram against the frequency with which it occurred (i.e. the number of pixels of a given intensity) as shown in Figure 6.3.

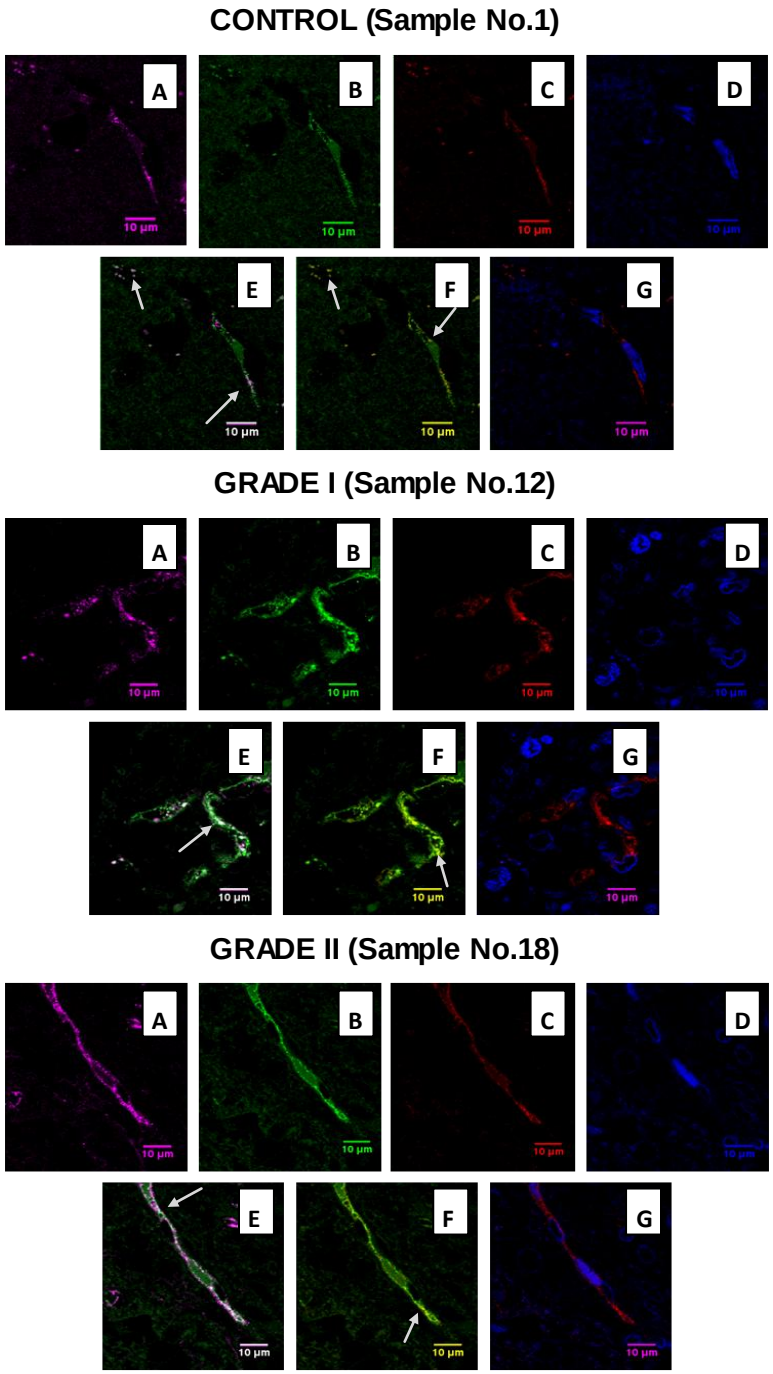

Figure 7.2 Immunohistological staining of human tissue sample from Control, Grade I and Grade II glioma brains.

All tissues were from a single slide containing multiple patient samples. Consequently all staining and imaging was conducted simultaneously for all patients. Imaging was conducted using the SP8 Confocal microscope with the same basic parameters used for all images, where false colour was added by the SP8 software.

A) CD34 , B) Pgp C) BCRP, D) DAPI, E) CD34+Pgp, F) Pgp+BCRP, G)DAPI+BCRP

Areas of co-localisation are highlighted by arrows.

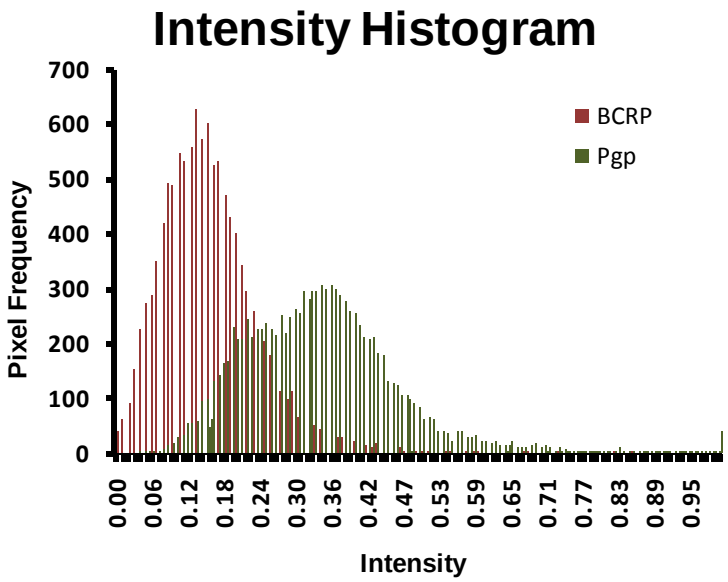

Figure 7.3 The frequencies of different staining intensities for Pgp and BCRP throughout a z-stack imaged from a Grade I astrocytoma (Sample No. 9)

Tissue was stained with BXP-21 (BCRP), JSB-1 (Pgp) and CD34 antibody. The CD34-positive pixels were mapped and the intensity of the BXP-21 and JSB-1 signals within the CD34-positive pixels was then measured through a z-stack of images (0.5µm per step). A histogram of the intensities (normalised between 0 minimum and 1 maximum) against frequency is shown. Data from one patient (No.9), >110000 CD34-positive pixels assessed.

To quantify BCRP and Pgp, the area under the curve (AUC) for each patient was calculated and normalised against the total number of CD34-positive pixels analysed for that patient. The fold change from control is shown in Figure 6.4.

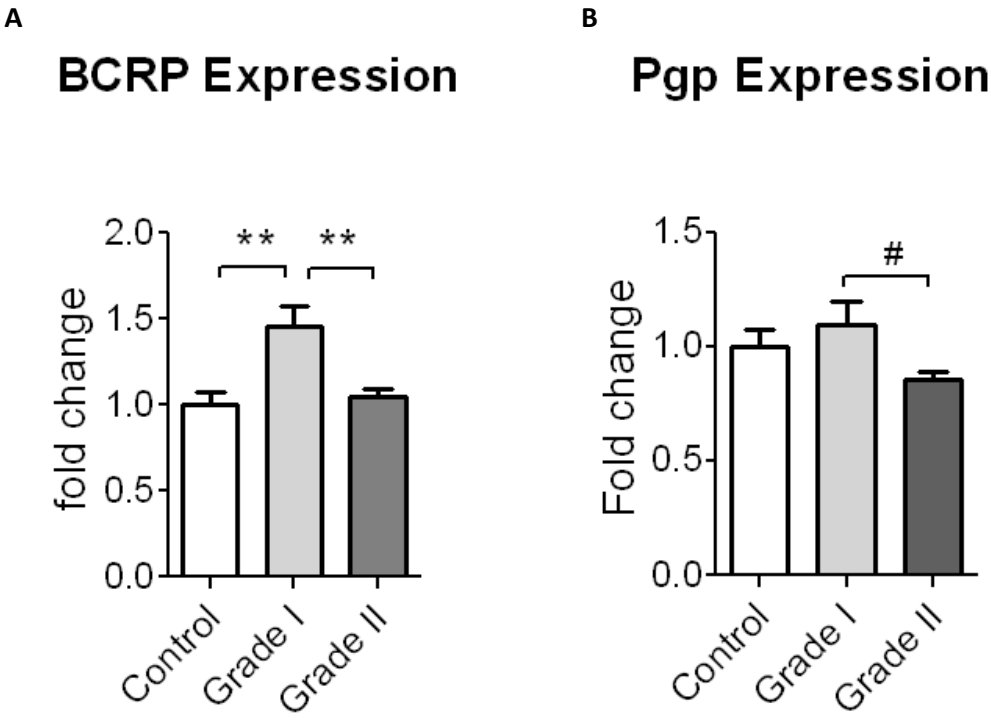

Figure 7.4 Relative BCRP and Pgp expression in astrocytoma microvessels

The expression of BCRP (A) and Pgp (B) was measured within human brain capillaries of Control, Grade I and Grade II astrocytoma tissues.

Capillaries were initially identified by staining positive for CD34 with nuclei present as indicated by DAPI and with diameters of < 7 µm. The CD34-postive pixels were then isolated and the intensity of Pgp and BCRP within the CD34-positive pixels were expressed as histograms. Transporter expression was then quantified as the area under the curve (AUC) of the histograms divided by the number of CD34-positive pixels. The results are expressed as fold change compared with control.

The values are mean ± SEM of n=3, n=4 and n=4 patient of Control, Grade I and Grade II astrocytomas, respectively.

**p<0.01 in 1-way ANOVA analysis using Newman-Keuls Multiple Comparison post test.

1 way ANOVA analysis of Pgp data showed unequal variances in Barlette's test (Barlette's statistic 12.15, P=0.0023) so data was analysed with unpaired 2 tailed t-test using Welch's correction for unequal variances. # p<0.05 difference in the t-test analysis.

The results showed a significant increase (1.6 fold) in BCRP expression in Grade I astrocytomas when compared with Control. Conversely, BCRP expression decreased in Grade II astrocytomas where the decrease resulted in the same amount of expression as in Control. Pgp expression decreased in Grade II astrocytomas when compared with Grade I astrocytoma.

Concerning the relative expression of Pgp and BCRP, the ratio of the expression of BCRP to Pgp showed an increase in Grade I astrocytomas but a decrease in Grade II astrocytoma (Table 6.2) indicating alterations in the relative expression of one or both of these transporters. The ratio mirrored the changes in BCRP expression (Figure 6.4) indicating changes in the ratio were largely due to changes in BCRP expression.

Table 7.2 The ratio of BCRP to Pgp expression in astrocytoma microvessels

8	BCRP/Pgp Ratio Mean ± SEM
Control	0.48±0.10
Grade I	0.66±0.13*****
Grade II	0.56±0.04

*p<0.05 significant difference from Control in unpaired 1-tailed t-test

8.1 Discussion

An initial observation of this study was the heterogeneity of efflux transporter staining within a single patient, especially for Pgp. Normal distributions of Pgp staining have been previously reported in rat brain vasculature (Saubamea *et al.*, 2012) showing that Pgp staining intensity varies. However, no similar information for BCRP or comparisons between BCRP and Pgp staining in human brain have been reported as far as is known. In the current study, Pgp intensity range (maximum intensity minus minimum intensity) was ~0.7 in control brain samples, with a more narrow range of BCRP intensities (~0.5), although there was some between-sample variation (e.g. similar intensity ranges for BCRP and Pgp in control Patient No.4). However, caution is needed with these control tissues since full details of their origin are unknown. Typically normal tissue is obtained from patients with neurological disorders (e.g. glioblastoma or epilepsy), from the periphery of the diseased area (Warren *et al.*, 2009, Shawahna *et al.*, 2011). Although attempts can be made to then select normal tissue

by using sections taken from as far away as possible from any diseased region (Shawahna et al., 2011), there is no guarantee that the tissue has not been influenced by the disease (e.g. by secreted factors).

BCRP expression was shown to be greater in Grade I astrocytoma when compared with control samples or with Grade II astrocytomas, indicating an increase in BCRP expression in Grade I astrocytomas that decreases back to basal/control levels by Grade II astrocytomas. Pgp showed no differences between control and Grade I astrocytomas, but showed significantly lower expression in Grade II astrocytoma samples, indicating that in microvessels of Grade I gliomas little change in Pgp protein expression occurs, however in later stages i.e. Grade II gliomas Pgp decreases. This is in some agreement with previous results by Sawada et al. (1999). Sawada et al. (1999) examined Pgp expression in capillaries isolated from 30 human brain tumour samples and showed a trend towards decreased Pgp expression with tumour grade. They found weaker Pgp staining in new tumour blood vessels compared with normal cerebral blood vessels, although Pgp was shown to be retained luminally expressed. An inverse correlation between Pgp expression and proliferation was noted, with Pgp expression reduced/absent in proliferating cells (Sawada et al., 1999).

Similarly, Toth *et al.* (1996), found that in Grade I and II tumours, Pgp staining of microvessels was as strong as in normal brain. Conversely, Grade IV glioblastoma vessels showed more heterogeneous staining, with both weak and strong Pgp staining observed, and 4 of the 18 samples tested being completely negative.

Disruption in Pgp staining was only noted in the vasculature of high grade tumours by Henson *et al.* (1992). This study showed that Pgp was expressed in the vasculature of low grade gliomas in all but 1 sample (17 samples total) although staining was quite variable, while in high grade gliomas 5/22 samples did not show positive and 10 samples only had weak staining

Together these observations indicate that large alterations to Pgp expression may not be seen until later stage gliomas, with the current study indicating changes begin at Grade II. Furthermore, if Pgp expression is linked to the proliferative state of the endothelial cells (as suggested by Sawada 1999), this could explain why lower grade tumours do not show large changes, since only in Grade IV gliomas are capillary endothelial cells proliferating (Grier & Batchelor, 2006).

Little research has been conducted concerning BCRP expression in glioma microvessels. Sakata *et al.* (2011) examined both Pgp and BCRP and found BCRP to

behave like Pgp; in low grade gliomas all samples showed stronger BCRP and Pgp staining of capillaries than the staining found in normal brains. Conversely, in high grade gliomas (28 samples) 77% showed strong BCRP and Pgp staining, with the rest showing weaker staining relative to normal brain. This suggests that both Pgp and BCRP may first increase in low grade tumours (hence showing stronger expression than normal brain vessels), but then decrease in higher grade tumours (hence showing weaker expression than normal brain vessels). Zhang *et al.* (2003) used laser capture microscopy to isolate tumour vessels from non-malignant tumours and glioblastoma tumours for QPCR, with results showing significantly higher BCRP mRNA in glioblastoma when compared with non-malignant vessels; this could indicate increase in BCRP mRNA in higher grade tumours**.** However, the mRNA expression of Pgp was not assessed and so relative expression of Pgp and BCRP in glioblastoma is unknown.

The fluctuations in BCRP expression found in the current study mirrors the expression pattern of BCRP in the Sakata *et al.* (2011) study, however does not fully agree for Pgp. In the current study expression BCRP and Pgp showed different changes in transporter expression in Grade I astrocytoma, which could indicate different and independent regulation of these efflux transporters during low stage glioma challenge. However, both transporters were shown to decrease in Grade II glioma, more in agreement with Sakata *et al.* (2011), indicative of common changes of the expression of the efflux transporters during higher grade glioma challenge. However, more research is needed to reach more decisive conclusions. A greater number of samples need to be analysed with a greater range of grades examined. Analysis of Grade III and Grade IV tumours is also needed to better compare the current results with previous studies.

9 Summary of the Project, General Discussion and Future Directions

The aim of the project was to investigate changes in the ABC transporters of the BBB during glioma challenge. Investigations are reported in Chapters 3-6 and the findings summarised here.

PBECs were used as an *in vitro* BBB model to study the ABC efflux transporters during glioma challenge. Chapter 3 showed that co-culture of PBECs with normal astrocytes alters their efflux capabilities, indicating that astrocyte co-culture provides a more physiological comparison for glioma co-culture. Comparisons of glioma co-cultures to mono-culture may be misleading since glioma cells can induce some of the same changes as normal glial cells (i.e. astrocytes) (e.g. increases in the overall rate of efflux).

By comparing PBECs in astrocyte co-culture with PBECs in glioma co-culture (Chapter 4), greater BCRP activity was demonstrated on the PBEC apical surface in the glioma co-cultures. This greater activity was shown when using PBECs in co-culture with rat cells and the 'humanised' PBEC co-culture with human astrocytes or human glioma. The greater BCRP activity in the rat glioma co-culture correlated with greater BCRP mRNA expression, indicating that the increased BCRP activity could be a result of increased BCRP transporter expression.

Since this was a non-contact co-culture system, the results further indicated that the changes induced by the glioma cells resulted from factors secreted by the glioma cells. This was confirmed by the use of conditioned medium from normal rat astrocyte or rat glioma cells, since PBECs grown in the rat glioma-conditioned medium showed higher levels of BCRP activity than the PBECs grown in normal rat astrocyte-conditioned medium (Chapter 5).

Concerning Pgp activity/expression, the results indicated that overall Pgp mRNA expression is not altered by glioma co-culture. However, alterations to the cellular polarity of Pgp were noted in the rat glioma co-culture, with significant Pgp activity on the basal surface not noted in rat astrocyte co-culture.

The BCRP and Pgp mRNA expression measured in the PBECs co-cultured with rat glioma cell (Chapter 4) agreed with the BCRP and Pgp protein expression measured in human glioma tissues (Chapter 6). Grade I glioma tissue showed increased BCRP expression, but no change in Pgp expression in the capillaries of the tumour tissue when compared with control brain capillaries. This indicates that PBECs co-cultured with rat glioma cells (after 4 days of co-culture) are a good model for Grade I glioma challenge *in vivo*. However, BCRP expression was shown to decrease back to basal levels (i.e. the levels seen in control tissue) in Grade II glioma samples (Chapter 6), showing that more work needs to be conducted to understand the longer-term changes in BCRP activity *in vivo*. Longer co-cultures (greater than four days) could be tried to replicate the higher grade glioma conditions.

Concerning possible signaling mechanism involved in inducing the changes in BCRP expression in the glioma co-culture, Chapter 5 investigated the affects of the Sonic Hedgehog and Wnt signaling pathways *in vitro* using PBECs grown in astrocyte-conditioned media or glioma-conditioned medium. Both signaling pathways were shown able to modulate BCRP and Pgp activity *in vitro*, with the Wnt pathways showing constitutive activity within the PBECs. This indicated that the Wnt pathway was at least partly responsible for the constitutive expression of the BCRP and Pgp efflux transporters within the PBECs. In addition, de-regulation of both pathways was shown in the PBECs treated with glioma-conditioned medium when compared with astrocyte-conditioned medium. Furthermore, since this was shown with the use of conditioned medium, it indicated that factors in the medium secreted by the glioma cells caused the changes in Sonic and Wnt signaling in the PBECs. However, since these two signaling pathways are interlinked it was not possible to distinguish whether both pathways were truly influenced by the secreted factors or whether de-regulation in one pathway led to alterations in the other. Dkk-1 was identified as a potential factor that might be secreted into the medium by glioma cells. This in an inhibitor of the Wnt pathway, and may have led to the changes in the Wnt pathway. However further work is needed to establish whether Dkk-1 is present in the glioma-conditioned medium, and if so, whether and how the sonic pathway could also be influenced.

In Chapter 5, the Sonic and Wnt pathways were shown to co-regulate both BCRP and Pgp activity. The literature suggested that this regulation is via inducing mRNA and protein changes. However, in the PBECs co-cultured with rat glioma cells, BCRP mRNA was increased but Pgp mRNA was not, indicating different regulation of the two transporters. Therefore the Sonic and Wnt pathways cannot be solely responsible for the changes noted in the PBEC-rat co-culture, as the presence of a BCRP-independent

regulator pathway is suggested by the work in Chapter 4. The involvement of a BCRP-independent pathway in modulating BCRP activity in cancer challenge is supported by the work in Chapter 6; BCRP expression increased in microvessels of Grade I glioma patients but Pgp showed no change in expression. More research needs to be conducted to identify which pathway(s) are responsible for the changes observed. In addition, the effects of Wnt and Sonic signaling molecules should also be tested on the PBECs in co-culture (as opposed to conditioned media) since in this model the polarity changes of the transporters (e.g. Pgp) can also be monitored. Furthermore, both Pgp and BCRP post-transcriptional regulation needs to be investigated, as some results in Chapter 4 indicated that transporter activity can be altered by glioma co-culture without alteration of transporter mRNA levels. Further work is also needed on the protein expression of the BCRP and Pgp transporters in the PBECs in co-culture with the glioma cells, to establish whether the increased BCRP mRNA does lead to increased BCRP protein expression and consequently increased activity.

Overall the project indicated that increased BCRP expression and activity occur as a result of early stage glioma challenge, which has implications in chemotherapeutic treatment of early stage gliomas since many chemotherapeutics are substrates of BCRP. However, more work is needed to identify the mechanism of BCRP increases and its implications for glioma treatment.

10 References

Abbott, N. J. 2013. Blood-brain barrier structure and function and the challenges for CNS drug delivery. *Journal of inherited metabolic disease* **36**:437-49.

Abbott, N. J., Patabendige, A. A., Dolman, D. E., Yusof, S. R. & Begley, D. J. 2010. Structure and function of the blood-brain barrier. *Neurobiology of disease* **37**:13-25.

Abbott, N. J., Ronnback, L. & Hansson, E. 2006. Astrocyte-endothelial interactions at the blood-brain barrier. *Nature reviews. Neuroscience* **7**:41-53.

Agarwal, S., Sane, R., Oberoi, R., Ohlfest, J. R. & Elmquist, W. F. 2011. Delivery of molecularly targeted therapy to malignant glioma, a disease of the whole brain. *Expert reviews in molecular medicine* **13**:e17.

Agnihotri, S., Burrell, K. E., Wolf, A., Jalali, S., Hawkins, C., Rutka, J. T. & Zadeh, G. 2013. Glioblastoma, a brief review of history, molecular genetics, animal models and novel therapeutic strategies. *Archivum immunologiae et therapiae experimentalis* **61**:25-41.

Allen, J. D., Brinkhuis, R. F., van Deemter, L., Wijnholds, J. & Schinkel, A. H. 2000. Extensive contribution of the multidrug transporters P-glycoprotein and Mrp1 to basal drug resistance. *Cancer research* **60**:5761-6.

Alvarez, J. I., Dodelet-Devillers, A., Kebir, H., Ifergan, I., Fabre, P. J., Terouz, S., Sabbagh, M., Wosik, K., Bourbonniere, L., Bernard, M., van Horssen, J., de Vries, H. E., Charron, F. & Prat, A. 2011. The Hedgehog pathway promotes blood-brain barrier integrity and CNS immune quiescence. *Science (New York, N.Y.)* **334**:1727-31.

Armulik, A., Genove, G., Mae, M., Nisancioglu, M. H., Wallgard, E., Niaudet, C., He, L., Norlin, J., Lindblom, P., Strittmatter, K., Johansson, B. R. & Betsholtz, C. 2010. Pericytes regulate the blood-brain barrier. *Nature* **468**:557-61.

Arshad, F., Wang, L., Sy, C., Avraham, S. & Avraham, H. K. 2010. Blood-brain barrier integrity and breast cancer metastasis to the brain. *Pathology research international* **2011**:920509.

Avdeef 2011. *In vitro* Brain endothelial cell models. European Journal of Pharmaceutical Science. 43:109

Ballerini, P., Di Iorio, P., Ciccarelli, R., Nargi, E., D'Alimonte, I., Traversa, U., Rathbone, M. P. & Caciagli, F. 2002. Glial cells express multiple ATP binding cassette proteins which are involved in ATP release. *Neuroreport* **13**:1789-92.

Barakat, S., Demeule, M., Pilorget, A., Regina, A., Gingras, D., Baggetto, L. G. & Beliveau, R. 2007. Modulation of p-glycoprotein function by caveolin-1 phosphorylation. *Journal of neurochemistry* **101**:1-8.

Bauer, B., Hartz, A. M. & Miller, D. S. 2007. Tumour necrosis factor alpha and endothelin-1 increase P-glycoprotein expression and transport activity at the blood-brain barrier. *Molecular pharmacology* **71**:667-75.

Beauchesne, E., Desjardins, P., Hazell, A. S. & Butterworth, R. F. 2009. Altered expression of tight junction proteins and matrix metalloproteinases in thiamine-deficient mouse brain. *Neurochemistry international* **55**:275-81.

Beaulieu, E., Demeule, M., Ghitescu, L. & Beliveau, R. 1997. P-glycoprotein is strongly expressed in the luminal membranes of the endothelium of blood vessels in the brain. *The Biochemical journal* **326 (Pt 2)**:539-44.

Begley, D. J. 2004. ABC transporters and the blood-brain barrier. *Current pharmaceutical design* **10**:1295-312.

Bell, R. D., Winkler, E. A., Sagare, A. P., Singh, I., LaRue, B., Deane, R. & Zlokovic, B. V. 2010. Pericytes control key neurovascular functions and neuronal phenotype in the adult brain and during brain aging. *Neuron* **68**:409-27.

Bendayan, R., Ronaldson, P. T., Gingras, D. & Bendayan, M. 2006. *In situ* localization of P-glycoprotein (ABCB1) in human and rat brain. *The journal of histochemistry and cytochemistry : official journal of the Histochemistry Society* **54**:1159-67.

Berezowski, V., Landry, C., Dehouck, M. P., Cecchelli, R. & Fenart, L. 2004. Contribution of glial cells and pericytes to the mRNA profiles of P-glycoprotein and multidrug resistance-associated proteins in an *in vitro* model of the blood-brain barrier. *Brain research* **1018**:1-9.

Bertossi, M., Virgintino, D., Maiorano, E., Occhiogrosso, M. & Roncali, L. 1997. Ultrastructural and morphometric investigation of human brain capillaries in normal and peritumoural tissues. *Ultrastructural pathology* **21**:41-9.

Betz, A. L. & Goldstein, G. W. 1978. Polarity of the blood-brain barrier: neutral amino acid transport into isolated brain capillaries. *Science (New York, N.Y.)* **202**:225-7.

Bleasby, K., Chauhan, S. & Brown, C. D. 2000. Characterization of MPP+ secretion across human intestinal Caco-2 cell monolayers: role of P-glycoprotein and a novel Na(+)-dependent organic cation transport mechanism. *British journal of pharmacology* **129**:619-25.

Bosch, I. & Croop, J. M. 1998. P-glycoprotein structure and evolutionary homologies. *Cytotechnology* **27**:1-30.

Boveri, M., Berezowski, V., Price, A., Slupek, S., Lenfant, A. M., Benaud, C., Hartung, T., Cecchelli, R., Prieto, P. & Dehouck, M. P. 2005. Induction of blood-brain barrier properties in cultured brain capillary endothelial cells: comparison between primary glial cells and C6 cell line. *Glia* **51**:187-98.

Braun, S., Oppermann, H., Mueller, A., Renner, C., Hovhannisyan, A., Baran-Schmidt, R., Gebhardt, R., Hipkiss, A., Thiery, J., Meixensberger, J. & Gaunitz, F. 2012. Hedgehog signaling in glioblastoma multiforme. *Cancer biology & therapy* **13**:487-95.

Bronger, H., Konig, J., Kopplow, K., Steiner, H. H., Ahmadi, R., Herold-Mende, C., Keppler, D. & Nies, A. T. 2005. ABCC drug efflux pumps and organic anion uptake transporters in human gliomas and the blood-tumour barrier. *Cancer research* **65**:11419-28.

Brown, R. C. & Davis, T. P. 2002. Calcium modulation of adherens and tight junction function: a potential mechanism for blood-brain barrier disruption after stroke. *Stroke; a journal of cerebral circulation* **33**:1706-11.

Brownson, E. A., Abbruscato, T. J., Gillespie, T. J., Hruby, V. J. & Davis, T. P. 1994. Effect of peptidases at the blood brain barrier on the permeability of enkephalin. *The Journal of pharmacology and experimental therapeutics* **270**:675-80.

Calatozzolo, C., Gelati, M., Ciusani, E., Sciacca, F. L., Pollo, B., Cajola, L., Marras, C., Silvani, A., Vitellaro-Zuccarello, L., Croci, D., Boiardi, A. & Salmaggi, A. 2005. Expression of drug resistance proteins Pgp, MRP1, MRP3, MRP5 and GST-pi in human glioma. *Journal of neuro-oncology* **74**:113-21.

Chambers, T. C., McAvoy, E. M., Jacobs, J. W. & Eilon, G. 1990. Protein kinase C phosphorylates P-glycoprotein in multidrug resistant human KB carcinoma cells. *The Journal of biological chemistry* **265**:7679-86.

Chen, Y. & Liu, L. 2012. Modern methods for delivery of drugs across the blood-brain barrier. *Advanced drug delivery reviews* **64**:640-65.

Chen, Y., Yue, S., Xie, L., Pu, X. H., Jin, T. & Cheng, S. Y. 2011. Dual Phosphorylation of suppressor of fused (Sufu) by PKA and GSK3beta regulates its stability and localization in the primary cilium. *The Journal of biological chemistry* **286**:13502-11.

Chen, Y. J., Kuo, C. D., Chen, S. H., Chen, W. J., Huang, W. C., Chao, K. S. & Liao, H. F. 2012. Small-molecule synthetic compound norcantharidin reverses multi-

drug resistance by regulating Sonic hedgehog signaling in human breast cancer cells. *PloS one* **7**:e37006.

Chen, Z. S., Lee, K. & Kruh, G. D. 2001. Transport of cyclic nucleotides and estradiol 17-beta-D-glucuronide by multidrug resistance protein 4. Resistance to 6-mercaptopurine and 6-thioguanine. *The Journal of biological chemistry* **276**:33747-54.

Chernausek, S. D., Murray, M. A. & Cheung, P. T. 1993. Expression of insulin-like growth factor binding protein-4 (IGFBP-4) by rat neural cells--comparison to other IGFBPs. *Regulatory peptides* **48**:123-32.

Cioni, C., Turlizzi, E., Zanelli, U., Oliveri, G. & Annunziata, P. 2012. Expression of Tight Junction and Drug Efflux Transporter Proteins in an *in vitro* Model of Human Blood-Brain Barrier. *Frontiers in psychiatry* **3**:47.

Cisternino, S., Mercier, C., Bourasset, F., Roux, F. & Scherrmann, J. M. 2004. Expression, up-regulation, and transport activity of the multidrug-resistance protein Abcg2 at the mouse blood-brain barrier. *Cancer research* **64**:3296-301.

Cisternino, S., Rousselle, C., Lorico, A., Rappa, G. & Scherrmann, J. M. 2003. Apparent lack of Mrp1-mediated efflux at the luminal side of mouse blood-brain barrier endothelial cells. *Pharmaceutical research* **20**:904-9.

Cohen-Kashi Malina, K., Cooper, I. & Teichberg, V. I. 2009. Closing the gap between the in-vivo and in-vitro blood-brain barrier tightness. *Brain research* **1284**:12-21.

Coomber, B. L. & Stewart, P. A. 1986. Three-dimensional reconstruction of vesicles in endothelium of blood-brain barrier versus highly permeable microvessels. *The Anatomical record* **215**:256-61.

Cooray, H. C., Blackmore, C. G., Maskell, L. & Barrand, M. A. 2002. Localisation of breast cancer resistance protein in microvessel endothelium of human brain. *Neuroreport* **13**:2059-63.

Crompton, T., Outram, S. V. & Hager-Theodorides, A. L. 2007. Sonic hedgehog signaling in T-cell development and activation. *Nature reviews. Immunology* **7**:726-35.

Cucullo, L., Hossain, M., Rapp, E., Manders, T., Marchi, N. & Janigro, D. 2007. Development of a humanized *in vitro* blood-brain barrier model to screen for brain penetration of antiepileptic drugs. *Epilepsia* **48**:505-16.

Daneman, R., Zhou, L., Kebede, A. A. & Barres, B. A. 2010. Pericytes are required for blood-brain barrier integrity during embryogenesis. *Nature* **468**:562-6.

Dauchy, S., Dutheil, F., Weaver, R. J., Chassoux, F., Daumas-Duport, C., Couraud, P. O., Schermann, J. M., De Waziers, I. & Decleves, X. 2008. ABC transporters,

cytochromes P450 and their main transcription factors: expression at the human blood-brain barrier. *Journal of neurochemistry* **107**:1518-28.

Dauchy, S., Miller, F., Couraud, P. O., Weaver, R. J., Weksler, B., Romero, I. A., Schermann, J. M., De Waziers, I. & Decleves, X. 2009. Expression and transcriptional regulation of ABC transporters and cytochromes P450 in hCMEC/D3 human cerebral microvascular endothelial cells. *Biochemical pharmacology* **77**:897-909.

Davson, H. & Oldendorf, W. H. 1967. Symposium on membrane transport. Transport in the central nervous system. *Proceedings of the Royal Society of Medicine* **60**:326-9.

Decleves, X., Bihorel, S., Debray, M., Yousif, S., Camenisch, G. & Scherrmann, J. M. 2008. ABC transporters and the accumulation of imatinib and its active metabolite CGP74588 in rat C6 glioma cells. *Pharmacological research : the official journal of the Italian Pharmacological Society* **57**:214-22.

Deeken, J. F. & Loscher, W. 2007. The blood-brain barrier and cancer: transporters, treatment, and Trojan horses. *Clinical cancer research : an official journal of the American Association for Cancer Research* **13**:1663-74.

Dehouck, M. P., Meresse, S., Delorme, P., Fruchart, J. C. & Cecchelli, R. 1990. An easier, reproducible, and mass-production method to study the blood-brain barrier *in vitro*. *Journal of neurochemistry* **54**:1798-801.

Dinda, A. K., Sarkar, C., Roy, S., Kharbanda, K., Mathur, M., Khosla, A. K. & Banerji, A. K. 1993. A transmission and scanning electron microscopic study of tumoural and peritumoural microblood vessels in human gliomas. *Journal of neuro-oncology* **16**:149-58.

Diradourian, C., Girard, J. & Pegorier, J. P. 2005. Phosphorylation of PPARs: from molecular characterization to physiological relevance. *Biochimie* **87**:33-8.

Dohgu, S., Yamauchi, A., Nakagawa, S., Takata, F., Kai, M., Egawa, T., Naito, M., Tsuruo, T., Sawada, Y., Niwa, M. & Kataoka, Y. 2004. Nitric oxide mediates cyclosporine-induced impairment of the blood-brain barrier in cocultures of mouse brain endothelial cells and rat astrocytes. *European journal of pharmacology* **505**:51-9.

Doyle, L. A., Yang, W., Abruzzo, L. V., Krogmann, T., Gao, Y., Rishi, A. K. & Ross, D. D. 1998. A multidrug resistance transporter from human MCF-7 breast cancer cells. *Proceedings of the National Academy of Sciences of the United States of America* **95**:15665-70.

Duport, S., Robert, F., Muller, D., Grau, G., Parisi, L. & Stoppini, L. 1998. An *in vitro* blood-brain barrier model: cocultures between endothelial cells and organotypic

brain slice cultures. *Proceedings of the National Academy of Sciences of the United States of America* **95**:1840-5.

Dwyer, J., Hebda, J. K., Le Guelte, A., Galan-Moya, E. M., Smith, S. S., Azzi, S., Bidere, N. & Gavard, J. 2012. Glioblastoma cell-secreted interleukin-8 induces brain endothelial cell permeability via CXCR2. *PloS one* **7**:e45562.

Ehrhardt, M., Lindenmaier, H., Burhenne, J., Haefeli, W. E. & Weiss, J. 2004. Influence of lipid lowering fibrates on P-glycoprotein activity *in vitro*. *Biochemical pharmacology* **67**:285-92.

Ehrlich P 1885 Das sauerstufbudurfnis des organismus, in *Eine Farbenanalytische Studie*, Hirschwald, Berlin.

Eisenblatter, T., Huwel, S. & Galla, H. J. 2003. Characterisation of the brain multidrug resistance protein (BMDP/ABCG2/BCRP) expressed at the blood-brain barrier. *Brain research* **971**:221-31.

Enokizono, J., Kusuhara, H., Ose, A., Schinkel, A. H. & Sugiyama, Y. 2008. Quantitative investigation of the role of breast cancer resistance protein (Bcrp/Abcg2) in limiting brain and testis penetration of xenobiotic compounds. *Drug metabolism and disposition: the biological fate of chemicals* **36**:995-1002.

Fagerholm, S., Ortegren, U., Karlsson, M., Ruishalme, I. & Stralfors, P. 2009. Rapid insulin-dependent endocytosis of the insulin receptor by caveolae in primary adipocytes. *PloS one* **4**:e5985.

Fattori, S., Becherini, F., Cianfriglia, M., Parenti, G., Romanini, A. & Castagna, M. 2007. Human brain tumours: multidrug-resistance P-glycoprotein expression in tumour cells and intratumoural capillary endothelial cells. *Virchows Archiv : an international journal of pathology* **451**:81-7.

Ferrara, N., Gerber, H. P. & LeCouter, J. 2003. The biology of VEGF and its receptors. *Nature medicine* **9**:669-76.

Ferreira, R. J., Ferreira, M. J. & dos Santos, D. J. 2013. Molecular docking characterizes substrate-binding sites and efflux modulation mechanisms within P-glycoprotein. *Journal of chemical information and modeling* **53**:1747-60.

Fricker, G., Nobmann, S. & Miller, D. S. 2002. Permeability of porcine blood brain barrier to somatostatin analogues. *British journal of pharmacology* **135**:1308-14.

Fukushima, H., Fujimoto, M. & Ide, M. 1990. Quantitative detection of blood-brain barrier-associated enzymes in cultured endothelial cells of porcine brain microvessels. *In vitro cellular & developmental biology : journal of the Tissue Culture Association* **26**:612-20.

Gaillard, P. J., van der Sandt, I. C., Voorwinden, L. H., Vu, D., Nielsen, J. L., de Boer, A. G. & Breimer, D. D. 2000. Astrocytes increase the functional expression of P-

glycoprotein in an *in vitro* model of the blood-brain barrier. *Pharmaceutical research* **17**:1198-205.

Gaillard, P. J., Voorwinden, L. H., Nielsen, J. L., Ivanov, A., Atsumi, R., Engman, H., Ringbom, C., de Boer, A. G. & Breimer, D. D. 2001. Establishment and functional characterization of an *in vitro* model of the blood-brain barrier, comprising a co-culture of brain capillary endothelial cells and astrocytes. *European journal of pharmaceutical sciences : official journal of the European Federation for Pharmaceutical Sciences* **12**:215-22.

Gerstner, E. R. & Fine, R. L. 2007. Increased permeability of the blood-brain barrier to chemotherapy in metastatic brain tumours: establishing a treatment paradigm. *Journal of clinical oncology : official journal of the American Society of Clinical Oncology* **25**:2306-12.

Ghosh, C., Gonzalez-Martinez, J., Hossain, M., Cucullo, L., Fazio, V., Janigro, D. & Marchi, N. 2010. Pattern of P450 expression at the human blood-brain barrier: roles of epileptic condition and laminar flow. *Epilepsia* **51**:1408-17.

Ginguene, C., Champier, J., Maallem, S., Strazielle, N., Jouvet, A., Fevre-Montange, M. & Ghersi-Egea, J. F. 2010. P-glycoprotein (ABCB1) and breast cancer resistance protein (ABCG2) localize in the microvessels forming the blood-tumour barrier in ependymomas. *Brain pathology (Zurich, Switzerland)* **20**:926-35.

Greenberger, L. M., Lothstein, L., Williams, S. S. & Horwitz, S. B. 1988. Distinct P-glycoprotein precursors are overproduced in independently isolated drug-resistant cell lines. *Proceedings of the National Academy of Sciences of the United States of America* **85**:3762-6.

Grier, J. T. & Batchelor, T. 2006. Low-grade gliomas in adults. *The oncologist* **11**:681-93.

Gros, P., Ben Neriah, Y. B., Croop, J. M. & Housman, D. E. 1986. Isolation and expression of a complementary DNA that confers multidrug resistance. *Nature* **323**:728-31.

Guerin, C., Wolff, J. E., Laterra, J., Drewes, L. R., Brem, H. & Goldstein, G. W. 1992. Vascular differentiation and glucose transporter expression in rat gliomas: effects of steroids. *Annals of neurology* **31**:481-7.

Haqqani, A. S., Delaney, C. E., Tremblay, T. L., Sodja, C., Sandhu, J. K. & Stanimirovic, D. B. 2013. Method for isolation and molecular characterization of extracellular microvesicles released from brain endothelial cells. *Fluids and barriers of the CNS* **10**:4.

Harati, R., Benech, H., Villegier, A. S. & Mabondzo, A. 2013. P-glycoprotein, breast cancer resistance protein, Organic Anion Transporter 3, and Transporting Peptide 1a4 during blood-brain barrier maturation: involvement of Wnt/beta-catenin and endothelin-1 signaling. *Molecular pharmaceutics* **10**:1566-80.

Hatherell, K., Couraud, P. O., Romero, I. A., Weksler, B. & Pilkington, G. J. 2011. Development of a three-dimensional, all-human *in vitro* model of the blood-brain barrier using mono-, co-, and tri-cultivation Transwell models. *Journal of neuroscience methods* **199**:223-9.

Hawkins, B. T., Rigor, R. R. & Miller, D. S. 2010a. Rapid loss of blood-brain barrier P-glycoprotein activity through transporter internalization demonstrated using a novel *in situ* proteolysis protection assay. *Journal of cerebral blood flow and metabolism : official journal of the International Society of Cerebral Blood Flow and Metabolism* **30**:1593-7.

Hawkins, B. T., Sykes, D. B. & Miller, D. S. 2010b. Rapid, reversible modulation of blood-brain barrier P-glycoprotein transport activity by vascular endothelial growth factor. *The Journal of neuroscience : the official journal of the Society for Neuroscience* **30**:1417-25.

Hayashi, Y., Nomura, M., Yamagishi, S., Harada, S., Yamashita, J. & Yamamoto, H. 1997. Induction of various blood-brain barrier properties in non-neural endothelial cells by close apposition to co-cultured astrocytes. *Glia* **19**:13-26.

Helms, H. C., Waagepetersen, H. S., Nielsen, C. U. & Brodin, B. 2010. Paracellular tightness and claudin-5 expression is increased in the BCEC/astrocyte blood-brain barrier model by increasing media buffer capacity during growth. *The AAPS journal* **12**:759-70.

Henson, J. W., Cordon-Cardo, C. & Posner, J. B. 1992. P-glycoprotein expression in brain tumours. *Journal of neuro-oncology* **14**:37-43.

Hirrlinger, J., Moeller, H., Kirchhoff, F. & Dringen, R. 2005. Expression of multidrug resistance proteins (Mrps) in astrocytes of the mouse brain: a single cell RT-PCR study. *Neurochemical research* **30**:1237-44.

Hobbs, S. K., Monsky, W. L., Yuan, F., Roberts, W. G., Griffith, L., Torchilin, V. P. & Jain, R. K. 1998. Regulation of transport pathways in tumour vessels: role of tumour type and microenvironment. *Proceedings of the National Academy of Sciences of the United States of America* **95**:4607-12.

Hoque, M. T., Robillard, K. R. & Bendayan, R. 2012. Regulation of breast cancer resistant protein by peroxisome proliferator-activated receptor alpha in human brain microvessel endothelial cells. *Molecular pharmacology* **81**:598-609.

Hori, S., Ohtsuki, S., Tachikawa, M., Kimura, N., Kondo, T., Watanabe, M., Nakashima, E. & Terasaki, T. 2004. Functional expression of rat ABCG2 on the luminal side of brain capillaries and its enhancement by astrocyte-derived soluble factor(s). *Journal of neurochemistry* **90**:526-36.

Ibrahim, S., Peggins, J., Knapton, A., Licht, T. & Aszalos, A. 2000. Influence of antipsychotic, antiemetic, and Ca(2+) channel blocker drugs on the cellular accumulation of the anticancer drug daunorubicin: P-glycoprotein modulation. *The Journal of pharmacology and experimental therapeutics* **295**:1276-83.

Jain, R., Griffith, B., Narang, J., Mikkelsen, T., Bagher-Ebadian, H., Nejad-Davarani, S. P., Ewing, J. R. & Arbab, A. S. 2012. Blood-Brain-Barrier Imaging in Brain Tumours: Concepts and Methods.

Janzer, R. C. & Raff, M. C. 1987. Astrocytes induce blood-brain barrier properties in endothelial cells. *Nature* **325**:253-7.

Jedlitschky, G., Burchell, B. & Keppler, D. 2000. The multidrug resistance protein 5 functions as an ATP-dependent export pump for cyclic nucleotides. *The Journal of biological chemistry* **275**:30069-74.

Jodoin, J., Demeule, M., Fenart, L., Cecchelli, R., Farmer, S., Linton, K. J., Higgins, C. F. & Beliveau, R. 2003. P-glycoprotein in blood-brain barrier endothelial cells: interaction and oligomerization with caveolins. *Journal of neurochemistry* **87**:1010-23.

Kamiie, J., Ohtsuki, S., Iwase, R., Ohmine, K., Katsukura, Y., Yanai, K., Sekine, Y., Uchida, Y., Ito, S. & Terasaki, T. 2008. Quantitative atlas of membrane transporter proteins: development and application of a highly sensitive simultaneous LC/MS/MS method combined with novel in-silico peptide selection criteria. *Pharmaceutical research* **25**:1469-83.

Kido, Y., Tamai, I., Nakanishi, T., Kagami, T., Hirosawa, I., Sai, Y. & Tsuji, A. 2002. Evaluation of blood-brain barrier transporters by co-culture of brain capillary endothelial cells with astrocytes. *Drug metabolism and pharmacokinetics* **17**:34-41.

Kise, Y., Morinaka, A., Teglund, S. & Miki, H. 2009. Sufu recruits GSK3beta for efficient processing of Gli3. *Biochemical and biophysical research communications* **387**:569-74.

Kuhnline Sloan, C. D., Nandi, P., Linz, T. H., Aldrich, J. V., Audus, K. L. & Lunte, S. M. 2012. Analytical and biological methods for probing the blood-brain barrier. *Annual review of analytical chemistry (Palo Alto, Calif.)* **5**:505-31.

Kusuhara, H. & Sugiyama, Y. 2005. Active efflux across the blood-brain barrier: role of the solute carrier family. *NeuroRx : the journal of the American Society for Experimental NeuroTherapeutics* **2**:73-85.

Kusuhara, H., Suzuki, H., Terasaki, T., Kakee, A., Lemaire, M. & Sugiyama, Y. 1997. P-Glycoprotein mediates the efflux of quinidine across the blood-brain barrier. *The Journal of pharmacology and experimental therapeutics* **283**:574-80.

Larsson, H. B., Stubgaard, M., Frederiksen, J. L., Jensen, M., Henriksen, O. & Paulson, O. B. 1990. Quantitation of blood-brain barrier defect by magnetic resonance imaging and gadolinium-DTPA in patients with multiple sclerosis and brain tumours. *Magnetic resonance in medicine : official journal of the Society of Magnetic Resonance in Medicine / Society of Magnetic Resonance in Medicine* **16**:117-31.

Lewandowsky M 1900 Zur lehre von der cerebrospinalflussigkeit. *Z Klin Med* **40:**480–494.

Lee, G., Babakhanian, K., Ramaswamy, M., Prat, A., Wosik, K. & Bendayan, R. 2007. Expression of the ATP-binding cassette membrane transporter, ABCG2, in human and rodent brain microvessel endothelial and glial cell culture systems. *Pharmaceutical research* **24**:1262-74.

Lee, Y. J., Kusuhara, H., Jonker, J. W., Schinkel, A. H. & Sugiyama, Y. 2005. Investigation of efflux transport of dehydroepiandrosterone sulfate and mitoxantrone at the mouse blood-brain barrier: a minor role of breast cancer resistance protein. *The Journal of pharmacology and experimental therapeutics* **312**:44-52.

Lemmen, J., Tozakidis, I. E. & Galla, H. J. 2013. Pregnane X receptor upregulates ABC-transporter Abcg2 and Abcb1 at the blood-brain barrier. *Brain research* **1491**:1-13.

Li, G., Yuan, W. & Fu, B. M. 2010. A model for the blood-brain barrier permeability to water and small solutes. *Journal of biomechanics* **43**:2133-40.

Lim, J. C., Kania, K. D., Wijesuriya, H., Chawla, S., Sethi, J. K., Pulaski, L., Romero, I. A., Couraud, P. O., Weksler, B. B., Hladky, S. B. & Barrand, M. A. 2008. Activation of beta-catenin signalling by GSK-3 inhibition increases p-glycoprotein expression in brain endothelial cells. *Journal of neurochemistry* **106**:1855-65.

Lim, J. C., Wolpaw, A. J., Caldwell, M. A., Hladky, S. B. & Barrand, M. A. 2007. Neural precursor cell influences on blood-brain barrier characteristics in rat brain endothelial cells. *Brain research* **1159**:67-76.

Lin, C. J., Tai, Y., Huang, M. T., Tsai, Y. F., Hsu, H. J., Tzen, K. Y. & Liou, H. H. 2010. Cellular localization of the organic cation transporters, OCT1 and OCT2, in brain microvessel endothelial cells and its implication for MPTP transport across the blood-brain barrier and MPTP-induced dopaminergic toxicity in rodents. *Journal of neurochemistry* **114**:717-27.

Linnet, K. & Ejsing, T. B. 2008. A review on the impact of P-glycoprotein on the penetration of drugs into the brain. Focus on psychotropic drugs. *European neuropsychopharmacology : the journal of the European College of Neuropsychopharmacology* **18**:157-69.

Liou, H. H., Hsu, H. J., Tsai, Y. F., Shih, C. Y., Chang, Y. C. & Lin, C. J. 2007. Interaction between nicotine and MPTP/MPP+ in rat brain endothelial cells. *Life sciences* **81**:664-72.

Liu, H., Liu, X., Jia, L., Liu, Y., Yang, H., Wang, G. & Xie, L. 2008. Insulin therapy restores impaired function and expression of P-glycoprotein in blood-brain barrier of experimental diabetes. *Biochemical pharmacology* **75**:1649-58.

Liu, W. Y., Wang, Z. B., Zhang, L. C., Wei, X. & Li, L. 2012. Tight junction in blood-brain barrier: an overview of structure, regulation, and regulator substances. *CNS neuroscience & therapeutics* **18**:609-15.

Liu, X., Jing, X. Y., Jin, S., Li, Y., Liu, L., Yu, Y. L., Liu, X. D. & Xie, L. 2011. Insulin suppresses the expression and function of breast cancer resistance protein in primary cultures of rat brain microvessel endothelial cells. *Pharmacological reports : PR* **63**:487-93.

Liu, X., Tu, M., Kelly, R. S., Chen, C. & Smith, B. J. 2004. Development of a computational approach to predict blood-brain barrier permeability. *Drug metabolism and disposition: the biological fate of chemicals* **32**:132-9.

Locher, K. P. 2009. Review. Structure and mechanism of ATP-binding cassette transporters. *Philosophical transactions of the Royal Society of London. Series B, Biological sciences* **364**:239-45.

Loscher, W. & Potschka, H. 2005. Drug resistance in brain diseases and the role of drug efflux transporters. *Nature reviews. Neuroscience* **6**:591-602.

Madden, S. L., Cook, B. P., Nacht, M., Weber, W. D., Callahan, M. R., Jiang, Y., Dufault, M. R., Zhang, X., Zhang, W., Walter-Yohrling, J., Rouleau, C., Akmaev, V. R., Wang, C. J., Cao, X., St Martin, T. B., Roberts, B. L., Teicher, B. A., Klinger, K. W., Stan, R. V., Lucey, B., Carson-Walter, E. B., Laterra, J. & Walter, K. A. 2004. Vascular gene expression in nonneoplastic and malignant brain. *The American journal of pathology* **165**:601-8.

Mao, Q. & Unadkat, J. D. 2005. Role of the breast cancer resistance protein (ABCG2) in drug transport. *The AAPS journal* **7**:E118-33.

Mandikova, J., Volkova, M., Pavek, P., Cesnek, M., Janeba, Z., Kubicek, V. & Trejtnar, F. 2013. Interactions with selected drug renal transporters and transporter-mediated cytotoxicity in antiviral agents from the group of acyclic nucleoside phosphonates. *Toxicology* **311**:135-46.

Marquet, G., Dameron, O., Saikali, S., Mosser, J. & Burgun, A. 2007. Grading glioma tumours using OWL-DL and NCI Thesaurus. *AMIA ... Annual Symposium proceedings / AMIA Symposium. AMIA Symposium*:508-12.

Martel, F., Calhau, C., Soares-da-Silva, P. & Azevedo, I. 2001. Transport of [3H]MPP+ in an immortalized rat brain microvessel endothelial cell line (RBE 4). *Naunyn-Schmiedeberg's archives of pharmacology* **363**:1-10.

Martinez, N., Boire, A. & Deangelis, L. M. 2013. Molecular interactions in the development of brain metastases. *International journal of molecular sciences* **14**:17157-67.

Matsson, P., Pedersen, J. M., Norinder, U., Bergstrom, C. A. & Artursson, P. 2009. Identification of novel specific and general inhibitors of the three major human ATP-binding cassette transporters P-gp, BCRP and MRP2 among registered drugs. *Pharmaceutical research* **26**:1816-31.

McAllister, M. S., Krizanac-Bengez, L., Macchia, F., Naftalin, R. J., Pedley, K. C., Mayberg, M. R., Marroni, M., Leaman, S., Stanness, K. A. & Janigro, D. 2001. Mechanisms of glucose transport at the blood-brain barrier: an *in vitro* study. *Brain research* **904**:20-30.

McMahon, H. T. & Boucrot, E. 2011. Molecular mechanism and physiological functions of clathrin-mediated endocytosis. *Nature reviews. Molecular cell biology* **12**:517-33.

Meng, X., Poon, R., Zhang, X., Cheah, A., Ding, Q., Hui, C. C. & Alman, B. 2001. Suppressor of fused negatively regulates beta-catenin signaling. *The Journal of biological chemistry* **276**:40113-9.

Merrill, M. J. & Oldfield, E. H. 2005. A reassessment of vascular endothelial growth factor in central nervous system pathology. *Journal of neurosurgery* **103**:853-68.

Meyer, J., Mischeck, U., Veyhl, M., Henzel, K. & Galla, H. J. 1990. Blood-brain barrier characteristic enzymatic properties in cultured brain capillary endothelial cells. *Brain research* **514**:305-9.

Miller, D. S. 2010. Regulation of P-glycoprotein and other ABC drug transporters at the blood-brain barrier. *Trends in pharmacological sciences* **31**:246-54.

Miller, D. S., Sussman, C. R. & Renfro, J. L. 1998. Protein kinase C regulation of p-glycoprotein-mediated xenobiotic secretion in renal proximal tubule. *The American journal of physiology* **275**:F785-95.

Min, T. H., Kriebel, M., Hou, S. & Pera, E. M. 2011. The dual regulator Sufu integrates Hedgehog and Wnt signals in the early Xenopus embryo. *Developmental biology* **358**:262-76.

Mitomo, H., Kato, R., Ito, A., Kasamatsu, S., Ikegami, Y., Kii, I., Kudo, A., Kobatake, E., Sumino, Y. & Ishikawa, T. 2003. A functional study on polymorphism of the ATP-binding cassette transporter ABCG2: critical role of arginine-482 in methotrexate transport. *The Biochemical journal* **373**:767-74.

Mittapalli, R. K., Manda, V. K., Bohn, K. A., Adkins, C. E. & Lockman, P. R. 2013. Quantitative fluorescence microscopy provides high resolution imaging of passive diffusion and P-gp mediated efflux at the *in vivo* blood-brain barrier. *Journal of neuroscience methods* **219**:188-95.

Mo, W. & Zhang, J. T. 2009. Oligomerization of human ATP-binding cassette transporters and its potential significance in human disease. *Expert opinion on drug metabolism & toxicology* **5**:1049-63.

Muller, A. M., Hermanns, M. I., Skrzynski, C., Nesslinger, M., Muller, K. M. & Kirkpatrick, C. J. 2002. Expression of the endothelial markers PECAM-1, vWf, and CD34 *in vivo* and *in vitro*. *Experimental and molecular pathology* **72**:221-9.

Nabors, M. W., Griffin, C. A., Zehnbauer, B. A., Hruban, R. H., Phillips, P. C., Grossman, S. A., Brem, H. & Colvin, O. M. 1991. Multidrug resistance gene (MDR1) expression in human brain tumours. *Journal of neurosurgery* **75**:941-6.

Narang, V. S., Fraga, C., Kumar, N., Shen, J., Throm, S., Stewart, C. F. & Waters, C. M. 2008. Dexamethasone increases expression and activity of multidrug resistance transporters at the rat blood-brain barrier. *American journal of physiology. Cell physiology* **295**:C440-50.

Nervi, P., Li-Blatter, X., Aanismaa, P. & Seelig, A. 2010. P-glycoprotein substrate transport assessed by comparing cellular and vesicular ATPase activity. *Biochimica et biophysica acta* **1798**:515-25.

Ni, Z., Bikadi, Z., Rosenberg, M. F. & Mao, Q. 2010. Structure and function of the human breast cancer resistance protein (BCRP/ABCG2). *Current drug metabolism* **11**:603-17.

Nies, A. T., Jedlitschky, G., Konig, J., Herold-Mende, C., Steiner, H. H., Schmitt, H. P. & Keppler, D. 2004. Expression and immunolocalization of the multidrug resistance proteins, MRP1-MRP6 (ABCC1-ABCC6), in human brain. *Neuroscience* **129**:349-60.

Nitta, T., Hata, M., Gotoh, S., Seo, Y., Sasaki, H., Hashimoto, N., Furuse, M. & Tsukita, S. 2003. Size-selective loosening of the blood-brain barrier in claudin-5-deficient mice. *The Journal of cell biology* **161**:653-60.

Ohuchi, N., Hayashi, K., Iwamoto, K., Koike, K., Kizawa, Y., Nukaga, M., Kakegawa, T. & Murakami, H. 2010. Thrombin-stimulated proliferation is mediated by endothelin-1 in cultured rat gingival fibroblasts. *Fundam Clin Pharmacol* **24**:501-8.

Olefsky, J. M. & Kao, M. 1982. Surface binding and rates of internalization of 125I-insulin in adipocytes and IM-9 lymphocytes. *The Journal of biological chemistry* **257**:8667-73.

Paolinelli, R., Corada, M., Orsenigo, F. & Dejana, E. 2011. The molecular basis of the blood brain barrier differentiation and maintenance. Is it still a mystery? *Pharmacological research : the official journal of the Italian Pharmacological Society* **63**:165-71.

Patabendige, A., Skinner, R. A. & Abbott, N. J. 2013a. Establishment of a simplified *in vitro* porcine blood-brain barrier model with high transendothelial electrical resistance. *Brain research* **1521**:1-15.

Patabendige, A., Skinner, R. A., Morgan, L. & Abbott, N. J. 2013b. A detailed method for preparation of a functional and flexible blood-brain barrier model using porcine brain endothelial cells. *Brain research* **1521**:16-30.

Patel, S. C., Jain R., and Wagner S. 2008. *Chapter 7. The Vasculature of the Human Brain,* Neuroscience in Medicine Conn, Michael (Ed.) 3rd ed. Humana Press

Perriere, N., Yousif, S., Cazaubon, S., Chaverot, N., Bourasset, F., Cisternino, S., Decleves, X., Hori, S., Terasaki, T., Deli, M., Scherrmann, J. M., Temsamani, J., Roux, F. & Couraud, P. O. 2007. A functional *in vitro* model of rat blood-brain barrier for molecular analysis of efflux transporters. *Brain research* **1150**:1-13.

Petty, M. A. & Lo, E. H. 2002. Junctional complexes of the blood-brain barrier: permeability changes in neuroinflammation. *Progress in neurobiology* **68**:311-23.

Pfeiffer, F., Schafer, J., Lyck, R., Makrides, V., Brunner, S., Schaeren-Wiemers, N., Deutsch, U. & Engelhardt, B. 2011. Claudin-1 induced sealing of blood-brain barrier tight junctions ameliorates chronic experimental autoimmune encephalomyelitis. *Acta neuropathologica* **122**:601-14.

Poller, B., Drewe, J., Krahenbuhl, S., Huwyler, J. & Gutmann, H. 2010. Regulation of BCRP (ABCG2) and P-glycoprotein (ABCB1) by cytokines in a model of the human blood-brain barrier. *Cellular and molecular neurobiology* **30**:63-70.

Poller, B., Gutmann, H., Krahenbuhl, S., Weksler, B., Romero, I., Couraud, P. O., Tuffin, G., Drewe, J. & Huwyler, J. 2008. The human brain endothelial cell line hCMEC/D3 as a human blood-brain barrier model for drug transport studies. *Journal of neurochemistry* **107**:1358-68.

Potschka, H., Fedrowitz, M. & Loscher, W. 2003. Multidrug resistance protein MRP2 contributes to blood-brain barrier function and restricts antiepileptic drug activity. *The Journal of pharmacology and experimental therapeutics* **306**:124-31.

Ramsauer, M., Krause, D. & Dermietzel, R. 2002. Angiogenesis of the blood-brain barrier *in vitro* and the function of cerebral pericytes. *FASEB journal : official publication of the Federation of American Societies for Experimental Biology* **16**:1274-6.

Raub, T. J., Kuentzel, S. L. & Sawada, G. A. 1992. Permeability of bovine brain microvessel endothelial cells *in vitro*: barrier tightening by a factor released from astroglioma cells. *Experimental cell research* **199**:330-40.

Regina, A., Demeule, M., Laplante, A., Jodoin, J., Dagenais, C., Berthelet, F., Moghrabi, A. & Beliveau, R. 2001. Multidrug resistance in brain tumours: roles of the blood-brain barrier. *Cancer metastasis reviews* **20**:13-25.

Regina, A., Jodoin, J., Khoueir, P., Rolland, Y., Berthelet, F., Moumdjian, R., Fenart, L., Cecchelli, R., Demeule, M. & Beliveau, R. 2004. Down-regulation of caveolin-1 in glioma vasculature: modulation by radiotherapy. *Journal of neuroscience research* **75**:291-9.

Regina, A., Koman, A., Piciotti, M., El Hafny, B., Center, M. S., Bergmann, R., Couraud, P. O. & Roux, F. 1998. Mrp1 multidrug resistance-associated protein and P-glycoprotein expression in rat brain microvessel endothelial cells. *Journal of neurochemistry* **71**:705-15.

Rigor, R. R., Hawkins, B. T. & Miller, D. S. 2010. Activation of PKC isoform beta(I) at the blood-brain barrier rapidly decreases P-glycoprotein activity and enhances drug delivery to the brain. *Journal of cerebral blood flow and metabolism : official journal of the International Society of Cerebral Blood Flow and Metabolism* **30**:1373-83.

Rist, R. J., Romero, I. A., Chan, M. W., Couraud, P. O., Roux, F. & Abbott, N. J. 1997. F-actin cytoskeleton and sucrose permeability of immortalised rat brain microvascular endothelial cell monolayers: effects of cyclic AMP and astrocytic factors. *Brain research* **768**:10-8.

Roberts, L. M., Black, D. S., Raman, C., Woodford, K., Zhou, M., Haggerty, J. E., Yan, A. T., Cwirla, S. E. & Grindstaff, K. K. 2008. Subcellular localization of

transporters along the rat blood-brain barrier and blood-cerebral-spinal fluid barrier by *in vivo* biotinylation. *Neuroscience* **155**:423-38.

Rubin, L. L., Hall, D. E., Porter, S., Barbu, K., Cannon, C., Horner, H. C., Janatpour, M., Liaw, C. W., Manning, K., Morales, J. & et al. 1991. A cell culture model of the blood-brain barrier. *The Journal of cell biology* **115**:1725-35.

Sachs, C. W., Chambers, T. C. & Fine, R. L. 1999. Differential phosphorylation of sites in the linker region of P-glycoprotein by protein kinase C isozymes alpha, betaI, betaII, gamma, delta, epsilon, eta, and zeta. *Biochemical pharmacology* **58**:1587-92.

Sakata, S., Fujiwara, M., Ohtsuka, K., Kamma, H., Nagane, M., Sakamoto, A. & Fujioka, Y. 2011. ATP-binding cassette transporters in primary central nervous system lymphoma: decreased expression of MDR1 P-glycoprotein and breast cancer resistance protein in tumour capillary endothelial cells. *Oncology reports* **25**:333-9.

Salama, N. N., Kelly, E. J., Bui, T. & Ho, R. J. 2005. The impact of pharmacologic and genetic knockout of P-glycoprotein on nelfinavir levels in the brain and other tissues in mice. *Journal of pharmaceutical sciences* **94**:1216-25.

Saubamea, B., Cochois-Guegan, V., Cisternino, S. & Scherrmann, J. M. 2012. Heterogeneity in the rat brain vasculature revealed by quantitative confocal analysis of endothelial barrier antigen and P-glycoprotein expression. *Journal of cerebral blood flow and metabolism : official journal of the International Society of Cerebral Blood Flow and Metabolism* **32**:81-92.

Savettieri, G., Di Liegro, I., Catania, C., Licata, L., Pitarresi, G. L., D'Agostino, S., Schiera, G., De Caro, V., Giandalia, G., Giannola, L. I. & Cestelli, A. 2000. Neurons and ECM regulate occludin localization in brain endothelial cells. *Neuroreport* **11**:1081-4.

Sawada, T., Kato, Y., Sakayori, N., Takekawa, Y. & Kobayashi, M. 1999. Expression of the multidrug-resistance P-glycoprotein (Pgp, MDR-1) by endothelial cells of the neovasculature in central nervous system tumours. *Brain tumour pathology* **16**:23-7.

Schiera, G., Bono, E., Raffa, M. P., Gallo, A., Pitarresi, G. L., Di Liegro, I. & Savettieri, G. 2003. Synergistic effects of neurons and astrocytes on the differentiation of brain capillary endothelial cells in culture. *Journal of cellular and molecular medicine* **7**:165-70.

Schlageter, K. E., Molnar, P., Lapin, G. D. & Groothuis, D. R. 1999. Microvessel organization and structure in experimental brain tumours: microvessel

populations with distinctive structural and functional properties. *Microvascular research* **58**:312-28.

Schroeter, M. L., Mertsch, K., Giese, H., Muller, S., Sporbert, A., Hickel, B. & Blasig, I. E. 1999. Astrocytes enhance radical defence in capillary endothelial cells constituting the blood-brain barrier. *FEBS letters* **449**:241-4.

Schroeter, M. L., Muller, S., Lindenau, J., Wiesner, B., Hanisch, U. K., Wolf, G. & Blasig, I. E. 2001. Astrocytes induce manganese superoxide dismutase in brain capillary endothelial cells. *Neuroreport* **12**:2513-7.

Seetharaman, S., Barrand, M. A., Maskell, L. & Scheper, R. J. 1998. Multidrug resistance-related transport proteins in isolated human brain microvessels and in cells cultured from these isolates. *Journal of neurochemistry* **70**:1151-9.

Shapiro, A. B., Corder, A. B. & Ling, V. 1997. P-glycoprotein-mediated Hoechst 33342 transport out of the lipid bilayer. *European journal of biochemistry / FEBS* **250**:115-21.

Sharom, F. J. 2008. ABC multidrug transporters: structure, function and role in chemoresistance. *Pharmacogenomics* **9**:105-27.

Shawahna, R., Uchida, Y., Decleves, X., Ohtsuki, S., Yousif, S., Dauchy, S., Jacob, A., Chassoux, F., Daumas-Duport, C., Couraud, P. O., Terasaki, T. & Scherrmann, J. M. 2011. Transcriptomic and quantitative proteomic analysis of transporters and drug metabolizing enzymes in freshly isolated human brain microvessels. *Molecular pharmaceutics* **8**:1332-41.

Shibata, S. 1989. Ultrastructure of capillary walls in human brain tumours. *Acta neuropathologica* **78**:561-71.

Shimomura, K., Okura, T., Kato, S., Couraud, P. O., Schermann, J. M., Terasaki, T. & Deguchi, Y. 2013. Functional expression of a proton-coupled organic cation (H+/OC) antiporter in human brain capillary endothelial cell line hCMEC/D3, a human blood-brain barrier model. *Fluids and barriers of the CNS* **10**:8.

Sims-Mourtada, J., Izzo, J. G., Ajani, J. & Chao, K. S. 2007. Sonic Hedgehog promotes multiple drug resistance by regulation of drug transport. *Oncogene* **26**:5674-9.

Singh, R. R., Kunkalla, K., Qu, C., Schlette, E., Neelapu, S. S., Samaniego, F. & Vega, F. 2011. ABCG2 is a direct transcriptional target of hedgehog signaling and involved in stroma-induced drug tolerance in diffuse large B-cell lymphoma. *Oncogene* **30**:4874-86.

Smith, A. J., Mayer, U., Schinkel, A. H. & Borst, P. 1998. Availability of PSC833, a substrate and inhibitor of P-glycoproteins, in various concentrations of serum. *Journal of the National Cancer Institute* **90**:1161-6.

Sobue, K., Yamamoto, N., Yoneda, K., Hodgson, M. E., Yamashiro, K., Tsuruoka, N., Tsuda, T., Katsuya, H., Miura, Y., Asai, K. & Kato, T. 1999. Induction of blood-brain barrier properties in immortalized bovine brain endothelial cells by astrocytic factors. *Neuroscience research* **35**:155-64.

Son, E., Jeong, J., Lee, J., Jung, D. Y., Cho, G. J., Choi, W. S., Lee, M. S., Kim, S. H., Kim, I. K. & Suk, K. 2005. Sequential induction of heme oxygenase-1 and manganese superoxide dismutase protects cultured astrocytes against nitric oxide. *Biochemical pharmacology* **70**:590-7.

Soontornmalai, A., Vlaming, M. L. & Fritschy, J. M. 2006. Differential, strain-specific cellular and subcellular distribution of multidrug transporters in murine choroid plexus and blood-brain barrier. *Neuroscience* **138**:159-69.

Staal, F. J., Luis, T. C. & Tiemessen, M. M. 2008. WNT signalling in the immune system: WNT is spreading its wings. *Nature reviews. Immunology* **8**:581-93.

Stamatovic, S. M., Keep, R. F. & Andjelkovic, A. V. 2008. Brain endothelial cell-cell junctions: how to "open" the blood brain barrier. *Current neuropharmacology* **6**:179-92.

Steg, A. D., Katre, A. A., Bevis, K. S., Ziebarth, A., Dobbin, Z. C., Shah, M. M., Alvarez, R. D. & Landen, C. N. 2012. Smoothened antagonists reverse taxane resistance in ovarian cancer. *Molecular cancer therapeutics* **11**:1587-97.

Steinberg, M. S. & McNutt, P. M. 1999. Cadherins and their connections: adhesion junctions have broader functions. *Current opinion in cell biology* **11**:554-60.

Stewart, P. A., Beliveau, R. & Rogers, K. A. 1996. Cellular localization of P-glycoprotein in brain versus gonadal capillaries. *The journal of histochemistry and cytochemistry : official journal of the Histochemistry Society* **44**:679-85.

Strom, S. C. & Michalopoulos, G. 1982. Collagen as a substrate for cell growth and differentiation. *Methods Enzymol* **82 Pt A**:544-55.

Sugiyama, D., Kusuhara, H., Lee, Y. J. & Sugiyama, Y. 2003. Involvement of multidrug resistance associated protein 1 (Mrp1) in the efflux transport of 17beta estradiol-D-17beta-glucuronide (E217betaG) across the blood-brain barrier. *Pharmaceutical research* **20**:1394-400.

Sun, H., Johnson, D. R., Finch, R. A., Sartorelli, A. C., Miller, D. W. & Elmquist, W. F. 2001. Transport of fluorescein in MDCKII-MRP1 transfected cells and mrp1-knockout mice. *Biochemical and biophysical research communications* **284**:863-9.

Tan, K. H., Dobbie, M. S., Felix, R. A., Barrand, M. A. & Hurst, R. D. 2001. A comparison of the induction of immortalized endothelial cell impermeability by astrocytes. *Neuroreport* **12**:1329-34.

Tang, F., Ouyang, H., Yang, J. Z. & Borchardt, R. T. 2004. Bidirectional transport of rhodamine 123 and Hoechst 33342, fluorescence probes of the binding sites on P-glycoprotein, across MDCK-MDR1 cell monolayers. *Journal of pharmaceutical sciences* **93**:1185-94.

Teng, H., Chopp, M., Hozeska-Solgot, A., Shen, L., Lu, M., Tang, C. & Zhang, Z. G. 2012. Tissue plasminogen activator and plasminogen activator inhibitor 1 contribute to sonic hedgehog-induced *in vitro* cerebral angiogenesis. *PloS one* **7**:e33444.

Tews, D. S., Nissen, A., Kulgen, C. & Gaumann, A. K. 2000. Drug resistance-associated factors in primary and secondary glioblastomas and their precursor tumours. *Journal of neuro-oncology* **50**:227-37.

Thottassery, J. V., Zambetti, G. P., Arimori, K., Schuetz, E. G. & Schuetz, J. D. 1997. p53-dependent regulation of MDR1 gene expression causes selective resistance to chemotherapeutic agents. *Proceedings of the National Academy of Sciences of the United States of America* **94**:11037-42.

Torok, M., Huwyler, J., Gutmann, H., Fricker, G. & Drewe, J. 2003. Modulation of transendothelial permeability and expression of ATP-binding cassette transporters in cultured brain capillary endothelial cells by astrocytic factors and cell-culture conditions. *Experimental brain research. Experimentelle Hirnforschung. Experimentation cerebrale* **153**:356-65.

Toth, K., Vaughan, M. M., Peress, N. S., Slocum, H. K. & Rustum, Y. M. 1996. MDR1 P-glycoprotein is expressed by endothelial cells of newly formed capillaries in human gliomas but is not expressed in the neovasculature of other primary tumours. *The American journal of pathology* **149**:853-8.

Tout, S., Chan-Ling, T., Hollander, H. & Stone, J. 1993. The role of Muller cells in the formation of the blood-retinal barrier. *Neuroscience* **55**:291-301.

Tsinman, O., Tsinman, K., Sun, N. & Avdeef, A. 2011. Physicochemical selectivity of the BBB microenvironment governing passive diffusion--matching with a porcine brain lipid extract artificial membrane permeability model. *Pharmaceutical research* **28**:337-63.

Uchida, Y., Ohtsuki, S., Katsukura, Y., Ikeda, C., Suzuki, T., Kamiie, J. & Terasaki, T. 2011. Quantitative targeted absolute proteomics of human blood-brain barrier transporters and receptors. *Journal of neurochemistry* **117**:333-45.

von Wedel-Parlow, M., Wolte, P. & Galla, H. J. 2009. Regulation of major efflux transporters under inflammatory conditions at the blood-brain barrier *in vitro*. *Journal of neurochemistry* **111**:111-8.

Wang, M. M., Lee, S. J., Kim, J., Majersik, J. J., Blaivas, M. & Borjigin, J. 2013. ABO blood antigens define human cerebral endothelial diversity. *Neuroreport* **24**:79-83.

Warren, M. S., Zerangue, N., Woodford, K., Roberts, L. M., Tate, E. H., Feng, B., Li, C., Feuerstein, T. J., Gibbs, J., Smith, B., de Morais, S. M., Dower, W. J. & Koller, K. J. 2009. Comparative gene expression profiles of ABC transporters in brain microvessel endothelial cells and brain in five species including human. *Pharmacological research : the official journal of the Italian Pharmacological Society* **59**:404-13.

Weiss, J., Sauer, A., Herzog, M., Boger, R. H., Haefeli, W. E. & Benndorf, R. A. 2009. Interaction of thiazolidinediones (glitazones) with the ATP-binding cassette transporters P-glycoprotein and breast cancer resistance protein. *Pharmacology* **84**:264-70.

Weksler, B. B., Subileau, E. A., Perriere, N., Charneau, P., Holloway, K., Leveque, M., Tricoire-Leignel, H., Nicotra, A., Bourdoulous, S., Turowski, P., Male, D. K., Roux, F., Greenwood, J., Romero, I. A. & Couraud, P. O. 2005. Blood-brain barrier-specific properties of a human adult brain endothelial cell line. *FASEB journal : official publication of the Federation of American Societies for Experimental Biology* **19**:1872-4.

Wen, P. Y. & Kesari, S. 2008. Malignant gliomas in adults. *The New England journal of medicine* **359**:492-507.

Willis, C. L., Leach, L., Clarke, G. J., Nolan, C. C. & Ray, D. E. 2004. Reversible disruption of tight junction complexes in the rat blood-brain barrier, following transitory focal astrocyte loss. *Glia* **48**:1-13.

Willis, C. L., Taylor, G. L. & Ray, D. E. 2007. Microvascular P-glycoprotein expression at the blood-brain barrier following focal astrocyte loss and at the fenestrated vasculature of the area postrema. *Brain research* **1173**:126-36.

Winkler, E. A., Bell, R. D. & Zlokovic, B. V. 2011. Central nervous system pericytes in health and disease. *Nature neuroscience* **14**:1398-405.

Wolburg, H., Noell, S., Mack, A., Wolburg-Buchholz, K. & Fallier-Becker, P. 2009. Brain endothelial cells and the glio-vascular complex. *Cell and tissue research* **335**:75-96.

Xiao, G. & Gan, L. S. 2013. Receptor-mediated endocytosis and brain delivery of therapeutic biologics. *International journal of cell biology* **2013**:703545.

Xue, Q., Liu, Y., Qi, H., Ma, Q., Xu, L., Chen, W., Chen, G. & Xu, X. 2013. A novel brain neurovascular unit model with neurons, astrocytes and microvascular endothelial cells of rat. *International journal of biological sciences* **9**:174-89.

Yauch, R. L., Gould, S. E., Scales, S. J., Tang, T., Tian, H., Ahn, C. P., Marshall, D., Fu, L., Januario, T., Kallop, D., Nannini-Pepe, M., Kotkow, K., Marsters, J. C., Rubin, L. L. & de Sauvage, F. J. 2008. A paracrine requirement for hedgehog signalling in cancer. *Nature* **455**:406-10.

Yin, X., Wright, J., Wall, T. & Grammas, P. 2010. Brain endothelial cells synthesize neurotoxic thrombin in Alzheimer's disease. *The American journal of pathology* **176**:1600-6.

Yousif, S., Chaves, C., Potin, S., Margaill, I., Scherrmann, J. M. & Decleves, X. 2012. Induction of P-glycoprotein and Bcrp at the rat blood-brain barrier following a subchronic morphine treatment is mediated through NMDA/COX-2 activation. *Journal of neurochemistry* **123**:491-503.

Yuan, W., Li, G., Zeng, M. & Fu, B. M. 2010. Modulation of the blood-brain barrier permeability by plasma glycoprotein orosomucoid. *Microvascular research* **80**:148-57.

Zenker, D., Begley, D., Bratzke, H., Rubsamen-Waigmann, H. & von Briesen, H. 2003. Human blood-derived macrophages enhance barrier function of cultured primary bovine and human brain capillary endothelial cells. *The Journal of physiology* **551**:1023-32.

Zhang, H., Hilton, D. A., Hanemann, C. O. & Zajicek, J. 2011. Cannabinoid receptor and N-acyl phosphatidylethanolamine phospholipase D--evidence for altered expression in multiple sclerosis. *Brain pathology (Zurich, Switzerland)* **21**:544-57.

Zhang, W., Mojsilovic-Petrovic, J., Andrade, M. F., Zhang, H., Ball, M. & Stanimirovic, D. B. 2003. The expression and functional characterization of ABCG2 in brain endothelial cells and vessels. *FASEB journal : official publication of the Federation of American Societies for Experimental Biology* **17**:2085-7.

Zhang, X., Chen, J., Davis, B. & Kiechle, F. 1999. Hoechst 33342 induces apoptosis in HL-60 cells and inhibits topoisomerase I *in vivo*. *Archives of pathology & laboratory medicine* **123**:921-7.

Zhang, Z., Wu, J. Y., Hait, W. N. & Yang, J. M. 2004. Regulation of the stability of P-glycoprotein by ubiquitination. *Molecular pharmacology* **66**:395-403.

Zhang, Z. Y. & Wong, Y. N. 2005. Enzyme kinetics for clinically relevant CYP inhibition. *Current drug metabolism* **6**:241-57.

Zhao, L. N., Yang, Z. H., Liu, Y. H., Ying, H. Q., Zhang, H. & Xue, Y. X. 2011. Vascular endothelial growth factor increases permeability of the blood-tumour barrier via

caveolae-mediated transcellular pathway. *Journal of molecular neuroscience : MN* **44**:122-9.

Zhou, Y., Liu, F., Xu, Q. & Wang, X. 2010. Analysis of the expression profile of Dickkopf-1 gene in human glioma and the association with tumour malignancy. *Journal of experimental & clinical cancer research : CR* **29**:138.

11 Appendix

11.1 Binding properties of ^{3}H-MPP^{+}

To determine whether the positive charge of MPP^{+} resulted in its binding to either plastics or cells, the binding properties of ^{3}H-MPP^{+} were assessed.

11.1.1 Binding to plastic

To assess whether ^{3}H-MPP^{+} significantly binds to plastics, the recovery of ^{3}H-MPP^{+} from a standard 96-well plate was determined. The recovery of ^{3}H-MPP^{+} into PBS and acid washes is shown in Table 9.1.1. PBS washes were used as standard since this is a common step in radioactive assay procedures. An acid wash was then used (after the PBS washes) to specifically target binding between the ^{3}H-MPP^{+} and the plastic plate, where a strong acid, 1M HCl, would displace any ^{3}H-MPP^{+} bound to the plastic. The results showed that only 0.1% of the ^{3}H-MPP^{+} was collected in the acid wash, with the majority recovered in the assay buffer (96%) and with 2.7% recovered in the PBS washes. This demonstrated that most of the excess ^{3}H-MPP^{+} could be removed by PBS washes.

Table A.^{3}H-MPP^{+} recovery from plastic plate

A

	DPMs Recovered			
DPMs Added to Well	**In the Removed Assay Buffer**	**In the Pooled PBS Washes**	**In the Acid Wash**	**Total**
133029 ± 717	127749 ± 1695	3541 ± 1159	150 ± 54	131440± 593

B

	% Recovered				
DPMs Added to Well	**In the Removed Assay Buffer**	**In the Pooled PBS Washes**	**In the Acid Wash**	**Total**	**% LOST**
133029 ± 717	96.0 ± 1.27	2.7 ± 0.87	0.1 ± 0.04	98.8 ± 0.45	1.2 ± 0.45

^{3}H-MPP^{+} was added to wells for 10 minutes at room temperature. The ^{3}H-MPP^{+} was then removed and kept (Removed Buffer) and the wells were washed with PBS three times with all the washes kept and pooled into a single sample (Pooled PBS Washes). The wells were then incubated with 1M HCl acid for 10 minutes. The acid wash was then collected (Acid wash sample).

The DPMs within each of the collected samples was measured using liquid scintillation counting and are shown in A. The percentage of ^{3}H-MPP^{+} recovery was then calculated as given in B.

Results are mean ± SEM of n=3.

11.1.2 Binding to the glycocalyx

To assess whether MPP+ was binding to the glycocalyx of the PBECs, alternative acid wash experiments were conducted. PBECs were incubated with ^{3}H-MPP^{+} for 1 hour, the cells were then washed with PBS three times, followed by a fourth wash with either PBS or Glycocalyx Acid wash (28mM Sodium Acetate, 20mM Barbitone sodium and 117mM NaCl) (Olefsky and Kao 1982) with the fourth wash kept for analysis. The cells were then lysed and the lysates were also analysed. If the MPP+ was binding to the glycocalyx, the acid wash would displace the MPP+ from cells, so more MPP+ would be found in the acid wash than in the PBS wash, and consequently less MPP+ would be found in the lysate when an acid wash was used.

The results show a trend towards greater amounts of ^{3}H-MPP^{+} within the acid wash and lower ^{3}H-MPP^{+} within the lysate when an acid wash had been used. However no significant differences between the percentage of ^{3}H-MPP^{+} measured within the PBS or acid wash, or within the cell lysates of the two conditions were observed, demonstrating that glycocalyx binding does not play a significant role in the assessment of ^{3}H-MPP^{+} uptake or efflux.

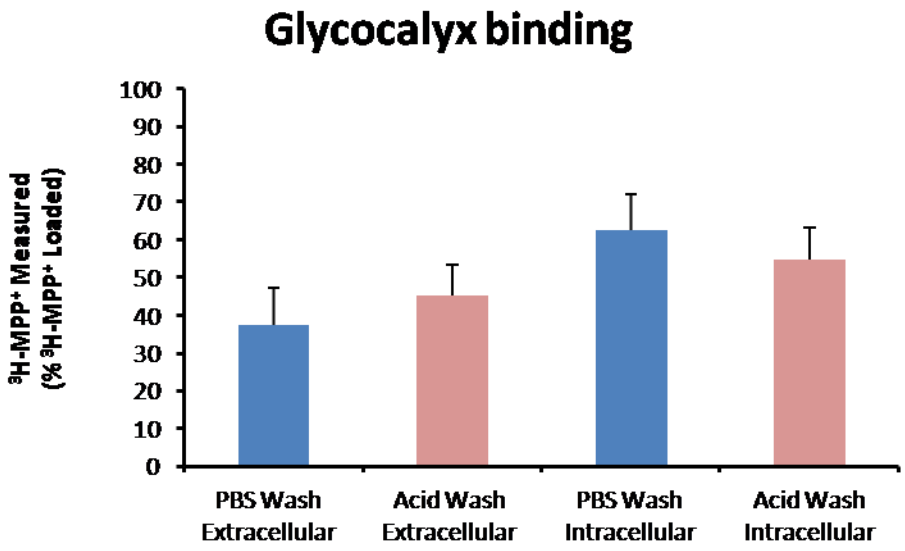

Figure A. Glycocalyx binding of ^{3}H-MPP$^+$

PBECs in 96-wells plates were incubated with ^{3}H-MPP$^+$ for 1 hour at 37ºC. The ^{3}H-MPP$^+$ was removed and the cells were washed three times with PBS. The cells were then incubated with either PBS or Glycocalyx Acid Wash for 6 minutes at 4ºC for a final 4th wash. The fourth wash was kept and the cells were lysed with the lysate also kept. The 4th wash (Extracellular sample, Extra) and lysate samples (Intracellular sample, Intra) were then analysed for the presence of ^{3}H-MPP$^+$ by scintillation counting with data corrected against ^{14}C-sucrose extracellular space marker.

The ^{3}H-MPP$^+$ measured within the 4th Wash or within the lysate was then expressed as a percentage of the total ^{3}H-MPP$^+$ loaded into the cells (prior to the start of the 4th wash).

Values are mean ± SEM of n=3.

No significant differences were noted in unpaired t-tests between PBS and Acid wash conditions in the 4th wash or the lysates.

11.2 Dose-response raw data

As detailed in 3.1.5 dose-response analysis of the ability of Pgp and BCRP inhibitors to inhibit ^{3}H-MPP^{+} efflux was assessed, using ^{3}H-MPP^{+} efflux assay in the presence of different concentrations of each inhibitor. The raw data (i.e. prior to normalisation) is shown below.

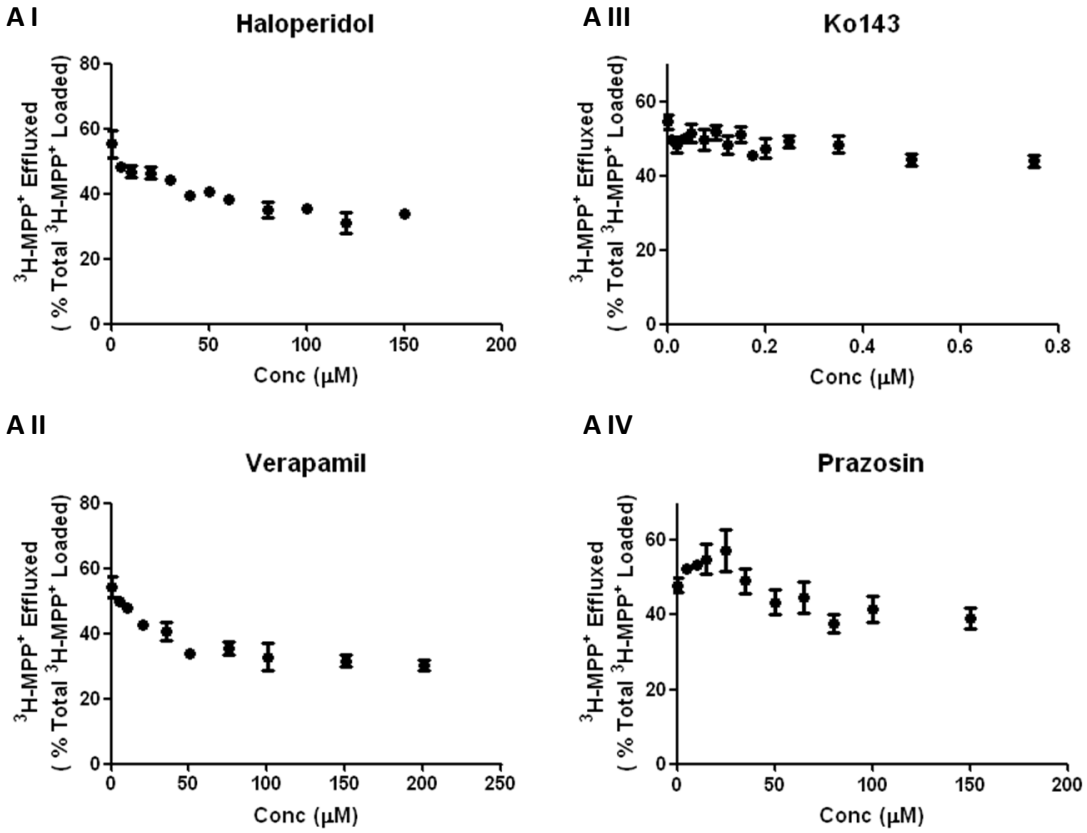

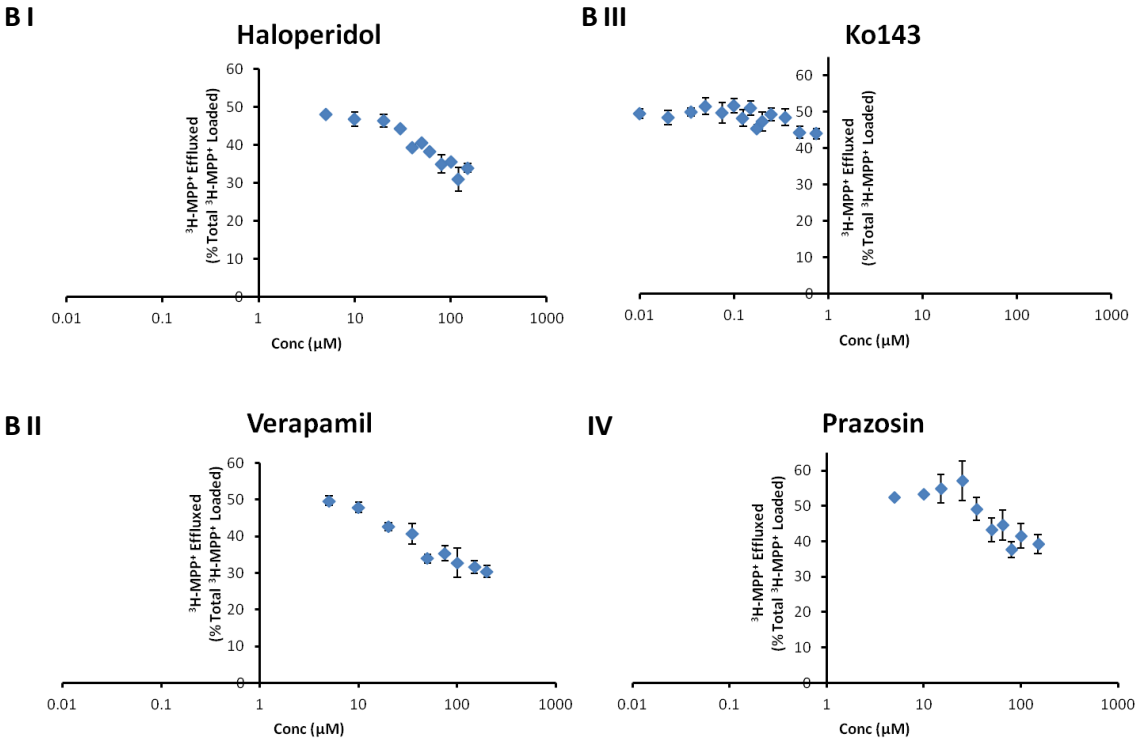

Figure B. Raw dose-response data

The PBECs grown on plates (PBECs-P) were loaded with ^{3}H-MPP^{+}. The loaded cells were then incubated with efflux buffer with or without ABC inhibitors (0 – 300 µM) for 35 minutes. The inhibitors used were the Pgp inhibitors haloperidol (I) and verapamil (II), and the BCRP inhibitors Ko143 (III) and prazosin (IV). The data is shown on a normal scale (A) and on a log scale (B).

The buffer was then collected and analysed by liquid scintillation counting for ^{3}H-MPP^{+} with correction for ^{14}C-sucrose.

The ^{3}H-MPP^{+} effluxed was then expressed as a percentage of the ^{3}H-MPP^{+} initially loaded into the cells.

The values are shown as mean ± SEM of 3-5 wells where possible, or as single mean point when less than 3 wells were tested at the same concentration. Values are pooled from 3-5 plates.

11.3 Effect of OCT inhibitor amantadine on ^{3}H-MPP^{+} uptake and efflux

To assess the involvement of OCT transporters in the uptake of ^{3}H-MPP^{+} into PBECs a ^{3}H-MPP^{+} uptake assay was conducted on PBECs grown in 96-well plates. Uptake was measured in the absence (Control) and presence of the OCT1/2 transporter amantadine. The concentration of amantadine used was 1mM, which has been previously shown to effectively inhibit OCT transporter activity (Shimomura *et al.*,

2013). In addition, 2mM amantadine was also used to assess whether a greater inhibition could be achieved with a higher concentration of amantadine.

The results (Figure C) showed that amantadine significantly decreased ^{3}H-MPP^{+} uptake by ~65% when 1mM or 2mM amantadine concentrations were used, indicating that uptake of ^{3}H-MPP^{+} into PBECs was OCT-dependent. No increase in inhibition was observed upon using 2mM as opposed to 1mM amantadine, indicating that 1mM amantadine was sufficient to maximally inhibit OCT-dependent ^{3}H-MPP^{+} uptake.

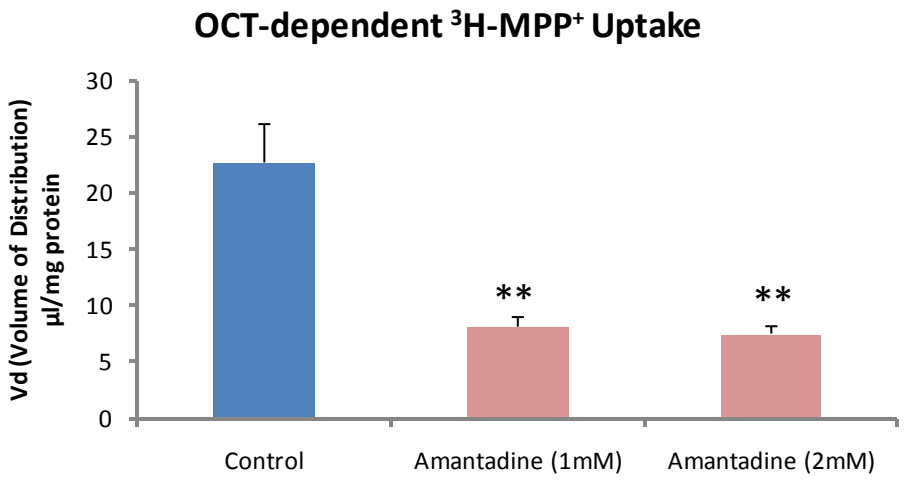

Figure C. OCT-dependent ^{3}H-MPP^{+}uptake

PBECs in 96-well plates were incubated with 9 nM (27.75 KBq.ml^{-1}) ^{3}H-MPP^{+} and ^{14}C-sucrose (5.55 KBq.ml^{-1}) for 1 hour, with^{14}C-sucrose as a marker for extracellular space. The cells were then washed and lysed. Half the lysate was analysed for ^{3}H-MPP^{+} and ^{14}C-sucrose and the other half of used for protein content measurement using a BCA assay.

Results are expressed as volume of distribution (Vd) in µl.mg^{-1} of protein after correction for ^{14}C-sucrose.

Values are mean ± SEM of n=5-6 wells from 2 different batches of PBECs.

**p<0.01 significant difference indicated conditions and control using an unpaired 2-tailed t-test.

To determine the involvement of the OCT transporters in the efflux of ^{3}H-MPP^{+} from PBECs, an ^{3}H-MPP^{+} efflux assay was conducted on PBECs-P (PBECs in 24 well plates) in the absence (Control) or presence of the OCT1/2 inhibitor amantadine (1mM), which was shown in the uptake assay to maximally inhibit uptake.

The results showed no significant difference in efflux or intracellular retention of ^{3}H-MPP^{+} in the absence or presence of amantadine, indicating that the OCT1/2 transporters were not significantly involved in the efflux of ^{3}H-MPP^{+}.

These results were compared to other results involving inhibition of Pgp by Haloperidol, where Haloperidol did significantly inhibit ^{3}H-MPP^{+} efflux, demonstrating that inhibition of ^{3}H-MPP^{+} efflux could be achieved, in this experiment.

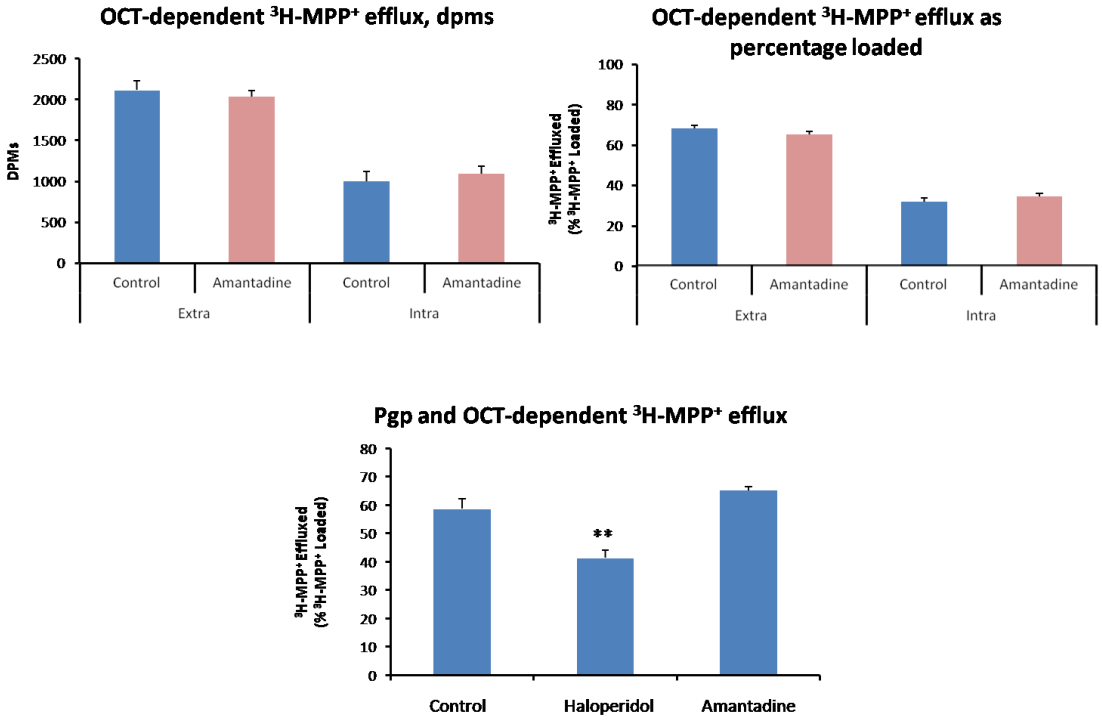

Figure D. OCT-dependent ^{3}H-MPP^{+} efflux

PBECs were grown on plates (PBECs-P), loaded with ^{3}H-MPP^{+} and then incubated with efflux buffer without (Control) or with the OCT 1/2 inhibitor Amantadine (1mM) for 35 minutes.

The buffer was then collected and the cells were lysed. The buffer and lysate samples were then analysed by liquid scintillation counting for ^{3}H-MPP^{+} with correction for ^{14}C-sucrose.

A I) The DPMs measured extracellularly (Extra, in the buffer) and intracellularly (Intra, in the lysate). AII) The ^{3}H-MPP^{+} effluxed extracellullarly or maintained intracellularly was then expressed as a percentage of the ^{3}H-MPP^{+} initially loaded into the cells.

B) The amantadine inhibition results were then compared to Haloperidol Inhibition results (Pgp inhibitor), where Haloperidol inhibition was conducted exactly as Amantadine inhibition experiment had been conducted, only using Haloperidol (60 µM) instead of Amantadine.

The values are shown as mean ± SEM of n=3-6.

11.4 RT-QPCR: Additional information

Additional information regarding the RT-PCR work conducted is given below.

11.4.1 RT-QPCT probe details

The details regarding the TaqMan Assay used are shown below (from Life Technology website). The exact probe sequences are not provided by the company, however the details of the target sequences are given.

Assay Design

The assay probe spans an exon junction.

Gene Transcripts

Gene Symbol	ABCB1
Entrez Gene ID	396910
Gene Name	ATP-binding cassette, sub-family B (MDR/TAP), member 1
Gene Aliases	MDR1, P-gp
NCBI Location Chromosome	Chr.9: 102530067 - 102626455
UniGene	Ssc.8764

Interrogated Sequence		Translated Protein	Exon Boundary	Assay Location	Amplicon Length
GenBank mRNA	AF403245.1	-	2 - 3	250	75
	AY825267.1	-	10 - 11	1401	75

Assay Design

The amplified product spans an exon junction and the probe and one of the primers sit within one exon. This assay may detect gDNA.

Gene Transcripts

Gene Symbol ABCG2
Entrez Gene ID 397073
Gene Name ATP-binding cassette, sub-family G (WHITE), member 2
Gene Aliases BMDP
NCBI Location Chromosome Chr.8: 140193291 - 140228765
UniGene Ssc.64

Interrogated Sequence		Translated Protein	Exon Boundary	Assay Location	Amplicon Length
RefSeq	NM_214010.1	NP_999175.1	15 - 15	1853	77
GenBank mRNA	AJ420927.1	-	15 - 15	1853	77
	AK239126.1	-	14 - 14	2264	77
	AY550047.1	-	2 - 2	76	77

Assay Design

The assay primers and probes lie within a single exon. This assay will detect gDNA.

Gene Transcripts

Gene Symbol ACTB
Entrez Gene ID 414396
Gene Name actin, beta
Gene Aliases -
NCBI Location Chromosome Chr.3: 4729266 - 4732657
UniGene Ssc.10316

Interrogated Sequence		Translated Protein	Exon Boundary	Assay Location	Amplicon Length
GenBank mRNA	AY550069.1	-	5 - 5	949	79
	DQ845171.1	-	3 - 3	528	79

Assay Design

The amplified product spans an exon junction and the probe and one of the primers sit within one exon. This assay may detect gDNA.

Gene Transcripts

Gene Symbol GAPDH
Entrez Gene ID 396823
Gene Name glyceraldehyde-3-phosphate dehydrogenase
Gene Aliases GAPD
NCBI Location Chromosome Chr.5: 66446302 - 66449510
UniGene Ssc.16135

Interrogated Sequence		Translated Protein	Exon Boundary	Assay Location	Amplicon Length
RefSeq	NM_001206359.1	NP_001193288.1	-	881	83
GenBank mRNA	AF069649.1	-	3 - 3	256	83
	AK234838.1	-	-	881	83
	DQ845173.1	-	-	564	83
	U48832.1	-	-	741	83
	U82261.1	-	-	262	83

11.4.2 Pgp and BCRP Ct values

The Ct values for Pgp and BCRP obtained from RT-PCR experiments are shown below.

A

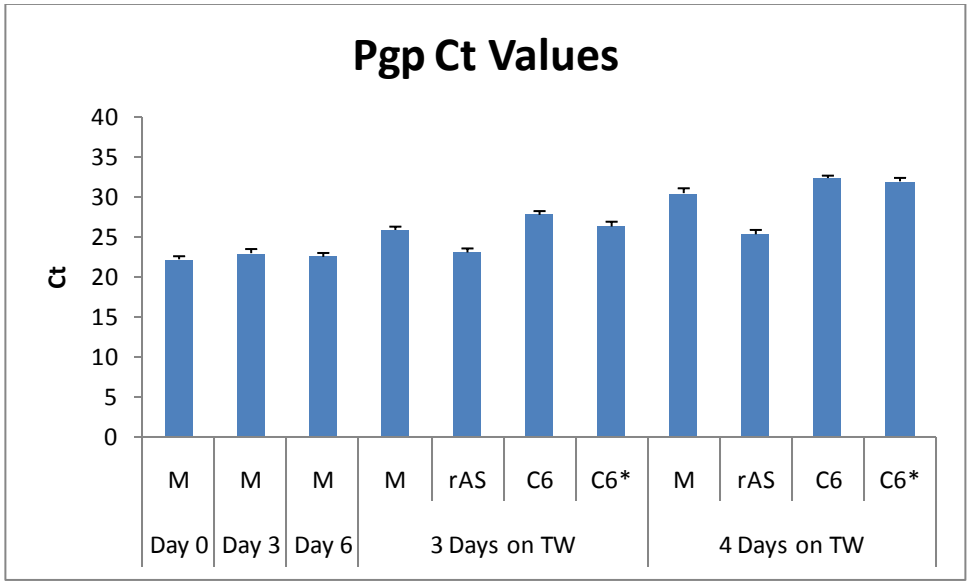

B

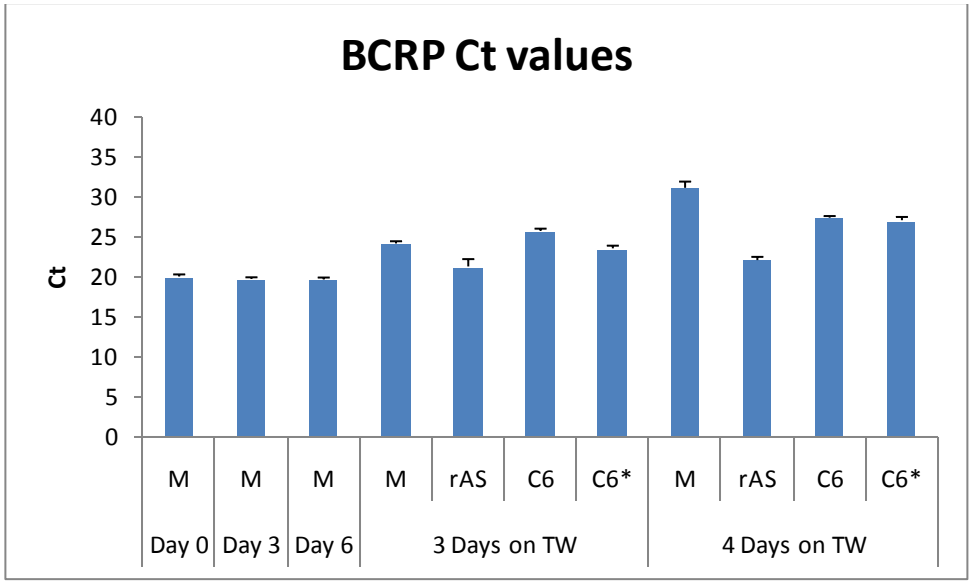

Figure E. Pgp and BCRP Ct values

The charts show the Ct values for Pgp (A) and BCRP (B) RNA from RT-QPCR experiments conducted on RNA collected from PBECs at different stages of the cell culture process.

Day 0 represents the primary isolated porcine capillaries. The PBECs were grown out from the capillaries for up to 6 days (the first 3 days in puromycin containing medium). RNA was isolated

after the 3 days of puromycin treatment (Day 3) and on day 6 when the cells were passaged to Transwells (Day 6).

Once on Transwells (TW), the PBECs were either grown alone (i.e. in mono-culture, M) or in co-culture with primary rat astrocytes (rAS) or C6 glioma cells (C6). The PBECs, in either mono-culture or in co-culture were grown on the Transwells for 3 days in serum-containing medium after which RNA was isolated (3 Days on TW). Alternatively, the PBECs, in either mono-culture or in co-culture were grown on the Transwells for 3 days in serum-containing medium, followed by 24 hours in serum-free medium containing 550 nM hydrocortisone, 250 µM CPT-cAMP and 17.5 µM Ro-20-1724, before RNA isolation (4 Days on TW). Two different C6 conditions were tested, one where the medium was changed on day two of co-culture and the other where the medium was not changed (the second is denoted by C6*).

Values are mean ± SEM of n=3 samples per condition, where PCR was conducted on triplicates per plate and n=3 plates were run.

11.5 Western Blotting Optimisations

Dot blot analysis was initially conducted to determine appropriate antibody concentrations for the anti-Pgp (C219) and the anti-BCRP (BXP-21) antibodies (Figure A), which showed positive staining of PBEC proteins by both antibodies.

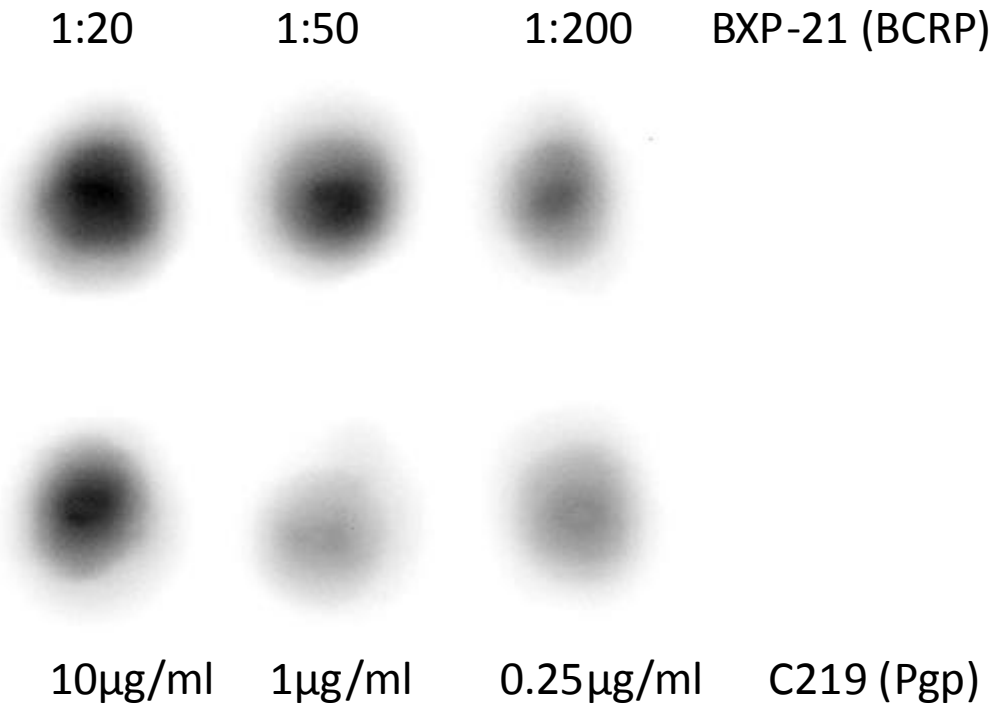

Figure F. Dot Blot for BCRP and Pgp

PBEC cell lysates obtained from mono-cultured cells was placed on a PVDF, using 2µl per dot. The blot was incubated with either mouse BXP-21 or mouse C219 antibody at the indicated concentration for 1 hour (room temp) washed then incubated with 1:1000 anti mouse IgG, HRP secondary antibody for 1 hour. HRP activity was then visualised with Syngene imager and Software.

Western Blots were then conducted of PBEC lysates using a standard blotting protocol, 10% Gels, 12-Wells 1mm thick, Tris-Glysine Transfer Buffer, Semi-Dry Transfer for 30 minutes at 20V, using 1:200 BXP-21 and/or 0.25µl/ml C219. BCRP was successfully deselected in PBEC cell lysates, lysed with 1% Triton-X 100 containing protease inhibitors for 1 hour (Figure B). However Pgp was not detected, either in samples or in the positive control.

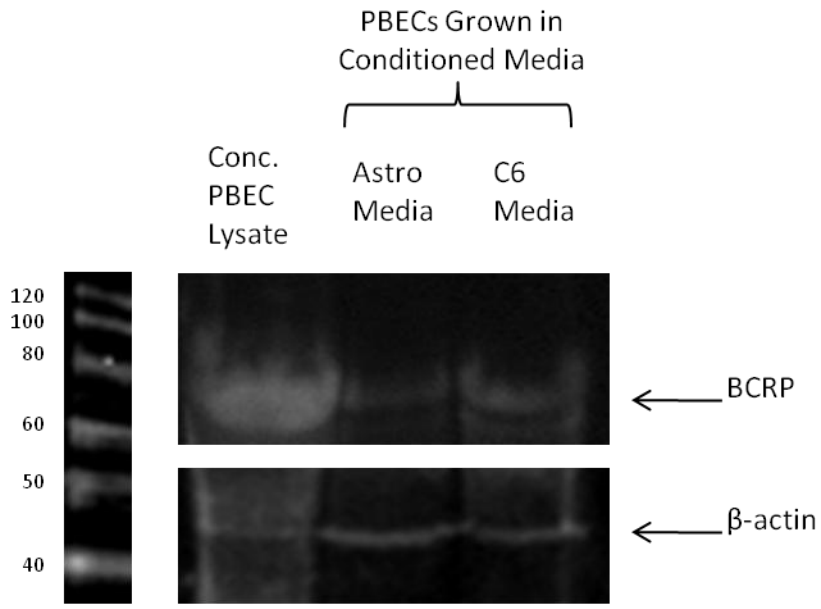

Figure G. Protein expression in PBECs grown in conditioned medium

PBECs were grown in rat astrocyte conditioned media (Astro Media) or C6 conditioned media (C6 Media). The cells were lysed and 20µg of protein lysates were loaded onto a 10% gel. The gels was transferred onto a PVDF membrane and incubated with anti-BCRP antibody (BXP-21, 1:200), anti-Pgp antibody (C219, 0.25µl/ml) and anti-βactin antibody (C-11, 1:1000) and respective secondary antibodies at 1:1000 dilutions.

The detected signals within the samples are shown in the image alongside a positive control from a pooled sample of PBEC cell lysates obtained from mono-cultured cells.

The lack of Pgp signal within the blot correlated with incomplete transfer of higher molecular proteins (including Pgp 170kDa). Therefore, thinner gels were run (0.75mm) in attempt to improve the transfer of Pgp and other higher molecular weight protein. In addition, different acrylamide percentages were also tested (6%, 8%, 10% and 12% gels). Transfer of higher molecular weight proteins improved with decreasing acrylamide concentrations. However, the 6% gels consistently melted during electrophoresis. Therefore 8% was decided on for western blotting experiments (data not shown). Furthermore, different transfer buffers were tested for different lengths of transfer times. The high pH Dunn's buffer with the addition of methanol and SDS, showed the best result with a transfer time of 75 minutes, where Pgp could be detected in rat liver positive control protein lysates (Figure C).

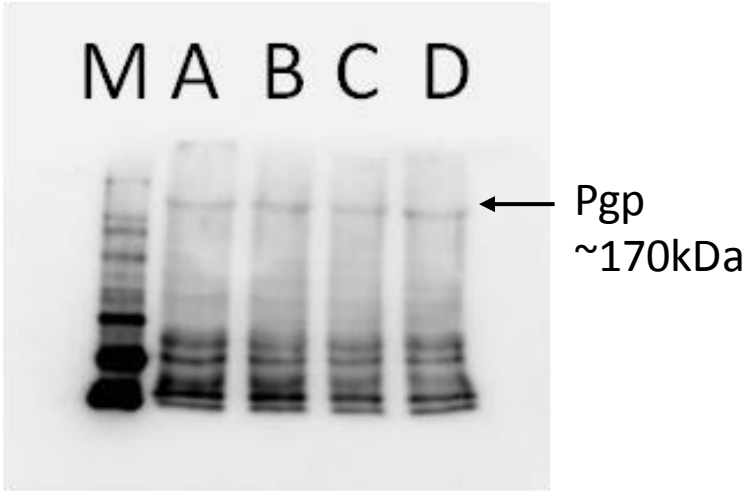

Figure H. Western Blotting for Pgp

Decreasing amounts of protein from a rat liver lysate underwent western blotting with anti-Pgp antibody (C219, 0.25µl/ml) and anti-βactin antibody (C-11, 1:1000) antibody A) 15 µg, B) 12.5 µg C) 10 µg D) 7.5 µg.

Using the optimised conditions, 0.75mm 8% Gel, Dunn's transfer buffer with methanol in bottom of the sandwich and SDS in the top of the sandwich, protein from PBECs-M,

PBECs-rAS, PBECs-C6 from after 3 days in co-culture was analysed by Western blotting (Figure D).

In attempt to correlate mRNA levels with protein levels, TRI isolation of RNA and protein from the same cells was conducted. TRI isolation was conducted from PBECs-M, PBECs-rAS and PBECs-C6. Due to phenol contamination from the TRI isolation process, accurate protein measurements of the protein samples isolated could not be obtained. Purification via TCA precipitation was attempted, but protein could not then be fully resuspendent into solution. Therefore, TCA purified protein was not appropriate for quantitative comparisons between the different PBEC conditions.

Instead, the equivalent of 1 Transwell of protein (i.e. the total protein isolated from a single Transwell) was loaded onto a 8%, 5-Well Gel without quantification. Western blotting was conducted using the optimised protocol, with antibodies against Pgp, BCRP and β-actin. The blot showed positive BCRP and Pgp within all the samples. However, due to insufficient time the western could not be repeated to achieve accurate quantification nor could western blots for other samples (e.g. samples from 4 days in co-culture) be conducted.

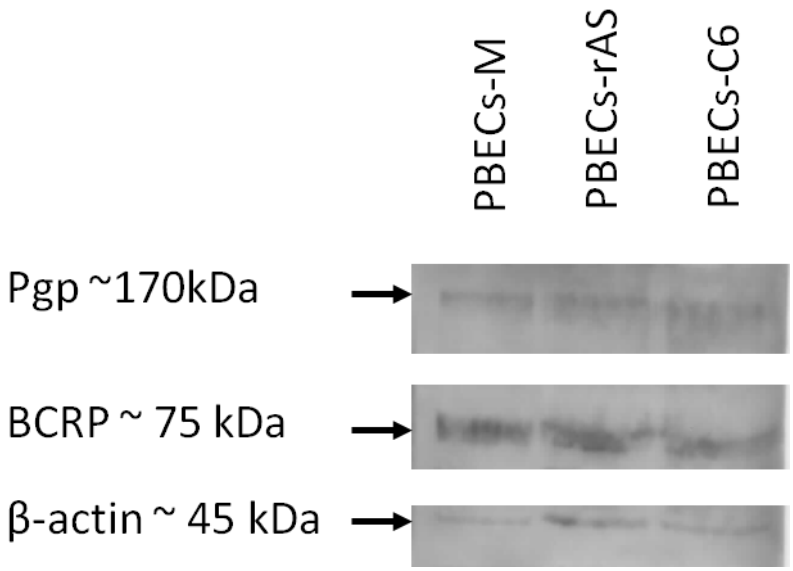

Figure I. BCRP and Pgp expression in PBECs after 3 days on Transwells

PBECs were grown on Transwells in mono-culture (PBECs-M) or in co-culture with rat astrocytes (PBECs-rAS) or C6 rat glioblastoma cells (PBCs-C6s) for a total of 3 days. The protein was isolated via TRI isolation and the equivalent of 1 Transwell of protein was loaded per well onto a 8%, 0.75mm gel. The gel underwent SDS-PAGE and transfer onto a PVDF

membrane, where blotting for Pgp, BCRP and actin was conduted using anti-Pgp antibody (C219, 0.25µl/ml), anti-BCRP antibody (BXP-21, 1:200), and anti-β-actin antibody (C-11, 1:1000) and respective secondary antibodies at 1:1000 for Pgp and BCRP and 1 in 25000 for β-actin.

The detected signals within the samples are shown after 5 minutes of imaging with Syngene imager and software.

11.6 Application of the PBECs-G7 as a Model of BBB Glioma Challenge

In collaboration with Steven Pollard's group (UCL) the following publication was achieved, where the extract shows the application of the humanised 2 day PBEC co-culture with G7s in drug screening process for glioblastoma.

OPEN ACCESS Freely available online

PLOS ONE

A High-Content Small Molecule Screen Identifies Sensitivity of Glioblastoma Stem Cells to Inhibition of Polo-Like Kinase 1

Davide Danovi[1¤a], Amos Folarin[1], Sabine Gogolok[1], Christine Ender[1], Ahmed M. O. Elbatsh[1], Pär G. Engström[2], Stefan H. Stricker[1], Sladjana Gagrica[1], Ana Georgian[3], Ding Yu[4], Kin Pong U[6], Kevin J. Harvey[5], Patrizia Ferretti[6], Patrick J. Paddison[4], Jane E. Preston[3], N. Joan Abbott[3], Paul Bertone[2,7,8], Austin Smith[8], Steven M. Pollard[1*¤b]

1 Samantha Dickson Brain Cancer Unit and Department of Cancer Biology, UCL Cancer Institute, University College London, London, United Kingdom, **2** European Bioinformatics Institute, European Molecular Biology Laboratory, Cambridge, United Kingdom, **3** Institute of Pharmaceutical Science, King's College London, London, United Kingdom, **4** Human Biology Division, Fred Hutchinson Cancer Research Center, Seattle, Washington, United States of America, **5** EMD Millipore Corporation, San Diego, California, United States of America, **6** Institute of Child Health, University College London, London, United Kingdom, **7** Genome Biology and Developmental Biology Units, European Molecular Biology Laboratory, Heidelberg, Germany, **8** Wellcome Trust–Medical Research Council Stem Cell Institute, University of Cambridge, Cambridge, United Kingdom

Abstract

Glioblastoma multiforme (GBM) is the most common primary brain cancer in adults and there are few effective treatments. GBMs contain cells with molecular and cellular characteristics of neural stem cells that drive tumour growth. Here we compare responses of human glioblastoma-derived neural stem (GNS) cells and genetically normal neural stem (NS) cells to a panel of 160 small molecule kinase inhibitors. We used live-cell imaging and high content image analysis tools and identified JNJ-10198409 (J101) as an agent that induces mitotic arrest at prometaphase in GNS cells but not NS cells. Antibody microarrays and kinase profiling suggested that J101 responses are triggered by suppression of the active phosphorylated form of polo-like kinase 1 (Plk1) (phospho T210), with resultant spindle defects and arrest at prometaphase. We found that potent and specific Plk1 inhibitors already in clinical development (BI 2536, BI 6727 and GSK 461364) phenocopied J101 and were selective against GNS cells. Using a porcine brain endothelial cell blood-brain barrier model we also observed that these compounds exhibited greater blood-brain barrier permeability *in vitro* than J101. Our analysis of mouse mutant NS cells (INK4a/ARF$^{-/-}$, or p53$^{-/-}$), as well as the acute genetic deletion of p53 from a conditional p53 floxed NS cell line, suggests that the sensitivity of GNS cells to BI 2536 or J101 may be explained by the lack of a p53-mediated compensatory pathway. Together these data indicate that GBM stem cells are acutely susceptible to proliferative disruption by Plk1 inhibitors and that such agents may have immediate therapeutic value.

Citation: Danovi D, Folarin A, Gogolok S, Ender C, Elbatsh AMO, et al. (2013) A High-Content Small Molecule Screen Identifies Sensitivity of Glioblastoma Stem Cells to Inhibition of Polo-Like Kinase 1. PLoS ONE 8(10): e77053. doi:10.1371/journal.pone.0077053

Editor: Kyung S. Lee, National Cancer Institute, NIH, United States of America

Received October 29, 2012; **Accepted** August 29, 2013; **Published** October 30, 2013

Funding: This work was supported by a grant from the EC-funded STREP project 'Neuroscreen,' EMBL, and grants from Cancer Research UK, Children with Cancer, and The Brain Tumour Charity. CE was supported by a FP7 Marie Curie Intra-European Fellowship. AS is an MRC Professor. SP was supported by an Alex Bolt Research Fellowship. The funders had no role in study design, data collection and analysis, decision to publish, or preparation of the manuscript.

Competing Interests: The authors have declared the following interests: Co-author Steven M. Pollard is a named inventor on the following patent using human NS cell culture condition for screening purposes (UK Patent Application 0503044.0, 'Neural Stem Cells')). However, he has no stock or consultancy duties for the company, which has exclusive rights to this patent (Stem Cells Inc.). Co-author Kevin Harvey is an employee of EMD Millipore Corporation. This does not alter the authors' adherence to all the PLOS ONE policies on sharing of data and materials.

* E-mail: steven.pollard@ed.ac.uk

¤a Current address: Centre for Stem Cells and Regenerative Medicine, King's College London, London, United Kingdom
¤b Current address: MRC Centre for Regenerative Medicine, University of Edinburgh, Edinburgh, United Kingdom

In vitro blood-brain barrier assay

Porcine brain endothelial cells (PBECs) were isolated and cultured as described [30,31]. Inserts with confluent PBECs were co-cultured with GNS cells and compounds applied to determine their capacity to cross the endothelial barrier to the GNS cells below. After 24 h the cell culture inserts containing PBECs were removed and GNS cells were cultured for a further 24 h, fixed, and then analysed by immunocytochemistry. Sodium fluorescein (Sigma) was used as a control to determine levels of paracellular permeability and therefore integrity of the barrier function of PBECs (applied at 7.5 µg/ml in the top insert). Samples of culture media below the insert were collected and fluorescence was measured at an excitation wavelength of 485 nm and an emission wavelength of 530 nm.

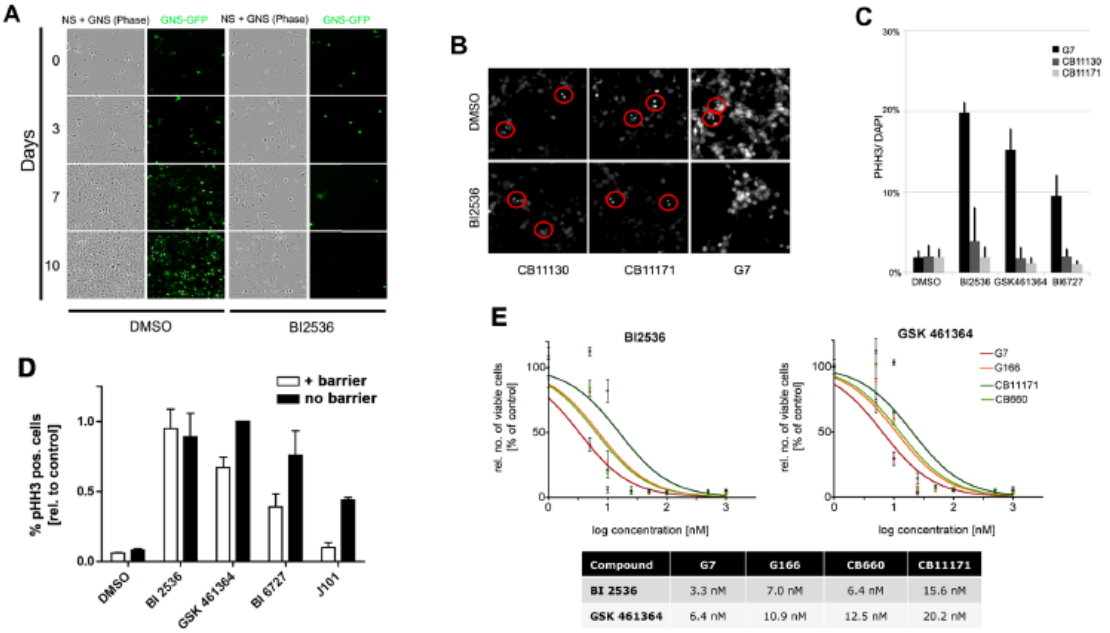

Compound	G7	G166	CB660	CB11171
BI 2536	3.3 nM	7.0 nM	6.4 nM	15.6 nM
GSK 461364	6.4 nM	10.9 nM	12.5 nM	20.2 nM

Figure 6. Alternative Plk1 inhibitors in clinical development compare favourably with BI 2536 in selectivity against GNS cells and blood-brain barrier permeability. (A) Co-culture of equal numbers of GFP-transfected G144 cell lines together with wild-type CB660 cells. In the presence of BI2536 GNS cells are selectively lost in the culture, while normal NS cells continue to proliferate. (B) DAPI staining of day 10 cultures of GNS or NS cells confirms that NS cells continue to undergo normal mitosis (anaphase events in red circles), without evidence of mitotic slippage and lagging chromosomes. (C) Two other Plk1 inhibitors in clinical development are selective against GNS cells (G7) compared to foetal NS cells (CB11130 and CB11171; chosen as they have a similar doubling time to G7). (D) Relative numbers of GNS cells arrested in mitosis after 48 h treatment with Plk1 inhibitors using an *in vitro* blood-brain barrier co-culture model. Inhibitors were added directly or via cell culture inserts containing a confluent layer of endothelial cells, and anti-mitotic responses were assessed in G7. J101 displayed poor blood-brain barrier permeability ($P<0.001$). GSK461364 performed similarly to BI 2536. Values shown are percentages of pHH3-positive cells relative to no-insert value of GSK 461364 treated GNS cells ($n=3$). (E) Dose-response curves and IC50 values for specific Plk1 inhibitors BI 2536 and GSK 461363. NS and GNS cells were treated with different concentrations of the Plk1 inhibitors BI 2536 and GSK461364. Five days after treatment the total number of viable cells was counted and normalised to DMSO control values. Calculation of IC50 values confirmed the differential effect of both inhibitors on NS and GNS cells, with G7 being most sensitive.

doi:10.1371/journal.pone.0077053.g006